

THE ITERATIVE SCHWINGER  
VARIATIONAL METHOD APPLIED TO  
ELECTRON-MOLECULE CONTINUUM  
PROCESSES

Thesis by  
Robert Ross Lucchese

In Partial Fulfillment of the Requirements  
for the Degree of  
Doctor of Philosophy

California Institute of Technology  
Pasadena, California

1982

(Submitted September 24, 1981)

To Kate

## ACKNOWLEDGMENTS

During my tenure as a graduate student at Caltech, I have had the privilege of working with and learning from many outstanding scientists. Foremost of these is my research advisor, Dr. McKoy who has both guided and stimulated my research as well as supporting it through his grants. I would also like to thank Drs. Debbie Watson, Arne Fliflet, Kazuo Takatsuka and Georges Raseev, who as postdocs and visiting associates have also been a source of encouragement and assistance in furthering my studies. I also acknowledge the generous support from a National Science Foundation Graduate Fellowship and from an Exxon Education Foundation Graduate Fellowship. Finally I would like to thank my wife, Kate, my parents and my brothers and sisters without whose support this degree would never have been earned.

## ABSTRACT

We have developed the iterative Schwinger variational method to study electron-molecule scattering problems within the Hartree-Fock approximation. The method is based on the iterative use of the Schwinger variational principle and can obtain exact static-exchange scattering solutions. This approach has been implemented using standard single-center expansion techniques. We present results using the Schwinger variational expression for e-He and e-He<sup>+</sup> collisions and find very rapid convergence of the phase shifts with increasing basis set size. We then discuss the iterative use of the Schwinger variational expression and give results for e-H<sub>2</sub> and e-H<sub>2</sub><sup>+</sup> scattering which show very rapid convergence of the iterative method. We have applied this method to low energy e-CO<sub>2</sub> scattering and obtained differential and integral elastic scattering cross sections. We determined that the <sup>2</sup>Π<sub>u</sub> shape resonance in this system occurs at an energy of 5.39 eV with a width of 0.64 eV in contrast to previously published static-exchange results.

We have also used the iterative Schwinger variational method to study the valence shell photoionization of N<sub>2</sub> and CO<sub>2</sub> as well as the K-shell photoionization of CO<sub>2</sub>. These results agree well with available experimental data. The vibrational branching ratios for photoionization of 3σ<sub>g</sub> level of N<sub>2</sub> were found to agree quantitatively with experimental measurements when an adequate number of internuclear spacings were considered. The effects of vibrational averaging on 4σ<sub>g</sub>

photoionization of  $\text{CO}_2$  were also studied. A detailed comparison of the results obtained using the Schwinger method and other theoretical methods for studying photoionization has been made.

The iterative Schwinger variational method has proven to be an accurate and efficient method for obtaining Hartree-Fock level scattering solutions, and it has allowed us to study electron-molecule continuum processes in more detail and for larger systems than previously possible.

## TABLE OF CONTENTS

<u>Chapter</u>	<u>Title</u>	<u>Page</u>
I.	DEVELOPMENT OF THE ITERATIVE SCHWINGER VARIATIONAL METHOD	1
	Introduction	2
A.	Application of the Schwinger Variational Principle to Electron Scattering [R.R. Lucchese and V. McKoy, J. Phys. B 12, L421 (1979)]	15
B.	Application of the Schwinger Variational Principle to Electron-Ion Scattering in the Static-Exchange Approximation [R.R. Lucchese and V. McKoy, Phys. Rev. A 21, 112 (1980)]	25
C.	Iterative Approach to the Schwinger Variational Principle for Electron- Molecule Collisions [R.R. Lucchese, D.K. Watson and V. McKoy, Phys. Rev. A 22, 421 (1980)]	69
D.	Iterative Approach to the Schwinger Variational Principle Applied to Electron-Molecular-Ion Collisions [R.R. Lucchese and V. McKoy, Phys. Rev. A 24, 770 (1981)]	90
II.	APPLICATION OF THE ITERATIVE SCHWINGER VARIATIONAL METHOD TO ELECTRON-MOLECULE SCATTERING	117
	Introduction	118
A.	A Study of Electron Scattering by CO <sub>2</sub> at the Static-Exchange Level [R.R. Lucchese and V. McKoy, Phys. Rev. A, accepted for publication]	120
III.	APPLICATION OF THE ITERATIVE SCHWINGER VARIATIONAL METHOD TO MOLECULAR PHOTOIONIZATION	140
	Introduction	141
A.	Studies of Differential and Total Photoionization Cross Sections of Molecular Nitrogen [R.R. Lucchese, G. Raseev and V. McKoy, Phys. Rev. A, accepted for publication]	145
B.	Accurate Hartree-Fock Vibrational Branching Ratios in 3σ <sub>g</sub> Photoionization of N <sub>2</sub> [R.R. Lucchese and V. McKoy, J. Phys. B, accepted for publication]	202
C.	Comparative Studies of a Shape-Resonant Feature in the Photoionization of CO <sub>2</sub> [R.R. Lucchese and V. McKoy, J. Phys. Chem. 85, 2166 (1981)]	217

- D. Studies of Differential and Total Photoionization Cross Sections of Carbon Dioxide 235  
[R.R. Lucchese and V. McKoy, Phys. Rev. A, submitted for publication]
- E. Vibrational Effects in the Photoionization Shape Resonance Leading to the  $C^2\Sigma_g^+$  State of  $CO_2^+$  282  
[R.R. Lucchese and V. McKoy, Phys. Rev. A, submitted for publication]

CHAPTER I

Development of the Iterative Schwinger Variational Method

## INTRODUCTION

Much theoretical research in recent years has been devoted to the understanding of molecular systems which contain continuum electrons.<sup>(1)</sup> There are many such physical processes, including electron-molecule scattering, which can be either elastic or rotationally, vibrationally, or electronically inelastic, dissociative attachment, dissociative recombination, photoionization, and photodetachment. These processes are important in understanding such physical systems as plasmas, the ionosphere of planets, gas lasers, and interstellar media. This thesis describes the development of the iterative Schwinger variational method which is a new theoretical approach for accurately describing the continuum electron problem for molecular systems. As presently applied this approach solves the continuum problem within the static-exchange and adiabatic-nuclei approximations for linear molecules. We have applied the iterative Schwinger variational method to photoionization of  $N_2$  and  $CO_2$  and to electron- $CO_2$  scattering.

The basic mathematical problem in molecular quantum mechanics, where one electron is in the continuum, is the solution of the time-independent Schrödinger equation

$$H(r, r_c, R)\Psi(r, r_c, R) = E\Psi(r, r_c, R) \quad (1)$$

where  $r_c$  represents the coordinates of the  $N+1$ st continuum electron,  $r$  represents the coordinates of the other  $N$  electrons and  $R$  represents the nuclear motion with the center of mass

motion removed. The total molecular Hamiltonian can be written as

$$H = T_R + T_{r_c} + T_r + V(r,R) + V_c(r_c,r,R) \quad (2)$$

with  $T$  being a kinetic energy operator,  $V$  being the potential energy of interaction without the  $N+1$ st particle present and  $V_c$  representing the additional interactions due to the  $N+1$ st particle. For problems where one electron is in the continuum (the  $N+1$ st particle as written here), the wave function  $\Psi$  is usually described using a target eigenfunction expansion.<sup>(2)</sup>

Thus the total molecular wave function is written as

$$\Psi(r,r_c,R) = \sum A \phi_i(r_c) \psi_i(r,R), \quad (3)$$

where  $\psi_i$  are eigenfunctions of the target Hamiltonian,

$$\{T_R + T_r + V(r,R)\} \psi_i(r,R) = E_i \psi_i(r,R), \quad (4)$$

$A$  is the usual antisymmetrizer, and  $\phi_i(r_c)$  is the wave function of the  $N+1$  particle. For open channels where  $E > E_i$ ,  $\phi_i$  will be an oscillatory function at  $r_c \rightarrow \infty$ , while for closed channels, where  $E_i > E$ ,  $\phi_i$  will be exponentially decaying at  $r_c \rightarrow \infty$ . Usually Eq. (2) is in turn expanded in adiabatic electronic eigenfunctions

$$\Psi(r,r_c,R) = \sum_{ij} A \phi_i(r_c) \psi_j^{FN}(r;R) \chi_{ji}(R) \quad (5)$$

where

$$\{T_r + V(r,k)\} \psi_j^{FN}(r;k) = E_j^{FN}(R) \psi_j^{FN}(r;k) \quad (6)$$

and  $\psi_i$  which satisfies Eq. (4) is given by

$$\psi_i(r, k) = \sum_j \psi_j^{\text{FN}}(r; k) \chi_{ji}(k). \quad (7)$$

Eq. (5) is known as the laboratory-frame expansion of the wave function. If the target wave functions  $\psi_j^{\text{FN}}$  and  $\chi_{ji}$  were known, then solution of Eq. (1) could be obtained by solving the set of coupled differential equations which result from substituting Eq. (5) into Eq. (1) and then multiplying on the left by target wave functions and integrating out the target coordinates  $r$  and  $R$ . However, for regions of configuration space where the continuum electron is close to the nuclei, the motion of the nuclei and that of the continuum electron are strongly correlated. For such regions the laboratory-frame expansion is slowly convergent, and a different approach is needed. An alternative wave function expansion, known as the body-frame expansion is of the form

$$\Psi(r, r_c, R) = \sum_j A_j u_j(r_c, R) \psi_j^{\text{FN}}(r; k). \quad (8)$$

Chang and Fano<sup>(3)</sup> suggested that a body-frame expansion be used for expanding the wave function when the continuum electron is close to the nuclei and then at some boundary, e.g., at  $r_c = r_F$ , the wave function should be transformed to the laboratory frame. This is known as the frame transformation procedure.

The function  $u$  in Eq. (8) can be expanded in fixed-nuclei continuum eigenfunctions

$$u_j = \sum_k \phi_{kj}^{\text{FN}}(r_c; R) \chi_k^{\wedge}(R) \quad (9)$$

where

$$\{T_r + T_{r_c} + V(r, R) + V_c(r_c, r, R)\} \sum_j A[\phi_{kj}^{\text{FN}}(r_c; R) \psi_j^{\text{FN}}(r; R)] = E_k \sum_j A[\phi_{kj}^{\text{FN}}(r_c; R) \psi_j^{\text{FN}}(r; R)]. \quad (10)$$

Then the molecular wave function is given by

$$\Psi(r, r_c, R) = \sum_{jk} A[\phi_{kj}^{\text{FN}}(r_c; R) \psi_j^{\text{FN}}(r; R)] \chi_k^{\wedge}(R). \quad (11)$$

Thus Eq. (11) can also be used as a basis for solving Eq. (1).

However, once the fixed-nuclei electronic wave functions are obtained and the problem has been reduced to just solving for  $\chi_k^{\wedge}$ , the resulting equations are a continuum of coupled differential equations. This situation is worse than what we had with the laboratory-frame expansion given in Eq. (5).

Fortunately, though, we can employ the Born-Oppenheimer approximation. If we restrict the use of the Born-Oppenheimer approximation to scattering energies not too close to threshold and only to describe the scattering close to the nuclei, then the usual arguments about the relative time scales hold, i.e., the characteristic time for molecular rotation is  $>10^{-12}$  sec, for molecular vibration it is  $10^{-14}$  sec, and for electronic motion it is  $10^{-16}$  sec, thus the electronic wave functions vary adiabatically with nuclear motion. Using the Born-Oppenheimer approximation, the molecular wave function can than be written as

$$\Psi_{k\nu}(r, r_c, R) = \sum_j A[\phi_{kj}^{FN}(r_c; R)\psi_j^{FN}(r; R)]\chi_{\nu}^{\leftarrow}(R). \quad (12)$$

The adiabatic nuclei approximation, given in Eq. (12), can in some cases satisfactorily describe the entire scattering process and in these situations one does not need to employ the frame transformation procedure. One case where the adiabatic-nuclei approximation is adequate is when the collision occurs rapidly enough so that the molecule is essentially fixed in space during the duration of the interaction. This is generally the case for non-resonant collisions above threshold where the anisotropic electron-molecule interactions are not of too long a range. One example where this is not true is in electron-dipolar molecule collisions where the integrated cross section is infinite in the adiabatic-nuclei approximation. A second case where the adiabatic-nuclei approximation is useful in scattering theory is in the case of resonant scattering, where one can define a new potential surface on which the nuclei move, due to the  $N+1$  particle resonant state. Such a potential surface is complex due to the finite lifetime of the resonant state.

For the systems we have considered in this thesis, the adiabatic-nuclei representation is adequate. We must then solve the purely electronic Schrodinger's equation given in Eq. (10). As a first approximation, we have solved the fixed-nuclei Schrodinger's equation using the Hartree-Fock approximation. Thus we have neglected all electron correlation effects, and we represent the total electronic wave function by a single

Slater determinant. The equation for determining the molecular continuum wave function is then reduced to a single-particle three-dimensional potential scattering problem where the interaction potential is non-spherical and non-local. The wave equation for such a system may be written as (in atomic units)

$$(-1/2\nabla^2 - \frac{k^2}{2})\psi(\underline{r}) = \int d^3\underline{r}' V(\underline{r}, \underline{r}')\psi(\underline{r}') \quad (13)$$

where  $V$  represents the effective scattering potential. This integro-differential equation can be rewritten as an integral equation by using the Green's function defined by

$$G^{(\pm)} = (\nabla^2 + k^2 \pm i\epsilon)^{-1}. \quad (14)$$

Eq. (13) then becomes the Lippmann-Schwinger equation

$$\begin{aligned} \psi_k^{(+)}(\underline{r}) = \phi_k(\underline{r}) + \int d^3\underline{r}' \int d^3\underline{r}'' G^{(+)}(\underline{r}, \underline{r}') \\ U(\underline{r}', \underline{r}'')\psi_k^{(+)}(\underline{r}'') \end{aligned} \quad (15)$$

where  $\phi_k$  is the free particle scattering solution (i.e., the solution in the absence of  $V$ ) and  $U = 2V$ .

The basic approach to take here in solving Eq. (15) is to approximate the kernel by a separable form. Thus we approximate the kernel with

$$\int d^3\underline{r}' G^{(+)}(\underline{r}, \underline{r}') U(\underline{r}', \underline{r}'') \approx \sum_{i=1}^N f_i(\underline{r}) g_i(\underline{r}''). \quad (16)$$

Using this approximation, the Lippmann-Schwinger equation becomes

$$\psi_k^{(+)}(x) = \phi_k(x) + \sum_i f_i(x) \langle g_i | \psi_k^{(+)} \rangle. \quad (17)$$

Multiplying on the left by  $g_i(x)$  and integrating over  $x$  we obtain

$$\langle g_j | \psi_k^{(+)} \rangle = \langle g_j | \phi_k \rangle + \sum_i \langle g_j | f_i \rangle \langle g_i | \psi_k^{(+)} \rangle \quad (18)$$

then it follows that

$$\psi_k^{(+)}(x) = \phi_k(x) + \sum_{ij} f_i(x) [(1-A)^{-1}]_{ij} \langle g_j | \phi_k \rangle \quad (19)$$

where

$$A_{ij} = \langle g_i | f_j \rangle. \quad (20)$$

We have tried two different approaches for approximating the kernel; these methods are known as the T-matrix and Schwinger variational methods. Both of these approaches approximate the potential  $V$  by a separable form and treat the Green's function exactly. This has the advantage that the resulting solutions have the correct analytic form and that these methods are not troubled by spurious singularities which occur when the Green's function is not treated exactly. (4)

First, we tried the approach of Rescigno et al. (5) where the potential is represented by

$$U^+(x', x) = \sum_{\alpha_i, \alpha_j \in R} \langle x' | \alpha_i \rangle \langle \alpha_i | U | \alpha_j \rangle \langle \alpha_j | x \rangle, \quad (21)$$

and where the set of functions  $R$  is taken to be a set of  $L^2$  functions. This approximation of the potential yields a scattering solution of the form

$$\psi_k^{(+)\prime}(\underline{x}) = \phi_k(\underline{x}) + \sum_{\alpha_i, \alpha_j, \alpha_1 \in R} \langle \underline{x} | G^{(+)} | \alpha_i \rangle \\ [(1-B)^{-1}]_{ij} \langle \alpha_j | U | \alpha_1 \rangle \langle \alpha_1 | \phi_k \rangle \quad (22)$$

with

$$B_{ij} = \sum_{\alpha_n \in R} \langle \alpha_i | U | \alpha_n \rangle \langle \alpha_n | G^{(+)} | \alpha_j \rangle. \quad (23)$$

The second method we examined was the Schwinger variational method where the separable potential is taken to be of the form

$$U^S(\underline{x}, \underline{x}') = \sum_{\alpha_i, \alpha_j \in R} \langle \underline{x} | U | \alpha_i \rangle [U^{-1}]_{ij} \langle \alpha_j | U | \underline{x}' \rangle. \quad (24)$$

The wave function in this case is given by

$$\psi_k^{(+)\prime}(\underline{x}) = \phi_k(\underline{x}) + \sum_{\alpha_i, \alpha_j \in R} \langle \underline{x} | G^{(+)} U | \alpha_i \rangle \\ [C^{-1}]_{ij} \langle \alpha_j | U | \phi_k \rangle \quad (25)$$

with

$$C_{ij} = \langle \alpha_i | U - UG^{(+)} U | \alpha_j \rangle. \quad (26)$$

In Section B of this chapter, we show that the T-matrix separable potential does not give as satisfactory a representation of the potential as does the Schwinger form. The superior results obtained from the Schwinger separable form can be attributed to the connection this form has with the Schwinger variational expression.<sup>(6)</sup> The Schwinger variational expression for the T-matrix is

$$T_{k,k'}^{\text{tr}} = \langle \phi_k | U | \psi_{k'}^{(+)\text{tr}} \rangle + \langle \psi_k^{(-)\text{tr}} | U | \phi_{k'} \rangle - \langle \psi_k^{(-)\text{tr}} | U - UG^{(+)}U | \psi_{k'}^{(+)\text{tr}} \rangle, \quad (27)$$

where  $\psi_k^{\text{tr}}$  is a trial wave function. One can show this is a variational expression by considering a trial wave function which differs from the exact wave function  $\psi^{\text{ex}}$  by a small amount

$$\psi^{\text{tr}} = \psi^{\text{ex}} + \delta\psi. \quad (28)$$

Then it follows that the errors in the variational T-matrix are second order in  $\delta\psi$ , thus

$$T_{k,k'}^{\text{tr}} = T_{k,k'}^{\text{ex}} + O(\delta\psi)^2. \quad (29)$$

Now if we expand  $\psi^{\text{tr}}$  in the basis set used in Eq. (25),

$$\psi_k^{(\pm)\text{tr}}(\mathbf{x}) = \sum_{\alpha_i \in R} C_{k,i}^{(\pm)} \alpha_i(\mathbf{x}), \quad (30)$$

and require that the T-matrix elements be stationary with respect to variations in the linear expansion parameters, i.e., require

$$\frac{\partial T_{k,k'}^{\text{tr}}}{\partial C_{k,i}^{(\pm)}} = 0, \quad (31)$$

then the resulting trial wave function is

$$\psi_k^{(+)\text{tr}}(r) = \sum_{\alpha_i, \alpha_j \in R} \alpha_i(r) [C^{-1}]_{ij} \langle \alpha_i | U | \phi_k \rangle, \quad (32)$$

and the variational T-matrix is given by

$$T_{k,k'}^S = \sum_{\alpha_i, \alpha_j \in R} \langle \phi_k | U | \alpha_i \rangle [C^{-1}]_{ij} \langle \alpha_j | U | \phi_{k'} \rangle. \quad (33)$$

Thus, the solutions of the Schwinger separable form given in Eq. (25) are related to the trial function of Eq. (32) by

$$\psi_k^{(+)\text{s}}(r) = \phi_k(r) + \langle r | GU | \psi_k^{(+)\text{tr}} \rangle. \quad (34)$$

Also, the asymptotic form of the solution obtained by this method is given by

$$\psi_k^{(+)\text{s}}(r) \underset{r \rightarrow \infty}{\sim} \phi_k(r) - \left[ \frac{\pi}{2} \right]^{1/2} T_{k\hat{r},k}^S \frac{\exp(ikr)}{r}, \quad (35)$$

and thus  $\psi^S$  is asymptotically variationally stable.

The use of the Schwinger variational method for molecular systems was first suggested by Watson and McKoy.<sup>(7)</sup> The original method proposed by Watson and McKoy computed the matrix element,  $\langle \alpha_i | UGU | \alpha_j \rangle$ , using an analytic approximation. As discussed in Sections A and B of this chapter, we developed a single-center expansion method to exactly evaluate these difficult matrix elements. In Section A we present the first exact application of the Schwinger variational expression to an atomic or molecular scattering system where exchange interactions have been accurately treated. In that section we present e-He scattering phase shifts in the static-exchange approximation. We find that for this simple system, the

scattering phase shifts are well converged using only five basis functions. In Section B we present details of the numerical procedures used to evaluate  $\langle \alpha_i | UGU | \alpha_j \rangle$  and give the appropriate modifications needed to consider electron-molecular ion collisions. In Section B we also give results for e-He<sup>+</sup> scattering and He photoionization. Again we find rapid convergence of the Schwinger results with increasing basis set size.

In an application of the Schwinger variational method to e-H<sub>2</sub> scattering,<sup>(8)</sup> we found that for certain channels it was useful to include continuum functions in the basis set for each scattering energy considered. This was in part due to the long range nature of electron-molecule potentials, which for H<sub>2</sub>, falls off asymptotically as  $1/r^3$  due to the quadrupole moment of H<sub>2</sub>. These early attempts to include continuum functions lead to the development of the iterative Schwinger variational method which is described in detail in Section C. It is known that if the exact continuum solutions were included in the basis set R of Eq. (25), then  $\psi^S$  would be exact.<sup>(9)</sup> The iterative method thus proceeds by starting with an L<sup>2</sup> basis which yields scattering solutions  $\psi^{S0}$  using Eq. (25). Then the continuum solutions are used to augment the L<sup>2</sup> basis set to produce a new set of solutions  $\psi^{S1}$ . The procedure then continues by replacing  $\psi^{S0}$  by  $\psi^{S1}$  in the basis set to produce  $\psi^{S2}$ . In Section C we discuss why this procedure should converge and show that when it does converge the resulting wave functions are exact solutions of Eq. (15).

Results of this procedure are given for e-H<sub>2</sub> scattering. We found that when the basis was adequate, the iterative method converged in one or two iterations. In Section D we give results obtained for e-H<sub>2</sub><sup>+</sup> scattering and for the photoionization of H<sub>2</sub>. We find similarly good convergence in these cases.

## References

1. See for example, Electron-Molecule and Photon-Molecule Collisions, ed. T. Rescigno, V. McKoy and B. Schneider, Plenum Press, New York (1979).
2. We have based much of this discussion on a recent review of electron-molecule collisions by N.F. Lane, Rev. Mod. Phys. 52, 29 (1980).
3. E.S. Chang and U. Fano, Phys. Rev. A 6, 173 (1972).
4. K. Takatsuka and V. McKoy, Phys. Rev. A 23, 2352 (1981).
5. T.N. Rescigno, C.W. McCurdy and V. McKoy, Chem. Phys. Lett. 27, 401 (1974).
6. This connection has been discussed by several authors including: W.H. Miller, J. Chem. Phys. 50, 407 (1969); S.K. Adhikari and I.H. Sloan, Phys. Rev. C 11, 1133 (1975); V.B. Belyaev, A.P. Podkopoyev, J. Wrzeczionko, A.L. Zubarev, J. Phys. B 12, 1225 (1979).
7. D.K. Watson and V. McKoy, Phys. Rev. A 20, 1474 (1979).
8. D.K. Watson, R.R. Lucchese, V. McKoy and T.N. Rescigno, Phys. Rev. A 21, 738 (1980).
9. D.J. Ernst, C.M. Shakin and R.M. Thaler, Phys. Rev. C 8, 46 (1973).

SECTION A

Application of the Schwinger Variational Principle to  
Electron Scattering

## 1. Introduction

The Schwinger variational principle is clearly a powerful formulation of the scattering problem and has several distinct advantages over other variational methods (Taylor 1972). For example, in the Schwinger method the trial scattering wavefunction need not satisfy any specific asymptotic boundary conditions. This feature makes the method particularly attractive for molecular applications since discrete basis functions, which do not satisfy the scattering boundary conditions, can be used in the solution of molecular collision problems. The Schwinger method is also not troubled by the spurious singularities that can arise in the Kohn variational method.

The main drawback to the application of the Schwinger variational principle is the occurrence of the term  $\langle \Psi_{\underline{k}}^{(-)} | V G_0 V | \Psi_{\underline{k}'}^{(+)} \rangle$  in the expression. Recently Watson and McKoy (1979) proposed an approximate, but analytical, procedure for applying the Schwinger principle to electron-molecule collisions. This scheme depends on the use of Cartesian Gaussian basis functions in both the expansion of the scattering function and the insertion of a completeness relationship in the evaluation of the matrix elements of  $V G_0 V$ . We have now developed an efficient numerical procedure for the correct evaluation of the Schwinger variational expression (Lucchese and McKoy 1979).

In this paper we present static-exchange K matrices for e-He scattering, obtained from the Schwinger variational expression. To our knowledge, these results represent the first exact use of the Schwinger variational principle in electron scattering with inclusion

of the exchange potential. For the expansion functions we choose Cartesian Gaussian functions. The results are very encouraging and indicate that the Schwinger variational method provides accurate solutions of the scattering problem and does not require expansions in large basis sets.

## 2. Theory

The Schwinger variational principle for the K-matrix can be written as

$$\langle \underline{k} | K | \underline{k}' \rangle = -\frac{\pi}{2} \frac{\langle \underline{k} | U | \Psi_{\underline{k}'}^{(P)} \rangle \langle \Psi_{\underline{k}}^{(P)} | U | \underline{k}' \rangle}{\langle \Psi_{\underline{k}}^{(P)} | U - U G_0^{(P)} U | \Psi_{\underline{k}'}^{(P)} \rangle} \quad (1)$$

where  $\Psi_{\underline{k}}^{(P)}$  is the scattering wavefunction with the standing-wave boundary condition,  $G_0^{(P)}$  the corresponding free-particle Green's function, and  $U = 2V$  with  $V$  the scattering potential. This expression for the K-matrix is stationary with respect to small variations of the exact state vector  $\Psi_{\underline{k}}^{(P)}$  about its correct value. Expanding  $\Psi_{\underline{k}}^{(P)}$  in the set of basis functions  $|\alpha\rangle$

$$|\Psi_{\underline{k}}^{(P)}\rangle = \sum_{\alpha} a_{\alpha}(\underline{k}) |\alpha\rangle \quad (2)$$

and requiring that equation (1) be stationary with respect to variation of the coefficients,  $a_{\alpha}(\underline{k})$ , leads to the Schwinger variational expression for the K-matrix

$$\tilde{K} = -\frac{\pi}{2} \sum_{\alpha, \beta} U | \alpha \rangle [D^{-1}]_{\alpha\beta} \langle \beta | U \quad (3)$$

with

$$D_{\alpha\beta} = \langle \alpha | U - UG_0^{(P)} U | \beta \rangle \quad (4)$$

This expression can also be obtained by assuming a separable expansion of the potential of the form

$$\tilde{U}(\underline{r}, \underline{r}') = \sum \langle \underline{r} | U | \alpha \rangle [d^{-1}]_{\alpha\beta} \langle \beta | U | \underline{r}' \rangle \quad (5)$$

where

$$d_{\alpha\beta} = \langle \alpha | U | \beta \rangle \quad (6)$$

Inserting this separable approximation to  $U$  into the Lippmann-Schwinger equation for  $K$

$$K = -\frac{\pi}{2} U + UG_0^{(P)} K \quad (7)$$

yields equation (3) for  $\tilde{K}$ .

For the expansion functions we choose Cartesian Gaussian functions of the form

$$\langle \underline{r} | \alpha \rangle = N_{\ell mn} (x - A_x)^\ell (y - A_y)^m (z - A_z)^n e^{-\alpha |\underline{r} - \underline{A}|^2} \quad (8)$$

where  $N_{\ell mn}$  is a normalization constant. Also, in actual calculations we use the partial wave K-matrix elements which are given by

$$\tilde{K}_{\ell\ell'm} = -k \sum_{\alpha,\beta} \langle j_{\ell}(kr) Y_{\ell m}(\hat{r}) | U | \alpha \rangle [D^{-1}]_{\alpha\beta} \langle \beta | U | j_{\ell'}(kr) Y_{\ell'm}(\hat{r}) \rangle \quad (9)$$

for linear molecules. For electron-molecule scattering, the matrix elements  $\langle j_{\ell}(kr) Y_{\ell m}(\hat{r}) | U | \alpha \rangle$  and  $\langle \alpha | U G_0^{(P)} U | \beta \rangle$  are evaluated numerically. These numerical integration schemes are efficient and rapid. A more detailed explanation of these procedures is given elsewhere (Lucchese and McKoy 1979, Fliflet and McKoy 1978).

### 3. Results

We have used the Schwinger variational principle to obtain s- and p-wave K-matrices for e-He scattering in the static-exchange approximation. The SCF wavefunction was obtained with Huzinaga's 10s basis set for helium (Huzinaga 1965). With this basis the SCF energy is -2.86167 a. u. In table 1 we list the exponents of the Cartesian Gaussian functions in which the scattering function is expanded. The same sets of exponents are used in both the s- and p-wave calculations.

The s- and p-wave K-matrices of this Schwinger variational calculation are shown in tables 2 and 3 respectively. The K-matrix elements agree very well with those of the Kohn variational calculations

of Sinfailam and Nesbet (1972). Even the results with the 3s scattering basis are close to those of Sinfailam and Nesbet (1972), indicating that the Schwinger variational principle can provide accurate results with small discrete basis sets.

#### 4. Conclusions

We have presented the results of the first rigorous application of the Schwinger variational principle to electron scattering with the inclusion of exchange (Altshuler 1953). The results of this application to e-He scattering show that the Schwinger variational principle is a powerful method for the accurate solution of the scattering problem with small discrete basis sets. This feature makes the Schwinger method particularly attractive for applications to electron-molecule collisions. Applications of the Schwinger method to electron-molecule scattering, including its multichannel extensions, are under way .

#### Acknowledgments

This work was supported in part by the National Science Foundation under grant number CHE76-05157, and by the National Resource for Computation in Chemistry under a grant from the National Science Foundation and the Basic Energy Sciences Division of the United States Department of Energy under Contract No. W-7405-ENG-48. One of us (RRL) acknowledges the support of a National Science Foundation Fellowship.

References

Altshuler S 1953 Phys. Rev. 89 1278-1283. These results are with the static potential of the H-atom.

Fliflet A W and McKoy V 1978 Phys. Rev. A 18 2107-2114

Huzinaga S 1965 J. Chem. Phys. 42 1293-1302

Lucchese R R and McKoy V 1979 Phys. Rev. A to be published

Sinfailam A L and Nesbet R K 1972 Phys. Rev. A 6 2118-2125

Taylor J R 1972 Scattering Theory (New York: Wiley)

Watson D K and McKoy V 1979 Phys. Rev. A to be published

Table 1. Exponents of the Cartesian Gaussian functions used in the Schwinger variational calculations.

3s and 3p set	5s and 5p set
20.	20.
1.41	4.47
0.1	1.0
	0.224
	0.05

Table 2. s-wave K-matrix elements for e- He scattering.

Momentum k	$\tilde{K}$ (3s)	$\tilde{K}$ (5s)	Sinfailam and Nesbet <sup>a</sup> K (SN)
0.01	-0.0151	-0.0148	--
0.1	-0.152	-0.149	-0.149
0.2	-0.309	-0.303	-0.303
0.3	-0.476	-0.467	-0.468
0.4	-0.660	-0.647	-0.647
0.5	-0.870	-0.853	-0.858
1.0	-3.081	-3.031	-3.026
2.0	3.103	3.321	--

<sup>a</sup> Sinfailam and Nesbet (1972)

Table 3. p-wave K-matrix elements for e - He scattering

Momentum k	$\tilde{K}$ (3p)	$\tilde{K}$ (5p)	Sinfailam and Nesbet <sup>a</sup> K (SN)
0.01	0.407(-6) <sup>b</sup>	0.422(-6)	--
0.1	0.404(-3)	0.419(-3)	0.6(-3) <sup>c</sup>
0.2	0.316(-2)	0.326(-2)	0.35(-2)
0.3	0.0103	0.0106	0.0108
0.4	0.0231	0.0236	0.0239
0.5	0.0420	0.0425	0.0426
1.0	0.184	0.185	0.187
2.0	0.320	0.337	--

<sup>a</sup>Sinfailam and Nesbet (1972)

<sup>b</sup>0.407(-6) =  $0.407 \times 10^{-6}$

<sup>c</sup>private communication, R. K. Nesbet

SECTION B

Application of the Schwinger Variational Principle to  
Electron-Ion Scattering in the Static-Exchange Approximation

## I. INTRODUCTION

In recent years several methods which employ discrete basis sets have been successfully developed to study electron-molecule scattering and photoionization processes in molecules. These methods include the R-matrix method used by Schneider for  $e^-$ -H<sub>2</sub>, N<sub>2</sub> and F<sub>2</sub><sup>1-3</sup> scattering, the T-matrix method introduced by Rescigno, McCurdy and McKoy,<sup>4,5</sup> and applied to  $e^-$ -H<sub>2</sub>, N<sub>2</sub> and CO,<sup>6-9</sup> and the Stieltjes imaging technique developed by Langhoff<sup>10,11</sup> and applied to photoionization cross sections of molecules including N<sub>2</sub>, CO, H<sub>2</sub>O and H<sub>2</sub>CO.<sup>12-15</sup>

In the present work, we compute static-exchange electron-ion scattering phase shifts by direct evaluation of the Schwinger variational expression for the K matrix. The Schwinger principle has several distinct advantages over other variational method. In the Schwinger method the trial function is not required to satisfy any specific asymptotic boundary condition. The method is also not troubled by the spurious singularities that can arise in the Kohn variational method. In the form used here, a trial wave function is constructed from a linear combination of Cartesian Gaussian functions.

The Schwinger variational expression also yields an approximate wave function expressed as a linear combination of discrete basis functions. With little additional computational effort, an improved

numerical wavefunction can be generated using the Lippman-Schwinger equation in an iterative fashion as suggested by Blatt and Jackson.<sup>16</sup> Thus the present application of the Schwinger principle also yields numerical wavefunctions with asymptotic forms corresponding to the variationally determined K matrix.

This method is well suited to electron-molecular ion scattering. The expressions presented in this paper are general for symmetric linear molecules. As a specific test case we have studied  $e^-$ -He<sup>+</sup> scattering. In addition to calculating s and p wave phase shifts, the scattering solutions have been used to calculate photoionization cross sections of the 1<sup>1</sup>S, 2<sup>1</sup>S and 2<sup>3</sup>S states of helium.

## II. THEORY

### A Electron-Ion Scattering

The Schrödinger equation for potential scattering from a molecular ion of net charge Z is of the form (in atomic units)

$$\left( -\nabla^2 - \frac{2Z}{r} + U^S(\underline{r}) - k^2 \right) \psi_{\underline{k}}(\underline{r}) = 0. \quad (1)$$

The potential  $U^S(\underline{r})$  is an optical potential representing the short-range interactions between the target and the scattered electron.

Instead of solving the Schrödinger equation directly, the Lippmann-Schwinger equation for the wavefunction is used. For electron-ion scattering considered here, the Lippmann-Schwinger equation is

$$\psi_{\underline{k}}^{(\pm)} = \psi_{\underline{k}}^{c(\pm)} + C^{c(\pm)} U^S \psi_{\underline{k}}^{(\pm)}, \quad (2)$$

where the Coulomb Green's function is

$$G^{c(\pm)} = \left( \nabla^2 + \frac{2Z}{r} + k^2 \pm i\epsilon \right)^{-1} \quad (3)$$

and  $U^S(\underline{r}) = 2V^S(\underline{r})$ . The wavefunction  $\psi_{\underline{k}}^{c(\pm)}$ , is the pure Coulomb scattering wavefunction which has the partial wave expansion given by

$$\psi_{\underline{k}}^{c(\pm)}(\underline{r}) = \sqrt{\frac{2}{\pi}} \sum_{\ell m} i^\ell e^{\pm i\sigma_\ell} \frac{F_\ell(\gamma; kr)}{kr} Y_{\ell m}(\hat{r}) Y_{\ell m}^*(\hat{k}), \quad (4)$$

where  $F_\ell(\gamma; kr)$  is the regular Coulomb function and

$$\gamma = -Z/k \quad \text{and} \quad \sigma_\ell = \arg[\Gamma(\ell + 1 + i\gamma)].$$

The partial wave expansion of the Coulomb Green's function  $G^{c(\pm)}$ <sup>17</sup> is

$$\begin{aligned} G^{c(\pm)}(\underline{r}, \underline{r}') &= -\frac{1}{k} \sum_{\ell m} Y_{\ell m}(\hat{r}) Y_{\ell m}^*(\hat{r}') r^{-1} r'^{-1} \\ &\times F_\ell(\gamma; kr_{<}) [G_\ell(\gamma; kr_{>}) \pm iF_\ell(\gamma; kr_{>})]. \end{aligned} \quad (5)$$

The asymptotic form of the scattering solution is then

$$\psi_{\underline{k}}^{(\pm)}(\underline{r}) \sim \psi_{\underline{k}}^{c(\pm)}(\underline{r}) + f_{\underline{k}}^{(\pm)}(\hat{r}) \frac{1}{(2\pi)^{\frac{3}{2}}} \frac{\exp[\pm i(kr - \gamma \ln 2kr)]}{r} \quad (6)$$

where

$$f_{\underline{k}}^{(\pm)}(\hat{r}) = -2\pi^2 \langle \psi_{\pm k\hat{r}}^{c(\mp)} | U^S | \psi_{\underline{k}}^{(\pm)} \rangle. \quad (7)$$

We can define the T matrix due to the short-range component of the potential,  $U^S$ , by

$$T^S(\pm) = U^S + U^S G^{c(\pm)} T^S(\pm). \quad (8)$$

It then follows that

$$T^S(\pm) | \psi_{\underline{k}}^{c(\pm)} \rangle = U^S | \psi_{\underline{k}}^{(\pm)} \rangle, \quad (9)$$

and hence

$$f_{\underline{k}}^{(\pm)}(\hat{f}) = -2\pi^2 \langle \psi_{\pm k \hat{f}}^{c(\mp)} | T^S(\pm) | \psi_{\underline{k}}^{c(\pm)} \rangle. \quad (10)$$

In actual calculations the principal value function, defined by

$$\psi_{\underline{k}}^{(P)} = \psi_{\underline{k}}^{c(P)} + G^{c(P)} U^S \psi_{\underline{k}}^{(P)}, \quad (11)$$

is used. We define the partial wave expansion of the principal value Coulomb function,  $\psi_{\underline{k}}^{c(P)}$  by

$$\psi_{\underline{k}}^{c(P)} = \sqrt{\frac{2}{\pi}} \frac{1}{kr} \sum_{\ell m} i^\ell F_\ell(\gamma; kr) Y_{\ell m}(\hat{f}) Y_{\ell m}^*(\hat{k}). \quad (12)$$

This definition for the principal value wavefunction is chosen so that  $\psi_{\underline{k}}^{c(P)}$  is normalized to  $\delta(k-k')$ . The expansion of  $\psi_{\underline{k}}^{c(P)}$  in Eq. (12) is similar to that given for  $\psi_{\underline{k}}^{c(\pm)}$  in Eq. (4), except that the partial wave radial functions have been made real, i. e., the factor  $e^{\pm i\sigma_\ell}$  has been dropped.

Defining the  $K^S$  matrix by

$$K^S = -\frac{\pi}{2} U^S + U^S G^{c(P)} K^S \quad (13)$$

with the partial wave  $K^S$  matrix elements given by

$$K_{\ell' \ell m}^S = \frac{2k}{\pi} \left\langle \frac{F_{\ell'}(\gamma; kr)}{kr} Y_{\ell' m}(\hat{f}) \middle| K^S \middle| \frac{F_{\ell m}(\gamma; kr)}{kr} Y_{\ell m}(\hat{f}) \right\rangle \quad (14)$$

and the partial wave expansion of  $\psi_{\underline{k}}^{(P)}(\underline{r})$  defined as

$$\psi_{\underline{k}}^{(P)}(\underline{r}) = \sqrt{\frac{2}{\pi}} \frac{1}{kr} \sum_{\ell\ell'm} i^\ell \psi_{\ell\ell'm}^{(P)}(r) Y_{\ell'm}(\hat{r}) Y_{\ell m}^*(\hat{k}) \quad (15)$$

we have for the asymptotic form of the partial wave functions

$$\psi_{\ell\ell'm}^{(P)} \sim F_\ell(\gamma; kr) \delta_{\ell\ell'} + G_\ell(\gamma; kr) K_{\ell'\ell m}^S. \quad (16)$$

The T matrix is related to the K matrix by defining the partial wave expansion of the on-shell T matrix as

$$\langle \psi_{(\pm)\underline{k}'}^{c(\mp)} | T^{S(\pm)} | \psi_{\underline{k}}^{c(\pm)} \rangle = \frac{1}{k} \sum_{\ell\ell'm} i^{\ell-\ell'} Y_{\ell'm}(\pm\hat{k}') T_{\ell'\ell m}^{S(\pm)} Y_{\ell m}^*(\hat{k}). \quad (17)$$

Then  $T_{\ell'\ell m}^{S(\pm)}$  is given by

$$T_{\ell'\ell m}^{S(\pm)} = \frac{2k}{\pi} e^{\pm i(\sigma_{\ell'} + \sigma_\ell)} \left\langle \frac{F_{\ell'}(\gamma; kr)}{kr} Y_{\ell'm}(\hat{r}) \middle| T^{S(\pm)} \middle| \frac{F_\ell(\gamma; kr)}{kr} Y_{\ell m}(\hat{r}) \right\rangle. \quad (18)$$

Now the T matrix can be obtained from the K matrix using

$$T_{\ell'\ell m}^{S(\pm)} = -\frac{2}{\pi} e^{\pm i(\sigma_{\ell'} + \sigma_\ell)} \sum_{\ell''} [(1 \mp iK^S)^{-1}]_{\ell'\ell'' m} K_{\ell''\ell m}^S. \quad (19)$$

The relation between  $\psi_{\underline{k}}^{(P)}$  and  $\psi_{\underline{k}}^{(\pm)}$  is then given by

$$\psi_{\ell\ell'm}^{(\pm)}(r) = e^{\pm i\sigma_\ell} \sum_{\ell''} [(1 \mp iK^S)^{-1}]_{\ell\ell'' m} \psi_{\ell''\ell'm}^{(P)}(r). \quad (20)$$

The approach taken here to solve the Lippmann-Schwinger equation for the K-matrix is to assume a separable potential of the form

$$\tilde{U}^S = \sum_{\alpha, \beta} U^S |\alpha\rangle [d^{-1}]_{\alpha\beta} \langle\beta| U^S, \quad (21)$$

where  $d_{\alpha\beta} = \langle\alpha| U^S |\beta\rangle$ . We chose the expansion functions to be Cartesian Gaussian functions of the form

$$\phi^{\alpha}(\underline{r}) = \langle\underline{r}|\alpha\rangle = N_{\ell mn} (x - A_x)^{\ell} (y - A_y)^m (z - A_z)^n e^{-\alpha |\underline{r} - \underline{A}|^2} \quad (22)$$

where  $\underline{A}$  locates the basis function center and  $N_{\ell mn}$  is a normalization factor. Substitution of this expression into the Lippmann-Schwinger equation yields

$$\tilde{K}^S = -\frac{\pi}{2} \sum_{\alpha\beta} U^S |\alpha\rangle [f^{-1}]_{\alpha\beta} \langle\beta| U^S, \quad (23)$$

where  $f_{\alpha\beta} = \langle\alpha| U^S |\beta\rangle - \langle\alpha| U^S G^c(iP) U^S |\beta\rangle$ . Adhikari and Sloan<sup>18</sup> have shown that a separable potential of this form in the Lippmann-Schwinger equation yields an expression for the K matrix which is equivalent to the Schwinger variational expression with trial wavefunctions expanded in the same bases, e.g.,  $\psi_{\underline{k}}^{t(iP)} = \sum_{\alpha} a_{\alpha}(\underline{k}) |\alpha\rangle$ .

### B. Static-Exchange Potential for $e^{-}$ -Ion Scattering

The potential,  $U^S(\underline{r})$ , used in the present work is just the static-exchange potential. For a two-electron system the electronic wavefunction is of the form

$$\psi(1, 2) = u'(1) u^0(2) \pm u'(2) u^0(1), \quad (24)$$

where the upper (lower) sign gives the singlet (triplet) solution. The one-electron orbital  $u'$  is taken to be a continuum orbital, and  $u^0$  is fixed as the bound orbital of the isolated one-electron ion. The electronic Hamiltonian for this two-particle system, where the ion is an atomic, homonuclear diatomic, or symmetric linear triatomic system is

$$H(1,2) = h(1) + h(2) + \frac{1}{r_{12}}, \quad (25)$$

where  $H(i) = -\frac{1}{2}\nabla_i^2 - \frac{Z_C}{r_i} - Z_A \left( \frac{1}{|\underline{r}_i - \underline{A}|} + \frac{1}{|\underline{r}_i + \underline{A}|} \right)$  and where

$Z_C$  and  $Z_A$  are the nuclear charges at the origin and at  $\underline{A}$  and  $-\underline{A}$ , respectively.

With the orbital  $u^0$  fixed, the solution of the Schrödinger equation

$$H\psi = E\psi \quad (26)$$

reduces to the one-electron equation for  $u'$ ,<sup>19-21</sup>

$$(h \pm Q^{u^0} \mp \epsilon_0 P^{u^0} + J^{u^0} \pm K^{u^0}) u' = \epsilon_1 (1 \pm P^{u^0}) u', \quad (27)$$

where the various operators are defined by

$$\begin{aligned} Q^{u^0}(\underline{r}) u'(\underline{r}) &= u^0(\underline{r}) \int d^3 \underline{r}' u^{0*}(\underline{r}') h(\underline{r}') u'(\underline{r}') \\ &+ h(\underline{r}) u^0(\underline{r}) \int d^3 \underline{r}' u^{0*}(\underline{r}') u'(\underline{r}') \\ P^{u^0}(\underline{r}) u'(\underline{r}) &= u^0(\underline{r}) \int d^3 \underline{r}' u^{0*}(\underline{r}') u'(\underline{r}') \end{aligned} \quad (28)$$

$$J^{u^0}(\underline{r}) u'(\underline{r}) = u'(\underline{r}) \int d^3 \underline{r}' \frac{u^{0*}(\underline{r}') u^0(\underline{r}')}{|\underline{r}' - \underline{r}|}$$

$$K^{u^0}(\underline{r}) u'(\underline{r}) = u^0(\underline{r}) \int d^3 \underline{r}' \frac{u^{0*}(\underline{r}') u'(\underline{r}')}{|\underline{r}' - \underline{r}|}$$

and where

$$\epsilon_0 = \int d^3 \underline{r} u^{0*}(\underline{r}) h(\underline{r}) u^0(\underline{r}) \quad (29)$$

and  $\epsilon_1 = E - \epsilon_0$ .

When  $u^0$  is an eigenfunction of  $h$ , Eq. 27 reduces to

$$(h \pm \epsilon_0 P^{u^0} + J^{u^0} \pm K^{u^0}) u' = \epsilon_1 (1 + P^{u^0}) u' \quad (30)$$

In the triplet case Eq. (30) is equivalent to the simpler equation

$$(h + J^{u^0} - K^{u^0}) u' = \epsilon_1 u' \quad (31)$$

since the solutions to Eq. (30) are just an arbitrary linear combination of  $u^0$  and the solutions to Eq. (31).<sup>19,22</sup> Thus the solutions to Eq. (3) are constrained to be orthogonal to the occupied bound orbital,  $u^0$ , where the solutions of Eq. (30) have no such orthogonality constraint imposed on them.

The potential in the static-exchange approximation is then

$$U^S(\underline{r}) = 2 \left\{ N^A(\underline{r}) + J^{u^0} \pm (K^{u^0} + Q^{u^0}) \mp (\epsilon_0 + \frac{1}{2} k^2) P^{u^0} \right\} \quad (32)$$

where

$$N^A(\underline{r}) = - \frac{(Z_c - Z)}{r} - Z_A \left( \frac{1}{|\underline{r} - \underline{A}|} + \frac{1}{|\underline{r} + \underline{A}|} \right) \quad (33)$$

Note that this potential is momentum dependent, although all of the individual operators are independent of momentum. The corresponding potential in the case where  $u^0$  is an eigenfunction of  $h$  is

$$U^S(\underline{r}) = 2\{N^A(\underline{r}) + J^{u^0} \pm K^{u^0} \pm (\epsilon_0 - \frac{1}{2}k^2)P^{u^0}\}. \quad (34)$$

In the triplet case the potential for the solution which is constrained to be orthogonal to the bound orbital is given by

$$U^S(\underline{r}) = 2\{N^A(\underline{r}) + J^{u^0} - K^{u^0}\}. \quad (35)$$

### III. IMPLEMENTATION

#### A. Matrix Elements

There are three types of matrix elements needed to evaluate the partial wave K matrix elements by the Schwinger variational principle:

$$\begin{aligned} \tilde{K}_{\ell\ell'm}^S = & -k \sum_{\alpha, \beta} \left\langle \frac{F_{\ell'}(\gamma; kr)}{kr} Y_{\ell'm}(\hat{f}) \middle| U^S | \alpha \right\rangle [f^{-1}]_{\alpha\beta} \\ & \times \left\langle \beta \middle| U^S \left| \frac{F_{\ell}(\gamma; kr)}{kr} Y_{\ell m}(\hat{f}) \right. \right\rangle, \end{aligned} \quad (36)$$

where  $[f^{-1}]_{\alpha\beta}$  is obtained by inverting the matrix with elements

$$f_{\alpha\beta} = \langle \alpha | U^S | \beta \rangle - \langle \alpha | U^S G^{c(P)} U^S | \beta \rangle. \quad (37)$$

The elements of the type  $\langle \alpha | U^S | \beta \rangle$  are available from standard bound state molecular integral programs. The other two types of matrix ele-

ments  $\langle \alpha | U^S | \frac{F_\ell(\gamma; kr)}{kr} Y_{\ell m}(\hat{r}) \rangle$  and  $\langle \alpha | U^S G^{c(P)} U^S | \beta \rangle$  are evaluated directly by numerical integration.

The initial step in the numerical procedure is to compute  $U^\alpha(\underline{r}) = \langle \underline{r} | U^S | \alpha \rangle$ . This is done by first partial-wave expanding the Cartesian Gaussian functions with

$$\phi^\alpha(\underline{r}) = \sum_{\ell m} \frac{\phi_{\ell m}^\alpha(r)}{r} Y_{\ell m}(\hat{r}). \quad (38)$$

These expansions are analytically known.<sup>23</sup> Then we define the partial wave expansion of the potential by

$$U^\alpha(\underline{r}) = \sum_{\ell m} \frac{U_{\ell m}^\alpha(r)}{r} Y_{\ell m}(\hat{r}). \quad (39)$$

In turn each operator which contributes to  $U^S$  can be similarly expanded.

For the case where the occupied orbital,  $u^0$ , is of sigma ( $m = 0$ ) symmetry, it has the partial wave expansion

$$u^0(\underline{r}) = \sum_{\ell} \frac{u_\ell^0(r)}{r} Y_{\ell 0}(\hat{r}). \quad (40)$$

Then the expansions of the operators J, K, N are<sup>23</sup>

$$J_{\ell m}^{u^0, \alpha}(r) = \sum_{\ell'=0}^{\infty} \sqrt{\frac{2\ell+1}{2\ell'+1}} \sum_{\lambda=0}^{\infty} (\ell \lambda 0 0 | \ell' 0) (\ell \lambda m 0 | \ell' m) \phi_{\ell' m}^\alpha(r) V_\lambda(r) \quad (41)$$

where

$$\begin{aligned}
V_{\lambda}^{\circ}(\mathbf{r}) &= \sum_{s, s'=0}^{\infty} \frac{[(2s+1)(2s'+1)]^{\frac{1}{2}}}{2\lambda} (ss'00|\lambda 0)^2 \\
&\times \left\{ \frac{1}{r^{\lambda+1}} \int_0^r dr' u_s^{\circ*}(r') u_{s'}^{\circ}(r') r'^{\lambda} \right. \\
&\quad \left. + r^{\lambda} \int_r^{\infty} dr' u_s^{\circ*}(r') u_{s'}^{\circ}(r') r'^{-\lambda-1} \right\} \quad (42)
\end{aligned}$$

and

$$\begin{aligned}
K_{\ell m}^{u^{\circ}, \alpha}(\mathbf{r}) &= \sum_{\ell'=0}^{\infty} \sum_{s, s', \lambda=0}^{\infty} A^{\circ}(\ell, \ell', m; s, s', \lambda) \\
&\times u_{s'}^{\circ}(\mathbf{r}) \left[ \frac{1}{r^{\lambda+1}} \int_0^r dr' u_s^{\circ*}(r') \phi_{\ell' m}^{\alpha}(r') r'^{\lambda} \right. \\
&\quad \left. + r^{\lambda} \int_r^{\infty} dr' u_s^{\circ*}(r') \phi_{\ell' m}^{\alpha}(r') r'^{-\lambda-1} \right] \quad (43)
\end{aligned}$$

and

$$\begin{aligned}
A^{\circ}(\ell, \ell', m; s, s', \lambda) &= \left[ \frac{(2s+1)(2s'+1)}{(2\ell+1)(2\ell'+1)} \right]^{\frac{1}{2}} \\
&\times (s\lambda 00|\ell' 0)(s'\lambda 00|\ell 0)(s\lambda 0m|\ell' m)(s'\lambda 0m|\ell m) \quad (44)
\end{aligned}$$

and

$$\begin{aligned}
N_{\ell m}^{\widehat{A}, \alpha}(\mathbf{r}) &= \sum_{\ell'=0}^{\infty} \frac{\sqrt{2\ell+1}}{2\ell'+1} \sum_{\lambda=0}^{\infty} (\ell\lambda 00|\ell' 0)(\ell\lambda m 0|\ell' m) \\
&\times \left[ -2Z_A \left( \frac{r^{\lambda}}{r^{\lambda+1}} \right)_A - \delta_{\lambda, 0} \left( \frac{Z_c - Z}{r} \right) \right] \phi_{\ell' m}^{\alpha}(\mathbf{r}) \quad (45)
\end{aligned}$$

with

$$\left( \frac{r^\lambda}{r^{\lambda+1}} \right)_A = \begin{cases} \frac{A^\lambda}{r^{\lambda+1}} & A < r \\ \frac{r^\lambda}{A^{\lambda+1}} & A > r \end{cases} \quad (46)$$

and  $\underline{A} = A\hat{z}$ . The quantities  $(j_1 j_2 m_1 m_2 | j_3 m_3)$  are Clebsch-Gordan coefficients. The expansions for the operators Q and P are

$$P_{\ell 0}^{u^0, \alpha}(r) = \langle u^0 | \alpha \rangle u_{\ell m}^0(r) \quad (47)$$

and

$$\begin{aligned} Q_{\ell m}^{u^0, \alpha}(r) &= \langle u^0 | h | \alpha \rangle u_{\ell m}^0(r) \\ &+ \langle u^0 | \alpha \rangle \left\{ -\frac{1}{2} \frac{d^2}{dr^2} + \frac{\ell(\ell+1)}{2r^2} - 2Z_A \left( \frac{r^\lambda}{r^{\lambda+1}} \right)_A \right. \\ &\left. - \delta_{\ell, 0} \frac{Z_c}{r} \right\} u_{\ell m}^0(r). \end{aligned} \quad (48)$$

In general  $u^0(\underline{r})$  is also a linear combination of Cartesian Gaussian functions. Thus the integrals  $\langle u^0 | \alpha \rangle$  and  $\langle u^0 | h | \alpha \rangle$  as well as the expansions  $u_{\ell n}^0(r)$  are evaluated analytically. The expanded potential is then given by

$$\begin{aligned} U_{\ell m}^\alpha(r) &= 2 \left\{ N_{\ell m}^A, \alpha(r) + J_{\ell m}^{u^0, \alpha}(r) \pm [K_{\ell m}^{u^0, \alpha}(r) + Q_{\ell m}^{u^0, \alpha}(r)] \right. \\ &\left. \pm (\epsilon_0 + \frac{1}{2} k^2) P_{\ell m}^{u^0, \alpha}(r) \right\}. \end{aligned} \quad (49)$$

The hybrid integrals are evaluated using

$$\langle \alpha | U^S | \frac{F_\ell(\gamma; kr)}{kr} Y_{\ell m}(\hat{r}) \rangle = \frac{1}{k} \int_0^\infty dr F_\ell(\gamma; kr) U_{\ell m}^\alpha(r) . \quad (50)$$

Finally the matrix element  $\langle \alpha | U^S G^{c(P)} U^S | \beta \rangle$  in the denominator of Eq. (36) is given by

$$\begin{aligned} \langle \alpha | U^S G^{c(P)} U^S | \beta \rangle &= -\frac{1}{k} \sum_{\ell m} \int_0^\infty dr U_{\ell m}^\alpha(r) \\ &\times \left\{ G_\ell(\gamma; kr) \int_0^r dr' U_{\ell m}^\beta(r') F_\ell(\gamma; kr') \right. \\ &\left. + F_\ell(\gamma; kr) \int_r^\infty dr' U_{\ell m}^\beta(r') G_\ell(\gamma; kr') \right\} . \quad (51) \end{aligned}$$

### B. Electron-Ion Scattering Wavefunctions

Numerical wavefunctions are generated from the K matrix using the method of Fliflet and McKoy.<sup>8</sup> The identity

$$U^S | \psi_{\underline{k}}^{(P)} \rangle = -\frac{2}{\pi} K^S | \psi_{\underline{k}}^{c(P)} \rangle \quad (52)$$

combined with Eq. (1), yields

$$\begin{aligned} \left( -\frac{d^2}{dr^2} + \frac{\ell(\ell+1)}{r^2} - \frac{2Z}{r} - k^2 \right) \psi_{\ell \ell' m}^{(P)}(r) = \\ + \frac{2k}{\pi} \langle Y_{\ell' m}(\hat{r}) | K^S | \frac{F_{\ell m}(\gamma; kr)}{kr} Y_{\ell m}(\hat{r}) \rangle . \quad (53) \end{aligned}$$

In the present formulation the right hand side of Eq. (53) is approximated by

$$\begin{aligned} & \frac{2k}{\pi} \langle Y_{\ell'm}(\mathbf{f}) | \tilde{K}^S | \frac{F_{\ell m}(\gamma; kr)}{kr} Y_{\ell m}(\mathbf{f}) \rangle \\ & = -k \sum_{\alpha, \beta} U_{\ell'm}^{\alpha}(\mathbf{r}) [f^{-1}]_{\alpha\beta} \langle \beta | U^S | \frac{F_{\ell m}(\gamma; kr)}{kr} Y_{\ell m}(\mathbf{f}) \rangle . \end{aligned} \quad (54)$$

These uncoupled ordinary differential equations are easily solved using the Numerov method subject to the boundary conditions<sup>8</sup>

$$\text{i) } r \rightarrow 0 \quad \psi_{\ell\ell'm}^{(P)}(r) = 0 \quad (55a)$$

$$\text{ii) } r \rightarrow \infty \quad \psi_{\ell\ell'm}^{(P)}(r) = F_{\ell}(\gamma; kr) \delta_{\ell\ell'} + \tilde{K}_{\ell', \ell m}^S G_{\ell}(\gamma; kr) . \quad (55b)$$

This prescription for generating numerical wavefunctions is equivalent to the iterative use of the Lippmann-Schwinger equation suggested by Blatt and Jackson.<sup>16</sup> For a given trial wavefunction,  $\psi_{\underline{k}}^{t(P)}$ , they suggested that it could be improved by using

$$\psi_{\underline{k}}^{t'(P)} = \psi_{\underline{k}}^{c(P)} + G^{c(P)} U^S \psi_{\underline{k}}^{t(P)} . \quad (56)$$

Thus the solution of Eqs. (53) and (54) is identical to the solution of Eq. (56) with the trial function,  $\psi_{\underline{k}}^{t(P)}$ , being given by

$$\psi_{\underline{k}}^{t(P)} = \sum_{\alpha, \beta} \phi^{\alpha}(\underline{r}) [f^{-1}]_{\alpha\beta} \langle \beta | U^S | \psi_{\underline{k}}^{c(P)} \rangle , \quad (57)$$

which is the trial wavefunction implied by the Schwinger variational expression given in Eq. (36).<sup>18</sup>

### C. Photoionization Cross Sections

In the present work, the electron-ion scattering solutions are also used to calculate photoionization cross sections. Photoionization from three initial states of helium are considered. The states are the ground state,  $1^1S$ , and two metastable states  $2^1S$  and  $2^3S$ .

The initial states in these calculations are of the functional form

$$\psi_1(1,2) = \frac{1}{\sqrt{2(1+S)}} (\phi_{ns'}(1)\phi_{1s}(2) \pm \phi_{1s}(1)\phi_{ns'}(2)) \quad (58)$$

where  $S = \langle ns' | 1s \rangle$ . In the  $1^1S$  calculation,  $\phi_{ns'}$  and  $\phi_{1s}$  are the same and are equal to the Hartree-Fock orbital of the ground state of helium in the basis set used. For the two metastable states,  $\phi_{1s}$  is constrained to be the same as in the ground state. The  $\phi_{ns'}$  functions are then eigenfunctions of the one-electron equation given in Eq. (27).

The final states used in the photoionization calculation are constructed from the solution of the electron-ion scattering problem where the bound orbital is fixed as the  $\phi_{1s}$  of the ground state. Hence the final orbital is the frozen core of the target. We measure all energies relative to the experimental ionization potentials and in this way compensate for some errors in the frozen core model. Thus the final states are of the form

$$\psi_{f,\underline{k}}(1,2) = \sqrt{\frac{k}{2}} [\phi_{1s}(1)\psi_{\underline{k}}^{(-)}(2) \pm \psi_{\underline{k}}^{(+)}(1)\phi_{1s}(2)] . \quad (59)$$

The differential dipole oscillator strength is then computed in either the length or velocity form as

$$\left(\frac{df}{dE}\right)_L = \sum_{\mu} \frac{2}{3} \Delta E \int d\Omega_{\hat{k}} |\langle \psi_i | r_{\mu} | \psi_{f,\hat{k}} \rangle|^2 \quad (60)$$

or

$$\left(\frac{df}{dE}\right)_V = \sum_{\mu} \frac{2}{3} \frac{1}{\Delta E} \int d\Omega_{\hat{k}} |\langle \psi_i | \nabla_{\mu} | \psi_{f,\hat{k}} \rangle|^2 \quad (61)$$

where  $\Delta E = \frac{1}{2}k^2 + I.P.$  and

$$r_{\mu} = \begin{cases} \mp (x \pm iy) / \sqrt{2} & \text{for } \mu = \pm 1 \\ z & \text{for } \mu = 0 \end{cases} \quad (62)$$

and

$$\nabla_{\mu} = \begin{cases} \mp \left( \frac{\partial}{\partial x} \pm i \frac{\partial}{\partial y} \right) / \sqrt{2} & \text{for } \mu = \pm 1 \\ \frac{\partial}{\partial z} & \text{for } \mu = 0. \end{cases} \quad (63)$$

If  $p_{\mu}$  stands for either  $r_{\mu}$  or  $\nabla_{\mu}$ , then since all bound orbitals are of gerade symmetry,

$$\langle \psi_i | p_{\mu} | \psi_{f,\hat{k}} \rangle = \sqrt{\frac{k}{(1 \pm S)}} \left[ S \langle \phi_{1S} | p_{\mu} | \psi_{\hat{k}}^{(-)} \rangle \pm \langle \phi_{NS'} | p_{\mu} | \psi_{\hat{k}}^{(-)} \rangle \right]. \quad (64)$$

The bound orbital  $\phi$  (either  $\phi_{1S}$  or  $\phi_{NS'}$ ) has the partial wave expansion

$$\phi(\underline{r}) = \sum_{\ell m} \frac{\phi_{\ell m}(\underline{r})}{r} Y_{\ell m}(\hat{r}), \quad (65)$$

then

$$\begin{aligned}
\langle \phi | p_\mu | \psi_{\underline{k}}^{(-)} \rangle &= \sqrt{\frac{2}{\pi}} \frac{1}{k} \sum_{\ell m} i^\ell Y_{\ell m}^*(\hat{k}) e^{-i\sigma_\ell} \sum_{\ell' m'} [(1 + iK)^{-1}]_{\ell \ell' m} \\
&\times \sum_{\ell'' \ell''' m''} \left\langle \frac{\phi_{\ell'' m''}}{r}(\mathbf{r}) Y_{\ell'' m''}(\hat{r}) \middle| p_\mu \middle| \frac{\psi_{\ell' \ell''' m}^{(P)}}{r}(\mathbf{r}) Y_{\ell' m}(\hat{r}) \right\rangle \quad (66)
\end{aligned}$$

The integral on the right-hand side of Eq. (66) in the length form is

$$\begin{aligned}
&\left\langle \frac{\phi_{\ell'' m''}}{r}(\mathbf{r}) Y_{\ell'' m''}(\hat{r}) \middle| r_\mu \middle| \frac{\psi_{\ell' \ell''' m}^{(P)}}{r}(\mathbf{r}) Y_{\ell' m}(\hat{r}) \right\rangle \\
&= C(\ell'', \ell''', m'', m, \mu) \times \int_0^\infty dr \phi_{\ell'' m''}^*(r) r \psi_{\ell' \ell''' m}^{(P)}(r) \quad , \quad (67)
\end{aligned}$$

where

$$\begin{aligned}
C(\ell'', \ell''', m'', m, \mu) &= \left( \frac{2\ell''' + 1}{2\ell'' + 1} \right)^{\frac{1}{2}} \times (1 \ell''' 0 0 | \ell'' 0) \\
&\times (1 \ell''' \mu m | \ell'' m''). \quad (68)
\end{aligned}$$

In the velocity form the integral in Eq. (66) is given by<sup>24</sup>

$$\begin{aligned}
&\left\langle \frac{\phi_{\ell'' m''}(r)}{r} Y_{\ell'' m''}(\hat{r}) \middle| \nabla_\mu \middle| \frac{\psi_{\ell' \ell''' m}^{(P)}(r)}{r} Y_{\ell' m}(\hat{r}) \right\rangle \\
&= C(\ell'', \ell''', m'', m, \mu) \times \int_0^\infty dr \phi_{\ell'' m''}^*(r) \left[ \frac{d}{dr} + \frac{\ell'''(\ell''' + 1) - \ell''(\ell'' + 1)}{2r} \right] \\
&\times \psi_{\ell' \ell''' m}^{(P)}(r). \quad (69)
\end{aligned}$$

## IV. RESULTS

### A. $e^-$ - $He^+$ Phase Shifts

The first application of the method presented here is to  $e^-$ - $He^+$  scattering. The  $He^+$  target is orbital is constructed from the Huzinaga hydrogen 10s basis set<sup>25</sup> with the exponents scaled up by a factor of 2. This basis set gives an energy of -1.999985 a. u. for  $He^+$ .

We perform the scattering calculation using three different methods. Besides the exact Schwinger method, we also computed an approximate form of the Schwinger expression as proposed by Watson and McKoy,<sup>26</sup> where the denominator  $f_{\alpha\beta}$  is approximated

$$f_{\alpha\beta}^I = \langle \alpha | U^S | \beta \rangle - \sum_{\gamma, \delta} \langle \alpha | U^S | \gamma \rangle \langle \gamma | G^{c(P)} | \delta \rangle \langle \delta | U^S | \beta \rangle . \quad (70)$$

A test of the accuracy of the approximation in Eq. (70) is important since this procedure is particularly attractive for molecular applications. The Schwinger K matrix with this approximation is then given by

$$\tilde{K}^{I(s)} = -\frac{\pi}{2} \sum_{\alpha\beta} U^S | \alpha \rangle [(f^I)^{-1}]_{\alpha\beta} \langle \beta | U^S . \quad (71)$$

In these calculations the basis set inserted in  $U^S G^{c(P)} U^S$  is the same set as is used in the rest of the scattering calculation. The third method is the uncorrected T-matrix method originally proposed by Rescigno, McCurdy and McKoy.<sup>4,5</sup> In this method the K matrix is calculated using

$$K^{T(s)} = -\frac{\pi}{2} \sum_{\alpha\beta\gamma\delta} | \alpha \rangle \langle \alpha | U^S | \beta \rangle [(f^I)^{-1}]_{\beta\gamma} \langle \gamma | U^S | \delta \rangle \langle \delta | . \quad (72)$$

The basis sets used in the exact Schwinger method and the approximate Schwinger method with insertion are given in Table I. The basis sets used in the T matrix calculations with Eq. (72) are given in Table II.

Results for  $^3S$  scattering, where the scattering solution is constrained to be orthogonal to the bound orbital, are presented in Table III. It is well known<sup>18,19</sup> that for triplet scattering this yields the same phase shift as the solution in which orthogonality is not imposed. The 5s Schwinger results are in excellent agreement with the numerical results of Sloan.<sup>27,28</sup> The 3s Schwinger phase shifts are within 3% of the correct values. The 3s phase shifts also smoothly approach the accurate phase shifts at higher momentum. The approximate Schwinger calculations with insertion in the denominator give very good results at low momentum but at higher momentum show discrepancies of up to 7%. Naturally the results of the Schwinger method in which the  $U^S G^{c(P)} U^S$  term is evaluated approximately, *i. e.*, with insertion, can be improved by using a larger basis set around  $G^{c(P)}$ . Uncorrected results using the T matrix equation [Eq. (72)] are presented for two basis sets. The 5s set which was also used in the two Schwinger calculations yields generally poor uncorrected T matrix results except for energies around  $k = 0.6$ , as can be seen in Figure 1. The 10s basis set gives much better T matrix phase shifts, which differ from the exact values by less than 2%.

The results for the  $^3S e^- He^+$  scattering calculations in which the scattering function is not constrained to be orthogonal to the bound

orbital, are given in Table IV. It can be seen that the 5s Schwinger phase shifts are again in good agreement with the numerical values, and they are almost identical to the phase shifts obtained from the constrained  $^3S$  scattering solution. However, the uncorrected T matrix 10s results are dramatically worse than in the constrained calculation. A larger 20s basis set does yield T matrix phase shifts which are again in close agreement with the accurate results.

The results for  $^1S$  scattering are presented in Table V. In this case, the Schwinger 5s and 10s T matrix calculations both agree well with Sloan's results.<sup>27,28</sup>

Phase shifts for  $^1P$  scattering are given in Table VI. In this symmetry the exact Schwinger and the approximate Schwinger (with insertion) expressions both give results in close agreement with the static-exchange phase shifts given by McGreevy and Stewart.<sup>29</sup>

Results for  $^3P$  scattering are given in Table VII. Again the Schwinger 5p and uncorrected 10p T matrix phase shifts are in close agreement.

### B. Photoionization Cross Sections

The initial state used in the ground-state photoionization calculation of helium is constructed from the 10s Gaussian set of Huzinaga<sup>25</sup> (also listed in Table VIII), which has a Hartree-Fock energy  $E = -2.861669$  a. u. For the two metastable states the 10s basis set is augmented by seven diffuse basis functions given in Table VIII. The orbital eigenvalues of the  $\phi_{2S'}$  orbitals, with the  $\phi_{1S}$  orbital taken as the Hartree-Fock orbital, are  $-0.141509$  a. u. for the  $2^1S$  state and  $-0.189942$  a. u. for the  $2^3S$  state. The more diffuse functions included

in this extended basis set are important in describing the Rydberg-like metastable states.

Results of photoionization cross section calculations for the  $1^1S$  state are presented in Table IX. Cross sections computed using all three methods employed in the scattering calculations are given. The IP was taken to be 0.9035 a. u. (24.59 eV) for the ground state.<sup>30</sup> The exact Schwinger results and approximate Schwinger results, with insertion in the denominator, are virtually identical. These results show that the total cross section is fairly insensitive to the variations in the accuracy of the continuum wavefunction generated by these various methods. This point is exemplified by the exact Schwinger  $1p$  cross sections presented in Table X. The difference between the  $1p$  and  $5p$  Schwinger cross sections is less than 1%. This result is put into perspective by comparing it to the cross section obtained by using a pure Coulomb wave as the continuum functions in the final state. The  $1p$  results can be seen to be an improvement over the pure Coulomb result which contains no short-range scattering information.

In Figure 2 the cross sections obtained from an exact Schwinger variational calculation with the  $5p$  basis given in Table I, are compared with experimental data given by Samson.<sup>30</sup> The difference between the two forms of the dipole cross section, the length and velocity forms, can be used as an estimate of correlation effects.<sup>31</sup> In the photoionization of the ground state of helium, the static-exchange velocity form yields cross sections closer to the experimental results than does the length form.

The photoionization cross sections of the two metastable states of He, the  $2^1S$  and  $2^3S$  states, are shown in Figures 3 and 4, respectively. The IP's of these states are taken to be 0.14595 a.u. (3.97 eV) for the  $2^1S$  state and 0.17524 a.u. (4.77 eV) for the  $2^3S$  state.<sup>32</sup> The static-exchange cross sections are compared to the calculated values of Norcross.<sup>33</sup> The calculations by Norcross used close-coupling final-state wavefunctions with three states included in the expansion. The initial states used by Norcross<sup>33</sup> were slightly different from ours, in that he used a  $\text{He}^+$  1s hydrogenic function for the frozen  $\phi_{1S}$  orbital. The dipole length cross section gives better agreement with Norcross results than does the velocity form. In general neither the dipole length nor dipole velocity forms seem to give more reliable static-exchange results.

## V. CONCLUSIONS

We have presented a method for calculating static-exchange electron-molecular ion scattering wavefunctions. The method should be directly applicable to molecular systems. In  $e^- - \text{He}^+$  scattering, the numerical evaluation of the exact Schwinger variational expression gives extremely accurate phase shifts with small basis sets. In molecular systems, the numerical integration of the matrix elements,  $\langle \alpha | U^S G^{c(P)} U^S | \beta \rangle$  may become extremely length. In this case, the approximate Schwinger expression with a large basis set inserted around  $G^{c(P)}$  may be a more economical procedure. As presented here, the approximate Schwinger method yields a single center

expansion of the scattering amplitude. This allows analytic averaging over target orientation. Both the exact Schwinger method and the approximate Schwinger method, with insertion in the denominator, can be used to compute accurate numerical scattering wavefunctions. These wavefunctions correspond to K-matrices which are variationally stable.

Accurate static-exchange wavefunctions can be utilized in various distorted-wave approximations. In the example presented in this paper, these wavefunctions can be used in the calculation of the photoionization cross section of helium, even when the scattering basis set is of very modest size. Another use for electron-ion scattering wavefunctions is in the study of electron impact ionization.

The application of the Schwinger variational principle to molecular systems is in progress.

## ACKNOWLEDGMENTS

This research was supported by grant No. CHE76-05157 from the National Science Foundation and by an Institutional Grant from the U.S. Department of Energy, No. EY-76-G-03-1305. We also acknowledge support by the National Resource for Computation in Chemistry under a grant from the National Science Foundation and the U.S. Department of Energy (Contract No. W-7405-ENG-48). One of us (RRL) acknowledges the support of a National Science Foundation Fellowship. We also thank Drs. A. W. Fliflet and D. K. Watson for many helpful and stimulating discussions.

References

- <sup>1</sup>B. I. Schneider, Phys. Rev. A 11, 1957 (1975).
- <sup>2</sup>B. I. Schneider and P. J. Hay, Phys. Rev. A 13, 2049 (1976).
- <sup>3</sup>M. A. Morrison and B. I. Schneider, Phys. Rev. A 16 1003 (1977).
- <sup>4</sup>T. N. Rescigno, C. W. McCurdy, and V. McKoy, Chem. Phys. Lett. 27, 401 (1974).
- <sup>5</sup>T. N. Rescigno, C. W. McCurdy, and V. McKoy, Phys. Rev. A 10, 2240 (1974).
- <sup>6</sup>T. N. Rescigno, C. W. McCurdy, and V. McKoy, Phys. Rev. A 11, 825 (1975).
- <sup>7</sup>A. W. Fliflet, D. A. Levin, M. Ma, and V. McKoy, Phys. Rev. A 17, 160 (1978).
- <sup>8</sup>A. W. Fliflet and V. McKoy, Phys. Rev. A 18, 2107 (1978).
- <sup>9</sup>D. A. Levin, A. W. Fliflet and V. McKoy, "Low-Energy e-CO Cross Sections in the Static Exchange Approximation," Phys. Rev. A, submitted for publication.
- <sup>10</sup>P. W. Langhoff, C. T. Corcoran, J. S. Sims, F. Weinhold and R. M. Glover, Phys. Rev. A 14, 1042 (1976).
- <sup>11</sup>C. T. Corcoran and P. W. Langhoff, J. Math. Phys. 18, 651 (1977).
- <sup>12</sup>T. N. Rescigno, C. F. Bender, B. V. McKoy and P. W. Langhoff, J. Chem. Phys. 68, 970 (1978).
- <sup>13</sup>N. Padial, G. Csanak, B. V. McKoy and P. W. Langhoff, J. Chem. Phys. 69, 2992 (1978).
- <sup>14</sup>G. R. J. Williams and P. W. Langhoff, Chem. Phys. Lett. 60, 201 (1979).

References (continued)

- <sup>15</sup>P. W. Langhoff, A. F. Orel, T. N. Rescigno and B. V. McKoy, *J. Chem. Phys.* 69, 4689 (1978).
- <sup>16</sup>J. M. Blatt and J. D. Jackson, *Phys. Rev.* 76, 18 (1949).
- <sup>17</sup>R. G. Newton, Scattering Theory of Waves and Particles, McGraw-Hill, New York (1966), p. 431.
- <sup>18</sup>S. K. Adhikari and I. H. Sloan, *Phys. Rev. C* 11, 1133 (1975). See also W. H. Miller, *J. Chem. Phys.* 50, 407 (1969).
- <sup>19</sup>M. E. Riley and D. G. Truhlar, *J. Chem. Phys.* 65, 792 (1976).
- <sup>20</sup>M. Cohen and R. P. McEachran, *Proc. Phys. Soc.* 92, 37 (1967).
- <sup>21</sup>M. J. Seaton, *Comments At. Molec. Phys.* 1, 184 (1970).
- <sup>22</sup>T. N. Rescigno, *J. Chem. Phys.* 66, 5255 (1977).
- <sup>23</sup>A. W. Fliflet and V. McKoy, *Phys. Rev. A* 18, 1048 (1978).
- <sup>24</sup>M. Rotenberg, R. Biyins, N. Metropolis and J. K. Wootin, The 3-j and 6j Symbols, MIT Press, Cambridge, (1959), p. 6.
- <sup>25</sup>S. Huzinaga, *J. Chem. Phys.* 42, 1293 (1965).
- <sup>26</sup>D. K. Watson and V. McKoy, "Discrete Basis Function Approach to Electron-Molecule Scattering," *Phys. Rev. A* (accepted for publication).
- <sup>27</sup>I. H. Sloan, *Proc. Roy. Soc. A* 281, 151 (1964).
- <sup>28</sup>N. F. Mott and H. S. Massey, The Theory of Atomic Collisions, Oxford, London, (1965), p. 559.
- <sup>29</sup>E. McGreevy and A. L. Stewart, *J. Phys. B* 10, L527 (1977).
- <sup>30</sup>J. A. R. Samson, *Adv. Molec. Phys.* 2, 177 (1966).
- <sup>31</sup>H. P. Kelly, *Chem. Phys. Lett.* 20, 547 (1973).

References (continued)

<sup>32</sup>M. Cohen and R. P. McEachran, Proc. Phys. Soc. 92, 37, 539 (1967).

<sup>33</sup>D. W. Norcross, J. Phys. B 4, 652 (1971).

TABLE I. Exponents for Cartesian Gaussian functions used in Schwinger variational calculations.

5s and 5p sets	3s set	1p set
100.0	100.0	0.500
21.1	4.47	
4.47	0.200	
0.946		
0.200		

TABLE II. Exponents for Cartesian Gaussian functions used in uncorrected T matrix calculations [Eq. (72)].

10s	10p	20s	
400.0	200.0	537.0	3.86
172.0	92.8	328.0	2.36
73.9	43.1	200.0	1.44
31.7	20.0	122.0	0.879
13.6	9.28	74.6	0.537
5.86	4.31	45.5	0.328
2.52	2.00	27.8	0.200
1.08	0.928	17.0	0.122
0.465	0.431	10.4	0.0746
0.200	0.200	6.32	0.0455

TABLE III. Phase shifts for triplet s wave scattering of helium ion.<sup>a</sup>

Momentum k	Schwinger <sup>b</sup> $\tilde{\delta}(5s)$	Schwinger <sup>c</sup> $\tilde{\delta}(3s)$	Approximate <sup>d</sup>		T matrix <sup>f</sup> $\delta^T(10s)$	Numerical <sup>g</sup> $\delta^N$
			Schwinger $\tilde{\delta}^I(5s)$	T matrix <sup>e</sup> $\delta^T(5s)$		
0.1	0.919	0.889	0.920	0.933	0.921	(k=0, $\delta^N=0.920$ )
0.3	0.910	0.880	0.913	0.918	0.910	↓
0.491	0.893	0.865	0.903	0.894	0.893	0.893
0.779	0.855	0.828	0.883	0.855	0.861	0.855
1.076	0.802	0.780	0.851	0.827	0.816	0.802
1.353	0.747	0.731	0.803	0.812	0.758	0.748
1.897	0.642	0.637	0.673	0.759	0.646	0.645
2.198	0.591	0.590	0.603	0.703	0.611	0.604

(footnotes, see next page)

Footnotes Table III.

- a) Phase shifts are for scattering solutions which are constrained to be orthogonal to the bound orbital, using the potential given by Eq. (35).
- b) Exact Schwinger variational phase shifts [Eq. (23)], for 5s basis set given in Table I.
- c) Exact Schwinger variational phase shifts for 3s basis set given in Table I.
- d) Approximate Schwinger variational phase shifts, with insertion in the denominator [Eq. (71)], for 5s basis set given in Table I.
- e) Uncorrected T matrix phase shifts [Eq. (72)] for 5s basis set given in Table I.
- f) Uncorrected T matrix phase shifts for 10s basis set given in Table II.
- g) Phase shifts of numerical solution of Schrödinger equation from Ref. 28.

TABLE IV. Phase shifts for triplet s wave scattering of helium ion<sup>a</sup>

Momentum k	Schwinger $\tilde{\delta}$ (5s)	T matrix $\delta^T$ (10s)	T matrix $\delta^T$ (20s)	Numerical <sup>b</sup> $\delta^N$
0.1	0.918	0.930	0.920	(k=0, $\delta^N=0.920$ )
0.3	0.909	0.911	0.916	-
0.491	0.893	0.964	0.907	0.893
0.779	0.855	1.334	0.854	0.855
1.076	0.802	1.332	0.809	0.802
1.353	0.747	0.998	0.750	0.748
1.897	0.641	0.750	0.645	0.645
2.198	0.590	0.910	0.605	0.604

<sup>a</sup>Phase shifts are for scattering solutions which are not constrained to be orthogonal to the bound orbital, using the potential given by Eq. (32).

<sup>b</sup>Numerical phase shifts from Ref. 28.

TABLE V. Phase shifts for singlet  $s$  wave scattering of helium ion.

Momentum $k$	Schwinger $\tilde{\delta}$ (5s)	T matrix $\delta^T$ (10s)	Numerical <sup>a</sup> $\delta^N$
0.1	0.386	0.400	( $k = 0$ , $\delta^N = 0.387$ )
0.3	0.378	0.388	-
0.491	0.366	0.361	0.366
0.779	0.341	0.341	0.341
1.076	0.317	0.325	0.318
1.353	0.302	0.314	0.302
1.897	0.290	0.289	0.290
2.198	0.290	0.289	0.283

<sup>a</sup>Numerical phase shifts from Ref. 28.

TABLE VI. Phase shifts for singlet p wave scattering of helium ion.

Momentum $k$	Schwinger $\tilde{\delta}(5p)$	Approximate		Numerical <sup>a</sup>	
		Schwinger $\tilde{\delta}(5p)$	T matrix $\delta^T(5p)$	T matrix $\delta^T(10p)$	Numerical <sup>a</sup> $\delta^N$
0.2	-0.0742	-0.0739	-0.0711	-0.0740	-0.0745
0.4	-0.0765	-0.0761	-0.0755	-0.0759	-0.0765
0.6	-0.0788	-0.0783	-0.0782	-0.0742	-0.0788
0.8	-0.0797	-0.0792	-0.0761	-0.0701	-0.0796
1.0	-0.0780	-0.0777	-0.0700	-0.0685	-0.0778
1.2	-0.0733	-0.0732	-0.0633	-0.0690	-0.0727
1.4	-0.0656	-0.0658	-0.0579	-0.0646	-0.0646
1.6	-0.0551	-0.0555	-0.0524	-0.0508	-0.0540

<sup>a</sup>Numerical phase shifts from Ref. 29.

TABLE VII. Phase shifts for triplet p wave scattering of helium ion.

Momentum k	Schwinger $\tilde{\delta}$ (5p)	T matrix $\delta^T$ (10p)
0.2	0.179	0.179
0.4	0.186	0.189
0.6	0.196	0.204
0.8	0.205	0.217
1.0	0.212	0.220
1.2	0.216	0.218
1.4	0.217	0.219
1.6	0.216	0.223

TABLE VIII. Exponents for Cartesian Gaussian functions used in initial state wavefunctions.

Huzinaga 10s basis set <sup>a</sup>	Additional diffuse functions for metastable states <sup>b</sup>
3293.694	0.0600
488.8941	0.0333
108.7723	0.0185
30.1799	0.0103
9.789053	0.00571
3.522261	0.00317
1.352436	0.00176
0.552610	
0.240920	
0.107951	

<sup>a</sup>This is the basis set, from Ref. 25, used in the  $1^1S$  ( $1s^2$ ) ground state of helium.

<sup>b</sup>The wavefunctions of the  $2^1S$  and  $2^3S$  ( $1s\ 2s$ ) metastable state of helium are constructed from the combined 17s basis set.

TABLE IX. Photoionization cross sections of the ground state of helium, using the length form of the dipole operator in megabarns ( $10^{-18} \text{ cm}^2$ ).

$\Delta E(\text{eV})$	Schwinger <sup>a</sup> $\tilde{\sigma} (5p)$	Approximate Schwinger <sup>b</sup> $\tilde{\sigma}^I (5p)$	T matrix <sup>c</sup> $\sigma^T (5p)$	T matrix $\sigma^T (10p)$
24.75	7.59	7.59	7.61	7.54
26.6	6.98	6.98	7.07	7.01
30.6	5.76	5.76	5.91	5.83
34.6	4.74	4.75	4.85	4.76
38.6	3.93	3.93	3.95	3.89
42.6	3.26	3.26	3.23	3.22
46.6	2.73	2.73	2.66	2.71

<sup>a</sup>The exact Schwinger photoionization cross section is computed using Eqs. (60), (64), (66), and (67), with the partial wave scattering solution,  $\psi_{\ell\ell'm}^{(P)}(\mathbf{r})$ , obtained from Eqs. (53) and (54) as described in the text. The 5p basis set given in Table I is used.

<sup>b</sup>The approximate Schwinger cross sections are obtained as in (a) except that  $K^S$  in Eq. (53) is approximated by  $\tilde{K}^{I(s)}$  given in Eq. (71).

<sup>c</sup>The uncorrected T-matrix cross sections are obtained as in (a) except that  $K^S$  in Eq. (53) is approximated by  $K^{T(s)}$  given in Eq. (72).

<sup>d</sup>Same calculation as in (c) except the 10p set given in Table II is used.

TABLE X. Photoionization cross sections of the ground state of helium using the length form of the dipole operator, in megabarns. Comparison of 5p and 1p exact Schwinger cross sections with Coulomb wave results.

$\Delta E(\text{eV})$	Schwinger $\tilde{\sigma}$ (5p)	Schwinger $\tilde{\sigma}$ (1p)	Coulomb wave <sup>a</sup> $\sigma^c$
24.75	7.59	7.60	7.73
26.6	6.98	7.00	6.91
30.6	5.76	5.79	5.44
34.6	4.74	4.77	4.34
38.6	3.93	3.94	3.53
42.6	3.26	3.27	2.90
46.6	2.73	2.72	2.41

<sup>a</sup>The Coulomb wave cross section is obtained by using  $\psi_{\ell\ell'm}^{(P)}(\mathbf{r}) = \delta_{\ell\ell'} F_{\ell}(\gamma;kr)$  in Eqs.(60), (64), (66) and (67).

### Figure Captions

Figure 1. Comparison of  $^3S$  phase shifts of helium ion, where the scattering solution is constrained to be orthogonal to the bound orbital: ———, exact Schwinger variational phase shifts with 5s basis set given in Table I; - - - - -, exact Schwinger variational phase shifts with 3s basis set given in Table I; ——— - ———, uncorrected T matrix phase shifts with 5s basis set given in Table I;  $\circ$ , numerical phase shifts given by Sloan.<sup>28</sup>

Figure 2. Photoionization cross sections of  $1^1S$  He, in megabarns (Mb): L, static exchange dipole length; V, static exchange dipole velocity;  $\circ$ , selected experimental cross sections from Samson.<sup>30</sup>

Figure 3. Photoionization cross sections of  $2^1S$  He, in Mb: L, static exchange dipole length; V, static exchange dipole velocity;  $\circ$ , numerical results of Norcross.<sup>33</sup>

Figure 4. Photoionization cross sections of  $2^3S$  He, in Mb: L, static exchange dipole length; V, static exchange dipole velocity;  $\circ$ , numerical results of Norcross.<sup>33</sup>

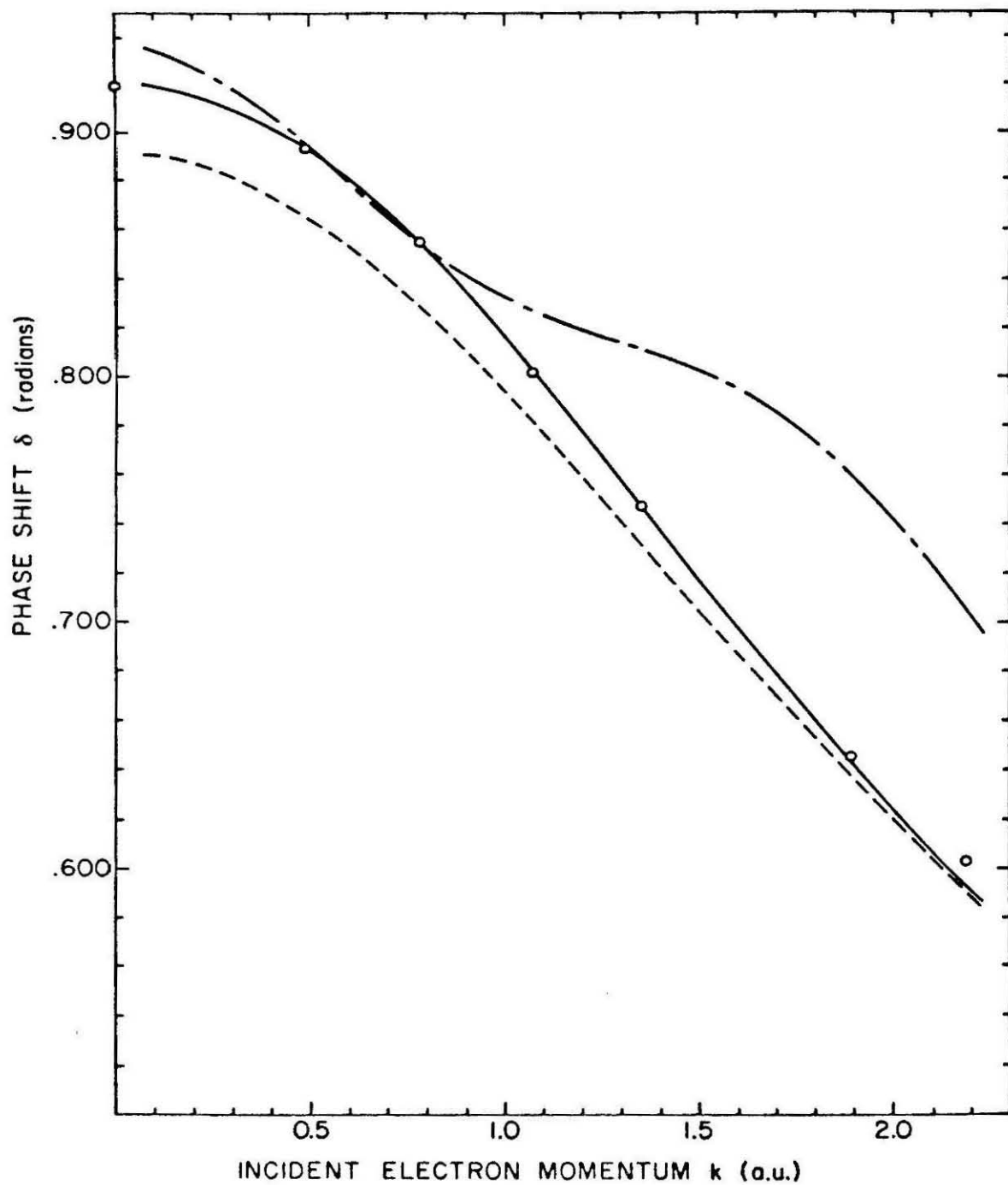


Figure 1

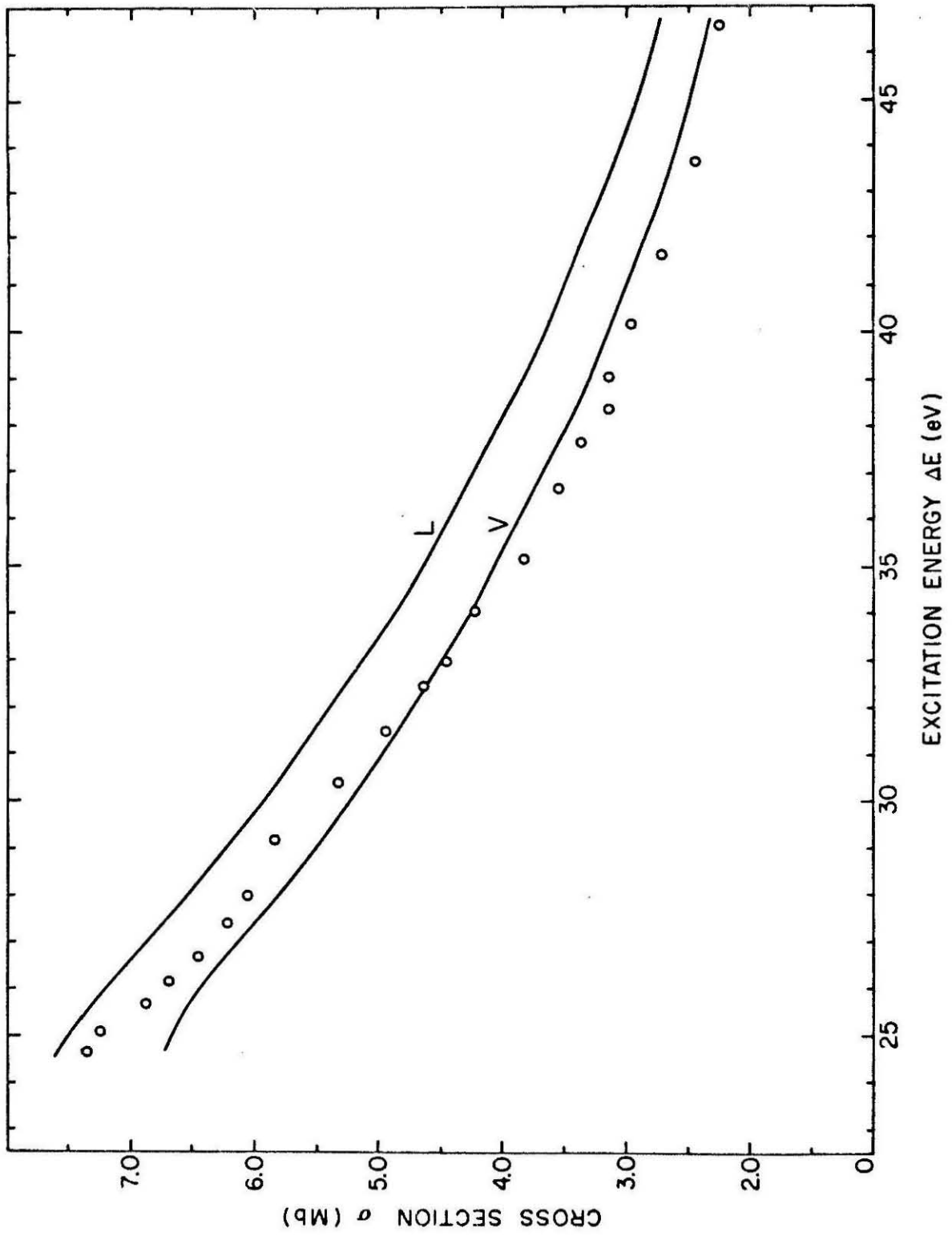


Figure 2

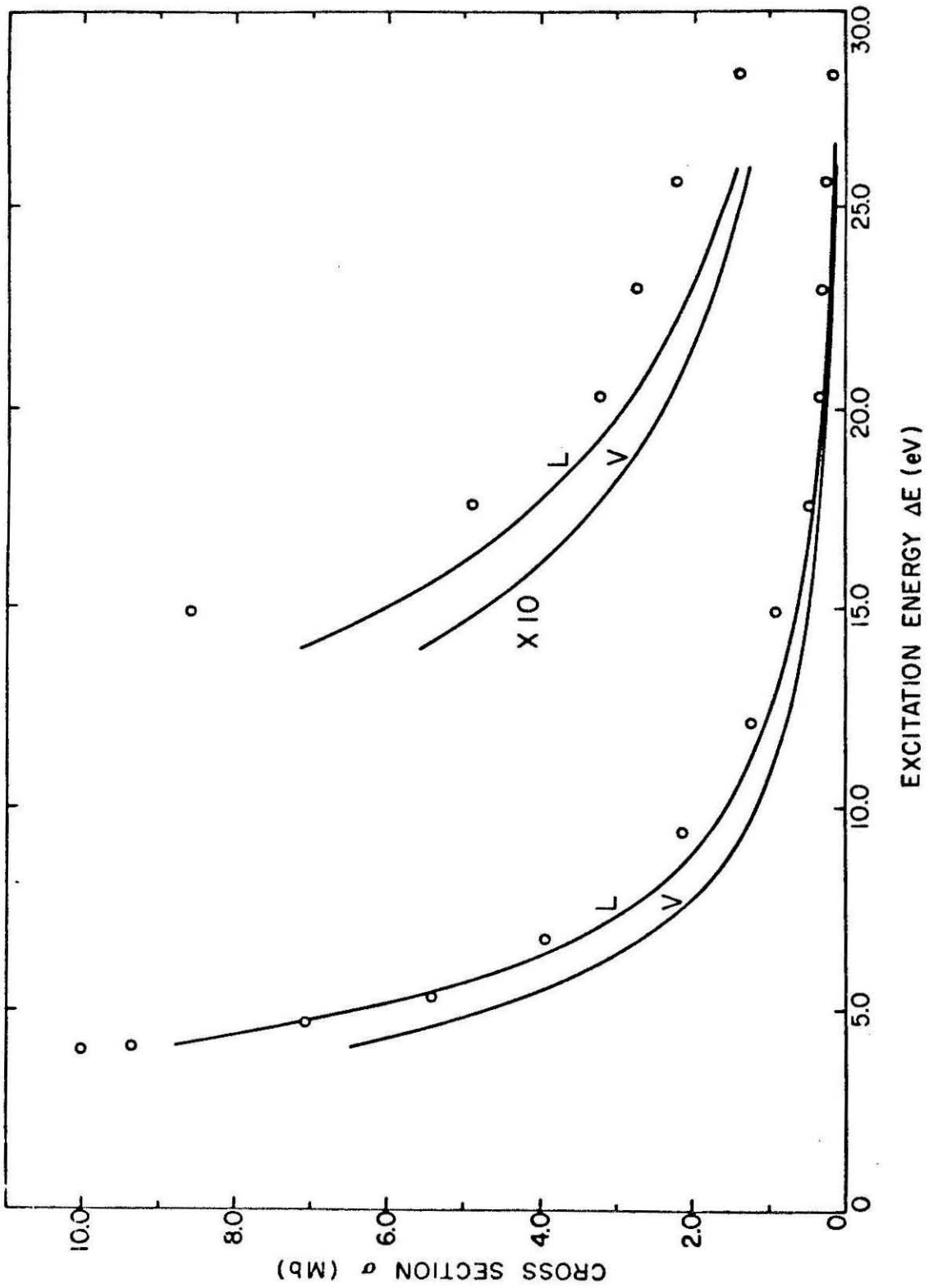


Figure 3

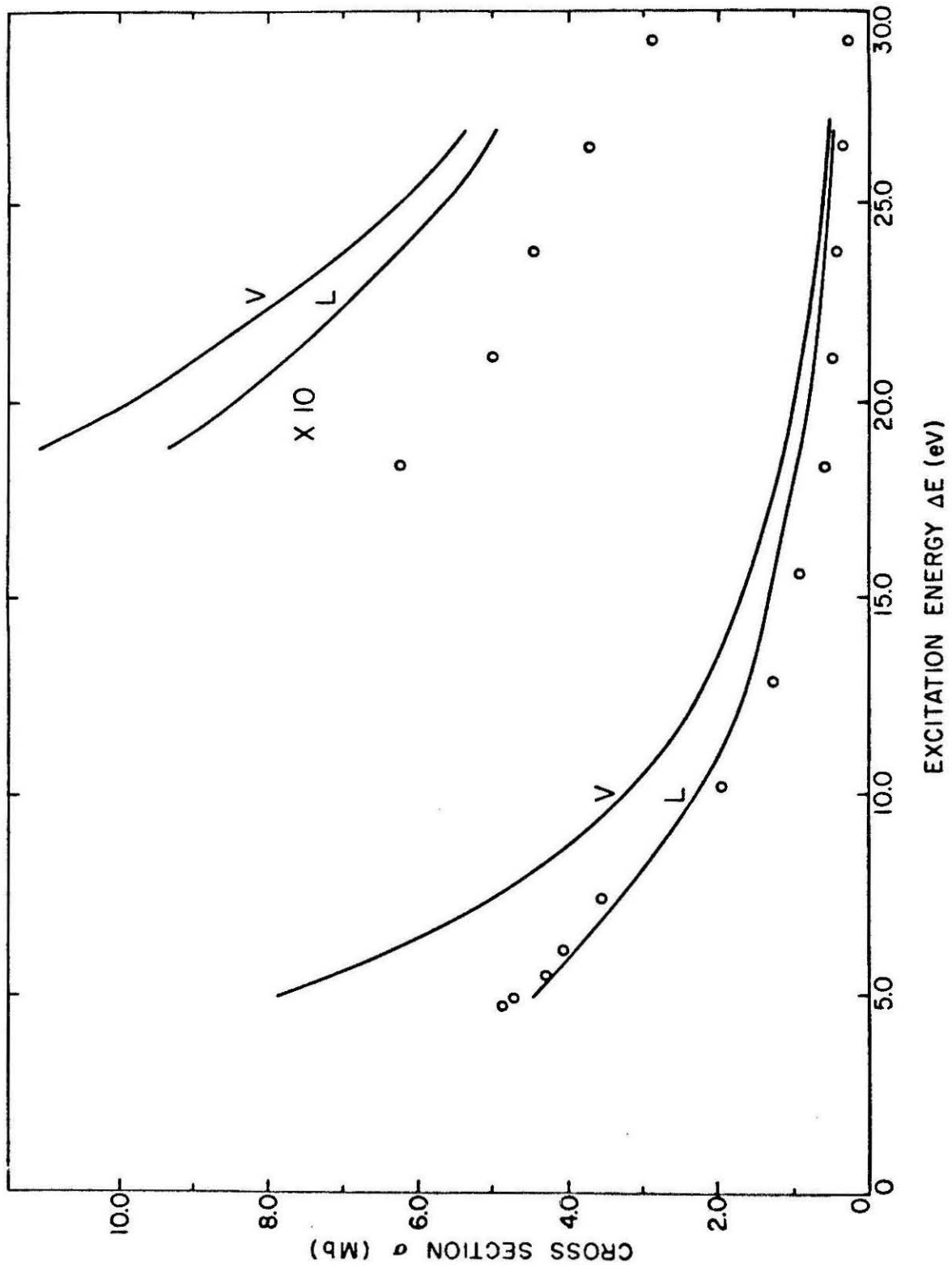


Figure 4

SECTION C

Iterative Approach to the Schwinger Variational Principle  
for Electron-Molecule Collisions

## I. INTRODUCTION

The Schwinger variational principle for the T matrix has been found to be very useful in obtaining accurate solutions for electron-molecule scattering. This method was introduced as a discrete basis function approach to scattering<sup>1</sup> and has evolved as a general numerical technique.<sup>2</sup> The Schwinger variational principle has been successfully applied to the scattering of low-energy electrons by He, He<sup>+</sup>, H<sub>2</sub>, H<sub>2</sub><sup>+</sup>, N<sub>2</sub><sup>+</sup>, and LiH.<sup>1-7</sup> In the present paper we apply an iterative approach to the Schwinger variational principle<sup>8-10</sup> to obtain scattering solutions to the electron-molecule collision problem. The method uses trial scattering wave functions which contain both discrete basis functions and numerical wave functions which explicitly satisfy the scattering boundary conditions. The discrete basis functions effectively describe the scattering wave function in the region near the nuclei where electron-exchange and partial-wave coupling are strong. The numerical wave functions are obtained from the Lippmann-Schwinger equation using a procedure which does not require solving coupled integro-differential equations. This is a powerful method for electron-molecule scattering combining the advantages of using discrete basis functions with an iterative procedure which allows convergence to an exact solution for the potential chosen to describe the interaction.

We apply the iterative Schwinger method to electron-H<sub>2</sub> scattering in the static-exchange approximation. The results of these applications show that the method is very effective and converges rapidly. Although the formal theory is given in terms of the T matrix and wave

functions which satisfy outgoing wave boundary conditions, for numerical convenience we actually perform all calculations using the K matrix and wave functions which satisfy standing wave boundary conditions.

## II. THEORY

The iterative Schwinger method starts with the solution of the Lippmann-Schwinger equation for the T matrix

$$T = U + U G_0^{(+)} T \quad (1)$$

using a separable approximation to the exact potential. The form of the separable potential used here is

$$\langle \underline{r} | U^{S_0} | \underline{r}' \rangle = \sum_{\alpha_i, \alpha_j \in R} \langle \underline{r} | U | \alpha_i \rangle [U^{-1}]_{ij} \langle \alpha_j | U | \underline{r}' \rangle \quad (2)$$

where R is an initial set of expansion functions and  $U = 2V$ . With this separable potential the solution of the Lippmann-Schwinger equation, Eq. (1), is given by

$$\langle \underline{r} | T^{S_0} | \underline{r}' \rangle = \sum_{\alpha_i, \alpha_j \in R} \langle \underline{r} | U | \alpha_i \rangle [(D^{(+)})^{-1}]_{ij} \langle \alpha_j | U | \underline{r}' \rangle \quad (3)$$

where

$$D_{ij}^{(+)} = \langle \alpha_i | U - U G_0^{(+)} U | \alpha_j \rangle. \quad (4)$$

As has been pointed out by several authors,<sup>11-13</sup> this form of the T matrix

is equivalent to that obtained from the Schwinger variational expression

$$T_{\ell\ell'm} = \langle \phi_{k\ell m} | T | \phi_{k\ell'm} \rangle = \frac{\langle \phi_{k\ell m} | U | \psi_{k\ell'm}^{(+)\dagger} \rangle \langle \psi_{k\ell m}^{(-)\dagger} | U | \phi_{k\ell'm} \rangle}{\langle \psi_{k\ell m}^{(-)\dagger} | U - UG_0^{(+)} U | \psi_{k\ell'm}^{(+)\dagger} \rangle} \quad (5)$$

where the partial wave trial functions are linear combinations of the expansion functions

$$\psi_{k\ell m}^{(\pm)\dagger}(\mathbf{r}) = \sum_{\alpha_i \in R} C_{k\ell m, i}^{(\pm)} \alpha_i(\mathbf{r}) . \quad (6)$$

The form of the T matrix given in Eq. (3) or equivalently Eq. (5), has been used by the present authors to obtain scattering results in several systems.<sup>1-5</sup> The errors that exist in this Schwinger variational T matrix are due to the difference between the exact potential U and the approximate separable potential  $U^{S_0}$  given in Eq. (2). It is possible to eliminate these errors due to the difference potential by an iterative procedure.

Our iterative procedure begins by constructing the scattering wave functions which correspond to the Schwinger T matrix given in Eq. (3). There are no coupled equations to solve to obtain these wavefunctions since the corresponding T matrix is exactly known. The scattering solutions are computed using the partial wave expansion of the wave function

$$\psi_{\mathbf{k}}^{(+)}(\mathbf{r}) = \sqrt{\frac{2}{\pi}} \sum_{\ell m} i^\ell \psi_{k\ell m}^{(+)}(\mathbf{r}) Y_{\ell m}^*(\hat{\mathbf{k}}). \quad (7)$$

For a linear target molecule,  $\psi_{klm}^{(+)}$  may in turn be expanded in a partial wave series by

$$\psi_{klm}^{(+)}(\underline{r}) = \sum_{\ell'} \psi_{\ell\ell'm}^{(+)}(k, r) Y_{\ell'm}(\hat{r}) . \quad (8)$$

The Lippmann-Schwinger equation for the wave function is

$$\psi_{klm}^{(+)\ S_0}(\underline{r}) = \phi_{klm}(\underline{r}) + \langle \underline{r} | G_0^{(+)\ S_0} U | \psi_{klm}^{(+)\ S_0} \rangle \quad (9)$$

where  $\phi_{klm}(\underline{r})$  are the free particle solutions

$$\phi_{klm}(\underline{r}) = j_\ell(kr) Y_{\ell m}(\hat{r}) . \quad (10)$$

By using the identity

$$\langle \underline{r} | U^{S_0} | \psi_{klm}^{(+)\ S_0} \rangle = \langle \underline{r} | T^{S_0} | \phi_{klm} \rangle , \quad (11)$$

we obtain an expression for the wave function in terms of the T matrix

$$\psi_{klm}^{(+)\ S_0}(\underline{r}) = \phi_{klm}(\underline{r}) + \langle \underline{r} | G_0^{(+)\ S_0} T^{S_0} | \phi_{klm} \rangle . \quad (12)$$

This equation for  $\psi_{klm}^{(+)\ S_0}$  is now uncoupled, and the partial-wave functions are given by

$$\begin{aligned} \psi_{\ell\ell'm}^{(+)\ S_0}(k, r) &= j_\ell(kr) \delta_{\ell\ell'} - \sum_{\alpha_i, \alpha_j \in R} k \langle j_{\ell'}(kr_{<}) h_{\ell'}^{(+)}(kr_{>}) Y_{\ell'm}(\hat{r}) \\ &\times |U| \alpha_i \rangle [(D^{(+)})^{-1}]_{ij} \langle \alpha_j | U | j_\ell(kr) Y_{\ell m}(\hat{r}) \rangle . \end{aligned} \quad (13)$$

The asymptotic form of the partial wave solutions are then

$$\psi_{\ell\ell'm}^{(+)\ S_0}(k, r) \sim j_\ell(kr) \delta_{\ell\ell'} - k \langle \phi_{k\ell'm} | T^{S_0} | \phi_{k\ell m} \rangle h_{\ell'}^{(+)}(kr) \quad (14)$$

The radial function,  $\psi_{\ell\ell'm}^{(+)}$ , is readily obtained from Eq. (13) by numerical integration.

The iterative procedure proceeds by augmenting the expansion set  $R$  of Eq. (2) by the set of functions  $S_0 = \{\psi_{k\ell_1 m}^{S_0}, \psi_{k\ell_2 m}^{S_0}, \dots, \psi_{k\ell_p m}^{S_0}\}$  which consists of the scattering solutions corresponding to the  $T$  matrix given in Eq. (3). Using this augmented set of functions, the first iteration is completed by calculating a new  $T$  matrix given by

$$\langle \underline{r} | T^{S_1} | \underline{r}' \rangle = \sum_{\chi_i, \chi_j \in R \cup S_0} \langle \underline{r} | U | \chi_i \rangle [(D^{(+)})^{-1}]_{ij} \langle \chi_j | U | \underline{r}' \rangle. \quad (15)$$

Note that the expansion functions contained in the set  $R \cup S_0$  include both the initial set of expansion functions  $R = \{\alpha_i\}$  and the continuum solutions given by Eq. (12).

A second iteration is begun by constructing the set of solutions  $S_1 = \{\psi_{k\ell_1 m}^{S_1}, \dots, \psi_{k\ell_p m}^{S_1}\}$  which are associated with the matrix  $T^{S_1}$  given by Eq. (15). The set  $S_1$  combined with the initial trial function set  $R$  yields a new  $T$  matrix  $T^{S_2}$ . In general,  $T^{S_n}$ ,  $\psi_{k\ell m}^{S_n}$  and the set of functions  $S_n$  are given by

$$\langle \underline{r} | T^{S_n} | \underline{r}' \rangle = \sum_{\chi_i, \chi_j \in R \cup S_{n-1}} \langle \underline{r} | U | \chi_i \rangle [(D^{(+)})^{-1}]_{ij} \langle \chi_j | U | \underline{r}' \rangle \quad (16)$$

and

$$S_n = \{ \psi_{kl_1 m}^{S_n}, \dots, \psi_{kl_p m}^{S_n} \} \quad (17)$$

where

$$\psi_{kl_i m}^{(+S_n)}(\underline{r}) = \phi_{kl_i m}(\underline{r}) + \langle \underline{r} | G_0^{(+)} T^{S_n} | \phi_{kl_i m} \rangle . \quad (18)$$

This iterative scheme is repeated until the wave functions converge.

If the wave functions do converge such that

$$\psi_{klm}^{(+S_{n+1})}(\underline{r}) = \psi_{klm}^{(+S_n)}(\underline{r}) \quad (19)$$

and if we have

$$\langle \psi_{kl_i m}^{(-S_n)} | U - U G_0^{(+)} U | \psi_{kl_j m}^{(+S_n)} \rangle = \langle \phi_{kl_i m} | U | \psi_{kl_j m}^{(+S_n)} \rangle \quad (20)$$

for  $1 \leq i \leq p$  and  $1 \leq j \leq p$ , and

$$\langle \psi_{kl_i m}^{(-S_n)} | U - U G_0^{(+)} U | \alpha_j \rangle = \langle \phi_{kl_i m} | U | \alpha_j \rangle \quad (21)$$

for  $1 \leq i \leq p$  and  $\alpha_j \in R$ , then it follows that the functions  $\psi_{klm}^{(+S_n)}$  satisfy the Lippmann-Schwinger equation for the exact potential  $U$ .

This can be demonstrated by substituting Eq. (16) into Eq. (18) to yield

$$\begin{aligned} \psi_{klm}^{(+)\mathcal{S}_{n+1}}(\underline{r}) &= \phi_{klm}(\underline{r}) + \sum_{\chi_i, \chi_j \in R \cup \mathcal{S}_n} \langle \underline{r} | G_0^{(+)} U | \chi_i \rangle \\ &\times [(D^{(+)})^{-1}]_{ij} \langle \chi_j | U | \phi_{klm} \rangle . \end{aligned} \quad (22)$$

Then using the relationships given in Eq. (20) and Eq. (21), Eq. (22) reduces to

$$\psi_{klm}^{(+)\mathcal{S}_{n+1}}(\underline{r}) = \phi_{klm}(\underline{r}) + \langle \underline{r} | G_0^{(+)} U | \psi_{klm}^{(+)\mathcal{S}_n} \rangle . \quad (23)$$

Thus if Eq. (19) is also satisfied, Eq. (23) reduces to

$$\psi_{klm}^{(+)\mathcal{S}_n}(\underline{r}) = \phi_{klm}(\underline{r}) + \langle \underline{r} | G_0^{(+)} U | \psi_{klm}^{(+)\mathcal{S}_n} \rangle \quad (24)$$

which is just the Lippmann-Schwinger equation for the exact potential  $U$ .

It is of interest to note that Eq. (20) and Eq. (21) are identically satisfied if  $\psi_{klm}^{\mathcal{S}_n}$  is the exact solution. This suggests that the degree of convergence of an approximate wave function can be judged by how well the relations given in Eq. (20) and Eq. (21) are satisfied. Also note that each side of Eq. (20) is a nonvariational approximation to the partial wave T matrix where  $\psi_{klm}^{\mathcal{S}_n}$  is an approximate trial function. Thus the convergence of the wave function can also be judged by how well the two sides of Eq. (20) compare with the variationally stable partial wave T matrix given by

$$\begin{aligned}
T_{\ell\ell'm}^{S_n} &= \langle \phi_{k\ell m} | T^{S_n} | \phi_{k\ell'm} \rangle = \sum_{\chi_i, \chi_j \in R \cup S_{n-1}} \langle \phi_{k\ell m} | U | \chi_i \rangle \\
&\times [(D^{(+)} )^{-1}]_{ij} \langle \chi_j | U | \phi_{k\ell'm} \rangle. \tag{25}
\end{aligned}$$

One of our original motivations for using the approximate solutions  $\psi_{k\ell m}^{S_0}$  in a new separable expansion, as a way of calculating an improved wave function, was an observation of Ernst *et al.*<sup>14</sup> They noted that if one had the exact solution to the Lippmann-Schwinger equation, then the potential given by a one-term separable approximation of the form in Eq. (2), where instead of the set  $R$  one uses the exact solutions, would give the exact on-shell and half off-shell  $T$  matrix. Thus it can be expected that the use of an approximate wave function satisfying the scattering boundary conditions in the separable expansion of Eq. (2) would give improved estimates of the  $T$  matrix from which an improved trial wave function could be calculated.

A more precise understanding of the nature of the convergence of the iterative procedure outlined above is obtained by dividing Eq. (16) into two parts giving<sup>15</sup>

$$\begin{aligned}
\langle \underline{r} | T^{S_n} | \underline{r}' \rangle &= \langle \underline{r} | T^{S_0} | \underline{r}' \rangle + \sum_{\substack{1 \leq i \leq p \\ 1 \leq j \leq p}} \langle \underline{r} | (1 + T^{S_0} G_0^{(+)} ) \Delta U | \\
&\times \psi_{k\ell_1 m}^{(+S_{n-1})} \rangle [(E^{(+)} )^{-1}]_{ij} \langle \psi_{k\ell_j m}^{(-S_{n-1})} | \Delta U (G_0^{(+)} T^{S_0} + 1) | \underline{r}' \rangle \tag{26}
\end{aligned}$$

where

$$E_{ij}^{(+)} = \langle \psi_{kl_i m}^{(-) S_{n-1}} | \Delta U - \Delta U G_S^{(+)} \Delta U | \psi_{kl_j m}^{(+)} S_{n-1} \rangle \quad (27)$$

and with

$$\Delta U = U - U^{S_0} . \quad (28)$$

Eq. (26) clearly shows the different contributions from the two sets of functions  $R$  and  $S_{n-1}$ . The Green's function  $G_S^{(+)}$  in Eq. (27) is the Green's function for the separable potential  $U^{S_0}$  and satisfies the Lippmann-Schwinger equation

$$G_S^{(+)} = G_0^{(+)} + G_0^{(+)} U^{S_0} G_S^{(+)} . \quad (29)$$

Thus  $G_S^{(+)}$  is given by

$$\begin{aligned} \langle \underline{r} | G_S^{(+)} | \underline{r}' \rangle &= \langle \underline{r} | G_0^{(+)} | \underline{r}' \rangle + \sum_{\alpha_i, \alpha_j \in R} \langle \underline{r} | G_0^{(+)} U | \alpha_i \rangle \\ &\times [(D^{(+)})^{-1}]_{ij} \langle \alpha_j | U G_0^{(+)} | \underline{r}' \rangle . \end{aligned} \quad (30)$$

The expression for the partial wave T matrix elements obtained from Eq. (26) is then

$$\begin{aligned} T_{ll'm}^{S_n} &= T_{ll'm}^{S_0} + \sum_{\substack{1 \leq i \leq p \\ 1 \leq j \leq p}} \langle \psi_{kl m}^{(-) S_0} | \Delta U | \psi_{kl_i m}^{(+)} S_{n-1} \rangle \\ &\times [(E^{(+)})^{-1}]_{ij} \langle \psi_{kl_j m}^{(-) S_{n-1}} | \Delta U | \psi_{kl' m}^{(+)} S_0 \rangle . \end{aligned} \quad (31)$$

Thus, after the first iteration, first and second order errors in the difference potential  $\Delta U$  have been eliminated from  $T_{\ell\ell'm}^{S_1}$  since with  $n = 1$ , Eq. (31) should give at least as good a correction to  $T_{\ell\ell'm}^{S_0}$  as a distorted-wave second Born approximation would.<sup>16</sup> Further iterations will give still higher order corrections.

### III. RESULTS

We have used the iterative method described above to study electron- $H_2$  scattering in the static-exchange approximation. The target SCF wave function is constructed from a (5s2z) Cartesian Gaussian basis set as given by Watson *et al.*<sup>4</sup> The Hartree-Fock energy for  $H_2$  in this basis set is -1.1330 au and the quadrupole moment is 0.452 au.

The results of a study of the convergence behavior of the iterative Schwinger method are given in Tables I-IV. The results presented in Tables I and II are obtained by starting the iterative procedure with  $\psi_{k\ell m}^{S_0}$  just equal to the free particle states  $\phi_{k\ell m}$ . This starting point corresponds to  $U^{S_0} = 0$ . It can be seen in Table I that the variational Schwinger K matrix converges to three places in four iterations. However, Table II shows that the nonvariational estimates of the partial wave K matrices from the left- and right-hand sides of Eq. (20) converge more slowly. In this calculation, these nonvariational K-matrices require another four iterations before they converge to three places. Table III gives the variational Schwinger K matrix for an iterative calculation where  $U^{S_0}$  is a one term separable approximation to  $U$ , constructed using a single s Cartesian Gaussian of exponent 0.5 centered on the nuclei. With this starting point, the iterative procedure

converges in two iterations. Also note that the nonvariationally stable matrix elements given in Table IV, which are associated with Eq. (20) and Eq. (21), are well converged by the second iteration also.

In Tables V and VI we present K matrix elements at several energies for both  ${}^2\Sigma$  and  ${}^2\Pi$  symmetries. We also compare the present results with those of Collins *et al.*<sup>17</sup> The separable potentials,  $U^{S_0}$ , used in these calculations are four term approximations. The potentials are constructed from Cartesian Gaussian functions centered at the nuclei. The Cartesian Gaussian functions have exponents of 0.3 and 1.0 and are of s and z types for the  ${}^2\Sigma$  symmetries and x and xz types for the  ${}^2\Pi$  symmetries. All variational K matrices converge to three places by the first iteration. This extremely rapid convergence is expected since the difference potential  $\Delta U$  should be small.

All integrals were calculated using single center expansions as is described elsewhere.<sup>3,18</sup> The integrations are performed on a grid extending to 40 au, except as noted in Tables V and VI where a grid extending to 125 au is used to accurately compute some integrals at low energy.

As can be seen, the K matrix elements are in good agreement with those of Collins *et al.*<sup>17</sup> The small discrepancies which exist are probably due to differences in the potentials used.

#### IV. CONCLUSIONS

The iterative Schwinger variational method presented here is a powerful method for computing electron-molecule scattering solutions. With a sufficient number of iterations, this method gives accurate scattering results which are independent of the initial discrete basis

set used. However, it is important to note that even though the variationally stable T matrix may converge in a particular calculation, it is necessary to check that the conditions given in Eqs. (19), (20), and (21) are satisfied to be assured that the T matrix has converged to the correct solution.

The Schwinger method does not require the solution of integro-differential equations. All equations are decoupled integral equations which are solved by straight forward integration procedures. With a reasonable choice of the initial separable potential  $U^{S_0}$ , this iteration method converges in only a few iterations. Applications to larger molecular systems are under way.

#### ACKNOWLEDGMENTS

This work was supported by the National Science Foundation under grant number CHE76-05157. We would like to thank Dr. Derek Robb for many helpful discussions and for providing us with results prior to publication. One of us (RRL) acknowledges the support of a National Science Foundation Predoctoral Fellowship.

The research reported in this paper made use of the Dreyfus-NSF Theoretical Chemistry Computer which was funded through grants from the Camille and Henry Dreyfus Foundation, the National Science Foundation (Grant No. CHE78-20235), and the Sloan Fund of the California Institute of Technology.

References

- <sup>1</sup>D. K. Watson and V. McKoy, Phys. Rev. A 20, 1474 (1979).
- <sup>2</sup>R. R. Lucchese and V. McKoy, J. Phys. B 12, L421 (1979).
- <sup>3</sup>R. R. Lucchese and V. McKoy, Phys. Rev. A 21, 112 (1980).
- <sup>4</sup>D. K. Watson, R. R. Lucchese, V. McKoy, and T. N. Rescigno, "The Schwinger Variational Principle for Electron-Molecule Scattering: Application to Electron-Hydrogen Scattering," Phys. Rev. A (to be published).
- <sup>5</sup>R. R. Lucchese and V. McKoy, Physica Scripta 21, 366 (1980).
- <sup>6</sup>R. R. Lucchese, G. Raseev, and V. McKoy, "Studies of Differential and Total Photoionization Cross Sections of N<sub>2</sub>," (in preparation).
- <sup>7</sup>D. K. Watson, V. McKoy, and T. N. Rescigno, "Application of the Schwinger Variational Principle to the Scattering of Electrons by Polar Molecules," (in preparation).
- <sup>8</sup>J. M. Blatt and J. D. Jackson, Phys. Rev. 76, 18 (1949).
- <sup>9</sup>T. Kato, Prog. Theo. Phys. 6, 295 (1951).
- <sup>10</sup>A. L. Zubarev, Sov. J. Part. Nucl. 7, 215 (1976).
- <sup>11</sup>W. H. Miller, J. Chem. Phys. 50, 407 (1969).
- <sup>12</sup>S. K. Adhikari and I. H. Sloan, Phys. Rev. C 11, 1133 (1975).
- <sup>13</sup>V. B. Belyaev, A. P. Podkopoyev, J. Wrzeczionko, and A. L. Zubarev, J. Phys. B 12, 1225 (1979).
- <sup>14</sup>D. J. Ernst, C. M. Shakin, and R. M. Thaler, Phys. Rev. C 8, 46 (1973).

- <sup>15</sup>We obtain Eq. (26) from Eq. (16) by partitioning the  $[D^{(+)}]_{ij}$  matrix and inverting. See, for example, C. E. Fröberg, Introduction to Numerical Analysis (Addison-Wesley, London, 1969) p. 108. Second Edition.
- <sup>16</sup>J. R. Taylor, Scattering Theory (Wiley, New York, 1972) p. 276.
- <sup>17</sup>L. Collins, D. Robb, and M. Morrison (private communication).
- <sup>18</sup>A. W. Fliflet and V. McKoy, Phys. Rev. A 18, 2107 (1978).

TABLE I. Convergence of the Schwinger variational K matrix starting from plane waves for  $^2\Sigma_g$  symmetry in  $H_2$  with  $k = 0.5$  au.

$(\ell, \ell')$	n=0	$S_n$ $K_{\ell\ell'0}$			
		1	2	3	4
(0, 0)	0.	-2.931	-1.701	-1.552	-1.548
(0, 2)	0.	0.128(-1)	0.133(-1)	0.134(-1)	0.134(-1)
(2, 2)	0.	0.163(-1)	0.163(-1)	0.163(-1)	0.163(-1)

TABLE II. Convergence of nonvariational approximations to the K matrix starting from plane waves for  ${}^2\Sigma_g$  symmetry in  $H_2$  with  $k = 0.5$  au.

$\langle \phi_{kl0}   U   \psi_{kl'0}^{s_n} \rangle$					
$(l, l')$	n=0	1	2	3	4
(0, 0)	3.055	-2.931	-1.331	-1.603	-1.515
(0, 2)	0.521(-1)	0.128(-1)	0.180(-1)	0.127(-1)	0.139(-1)
(2, 0)	0.521(-1)	0.128(-1)	0.135(-1)	0.135(-1)	0.134(-1)
(2, 2)	0.165(-1)	0.163(-1)	0.163(-1)	0.163(-1)	0.163(-1)
$\langle \psi_{kl0}^{s_n}   U - U G_0^{(P)} U   \psi_{kl'0}^{s_n} \rangle$					
$(l, l')$	n=0	1	2	3	4
(0, 0)	-2.921	-5.045	-1.139	-1.659	-1.483
(0, 2)	0.129(-1)	0.120(-1)	0.180(-1)	0.128(-1)	0.138(-1)
(2, 2)	0.163(-1)	0.162(-1)	0.163(-1)	0.163(-1)	0.163(-1)

TABLE III. Convergence of the Schwinger variational K matrix starting from one discrete scattering function for  ${}^2\Sigma_g$  symmetry in  $H_2$  with  $k = 0.5$  au.

$(l, l')$	$K_{ll'0}^{s_n}$		
	n=0	1	2
(0, 0)	-2.045	-1.552	-1.548
(0, 2)	-0.276(-1)	0.133(-1)	0.134(-1)
(2, 2)	-0.372(-3)	0.163(-1)	0.163(-1)

TABLE IV. Convergence of nonvariational approximations to the K matrix and of matrix elements involving the discrete function starting from one discrete scattering function for  ${}^2\Sigma_g$  symmetry in  $H_2$  with  $k = 0.5$  au.

$\langle \phi_{kl0}   U   \psi_{kl'0}^{S_n} \rangle$			
$(l, l')$	n=0	1	2
(0, 0)	-1.602	-1.567	-1.549
(0, 2)	0.179(-1)	0.131(-1)	0.134(-1)
(2, 0)	-0.107(-1)	0.136(-1)	0.135(-1)
(2, 2)	0.161(-1)	0.163(-1)	0.163(-1)

$\langle \psi_{kl0}^{S_n}   U - UG_0^{(P)} U   \psi_{kl'0}^{S_n} \rangle$			
$(l, l')$	n=0	1	2
(0, 0)	-1.642	-1.586	-1.550
(0, 2)	0.667(-2)	0.132(-1)	0.135(-1)
(2, 2)	0.155(-1)	0.162(-1)	0.163(-1)

$\langle \phi_{kl0}   U   \alpha \rangle^a$			
$l$			
	0	6.180	
	2	0.834(-1)	

$\langle \psi_{kl0}^{S_n}   U - UG_0^{(P)} U   \alpha \rangle^a$			
$l$	n=0	1	2
0	6.190	6.224	6.180
2	0.170	0.824(-1)	0.830(-1)

<sup>a</sup> See Eq. (21).

TABLE V. Iterated Schwinger variational K matrix elements for  ${}^2\Sigma$  symmetry in  $H_2$ .

k	${}^2\Sigma_g^+$		${}^2\Sigma_u^+$	
	$K_{000}^S$	$K_{000}^{CRM}$	$K_{110}^S$	$K_{110}^{CRM}$
0.1	-0.217	-0.217 <sup>a</sup>	0.123(-1) <sup>b</sup>	0.127(-1) <sup>a</sup>
0.3	-0.722	-0.722	0.113	0.119
0.5	-1.55	-1.55	0.411	0.421
1.0	8.04	8.05	1.34	1.34
k	$K_{020}^S$	$K_{020}^{CRM}$	$K_{130}^S$	$K_{130}^{CRM}$
0.1	0.406(-2)	0.39(-2)	0.105(-2) <sup>b</sup>	0.15(-2)
0.3	0.978(-2)	0.11(-1)	0.335(-2)	0.34(-2)
0.5	0.134(-1)	0.15(-1)	0.703(-2)	0.71(-2)
1.0	0.122	0.11	0.304(-1)	0.29(-1)
k	$K_{220}^S$	$K_{220}^{CRM}$	$K_{330}^S$	$K_{330}^{CRM}$
0.1	0.165(-2)	0.21(-2)	0.971(-3) <sup>b</sup>	0.73(-3)
0.3	0.687(-2)	0.74(-2)	0.290(-2)	0.31(-2)
0.5	0.163(-1)	0.18(-1)	0.520(-2)	0.56(-2)
1.0	0.914(-1)	0.93(-1)	0.190(-1)	0.20(-1)

<sup>a</sup> All numbers in this column are from Ref. 17.

<sup>b</sup> A grid extending to 125 au is used to obtain this K matrix element.

TABLE VI. Iterated Schwinger variational K matrix elements for  $^2\Pi$  symmetry in  $H_2$

k	$^2\Pi_u$		$^2\Pi_g$	
	$K_{111}^S$	$K_{111}^{CRM}$	$K_{221}^S$	$K_{221}^{CRM}$
0.1	-0.296(-2)	-0.306(-2) <sup>a</sup>	0.106(-2) <sup>b</sup>	0.103(-2) <sup>a</sup>
0.3	0.195(-1)	0.218(-1)	0.368(-2)	0.400(-2)
0.5	0.102	0.108	0.103(-1)	0.114(-1)
1.0	0.334	0.335	0.692(-1)	0.713(-1)
k	$K_{131}^S$	$K_{131}^{CRM}$	$K_{241}^S$	$K_{241}^{CRM}$
	0.1	0.110(-2)	0.12(-2)	0.493(-3) <sup>b</sup>
0.3	0.267(-2)	0.28(-2)	0.148(-2)	0.15(-2)
0.5	0.483(-2)	0.50(-2)	0.235(-2)	0.24(-2)
1.0	0.142(-1)	0.14(-1)	0.564(-2)	0.58(-2)
k	$K_{331}^S$	$K_{331}^{CRM}$	$K_{441}^S$	$K_{441}^{CRM}$
	0.1	0.286(-3)	0.55(-3)	0.465(-3) <sup>b</sup>
0.3	0.217(-2)	0.23(-2)	0.139(-2)	0.15(-2)
0.5	0.392(-2)	0.42(-2)	0.245(-2)	0.26(-2)
1.0	0.157(-1)	0.17(-1)	0.611(-2)	0.67(-2)

<sup>a</sup> All numbers in this column are from Ref. 17.

<sup>b</sup> A grid extending to 125 au is used to obtain this K matrix element.

SECTION D

Iterative Approach to the Schwinger Variational Principle  
Applied to Electron-Molecular-Ion Collisions

I. INTRODUCTION

Considerable effort has been devoted to the development of efficient and accurate methods for solving the electron-molecule collision problem.<sup>1</sup> The main difficulties encountered in solving this problem are the non-spherical nature of the potential and the accurate treatment of the non-local exchange potential. Our approach to the solution of the electron-molecule collision problem is to use the Schwinger variational principle. The first application of the Schwinger variational principle to this problem was an approximate discrete basis function approach.<sup>2</sup> We then implemented the Schwinger variational principle exactly using numerical techniques.<sup>3,4</sup> This method has been successfully applied to the scattering of low-energy electrons by He, He<sup>+</sup>, H<sub>2</sub>, H<sub>2</sub><sup>+</sup>, N<sub>2</sub><sup>+</sup>, and LiH.<sup>3-9</sup> In the present paper we give results for the e<sup>-</sup>-H<sub>2</sub><sup>+</sup> system<sup>7</sup> using a recently developed iterative technique based upon the Schwinger variational principle.<sup>6</sup>

In this study of the e<sup>-</sup>-H<sub>2</sub><sup>+</sup> scattering system we make several standard simplifying assumptions. First we work within the fixed-nuclei approximation. We also assume that the interaction between the continuum electron and the molecular ion is described by the static-exchange potential, and hence we neglect electron correlation.

The iterative method used here<sup>6</sup> for solving the resulting scattering equations begins by exactly solving the equations for a separable approximation to the static-exchange potential. The separable approximation used in this study is constructed from a set of Cartesian Gaussian functions. The iterative method then proceeds by using the exact solutions to the approximate separable potential in a distorted

wave Schwinger variational calculation on the difference potential (i. e., the difference between the exact static-exchange potential and the approximate separable potential). Further iterations proceed to give higher order corrections.

We present converged results for both elastic  $e^-H_2^+$  scattering and photoionization cross sections of  $H_2$ . We found that our iterative method converged rapidly in all calculations presented here. We have studied  $e^-H_2^+$  scattering as the first test case for applying the iterative Schwinger method to electron molecular-ion scattering. We have chosen this system since standard single-center expansion methods should work well and thus provide us with accurate results to compare with. We have compared our results with the accurate static-exchange results of Collins and Robb,<sup>10</sup> which were obtained using such a single center expansion method. There have been other studies of  $e^-H_2^+$  systems,<sup>11-13</sup> but the study of Collins and Robb<sup>10</sup> is the most accurate to date. For all channels and energies considered here, the results of the iterative Schwinger variational method are in good agreement with those of Collins and Robb.<sup>10</sup>

## II. THEORY

The Schrödinger equation for electron-molecular ion scattering in the static-exchange approximation is (in atomic units)

$$\left(-\frac{1}{2}\nabla^2 - \frac{Z}{r} + V(r) - \frac{k^2}{2}\right)\psi_{\mathbf{k}}^{(+)}(\mathbf{r}) = 0, \quad (1)$$

where  $Z$  is the net charge on the isolated ion and  $V(r)$  is the residual short-range potential. This Schrödinger equation is equivalent to the Lippmann-Schwinger equation

$$\psi_{\mathbf{k}}^{(+)} = \psi_{\mathbf{k}}^{C(+)} + G^{C(+)} U \psi_{\mathbf{k}}^{(+)}, \quad (2)$$

where

$$U(\mathbf{r}) = 2V(\mathbf{r}) \quad (3)$$

and the Coulomb Green's function is defined by

$$G^{c(\pm)} = (\nabla^2 + \frac{2Z}{r} + k^2 \pm i\epsilon)^{-1} . \quad (4)$$

The function  $\Psi_{\underline{k}}^{c(\pm)}$  is the pure Coulomb scattering function and is given in terms of its partial-wave expansion as

$$\Psi_{\underline{k}}^{c(\pm)}(\mathbf{r}) = \left(\frac{2}{\pi}\right)^{1/2} \sum_{\ell, m} i^\ell \phi_{k\ell m}^{c(\pm)}(\mathbf{r}) Y_{\ell m}^*(\hat{\mathbf{k}}) , \quad (5)$$

where  $\phi_{k\ell m}^{c(\pm)}$  is the partial-wave Coulomb function defined by

$$\phi_{k\ell m}^{c(\pm)}(\mathbf{r}) = e^{(\pm)i\sigma_\ell} \frac{F_\ell(\gamma; kr)}{kr} Y_{\ell m}(\hat{\mathbf{r}}) . \quad (6)$$

The function  $F_\ell(\gamma; kr)$  is the regular Coulomb function with  $\gamma = -Z/k$  and  $\sigma_\ell$  is the Coulomb phase shift defined as  $\sigma_\ell = \arg[\Gamma(\ell + 1 + i\gamma)]$ .

The wave function  $\Psi_{\underline{k}}^{(+)}$ , which has incoming waves with momentum  $\underline{k}$ , can be expanded in the partial-wave series

$$\Psi_{\underline{k}}^{(+)}(\mathbf{r}) = \left(\frac{2}{\pi}\right)^{1/2} \sum_{\ell m} i^\ell \psi_{k\ell m}^{(+)}(\mathbf{r}) Y_{\ell m}^*(\hat{\mathbf{k}}) . \quad (7)$$

Computing the wave function in the partial-wave form allows the dependence of the scattering solution on the target orientation to be treated

analytically. The Lippmann-Schwinger equation for the partial-wave states is then

$$\psi_{k\ell m}^{(+)}(\underline{r}) = \phi_{k\ell m}^{c(+)}(\underline{r}) + \langle \underline{r} | G^{c(+)} U | \psi_{k\ell m}^{(+)} \rangle . \quad (8)$$

Instead of solving for the scattering solutions directly, one can equivalently solve for the T matrix due to only the short-range component of the potential which satisfies the Lippmann-Schwinger equation

$$T = U + U G^{c(+)} T . \quad (9)$$

Then using the identity

$$T | \phi_{k\ell m}^{c(+)} \rangle = U | \psi_{k\ell m}^{(+)} \rangle \quad (10)$$

and Eq. (8), the partial-wave solutions are obtained from

$$\psi_{k\ell m}^{(+)}(\underline{r}) = \langle \underline{r} | 1 + G^{c(+)} T | \phi_{k\ell m}^{c(+)} \rangle . \quad (11)$$

We solve the Lippmann-Schwinger equation, Eq. (8), with an iterative procedure based upon the Schwinger variational principle.<sup>6</sup> The iterative method begins by approximating the short-range potential by a separable potential of the form

$$\langle \underline{r} | U^{S_0} | \underline{r}' \rangle = \sum_{\alpha_i, \alpha_j \in R} \langle \underline{r} | U | \alpha_i \rangle [U^{-1}]_{ij} \langle \alpha_j | U | \underline{r}' \rangle , \quad (12)$$

where  $R$  is some initial set of expansion functions. For this approximate separable potential, the solution of the Lippmann-Schwinger equation for the  $T$  matrix (Eq. (9)) is given by

$$\langle \underline{r} | T^{S_0} | \underline{r}' \rangle = \sum_{\alpha_i, \alpha_j \in R} \langle \underline{r} | U | \alpha_i \rangle [(D^{(+)})^{-1}]_{ij} \langle \alpha_j | U | \underline{r}' \rangle \quad (13)$$

where

$$D_{ij}^{(+)} = \langle \alpha_i | U - UG^{c(+)} U | \alpha_j \rangle . \quad (14)$$

As has been pointed out by several authors,<sup>14-16</sup> this form of the  $T$  matrix is equivalent to that obtained from finding stationary values of the Schwinger variational expression

$$T_{ll'm} = \langle \phi_{klm}^{c(-)} | T | \phi_{kl'm}^{c(+)} \rangle = \frac{\langle \phi_{klm}^{c(-)} | U | \psi_{kl'm}^{(+t)} \rangle \langle \psi_{klm}^{(-t)} | U | \phi_{kl'm}^{c(+)} \rangle}{\langle \psi_{klm}^{(-t)} | U - UG^{c(+)} U | \psi_{kl'm}^{(+t)} \rangle} \quad (15)$$

by varying the partial-wave trial functions which are linear combinations of the expansion functions,

$$\psi_{klm}^{(\pm)t}(\underline{r}) = \sum_{\alpha_i \in R} C_{klm,i}^{(\pm)} \alpha_i(\underline{r}) . \quad (16)$$

The scattering solutions  $\psi_{klm}^{(+S_0}$  corresponding to the approximate separable potential  $U^{S_0}$  are obtained using Eq. (11) giving

$$\psi_{klm}^{(+S_0)}(\underline{r}) = \phi_{klm}^{c(+)}(\underline{r}) + \langle \underline{r} | G^{c(+)} T^{S_0} | \phi_{klm}^{c(+)} \rangle . \quad (17)$$

The iterative procedure is continued by augmenting the expansion set  $R$ , of Eq. (12), by the set of functions

$$S_0 = \{ \psi_{kl_1 m}^{S_0}, \psi_{kl_2 m}^{S_0}, \dots, \psi_{kl_p m}^{S_0} \}, \quad (18)$$

which are the scattering solutions given by Eq. (17). Using this augmented set of functions, the first iteration is completed by calculating a new  $T$  matrix given by

$$\begin{aligned} \langle \mathcal{E} | T^{S_1} | \mathcal{E}' \rangle &= \sum_{\chi_i, \chi_j \in R \cup S_0} \langle \mathcal{E} | U | \chi_i \rangle [(D^{(+)})^{-1}]_{ij} \\ &\quad \times \langle \chi_j | U | \mathcal{E}' \rangle. \end{aligned} \quad (19)$$

Note that the variational basis set  $R \cup S_0$  used in Eq. (19) contains both the initial expansion set  $R = \{ \alpha_i \}$  and the continuum solutions given by Eq. (17). Thus, for example, the  $D_{ij}^{(+)}$  matrix will contain matrix elements of the form  $\langle \psi_{klm}^{S_0} | U - UG^{C^{(+)}} U | \alpha_j \rangle$  and  $\langle \psi_{klm}^{S_0} | U - UG^{C^{(+)}} U | \psi_{kl'm}^{S_0} \rangle$  as well as the type given in Eq. (14).

A second iteration is begun by constructing the set of solutions  $S_1 = \{ \psi_{kl_1 m}^{S_1}, \dots, \psi_{kl_p m}^{S_1} \}$  which is associated with the matrix  $T^{S_1}$  given by Eq. (19). The set  $S_1$ , combined with the initial trial functions set  $R$ , yields a new  $T$  matrix,  $T^{S_2}$ . In general,  $T^{S_n}$  and the set of functions  $S_n$  are given by

$$\begin{aligned} \langle \mathcal{E} | T^{S_n} | \mathcal{E}' \rangle &= \sum_{\chi_i, \chi_j \in R \cup S_{n-1}} \langle \mathcal{E} | U | \chi_i \rangle [(D^{(+)})^{-1}]_{ij} \\ &\quad \times \langle \chi_j | U | \mathcal{E}' \rangle \end{aligned} \quad (20)$$

and

$$S_n = \{ \psi_{kl_1 m}^{S_n}, \dots, \psi_{kl_p m}^{S_n} \}, \quad (21)$$

where

$$\psi_{\mathbf{k}\ell_1 m}^{(+)\mathbf{S}_n}(\mathbf{r}) = \phi_{\mathbf{k}\ell_1 m}^{c(+)}(\mathbf{r}) + \langle \mathbf{r} | G^{c(+)} T^{\mathbf{S}_n} | \phi_{\mathbf{k}\ell_1 m}^{c(+)} \rangle . \quad (22)$$

This iterative procedure is continued until the wave functions converge. When the wave functions do converge, it can be shown that they are solutions of the Lippmann-Schwinger equation for the exact potential  $U$ .<sup>6</sup>

In the fixed-nuclei approximation, the differential cross section (DCS) averaged over molecular orientation is given by<sup>12</sup>

$$\begin{aligned} \frac{d\sigma}{d\Omega} = & \frac{\gamma^2}{4k^2 \sin^4(\frac{\theta}{2})} + \sum_L A_L P_L(\cos \theta) + \frac{1}{\sin^2(\frac{\theta}{2})} \\ & \times \sum_L B_L(\theta) P_L(\cos \theta) , \end{aligned} \quad (23)$$

where

$$\begin{aligned} A_L = & \frac{1}{4\pi} \sum_{\ell, \ell', \lambda, \lambda', m, \mu} a_{\ell \ell' m} a_{\lambda \lambda' \mu}^* \left( \frac{2L+1}{2\lambda'+1} \right) \left( \frac{2L+1}{2\lambda+1} \right)^{1/2} \\ & \times (L \ell 0 0 | \lambda 0) (L \ell' 0 0 | \lambda' 0) (L \ell \mu -m m | \lambda \mu) (L \ell' \mu -m m | \lambda' \mu) , \end{aligned} \quad (24)$$

and

$$B_L(\theta) = -\frac{\gamma}{k} \sum_m \frac{1}{(4\pi(2\ell+1))^{1/2}} \operatorname{Re} \left\{ \exp \left[ i\gamma \ell n \left( \sin^2 \frac{\theta}{2} \right) - 2i\sigma_0 \right] \times a_{LLm} \right\}, \quad (25)$$

and where  $(j_1 j_2 m_1 m_2 | jm)$  is a Clebsch-Gordan coefficient. The fixed-nuclei dynamical coefficients  $a_{\ell\ell'm}$  are defined by<sup>12</sup>

$$a_{\ell\ell'm} = -\frac{\pi^{3/2}}{k} i^{\ell'-\ell} (2\ell'+1)^{1/2} T_{\ell\ell'm}. \quad (26)$$

In the present study, the partial-wave T matrix elements are approximated at the n'th iteration by  $T_{\ell\ell'm}^{S_n}$  which is given by

$$T_{\ell\ell'm}^{S_n} = \sum_{\chi_i, \chi_j \in R \cup S_{n-1}} \langle \phi_{k\ell m}^{c(-)} | U | \chi_i \rangle [(D^{(+)})^{-1}]_{ij} \langle \chi_j | U | \phi_{k\ell m}^{c(+)} \rangle. \quad (27)$$

From Eq. (23) it is clearly seen that the DCS is the sum of the pure Coulomb scattering DCS plus the DCS due to the short-range potential plus an interference term.

We have only considered the interaction between the scattered electron and the target in the static-exchange approximation. The static-exchange potential due to a one-electron target is of the form,<sup>4</sup>

$$U(\underline{r}) = 2 \left\{ N^A(\underline{r}) + J^{u^0} \pm (K^{u^0} + Q^{u^0}) \mp (\epsilon_0 + \frac{1}{2} k^2) P^{u^0} \right\}. \quad (28)$$

where  $u^0(\underline{r})$  is the orbital of the bound electron, and where the upper (lower) sign is for singlet (triplet) scattering. In Eq. (28),  $N^A$  is the nuclear attraction term minus the long-range  $-Z/r$  term in Eq. (1).

The operators  $J^{u^0}$  and  $K^{u^0}$  are the standard Coulomb and exchange operators of the orbital  $u^0$ . The  $Q^{u^0}$  and  $P^{u^0}$  operators are included to allow for possible non-orthogonality between the bound orbital and the continuum orbital. These operators are defined by

$$\langle \mathcal{F} | Q^{u^0} | \chi \rangle = \langle \mathcal{F} | u^0 \rangle \langle u^0 | h | \chi \rangle + \langle \mathcal{F} | h | u^0 \rangle \langle u^0 | \chi \rangle \quad (29)$$

and

$$\langle \mathcal{F} | P^{u^0} | \chi \rangle = \langle \mathcal{F} | u^0 \rangle \langle u^0 | \chi \rangle, \quad (30)$$

where

$$h(i) = -\frac{1}{2} \nabla_i^2 + N^A \left( \frac{r_i}{r_i} \right) - \frac{Z}{r_i}. \quad (31)$$

The one electron energy  $\epsilon_0$  of the orbital  $u^0$  is thus given by

$$\epsilon_0 = \langle u^0 | h | u^0 \rangle. \quad (32)$$

### III. RESULTS FOR $e^- - H_2^+$ SCATTERING

In the present study of  $e^- - H_2^+$  elastic scattering, we used a target molecular orbital constructed from the 8s4z Cartesian Gaussian basis set which is given in Table I. This basis set is the 6s Gaussian fit to the hydrogen 1s function given by Huzanaga,<sup>17</sup> augmented by four z functions and two diffuse s functions. The internuclear separation for  $H_2^+$  was  $R = 2.0$  au. The target energy in this basis was  $E = -1.102292$  au and the quadrupole moment was  $-1.533$  au.

The initial scattering basis set, set R, is given in Table II. For the present study, R consisted of a set of nuclear and bond mid-point

centered Cartesian Gaussian functions. For all symmetries considered, the scattering basis set consisted of only five functions. We found that inclusion of bond mid-point centered functions in the initial scattering set yielded more rapidly converging wave functions than those obtained starting from basis sets not containing such functions. We believe that this is due to the way the short-range potential  $U$  as given in Eq. (28) is constructed. The short-range potential  $U$  is obtained from the full static-exchange potential by the addition of the term  $Z/r$ . This just cancels the long-range tail of the full potential, but this method thus makes  $U$  strongly repulsive near the origin. It seems that in order to describe the scattering due to this repulsive potential it is important to have functions centered at the origin.

In Tables III and IV we present our converged results for  $\Sigma$  and  $\Pi$  symmetries and compare them with those of Collins and Robb.<sup>10</sup> Our results generally agree very well with those of Collins and Robb. Any discrepancies are probably due to the different target orbitals used. Collins and Robb use a target orbital constructed from Slater-type functions which probably gives a more accurate orbital than that constructed from our Cartesian Gaussian functions. It is interesting to note that in an earlier study,<sup>7</sup> we used a target constructed from a smaller  $5s2z$  Cartesian Gaussian basis set. Using the iterative Schwinger method with this target, we found that in the  ${}^1\Sigma_u$  channel there were discrepancies of  $\sim 0.05$  radians in the converged eigenphase sums compared with the results of Collins and Robb. This large difference had not been evident in any of the other channels considered. We then performed a scattering calculation in which no exchange interaction was considered. This calculation with the direct potential only

yielded excellent agreement with the equivalent calculation performed by Collins and Robb. This somewhat anomalous behavior in the  ${}^1\Sigma_u$  channel prompted us to try the more accurate 8s4z target which then gave very good agreement in this channel. It is believed that this strong dependence on the target orbital is indicative of resonant-like scattering in the  ${}^1\Sigma_u$  channel.

The iterative procedure used in the present study was found to converge very rapidly. In Table V we present a representative calculation showing how the eigenphases converged. The higher partial-wave eigenphases were not accurately obtained using only the discrete basis set in the zero'th iteration result. However, these eigenphases are quickly corrected in the first iteration since they are Born-dominated.

All integrals were computed using numerical quadrature as is described elsewhere.<sup>4,16</sup> The integrals were evaluated on a grid of 780 points extending out to 66.2 au. All basis functions and the target orbital were expanded up to  $l = 13$ . The exchange and direct integrals were then computed exactly with no further truncations in  $l$ . We have computed partial wave solutions up to  $l_p = 7$ . This truncation of the sum in  $l_p$  in general gives eigenphase sums converged to better than 1%. Cutting off the  $l_p$  sum does represent an approximation to the total wave function  $\Psi_k$ , however each individual partial wave function  $\psi_{klm}$  which is included in the calculation will still be obtained exactly within the static-exchange approximation if the iterative solution converges.

In Fig. 1 we present the spin-averaged DCS obtained at the three energies considered here. These curves clearly show the dominance of Coulomb scattering at low angle and the effects of scattering due to the short-range potential at large angles.

#### IV. RESULTS FOR PHOTOIONIZATION OF $H_2$

We use the electron-molecular ion scattering wave functions obtained here to study the photoionization of  $H_2$  in its ground state. We have used the method outlined in our earlier paper<sup>4</sup> to obtain the photoionization

cross section. The fixed-nuclei photoionization cross section is obtained in both the dipole-length and dipole-velocity approximations.

The initial state wave function  $\Psi_i(\mathbf{r}_1, \mathbf{r}_2)$  used in these calculations is a Hartree-Fock wave function. The initial state is thus of the form

$$\Psi_i(\mathbf{r}_1, \mathbf{r}_2) = \phi_{1\sigma}(\mathbf{r}_1) \phi_{1\sigma}(\mathbf{r}_2) \left( \frac{\alpha(1)\beta(2) - \beta(1)\alpha(2)}{2^{1/2}} \right). \quad (33)$$

The one electron orbital  $\phi_{1\sigma}$  was constructed from a 5s2z Cartesian Gaussian basis given by Watson et al.<sup>5</sup> The Hartree-Fock energy for  $H_2$  in this basis set is -1.1330 au. The final state wave function is taken to be the electron-ion scattering wave function where the target orbital is fixed as the  $\phi_{1\sigma}$  orbital of  $H_2$ . Thus the final states are of the form

$$\Psi_{f, \underline{k}}(\mathbf{r}_1, \mathbf{r}_2) = \left(\frac{k}{2}\right)^{1/2} \left[ \phi_{1\sigma}(\mathbf{r}_1) \Psi_{\underline{k}}^{(-)}(\mathbf{r}_2) + \Psi_{\underline{k}}^{(-)}(\mathbf{r}_1) \phi_{1\sigma}(\mathbf{r}_2) \right] \left( \frac{\alpha(1)\beta(2) - \beta(1)\alpha(2)}{2^{1/2}} \right). \quad (34)$$

The differential dipole oscillator strengths are then computed in either the length or velocity form using

$$\left( \frac{df}{dE} \right)_L = \sum_{\mu} \frac{2}{3} E \int d\Omega_{\underline{k}} \left| \langle \Psi_i | r_{\mu} | \Psi_{f, \underline{k}} \rangle \right|^2 \quad (35)$$

or

$$\left(\frac{df}{dE}\right)_v = \sum_{\mu} \frac{2}{3} \frac{1}{E} \int d\Omega_{\hat{k}} |\langle \Psi_i | \nabla_{\mu} | \Psi_{f, \hat{k}} \rangle|^2 \quad (36)$$

where the photon energy is  $E = \frac{1}{2}k^2 + \text{IP}$ . The photoionization cross section is then given by

$$\sigma(E) = \frac{2\pi^2}{c} \left(\frac{df}{dE}\right). \quad (37)$$

The initial scattering basis set in these calculations was the same basis set we used for  $e^- - \text{H}_2^+$  scattering and is given in Table II. The rate of convergence in these photoionization calculations was similar to that obtained in  $e^- - \text{H}_2^+$  scattering. In Table VI we give an example which shows the rate of convergence for a selected energy in the  $^1\Sigma_u$  symmetry. Both the eigenphase sums and the cross sections were converged to three decimal places by the second iteration for all energies considered in this study. In Fig. 2 we present the converged photoionization cross sections for  $\text{H}_2$  in both the length and velocity forms. We also compare the present calculated cross section with some experimental results.<sup>19,20</sup> Since we have not treated the vibrational motion in the  $\text{H}_2 - \text{H}_2^+$  system, we have only compared our calculated results with experimental results which correspond to photon energies for which the sum of all Franck-Condon factors for the open vibrational channels of  $\text{H}_2^+$  is close to unity. For the  $\text{H}_2 - \text{H}_2^+$  system this corresponds to photon energies greater than  $\sim 18 \text{ eV}$ .<sup>21,22</sup> The equivalence of the dipole length and dipole velocity forms of the photoionization cross section is

a necessary but not a sufficient condition for the exact solution.<sup>21</sup> Thus, we may use this difference to estimate the minimum possible error in the calculation. For the photoionization of  $H_2$ , as shown in Fig. 2, the length and velocity forms bracket the experimental results except at the lowest energy. Thus in this case the difference between the length and velocity forms gives a good estimate to the true error in the calculation.

## V. CONCLUSION

In this study we have extended the iterative Schwinger variational method to include electron-molecular ion collisions. For the  $e^- - H_2^+$  system we found rapid convergence of the iterative scheme. The resulting eigenphases are in close agreement with the accurate static-exchange results of Collins and Robb.<sup>10</sup>

We have also shown that the photoionization cross sections obtained using the method presented here agree well with the observed cross sections. The application of the iterative Schwinger method to the photoionization of  $N_2$  and  $CO_2$  is in progress.

## ACKNOWLEDGMENTS

This work was supported by the National Science Foundation under grant number CHE79-15807 and was supported in part by the National Resource for Computation in Chemistry under a grant from the National Science Foundation and the Basic Energy Sciences Division of the United States Department of Energy under Contract No. W-7405-ENG-48. We would like to thank Dr. Derek Robb for many helpful

discussions and for providing us with results prior to publication. One of us (RRL) acknowledges the support of a National Science Foundation Predoctoral Fellowship.

The research reported in this paper made use of the Dreyfus-NSF Theoretical Chemistry Computer which was funded through grants from the Camille and Henry Dreyfus Foundation, the National Science Foundation (Grant No. CHE78-20235), and the Sloan Fund of the California Institute of Technology.

References

\* Contribution No. 6224

<sup>1</sup> See for example, Proceedings of the First Asilomar Conference on Electron-Molecule and Photon-Molecule Collisions, Pacific Grove, CA, August 1-4, 1978, ed. by Thomas Rescigno, Vincent McKoy, and Barry Schneider (Plenum Press, New York, London, 1979).

<sup>2</sup> D. K. Watson and V. McKoy, Phys. Rev. A 20, 1474 (1979).

<sup>3</sup> R. R. Lucchese and V. McKoy, J. Phys. B 12, 421 (1979).

<sup>4</sup> R. R. Lucchese and V. McKoy, Phys. Rev. A 21, 112 (1980).

<sup>5</sup> D. K. Watson, R. R. Lucchese, V. McKoy, and T. N. Rescigno, Phys. Rev. A 21, 738 (1980).

<sup>6</sup> R. R. Lucchese, D. K. Watson, and V. McKoy, "An Iterative Approach to the Schwinger Variational Principle for Electron-Molecule Collisions," Phys. Rev. A (submitted for publication).

<sup>7</sup> For some preliminary results using discrete basis functions, see R. R. Lucchese and V. McKoy, Physica Scripta 21, 366 (1980).

<sup>8</sup> R. R. Lucchese, G. Raseev, and V. McKoy, "Studies of Differential and Total Photoionization Cross Sections of N<sub>2</sub>," (in preparation).

<sup>9</sup> D. K. Watson, V. McKoy, and T. N. Rescigno, "Application of the Schwinger Variational Principle to the Scattering of Electrons by Polar Molecules," (in preparation).

- <sup>10</sup> L. Collins and D. Robb (private communication).
- <sup>11</sup> A. Temkin and K. V. Vasavada, *Phys. Rev.* 160, 109 (1967).
- <sup>12</sup> A. Temkin, K. V. Vasavada, E. S. Chang, and A. Silver, *Phys. Rev.* 186, 57 (1969).
- <sup>13</sup> B. R. Tambe and B. Ritchie, *J. Chem. Phys.* 68, 3595 (1978).
- <sup>14</sup> W. H. Miller, *J. Chem. Phys.* 50, 407 (1969).
- <sup>15</sup> S. K. Adhikari and I. H. Sloan, *Phys. Rev. C* 11, 1133 (1975).
- <sup>16</sup> V. B. Belyaev, A. P. Podkopoyev, J. Wrzecionko, and A. L. Zubarev, *J. Phys. B* 12, 1225 (1979).
- <sup>17</sup> S. Huzinaga, *J. Chem. Phys.* 42, 1293 (1965).
- <sup>18</sup> A. W. Fliflet and V. McKoy, *Phys. Rev. A* 18, 2107 (1978).
- <sup>19</sup> G. R. Cook and P. H. Metzger, *J. Opt. Soc. Am.* 54, 968 (1964).
- <sup>20</sup> J. A. R. Samson and R. B. Cairns, *J. Opt. Soc. Am.* 55, 1035 (1965).
- <sup>21</sup> H. P. Kelly, *Chem. Phys. Lett.* 20, 547 (1973).
- <sup>22</sup> P. H. S. Martin, T. N. Rescigno, V. McKoy, W. H. Henneker  
*Chem. Phys. Lett.* 29, 496 (1974).

TABLE I. Target wave function for  $H_2^+$ .<sup>a</sup>

Type of function <sup>b</sup>	Exponent	Coefficient
<b>s</b>	68.1600	0.00205
s	10.2465	0.01596
s	2.34648	0.07150
s	0.673320	0.25547
s	0.224660	0.27003
s	0.082217	0.00953
<b>s</b>	0.04	0.00988
s	0.02	-0.00342
<b>z</b>	1.35	-0.01710
z	0.45	-0.04320
z	0.15	-0.01389
<b>z</b>	0.05	-0.00095

<sup>a</sup>The first six s type functions are from Ref. 17.

<sup>b</sup>The basis functions are symmetry adapted functions constructed from Cartesian Gaussian functions of the given type.

TABLE II. Scattering basis set.<sup>a</sup>

Type of function for the scattering symmetry <sup>b</sup>				Function Center	Exponent
$\Sigma_g$	$\Sigma_u$	$\Pi_g$	$\Pi_u$		
s	s	x	x	nuclei	1.0
s	s	x	x	nuclei	0.3
z	z	xz	xz	nuclei	1.0
z	z	xz	xz	nuclei	0.3
s	z	xz	x	bond mid-point	1.0

<sup>a</sup>These basis sets correspond to the set R of Eq. (12).

<sup>b</sup>See footnote (b) of Table I.

TABLE III. Converged eigenphase sums for  $\Sigma$  symmetries in  $e^- - H_2^+$  scattering.

Symmetry	Momentum			
	k = 0.2	k = 0.5	k = 1.0	
$^1\Sigma_g$	LM <sup>a</sup>	-0.366	-0.377	-0.352
	CR <sup>b</sup>	-0.363	-0.384	-0.350
$^3\Sigma_g$	LM	0.235	0.238	0.243
	CR	0.230	0.233	--
$^1\Sigma_u$	LM	0.349	0.401	0.519
	CR	0.359	0.412	--
$^3\Sigma_u$	LM	1.408	1.296	1.074
	CR	1.400	1.287	--

<sup>a</sup>Results of the present study.

<sup>b</sup>Results from Ref. 10.

TABLE IV. Converged eigenphase sums for  $\Pi$  symmetries in  $e^-$ - $H_2^+$  scattering.

Symmetry	Momentum			
	$k = 0.2$	$k = 0.5$	$k = 1.0$	
$^1\Pi_g$	LM <sup>a</sup>	0.042	0.042	0.049
	CR <sup>b</sup>	0.045	0.045	0.054
$^3\Pi_g$	LM	0.094	0.122	0.183
	CR	0.097	0.128	0.194
$^1\Pi_u$	LM	-0.344	-0.330	-0.281
	CR	-0.347	-0.331	-0.273
$^3\Pi_u$	LM	0.141	0.137	0.107
	CR	0.154	0.150	0.119

<sup>a</sup> Results of the present study.

<sup>b</sup> Results from Ref. 10.

TABLE V. Convergence of eigenphases using the iterative Schwinger variational method.<sup>a</sup>

Iteration Number	Eigenphase <sup>b</sup>				Sum
	0	2	4	6	
0	-0.497	0.055	-0.000	0.000	-0.443
1	-0.488	0.083	0.019	0.006	-0.379
2	-0.487	0.084	0.019	0.006	-0.377
CR <sup>c</sup>	-0.497	0.088	0.019	0.006	-0.384

<sup>a</sup>The results given are for  $^1\Sigma_g$  scattering in  $e^- - H_2^+$  at  $k = 0.5$  au.

<sup>b</sup>These values of  $l$  correspond to the principal component of the given eigenphase.

<sup>c</sup>Results from Ref. 10.

TABLE VI. Convergence of eigenphase sums and cross sections using the iterative Schwinger variational method to compute photoionization cross sections of  $H_2$ .<sup>a</sup>

Iteration Number	Eigenphase Sum	Length	$\sigma$ (Mb) <sup>b</sup>	Velocity
0	0.181	4.59		2.62
1	0.213	4.62		2.64
2	0.213	4.62		2.64

<sup>a</sup>The results given are for  $^1\Sigma_u$  scattering at  $k = 0.4287$  or  $E = 18.9$  eV.

<sup>b</sup>In megabarns ( $10^{-18}$  cm<sup>2</sup>).

Figure Captions

Fig. 1 Spin averaged elastic DCS for  $e^-$ - $H_2^+$  collisions.

Fig. 2 Total photoionization cross section of  $H_2$  in megabarns: ——— static-exchange dipole length; --- static-exchange dipole velocity;  $\odot$  experimental points from Cook and Metzger (Ref. 19);  $\Delta$  experimental points from Samson and Carins (Ref. 20). The ionization potential for  $H_2$  was taken to be 16.4 eV.

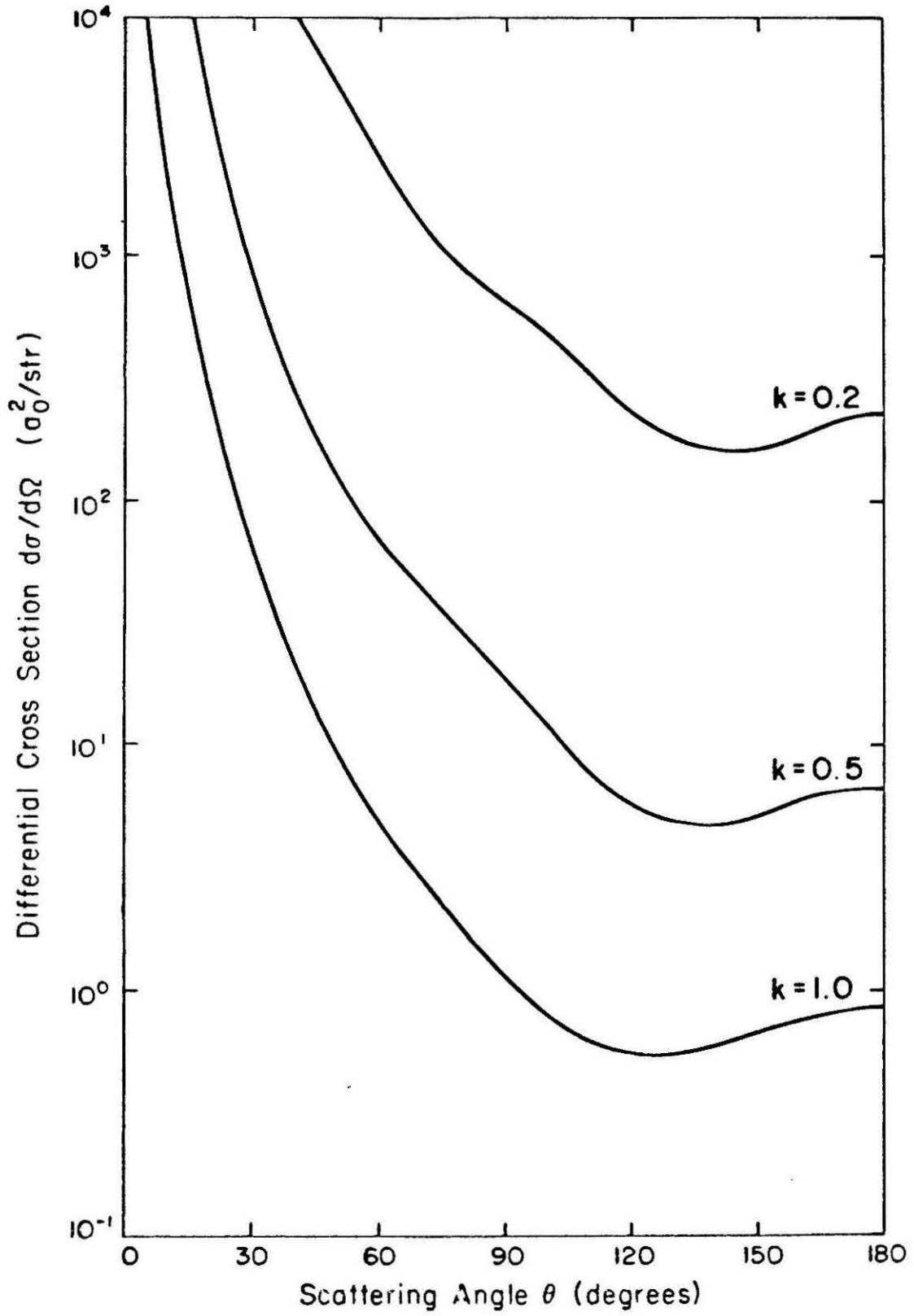


Figure 1

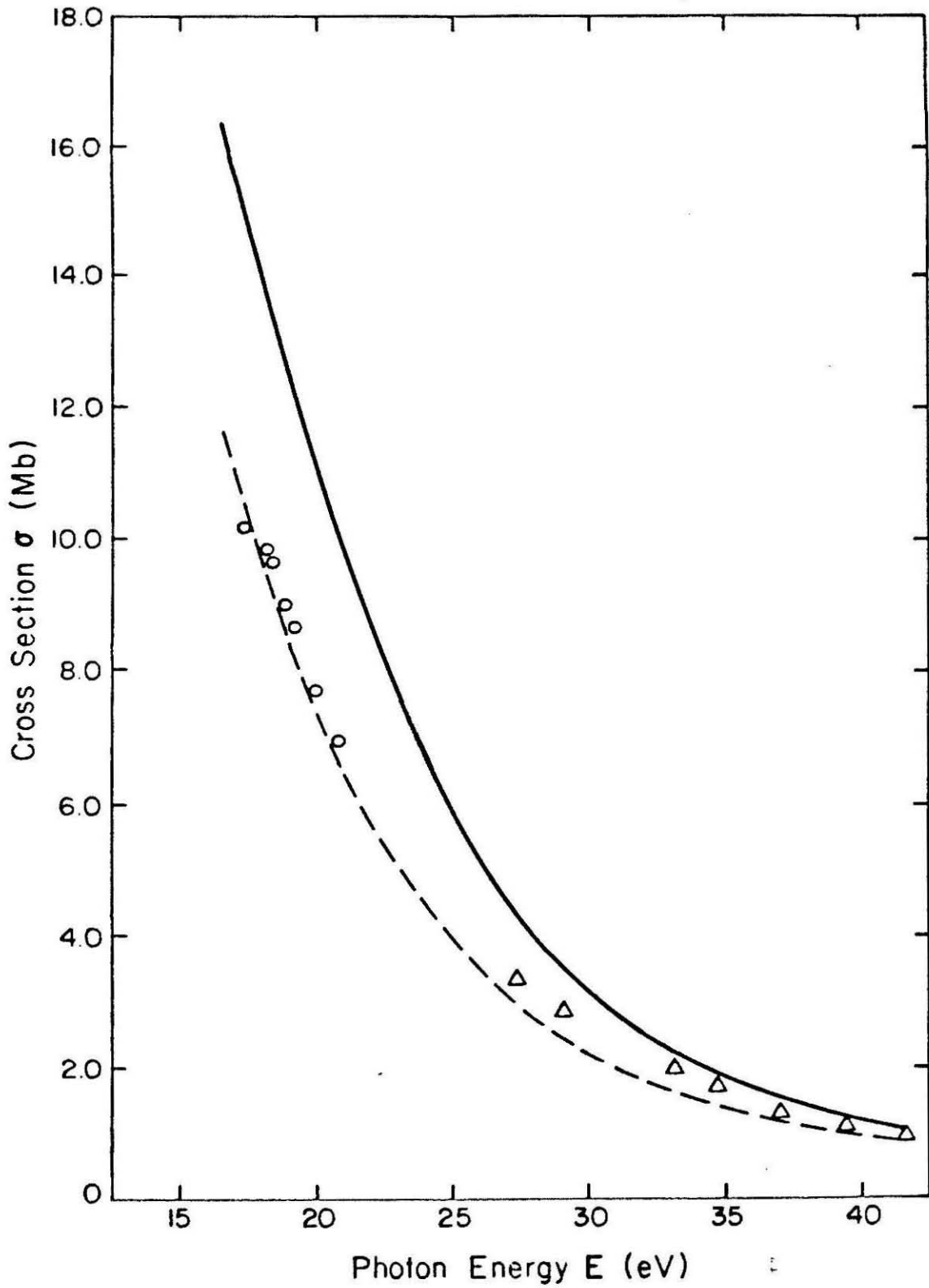


Figure 2

CHAPTER II

Application of the Iterative Schwinger Variational Method  
to Electron-Molecule Scattering

## INTRODUCTION

The efficiency of the iterative Schwinger method discussed in Chapter I allows us to obtain accurate static-exchange results for electron-molecule scattering using converged single-center expansions. This chapter presents the results of a study of e-CO<sub>2</sub> scattering in the static-exchange approximation. Although these results are not expected to compare exactly with experimental results due to neglect of correlation effects, they provide the first accurate ab initio scattering results for the e-CO<sub>2</sub> system. We have compared the present results with those obtained using a model-exchange potential<sup>(1)</sup> and with results obtained using an unconverged single-center expansion method.<sup>(2)</sup> One feature of interest in this system is the  $^2\Pi_u$  shape resonance. Both previous results placed this feature at 8 eV and with a fairly broad width. The present results show that in the static-exchange approximation the resonance lies at 5.39 eV and has a width of 0.64 eV. This indicates that the semi-empirical polarization potential of Morrison et al.<sup>(1)</sup> also corrected for deficiencies in the model-exchange potential as well as including some effects of polarization. We feel that it is important to determine the static-exchange result accurately before attempting to include such polarization effects.

## References

1. M.A. Morrison, N.F. Lane and L.A. Collins, Phys. Rev. A 15, 2186 (1977).
2. B.I. Schneider and L.A. Collins, J. Phys. B 14, L101 (1981).

SECTION A

A Study of Electron Scattering by  $\text{CO}_2$  at the  
Static-Exchange Level

Collisions of low-energy electrons with  $\text{CO}_2$  molecules are of significant experimental and theoretical interest. Morrison *et al.*<sup>1</sup> have studied the scattering of electrons by  $\text{CO}_2$  in the energy range 0.07-10.0 eV. In these studies, exchange and polarization effects in the scattering potential were approximated by a local energy-dependent potential and a semi-empirical polarization potential respectively. The coupled radial equations resulting from the partial wave expansions of the wave function of the scattered electron and the potential were numerically integrated. Dill *et al.*<sup>2</sup> have used the continuum multiple scattering model to study the scattering of electrons by  $\text{CO}_2$ . The emphasis of these studies was the role of shape resonances in the enhancement of vibrational excitation at intermediate energies in electron-molecule scattering. Among several approximations for the scattering potential the continuum multiple scattering model also uses a local exchange approximation. Onda and Truhlar<sup>3</sup> have also reported differential and integral cross sections for electron- $\text{CO}_2$  elastic scattering at 20 eV. These studies used a semi-empirical scattering potential.

In this paper we present the results of studies of the scattering of low-energy electrons by  $\text{CO}_2$  in the static-exchange approximation. These studies were done with the iterative Schwinger variational method which we have recently developed for studying electron-molecule and electron-molecular ion collisions. Although these studies neglect the effects of polarization, we believe that it is important to determine the converged scattering solutions for the  $e^- - \text{CO}_2$  system at the static-exchange level. These static-exchange results are not only useful in

several applications, such as in the calculation of vibrational excitation cross sections at energies where polarization effects are not dominant, and of electronic excitation cross sections, but they are also needed in order to realistically assess approximate schemes such as the local exchange approximation. It has also been shown that the static-exchange approximation with an appropriately distorted charge density derived from the negative ion wave function can provide reliable resonance vibrational excitation cross sections.<sup>4,5</sup>

In the next section we give a very brief outline of the method used in these studies. In Section III we present the  ${}^2\Sigma_g$ ,  ${}^2\Sigma_u$ ,  ${}^2\Pi_u$ , and  ${}^2\Pi_g$  eigenphases at incident momenta of 0.1, 0.3, 0.5, 0.7, 0.8573, and 1.0. All the required matrix elements were evaluated with the use of single-center partial wave expansions. In these studies of e-CO<sub>2</sub> scattering with its highly anisotropic interaction we have carried out the single-center expansions to high  $l$  values to assure that our results are converged. The eigenphase sums for the resonant  ${}^2\Pi_u$  channel are of particular importance in this regard. The parameters for this  ${}^2\Pi_u$  resonance extracted from our eigenphase sums are 0.64 eV for the width and 5.39 eV for the position. We also compare our calculated cross sections with measured elastic scattering cross sections.

## II. THEORY

In these studies we use the iterative Schwinger variational method to solve the collision equations for the e-CO<sub>2</sub> system. Briefly, the iterative Schwinger variational method<sup>6</sup> is a method to solve the partial wave Lippmann-Schwinger equation

$$\psi_{k\ell m}^{(+)} = \phi_{k\ell m} + G^{(+)}(E)U\psi_{k\ell m}^{(+)} \quad (1)$$

where  $\phi_{k\ell m}$  is a component of the incident plane wave,  $G^{(+)}$  the Green's function with outgoing wave boundary conditions, and  $U = 2V$  with  $V$  the effective interaction between the target and the scattered electron. The partial wave component of the total scattering wave function is defined by

$$\Psi_{\underline{k}}^{(+)} = \left(\frac{2}{\pi}\right)^{1/2} \sum_{\ell m} i^{\ell} \psi_{k\ell m}^{(+)}(\underline{r}) Y_{\ell m}^*(\Omega_{\hat{k}}) \quad (2)$$

The Schwinger variational expression for the partial wave elastic T matrix elements can be written as<sup>7</sup>

$$\tilde{T}_{\ell\ell'm} = \frac{\langle \phi_{k\ell m} | U | \tilde{\psi}_{k\ell'm}^{(+)} \rangle \langle \tilde{\psi}_{k\ell'm}^{(-)} | U | \phi_{k\ell'm} \rangle}{\langle \tilde{\psi}_{k\ell'm}^{(-)} | U - UG^{(+)}U | \tilde{\psi}_{k\ell'm}^{(+)} \rangle} \quad (3)$$

where  $\tilde{\psi}_{k\ell m}$  is a trial scattering function and we have assumed the molecule to be linear. Expansion of the trial scattering function in basis functions and variation of the linear expansion coefficients give the stationary result

$$T_{\ell\ell'm}^{S_0} = \sum_{\alpha_i, \alpha_j}^N \langle \phi_{k\ell m} | U | \alpha_i \rangle [(D^{(+)})^{-1}]_{ij} \langle \alpha_j | U | \phi_{k\ell'm} \rangle \quad (4)$$

where the  $\alpha$ 's are the expansion functions and

$$D_{ij}^{(+)} = \langle \alpha_i | U - UG^{(+)}U | \alpha_j \rangle \quad (5)$$

As is well-known, the T-matrix of Eq. (4) is equivalent to solving the Lippmann-Schwinger equation, Eq. (1), with a separable potential of the form

$$U^S(\underline{r}, \underline{r}') = \sum_{\alpha_i, \alpha_j} \langle \underline{r} | U | \alpha_i \rangle (U^{-1})_{ij} \langle \alpha_j | U | \underline{r}' \rangle \quad (6)$$

where the matrix of  $(U^{-1})_{ij}$  is the inverse of the potential matrix  $U_{ij}$ . The corresponding approximate scattering solution of Eq. (1) is then

$$\psi_{klm}^{S_0}(\underline{r}) = \phi_{klm}(\underline{r}) + \sum_{\alpha_i, \alpha_j} \langle \underline{r} | G^{(+)} U | \alpha_i \rangle (D^{-1})_{ij} \langle \alpha_j | U | \phi_{klm} \rangle. \quad (7)$$

At this point we have obtained an approximate noniterative solution to the scattering equations. We have developed a method to iteratively improve the scattering function in Eq. (7).<sup>6</sup> As noted by Ernst et al.,<sup>8</sup> if the expansion set used in Eqs. (6) and (7) contained the exact solution, then the solution given back by Eq. (7) would again be the exact solution. Then our iterative method proceeds by augmenting the expansion set used in Eq. (6) by including the approximate solutions  $\psi_{klm}^{S_0}(\underline{r})$ . Equation (7) will then yield a new and probably improved solution,  $\psi_{klm}^{S_1}$ , to Eq. (1). The next iteration proceeds in a similar fashion by replacing the solutions  $\psi_{klm}^{S_0}$  in the expansion sets by those of the first iteration,  $\psi_{klm}^{S_1}$ . This new expansion set then yields a new set of approximate solutions  $\psi_{klm}^{S_2}$ . This procedure can be continued until convergence. Various criteria can be developed to establish when the

exact solutions to the scattering equations have been obtained.<sup>6</sup>

### III. RESULTS AND DISCUSSION

We have applied the Schwinger variational method in its iterative form to study the scattering of low-energy electrons by CO<sub>2</sub>. For the scattering potential we use the static-exchange approximation which was obtained from an SCF calculation in a [3s2p1d] contracted Cartesian Gaussian basis.<sup>9</sup> The SCF energy for CO<sub>2</sub> in this basis is -187.674286 a. u. and the quadrupole moment is -4.013 a. u. for a C-O bond distance of 2.1944 a. u.

We have carried out calculations for the  ${}^2\Sigma_g$ ,  ${}^2\Sigma_u$ ,  ${}^2\Pi_u$ , and  ${}^2\Pi_g$  eigenphases. The expansion functions used to construct the separable approximation to the scattering potential, Eq. (6), in the initial step of the iterative procedure are spherical Gaussian functions defined by

$$\phi_{\ell m}^{\alpha}(\underline{r}) = N_{\ell m}^{\alpha} |\underline{r} - \underline{A}|^{\ell} e^{-\alpha |\underline{r} - \underline{A}|^2} Y_{\ell m}(\Omega_{\underline{r} - \underline{A}}). \quad (8)$$

The spherical Gaussians as defined in Eq. (8), can be expanded onto a different center by taking linear combinations of expansions of the appropriate Cartesian Gaussian functions.<sup>10</sup> However, for spherical Gaussian functions with larger values of  $\ell$ , the required expressions can be more easily obtained by noting that a spherical Gaussian is the product of a simple s-type Gaussian function and a solution to Laplace's equation, both of which have simple expressions for their expansion about another center.<sup>10, 11</sup> The basis sets for the different symmetries are given in Table I. The total number of basis functions

for the  ${}^2\Sigma_g$ ,  ${}^2\Sigma_u$ ,  ${}^2\Pi_u$ , and  ${}^2\Pi_g$  symmetries are 30, 24, 19, and 19 respectively. All matrix elements were evaluated with the use of single-center expansions and Simpson's rule quadrature for the radial integrals. The grid for the quadrature contained 1000 points and extended out to 80  $a_0$ . In the static potential partial waves through  $\ell = 59$  were retained while in the expansion of the occupied orbitals in the exchange kernel we used enough partial waves so that each orbital was normalized to better than 0.99. For the  $1\sigma_g$ ,  $2\sigma_g$ ,  $3\sigma_g$ , and  $4\sigma_g$  orbitals this required  $\ell$  values up to 38, 10, 24, and 16 respectively and  $\ell$  values up to 39, 23, 15, 15, and 16 for the  $1\sigma_u$ ,  $2\sigma_u$ ,  $3\sigma_u$ ,  $1\pi_u$ , and  $1\pi_g$  orbitals respectively in the exchange kernel. In the expansion of  $1/r_{12}$  we retained partial waves up to  $\ell = 108$  in the direct potential and up to 40 in the exchange potential. The maximum partial wave retained in the expansion of all other functions in the calculation, e. g., in  $\tilde{\psi}$ ,  $V\tilde{\psi}$ , and  $G V\tilde{\psi}$ , was  $\ell = 59$ .

In Tables II-V we show the eigenphases and eigenphase sums at  $k = 0.1, 0.3, 0.5, 0.7, 0.8573$  and  $1.0$  for the  ${}^2\Sigma_g$ ,  ${}^2\Sigma_u$ ,  ${}^2\Pi_u$  and  ${}^2\Pi_g$  channels. These eigenphases were obtained from the second iteration of our iterative procedure and are quite well converged. We have chosen to show these results in tabular form since in this form they will be more useful for comparison with results of other approaches to the solution of the scattering equations or with the results of model calculations. To our knowledge the only other published eigenphases for e-CO<sub>2</sub> scattering in this energy range are those of the multiple scattering model by Dill et al.<sup>2</sup> We do not compare the present static-exchange eigenphase sums with their results in any detail since their actual numerical values are not given.<sup>2</sup> However, several qualitative features of our results

agree with theirs. For example, the increase in our  $\sigma_g$  eigenphase sum at around  $k = 1.0$  clearly also locates a high energy shape resonance in this channel. The eigenphases of Table II show that the resonance contains a strong mixture of s, d, and g waves. The resonant behavior in the  ${}^2\Pi_u$  eigenphase sum is due to the well-known shape resonance in the e-CO<sub>2</sub> system. A simple fit of the eigenphase sums to a Breit-Wigner form including a background term gives a resonance position of 5.39 eV and a width of 0.64 eV. Experimentally<sup>12</sup> this shape resonance occurs at around 3.8 eV. This difference of about 1.6 eV between the position of this resonance in the static-exchange model and its actual location is obviously due to polarization effects. A difference of this magnitude is quite consistent with the results of similar studies of shape resonances in the e-N<sub>2</sub> and e-CO systems.<sup>12, 13, 14</sup> The multiple scattering model<sup>2</sup> predicts a resonance position of 3.4 eV in this  ${}^2\Pi_u$  channel.

In Fig. 1 we compare our calculated total elastic scattering cross sections with those calculated with a local model exchange potential by Morrison et al.<sup>1</sup> A comparison of these cross sections shows that with this local exchange approximation the  ${}^2\Pi_u$  shape resonance comes out at about 8 eV which is about 3 eV higher than our calculated position of 5.39 eV. A semi-empirical polarization potential with a single adjustable parameter was then added to this local exchange potential so as to move this shape resonance down to its experimental location of 3.8 eV. The present results, in which the  ${}^2\Pi_u$  resonance is seen to be at around 5.4 eV at the static-exchange level, show that polarization effects have been overestimated in the semi-empirical potential as used by Morrison et al.<sup>1</sup> Figure 1 also shows that the magnitude and shape of

the total elastic cross section obtained with the local exchange approximation<sup>1</sup> are quite different from the present calculated static-exchange values. To obtain the total elastic cross sections shown in Fig. 1 we added first-Born estimates for the  ${}^2\Delta_g$  and  ${}^2\Delta_u$  symmetries to the actual static-exchange contributions for the  ${}^2\Sigma_g$ ,  ${}^2\Sigma_u$ ,  ${}^2\Pi_u$ , and  ${}^2\Pi_g$  channels. For comparison we also show in Fig. 1 measured values of the total elastic cross sections.<sup>15, 16</sup>

In Fig. 2 we show the elastic differential cross sections for the scattering of 10 eV electrons by  $\text{CO}_2$ . These static-exchange cross sections agree quite well with the recent measured values of Register *et al.*<sup>16</sup>

Recently Schneider and Collins<sup>17</sup> reported some results from their preliminary static-exchange calculations for electron scattering by  $\text{CO}_2$ . Specifically they report the  ${}^2\Pi_u$  resonance at 8.2 eV with a width of 2 eV. They<sup>17</sup> also indicate that these results are converged to about 15%. These results differ significantly from our calculated position of 5.39 eV and a width of 0.64 eV. To try to understand these calculated positions and widths for this resonance we have repeated our calculation with a reduced number of partial waves in the various expansions in the evaluation of the matrix elements of Eq. (4). Specifically, the maximum partial wave retained in the expansion of any function in Eq. (4) was reduced from 59 to 27 while only partial waves up to 54 were retained in the expansion of  $\frac{1}{r_{12}}$  in the direct potential. In the expansion of the occupied orbitals in the exchange potential we retained partial waves up to 4, 5, 5, and 6 for the  $\sigma_g$ ,  $\sigma_u$ ,  $\pi_u$ , and  $\pi_g$  orbitals respectively. In the expansion of the continuum orbital in the exchange potential we retained partial waves up to  $l = 5$ . With these reduced

partial wave expansions we obtained eigenphase sums which give a resonance position of 7.33 eV and a width of 1.47 eV. This change of about 2 eV and 0.83 eV in the position and width of the resonance respectively due to the reduction in the partial wave expansions suggest that the results of Schneider and Collins<sup>17</sup> may not be adequately converged. We also note that Čadež *et al.*<sup>18</sup> found that with a value of 0.31 eV for the width of this resonance at the ground state equilibrium geometry in the boomerang model<sup>19</sup> they could accurately describe the observed resonant vibrational excitation cross sections at 4 eV impact. A static-exchange value of 0.64 eV for the width of the resonance seems quite consistent with their assumed value of 0.31 eV since one expects polarization effects to reduce the static-exchange width by about a factor of 2, e. g., in the e-N<sub>2</sub> system.<sup>5</sup> Calculations which include such polarization effects in e-CO<sub>2</sub> collisions are under way.

#### ACKNOWLEDGMENTS

This research is based upon work supported by the National Science Foundation under Grant No. CHE79-15807. One of us (R. R. L) acknowledges support from an Exxon Educational Foundation Fellowship. The research reported in this paper made use of the Dreyfus-NSF Theoretical Chemistry Computer which was funded through grants from the Camille and Henry Dreyfus Foundation, the National Science Foundation (Grant No. CHE78-20235), and the Sloan Fund of the California Institute of Technology. This research was also supported in part by an Institutional Grant from the United States Department of Energy, No. EY-76-G-03-1305.

References

- <sup>1</sup>M. A. Morrison, N. F. Lane, and L. A. Collins, *Phys. Rev. A* 15, 2186 (1977).
- <sup>2</sup>D. Dill, J. Welch, J. L. Dehmer, and J. Siegel, *Phys. Rev. Lett.* 43, 1236 (1979).
- <sup>3</sup>K. Onda and D. G. Truhlar, *J. Phys. B* 12, 283 (1979).
- <sup>4</sup>B. I. Schneider, M. Le Dourneuf, and Vo Ky Lan, *Phys. Rev. Lett.* 43, 1926 (1979).
- <sup>5</sup>A. U. Hazi, T. N. Rescigno, and M. Kurilla, *Phys. Rev. A* 23, 1089 (1981).
- <sup>6</sup>R. R. Lucchese, D. K. Watson, and V. McKoy, *Phys. Rev. A* 22, 421 (1980).
- <sup>7</sup>R. G. Newton, Scattering Theory of Waves and Particles (McGraw-Hill, New York, 1966), p. 319.
- <sup>8</sup>D. J. Ernst, C. M. Shakin, and R. M. Thaler, *Phys. Rev. C* 8, 46 (1973).
- <sup>9</sup>T. H. Dunning, Jr. and P. J. Hay, "Gaussian Basis Sets for Molecular Calculations" in Methods of Electronic Structure Theory, ed. H. F. Shaefer III (Plenum, New York, 1977), p. 1.
- <sup>10</sup>A. W. Fliflet and V. McKoy, *Phys. Rev. A* 18, 1048 (1978).

- <sup>11</sup> P. M. Morse and H. Feshbach, Methods of Theoretical Physics, Part II (McGraw-Hill, New York, 1953), p. 1271.
- <sup>12</sup> G. J. Schulz, *Rev. Mod. Phys.* 45, 378 (1973).
- <sup>13</sup> A. W. Fliflet, D. A. Levin, M. Ma, and V. McKoy, *Phys. Rev. A* 17, 160 (1978).
- <sup>14</sup> D. A. Levin, A. W. Fliflet, and V. McKoy, *Phys. Rev. A* 21, 1202 (1980).
- <sup>15</sup> T. W. Shyn, W. E. Sharp, and G. R. Carignan, *Phys. Rev. A* 17, 1855 (1978).
- <sup>16</sup> D. F. Register, H. Nishimura, S. Trajmar, *J. Phys. B* 13, 1651 (1980).
- <sup>17</sup> B. I. Schneider and L. A. Collins, *J. Phys. B* 14, L101 (1981).
- <sup>18</sup> I. Čadež, F. Gresteau, M. Tronc, and R. I. Hall, *J. Phys. B* 10, 3821 (1977).
- <sup>19</sup> D. Birtwistle and A. Herzenberg, *J. Phys. B* 4, 53 (1971).

TABLE I. Basis sets used in the initial step of the iterative procedure.<sup>a</sup>

${}^2\Sigma_g$ symmetry					${}^2\Sigma_u$ symmetry				
Number of Functions <sup>b</sup>	Center	$l$	$m$	Range of Exponent	Number of Functions	Center	$l$	$m$	Range of Exponent
6	O	0	0	8.0-0.25	6	O	0	0	8.0-0.25
4	O	1	0	2.0-0.25	4	O	1	0	2.0-0.25
3	O	2	0	1.0-0.25	1	O	2	0	0.5
2	O	3	0	1.0-0.5	5	C	1	0	8.0-0.5
1	O	4	0	0.5	4	C	3	0	2.0-0.25
6	C	0	0	8.0-0.25	3	C	5	0	2.0-0.5
4	C	2	0	2.0-0.25	1	C	7	0	1.0
3	C	4	0	2.0-0.5					
1	C	6	0	1.0					
${}^2\Pi_u$ symmetry					${}^2\Pi_g$ symmetry				
5	O	1	1	4.0-0.25	5	O	1	1	4.0-0.25
4	O	2	1	2.0-0.25	4	O	2	1	2.0-0.25
5	C	1	1	4.0-0.25	5	C	2	1	4.0-0.25
4	C	3	1	2.0-0.25	4	C	4	1	2.0-0.25
1	C	5	1	0.5	1	C	6	1	0.5

<sup>a</sup>See Eq. (8).

<sup>b</sup>Total number of basis functions on a given center with the same value of  $l$  and  $m$ . The exponents of the basis functions form a geometric series with a ratio of 2.0.

TABLE II.  $^2\Sigma_g$  eigenphases and eigenphase sums for e-CO<sub>2</sub> collisions.

$k^a$	$\delta_{\text{sum}}^b$	$\ell_{\text{max}}^c$	$\delta_0^d$	$\delta_2$	$\delta_4$	$\delta_6$	$\delta_8$	$\delta_{10}$
0.1	-0.15	10	-0.14	-0.01				
0.3	-0.47	24	-0.40	-0.04	-0.01	-0.01		
0.5	-0.76	38	-0.60	-0.10	-0.03	-0.01	-0.01	
0.7	-1.08	52	-0.71	-0.29	-0.03	-0.02	-0.01	-0.01
0.8573	-1.18	58	-0.46	-0.67	0.02	-0.03	-0.01	-0.01
1.0 <sup>e</sup>	-0.88	58	-0.29	-0.82	0.31	-0.03	-0.01	-0.01

<sup>a</sup>Incident momentum in a. u.

<sup>b</sup>Eigenphase sum.

<sup>c</sup>Dimensionality of the partial wave K-matrix used.

<sup>d</sup> $\delta_\ell$  is the eigenphase whose principal partial wave component is  $\ell$ .

<sup>e</sup>Convergence not complete. This eigenphase sum could be in error by  $\pm 0.01$  radians.

TABLE III.  $\Sigma_u^2$  eigenphases and eigenphase sums for e-CO<sub>2</sub> collisions.<sup>a</sup>

k	$\delta_{\text{sum}}$	$\ell_{\text{max}}$	$\delta_1$	$\delta_3$	$\delta_5$	$\delta_7$	$\delta_9$	$\delta_{11}$
0.1	-0.088	9	-0.078	-0.009				
0.3	-0.35	23	-0.30	-0.03	-0.01			
0.5	-0.71	39	-0.63	-0.04	-0.02	-0.01		
0.7	-1.08	53	-0.99	-0.04	-0.02	-0.01	-0.01	
0.8573	-1.34	59	-1.25	-0.04	-0.02	-0.01	-0.01	
1.0	-1.55	59	-1.45	-0.02	-0.03	-0.02	-0.01	-0.01

<sup>a</sup>See footnotes for Table II.

TABLE IV.  $^2\Pi_u$  eigenphases and eigenphase sums for e-CO<sub>2</sub> collisions.<sup>a</sup>

k	$\delta_{\text{sum}}$	$l_{\text{max}}$	$\delta_1$	$\delta_3$	$\delta_5$	$\delta_7$	$\delta_9$	$\delta_{11}$
0.1	0.027	9	0.037	-0.009	-0.002	0.001		
0.3	-0.036	23	0.020	-0.034	-0.011	-0.005	-0.003	-0.002
0.5	-0.20	39	-0.18	0.03	-0.02	-0.01	-0.01	
0.5745	-0.13	45	-0.25	0.18	-0.02	-0.01	-0.01	
0.6083	0.24	47	-0.28	0.58	-0.02	-0.01	-0.01	
0.6403	1.59	49	-0.31	1.96	-0.02	-0.01	-0.01	
0.6708	2.12	51	-0.33	2.50	-0.02	-0.01	-0.01	
0.7	2.22	53	-0.53	2.82	-0.02	-0.01	-0.01	
0.8573	2.12	59	-0.62	2.82	-0.03	-0.01	-0.01	-0.01
1.0	1.92	59	-0.77	2.77	-0.03	-0.02	-0.01	-0.01

<sup>a</sup>See footnotes for Table II.

TABLE V.  $^2\Pi_g$  eigenphases and eigenphase sums for e-CO<sub>2</sub> collisions.<sup>a</sup>

k	$\delta_{\text{sum}}$	$l_{\text{max}}$	$\delta_2$	$\delta_4$	$\delta_6$	$\delta_8$	$\delta_{10}$	$\delta_{12}$
0.1	-0.014	10	-0.012	-0.003	0.001			
0.3	-0.065	24	-0.040	-0.012	-0.006	-0.003	-0.002	-0.001
0.5	-0.16	38	-0.11	-0.02	-0.01	-0.01		
0.7	-0.32	52	-0.25	-0.03	-0.01	-0.01	-0.01	
0.8573	-0.47	58	-0.39	-0.03	-0.01	-0.01	-0.01	
1.0	-0.59	58	-0.53	0.02	-0.03	-0.01	-0.01	-0.01

<sup>a</sup>See footnotes for Table II.

Fig. 1 Total elastic cross section for e-CO<sub>2</sub> scattering: —○— exact static exchange results of present study; ---●--- static plus model exchange from Ref. 1; □ experimental data from Ref. 15; Δ experimental data from Ref. 16.

Fig. 2 Elastic differential cross section for scattering 10 eV electrons by CO<sub>2</sub>: ————— exact static exchange results of present study; Δ experimental data from Ref. 16, (Δ) indicates an extrapolated value.

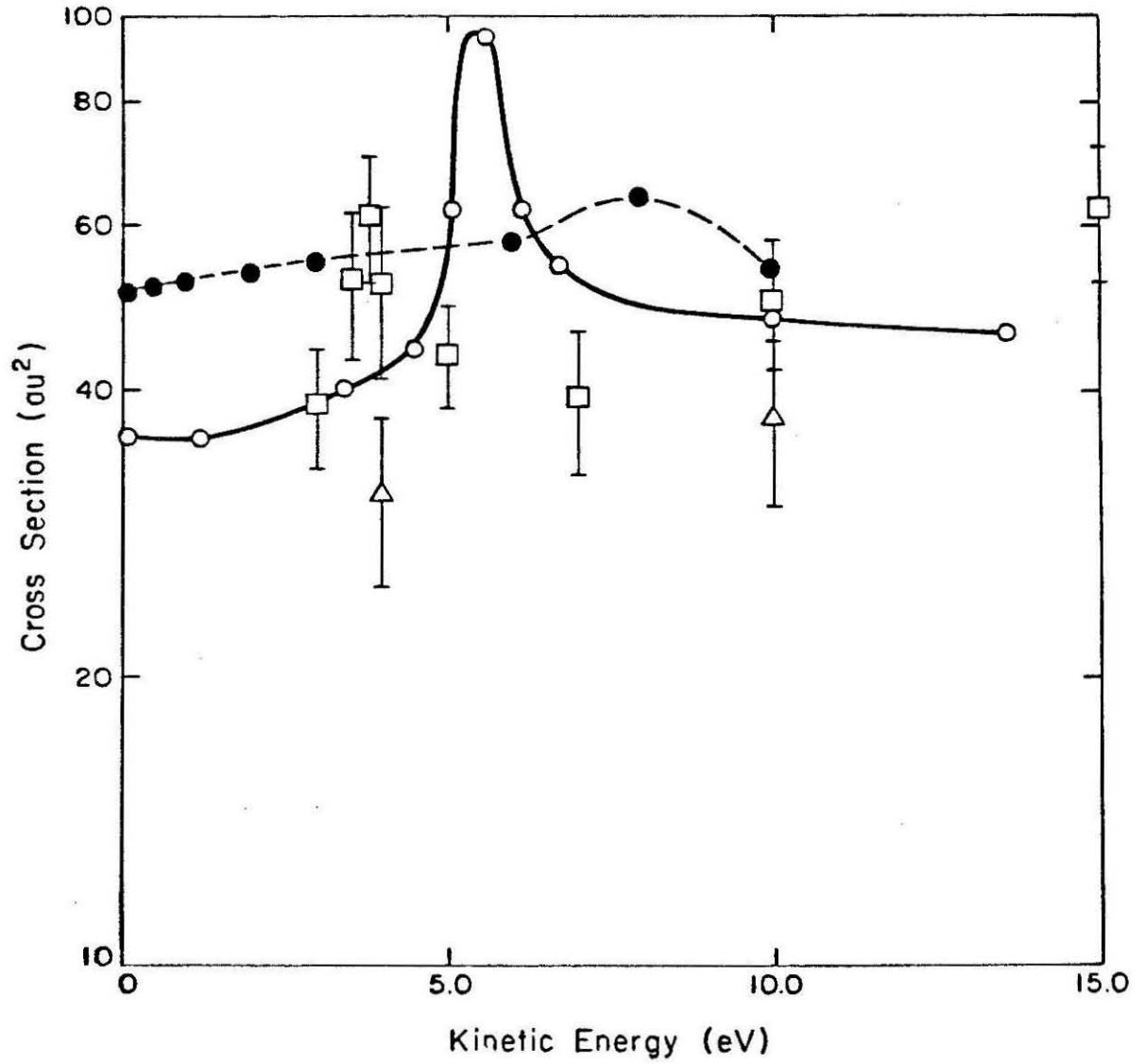


Fig. 1

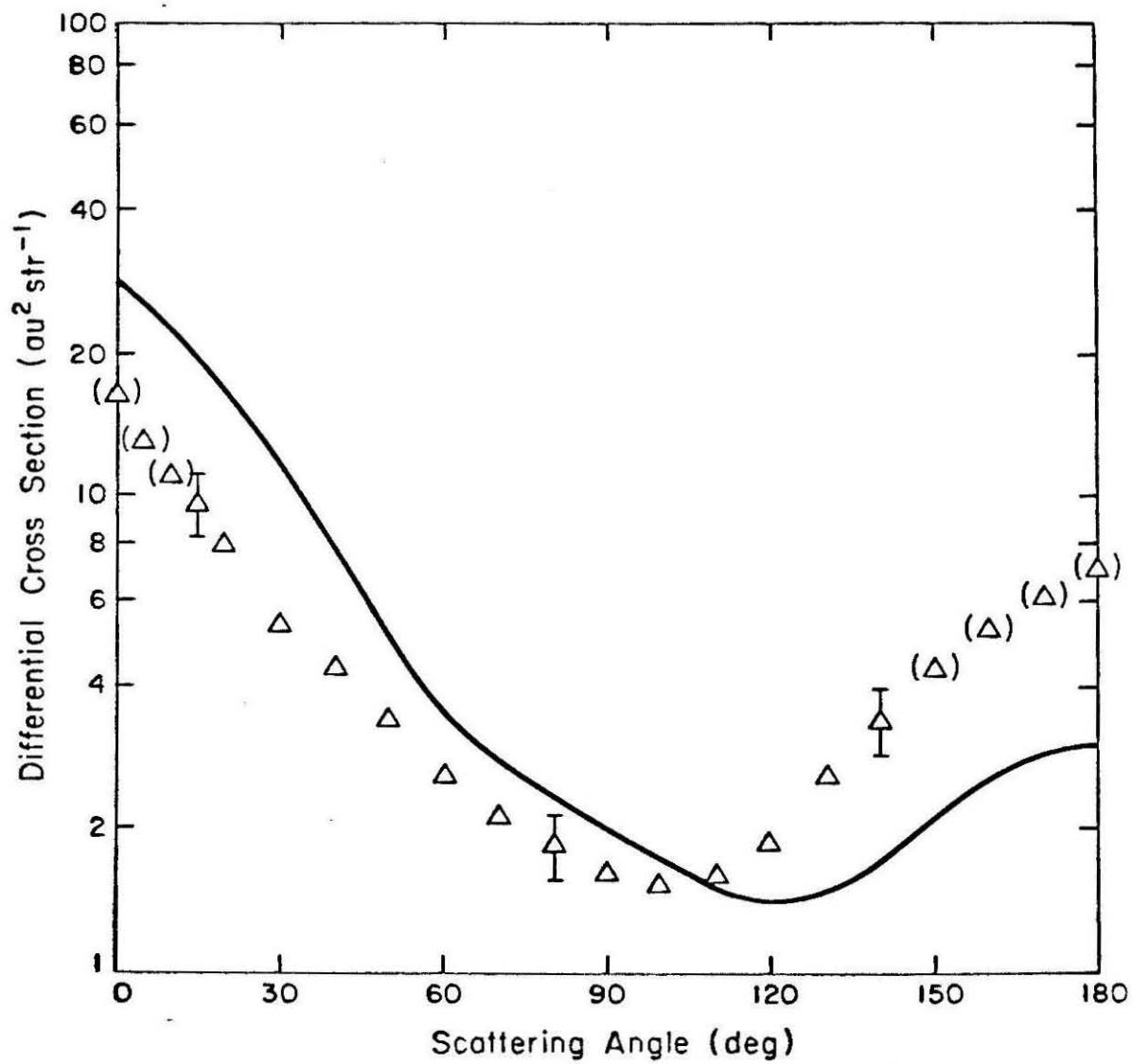


Fig. 2

CHAPTER III

Application of the Iterative Schwinger Variational Method  
to Molecular Photoionization

## INTRODUCTION

In this chapter we give the results of the iterative Schwinger variational method applied to molecular photoionization of  $N_2$  and  $CO_2$ . As in our discussion of electron-molecule scattering in Chapter II, one of the interesting features of molecular photoionization is the appearance of shape resonances. Shape resonances appear prominently in the photoionization of both  $N_2$  and  $CO_2$ . Such resonances can lead to enhanced total photoionization cross sections as well as non-Franck-Condon vibrational effects and rapidly changing photoelectron angular differential cross sections.

We make detailed comparisons of our computed total and differential photoionization cross sections of  $N_2$  and  $CO_2$  with available experimental data and with the results of other theoretical methods. In general we find that the Frozen-Core Hartree-Fock (FCHF) model of photoionization used here represents the valence shell photoionization cross sections of  $N_2$  and  $CO_2$  very well. We also have found that inclusion of initial-state correlation effects can be important in obtaining quantitative agreement with experimental results. We have compared our cross sections to the theoretical results given by the Continuum Multiple Scattering Method (CMSM) and by the Stieltjes-Tchebycheff Moment Theory (STMT) approach for molecular photoionization in the FCHF approximation.<sup>(1)</sup> These two methods are the only other methods, besides the Schwinger approach presented here, which have been used to obtain

the photoionization cross sections of  $N_2$  and  $CO_2$  for the valence shell level.<sup>(2)</sup> We find that the CMSM cross sections generally reproduced all of the qualitative features obtained in the Schwinger results but the quantitative results of the CMSM method were sometimes in error by more than a factor of 2. The STMT method is found to give reasonable absolute values for the photoionization cross sections but this method does not reliably reproduce effects due to shape resonances. The CMSM method obtains exact scattering solutions but of a highly simplified model potential which is used to represent the static-exchange interactions. The STMT method on the other hand uses the exact static-exchange interactions but does not explicitly solve the scattering equations.

The development of the iterative Schwinger method has allowed us to directly solve the scattering equations using the correct static-exchange potential, with a reasonable computational effort. The cross sections given by the iterative Schwinger method allow us to interpret reliably experimental results using the FCHF model without uncertainty concerning the accuracy of the computed cross sections.

In Section A of this chapter, we give results for the valence photoionization of  $N_2$  in the fixed-nuclei approximation. Section B gives vibrational branching ratios for the resonant photoionization channel of  $N_2$  leading to the  $X^2\Sigma_g^+$  state of  $N_2^+$ . In Section C we give a detailed comparison of the results of the STMT, CMSM and Schwinger methods for the photoionization of  $CO_2$  leading to the  $C^2\Sigma_g^+$  state of  $CO_2^+$ . In Section D we give

the results for valence and K-shell photoionization cross sections of  $\text{CO}_2$  in the fixed-nuclei approximation. In Section E we examine the effects of vibrational averaging on the photoionization cross section (both total and differential) leading to the  $\text{C}^2\Sigma_g^+$  state of  $\text{CO}_2^+$ .

## References

1. For a general discussion of the CMSM and STMT methods see chapters by J.L. Dehmer and D. Dill and by P.W. Langhoff in, Electron-Molecule and Photon-Molecule Collisions, ed. T. Rescigno, V. McKoy and B. Schneider, Plenum Press, New York (1979).
2. The only other studies at the FCHF level are of one channel in  $N_2$  photoionization by G. Rasee, V.H. LeRovzo and H. Lefebvre-Brion, J. Chem. Phys. 72, 5701 (1980), and by W.D. Robb and L.A. Collins, Phys. Rev. A 22, 2474 (1981). Both of these studies used single-center techniques and neither study was well converged.

SECTION A

Studies of Differential and Total Photoionization  
Cross Sections of Molecular Nitrogen

## I. INTRODUCTION

The photoionization of molecular systems is a topic of much current theoretical interest.<sup>1</sup> As a prototypical system, the photoionization of molecular nitrogen has been studied using several different methods including the Continuum Multiple Scattering Method (CMSM),<sup>2</sup> the Stieltjes-Tchebycheff Moment Theory approach (STMT), both in the Hartree-Fock (HF) approximation<sup>3,4</sup> and the Random-Phase Approximation with Exchange (RPAE),<sup>5</sup> and several numerical single-center expansion methods.<sup>6</sup> The single-center expansion methods applied to the photoionization of molecular nitrogen have treated the interaction potential in several different ways. There have been static and static-plus-orthogonalization calculations,<sup>7</sup> static-plus-model-exchange calculations,<sup>8</sup> and exact static-exchange calculations.<sup>9,10</sup> Most previous studies have attempted to obtain the continuum solution for the final state using the Frozen-Core Hartree-Fock (FCHF) approximation.<sup>9</sup> The present study is directed at obtaining accurate and converged FCHF solutions for the final-state wave function, using the body-fixed frame, fixed nuclei approach.<sup>6</sup> We compare our results with some of the other theoretical results mentioned above and with the experimental results of continuous source experiments by Plummer *et al.*<sup>11</sup> and Marr *et al.*<sup>12</sup> using synchrotron radiation, and by Hamnett *et al.*<sup>13</sup> and Wight *et al.*<sup>14</sup> obtained using an (e, 2e) technique.

We have considered the photoionization leading to the  $X^2\Sigma_g^+$ ,  $A^2\Pi_u$ , and  $B^2\Sigma_u^+$  states of  $N_2^+$ . Both total and partial photoionization cross

sections and angular distributions for these states are reported. Following the suggestion of Wallace and Dill,<sup>15</sup> we give both the asymmetry parameter for the usual Integrated Target Angular Distribution (ITAD), denoted here by  $\beta_{\hat{k}}$ , and the Integrated Detector Angular Distribution (IDAD), denoted by  $\beta_{\hat{n}}$ . In combination with accurate FCHF final-state wave functions, we have considered the effect of initial-state correlation by comparing the results obtained using both HF and Configuration Interaction (CI) type initial-state wave functions. The difference between the dipole length and dipole velocity forms of the cross sections is used to estimate the remaining final state correlation effects.

We solve the static-exchange continuum equations using the iterative Schwinger method.<sup>16,17</sup> This method is essentially a single-center expansion technique comparable to the methods used by Raseev *et al.*<sup>9</sup> and Robb and Collins.<sup>10</sup> The iterative Schwinger method has been earlier applied to the photoionization of  $H_2$  and  $CO_2$ ,<sup>18,19</sup> as well as to electron-molecule collisions for the  $e-H_2$ ,  $e-LiH$  and  $e-CO_2$  systems.<sup>16,20,21</sup> We find in this study of the photoionization of  $N_2$  that the iterative Schwinger method converges rapidly.

The present results are compared with the results of other single-center expansion methods. We find that, for the shape resonance in the photoionization channel leading to the  $X^2 \Sigma_g^+$  state of  $N_2^+$ , the previous results of Raseev *et al.*<sup>9</sup> and Robb *et al.*<sup>10</sup> are not well converged. In particular, their peak cross section occurs at a photon energy of 31 eV which differs from the present result of 29 eV. In this regard,

we have determined empirically that the energy of the peak cross section in this shape resonance, for which the continuum function is of  $\sigma_u$  symmetry, converges as

$$E_{\max}^{\ell} - E_{\max}^{\infty} \propto \frac{1}{\ell^3}, \quad (1)$$

where  $\ell$  is the maximum  $\ell$  included in the partial wave expansion of the continuum function. We also compare our accurate static-exchange results with the results obtained using the CMSM and STMT methods.<sup>2-4</sup> This comparison shows that the CMSM and STMT results are qualitatively similar to accurate static-exchange results but neither the CMSM nor STMT is in quantitative (better than 10 %) agreement with the present results. Finally, the comparison with experimental results<sup>11-14</sup> shows that the FCHF final-state model reproduces the experimental cross section well except in the energy regions where two-electron resonances, such as autoionization, are important.

We find that the inclusion of initial-state correlation brings the dipole length and velocity forms of the photoionization cross section into better agreement with experimental results. This result for molecular systems is similar to that found by Swanson and Armstrong for atomic systems.<sup>22</sup> In the region of the shape resonance leading to the  $X^2 \Sigma_g^+$  state of  $N_2^+$ , the combination of correlated initial-state wave function and FCHF final-state wave function is found to be particularly effective.

## II. METHOD

### A. Iterative Schwinger Variational Method

We compute the final-state photoionization wave functions using the

FCHF approximation.<sup>9</sup> This implies that the final state is described by a single electronic configuration in which the ionic core orbitals are constrained to be identical to the HF orbitals of the neutral molecule. The Schrödinger equation for the remaining continuum orbital is then (in atomic units)

$$\left(-\frac{1}{2}\nabla^2 - \frac{1}{r} + V(\vec{r}) - \frac{k^2}{2}\right) \Psi_{\vec{K}}^{(\pm)}(\vec{r}) = 0, \quad (2)$$

where  $V(\vec{r})$  is the short-range portion of the static-exchange potential and  $\vec{k}$  is the momentum of the continuum electron. By using the FCHF approximation, the final-state photoionization problem is reduced to solving a single-particle potential scattering problem.

The Schrödinger equation given in Eq. (2) is equivalent to the Lippmann-Schwinger equation

$$\Psi_{\vec{K}}^{(\pm)} = \Psi_{\vec{K}}^{c(\pm)} + G^{c(\pm)} U \Psi_{\vec{K}}^{(\pm)}, \quad (3)$$

where  $U(\vec{r}) = 2V(\vec{r})$  and  $G^{c(\pm)}$  is the Coulomb Green's function defined by

$$G^{c(\pm)} = \left(\nabla^2 + \frac{2}{r} + k^2 \pm i\epsilon\right)^{-1}. \quad (4)$$

The function  $\Psi_{\vec{K}}^{c(\pm)}$  is the pure Coulomb scattering function and is given in terms of its partial-wave expansion as

$$\Psi_{\vec{K}}^{c(\pm)}(\vec{r}) = \left(\frac{2}{\pi}\right)^{1/2} \sum_{\ell, m} i^\ell \phi_{\ell m}^{c(\pm)}(\vec{r}) Y_{\ell m}^*(\Omega_{\hat{k}}), \quad (5)$$

where  $\phi^{c(\pm)}$  is the partial-wave Coulomb function defined by

$$\phi_{k\ell m}^{c(\pm)}(\vec{r}) = e^{\pm i\sigma_\ell} \frac{F_\ell(\gamma; kr)}{kr} Y_{\ell m}(\Omega_{\hat{r}}). \quad (6)$$

The function  $F_\ell(\gamma; kr)$  is the regular Coulomb function with  $\gamma = -1/k$  and  $\sigma_\ell$  is the Coulomb phase shift defined as  $\sigma_\ell = \arg [\Gamma(\ell + 1 + i\gamma)]$ .<sup>23</sup>

The wave function  $\Psi_{\vec{k}}^{(-)}$ , which represents the ejected electron with momentum  $\vec{k}$ , is then expanded in the partial-wave series

$$\Psi_{\vec{k}}^{(-)}(\vec{r}) = \left(\frac{2}{\pi}\right)^{\frac{1}{2}} \sum_{\ell=0}^{\ell_p} \sum_{m=-\ell}^{+\ell} i^\ell \psi_{k\ell m}^{(-)}(\vec{r}) Y_{\ell m}^*(\Omega_{\hat{k}}), \quad (7)$$

where an infinite sum over  $\ell$ 's has been truncated at  $\ell = \ell_p$ . Computing the wave function in the partial-wave form allows the dependence of the scattering solution on the target orientation to be treated analytically. The Lippmann-Schwinger equation for the partial-wave states is then

$$\psi_{k\ell m}^{(-)}(\vec{r}) = \phi_{k\ell m}^{c(-)}(\vec{r}) + \langle \vec{r} | G^{c(-)} U | \psi_{k\ell m}^{(-)} \rangle. \quad (8)$$

We solve Eq. (8) using an iterative procedure.<sup>16</sup> The iterative method begins by approximating the short-range potential by a separable potential of the form

$$\langle \vec{r} | U^{S_0} | \vec{r}' \rangle = \sum_{\alpha_i, \alpha_j \in R} \langle \vec{r} | U | \alpha_i \rangle [U^{-1}]_{ij} \langle \alpha_j | U | \vec{r}' \rangle, \quad (9)$$

where  $R$  is some initial set of expansion functions and  $[U^{-1}]_{ij}$  is the matrix inverse of  $U_{ij}$ . Inserting this approximation to  $U$  in to Eq. (8) allows the Lippmann-Schwinger equation to be solved since the kernel of the integral equation is now separable.<sup>24</sup> The solution to Eq. (8)

with the potential approximated by  $U^{S_0}$  is

$$\begin{aligned} \psi_{k\ell m}^{(-)S_0}(\vec{r}) &= \phi_{k\ell m}^{c(-)}(\vec{r}) \\ &+ \sum_{\alpha_i, \alpha_j \in R} \langle \vec{r} | G^{c(-)} U | \alpha_i \rangle [D^{-1}]_{ij} \langle \alpha_j | U | \phi_{k\ell m}^{c(-)} \rangle \end{aligned} \quad (10)$$

where

$$D_{ij} = \langle \alpha_i | U - UG^{c(-)}U | \alpha_j \rangle . \quad (11)$$

The use of a separable potential of the form given in Eq. (9) to solve the Lippmann-Schwinger equation is known to be identical to the use of the Schwinger variational expression,<sup>25-27</sup> and hence we call this method the iterative Schwinger variational method.

The iterative method is continued by augmenting the expansion set  $R$ , of Eq. (9) by the set of functions

$$S_0 = \{ \psi_{k\ell_1 m}^{S_0}, \psi_{k\ell_2 m}^{S_0}, \dots, \psi_{k\ell_p m}^{S_0} \}, \quad (12)$$

which are the scattering solutions given by Eq. (10), and where  $\ell_p$  is the maximum  $\ell$  included in the expansion of the scattering solution as given in Eq. (7). Using this augmented set of functions, a second set of scattering solutions

$$S_1 = \{ \psi_{k\ell_1 m}^{S_1}, \dots, \psi_{k\ell_p m}^{S_1} \}$$

is obtained using Eq. (10). In general, the set of scattering solutions at the  $n$ 'th iteration

$$S_n = \{ \psi_{k\ell_1 m}^{S_n}, \dots, \psi_{k\ell_p m}^{S_n} \} \quad (13)$$

is obtained from the previous set of solutions  $S_{n-1}$  from

$$\begin{aligned} \psi_{\mathbf{k}\ell m}^{(-)S_n}(\bar{\mathbf{r}}) = & \phi_{\mathbf{k}\ell m}^{c(-)}(\bar{\mathbf{r}}) + \\ & \sum_{\chi_i, \chi_j \in R \cup S_{n-1}} \langle \bar{\mathbf{r}} | G^{c(-)} U | \chi_i \rangle [D^{-1}]_{ij} \\ & \times \langle \chi_j | U | \phi_{\mathbf{k}\ell m}^{c(-)} \rangle . \end{aligned} \quad (14)$$

This iterative procedure is continued until the wave functions converge. When the wave functions do converge, it can be shown that they are solutions of the Lippmann-Schwinger equation for the exact potential  $U$ .<sup>16</sup>

### B. Frozen Core Hartree-Fock Static-Exchange Potential

In this section we will discuss the form of the static-exchange potential, obtained from the FCHF approximation, which describes the interaction of the ionized electron with the open-shell ionic core.<sup>28</sup> First consider the HF wave function of a closed shell molecule such as  $N_2$ . The HF wave function is simply written as a single Slater determinant

$$\Psi = |\phi_1\alpha\phi_1\beta \dots \phi_n\alpha\phi_n\beta| . \quad (15)$$

The photoionization final-state wave function in the FCHF approximation, where the ionized electron is removed from orbital  $\phi_n$ , is written as

$$\begin{aligned} \Psi_{\mathbf{k}}^- = & \left(\frac{1}{2}\right)^{\frac{1}{2}} \{ |\phi_1\alpha\phi_1\beta \dots \phi_n\alpha\phi_{\mathbf{k}}\beta| \\ & + |\phi_1\alpha\phi_1\beta \dots \phi_{\mathbf{k}}\alpha\phi_n\beta| \} , \end{aligned} \quad (16)$$

assuming that  $\phi_n$  is a nondegenerate orbital. Then the correct single-particle equation for the continuum electron is obtained from

$$\langle \delta \Psi_{\mathbf{k}}^- | H - E | \Psi_{\mathbf{k}}^- \rangle = 0 \quad (17)$$

where

$$\begin{aligned} \delta \Psi_{\mathbf{k}}^- = & \left(\frac{1}{2}\right)^{\frac{1}{2}} \{ |\phi_1 \alpha \phi_1 \beta \dots \phi_n \alpha \delta \phi_{\mathbf{k}}^- \beta| \\ & + |\phi_1 \alpha \phi_1 \beta \dots \delta \phi_{\mathbf{k}}^- \alpha \phi_n \beta| \} \end{aligned} \quad (18)$$

and where Eq. (17) holds for all possible  $\delta \phi_{\mathbf{k}}^-$ .

The electronic Hamiltonian can be written as

$$H = \sum_{i=1}^N f(i) + \sum_{i < j}^N \frac{1}{r_{ij}} \quad (19)$$

with

$$f(i) = -\frac{1}{2} \nabla_i^2 - \sum_{\alpha} \frac{Z_{\alpha}}{r_{i\alpha}} \quad (20)$$

where  $Z_{\alpha}$  are the nuclear charges and  $N = 2n$  is the number of electrons. The one-electron HF Hamiltonian can be written in this form as

$$H^{\text{HF}} = f + \sum_{i=1}^n 2J_i - K_i, \quad (21)$$

where  $f$  is the one-electron operator defined in Eq. (20) and  $J_i$  and  $K_i$  are the usual Coulomb and exchange operators.<sup>29</sup> Thus the HF orbitals satisfy

$$H^{\text{HF}} \phi_n = \epsilon_n \phi_n. \quad (22)$$

If we assume that the orbitals  $\phi_{\vec{k}}$  and  $\delta\phi_{\vec{k}}$  are not necessarily orthogonal to each other nor to the orthonormal set of occupied HF orbitals, then Eq. (17) can be expanded to give

$$\begin{aligned}
0 = & \langle (P\delta\phi_{\vec{k}}) | \tilde{H} - \epsilon + J_n + K_n | P\phi_{\vec{k}} \rangle \\
& + 2\langle \delta\phi_{\vec{k}} | \phi_n \rangle \langle \phi_n | \tilde{H} - \epsilon + J_n | \phi_n \rangle \langle \phi_n | \phi_{\vec{k}} \rangle \\
& + 2\langle \delta\phi_{\vec{k}} | \phi_n \rangle \langle \phi_n | \tilde{H} + J_n | P\phi_{\vec{k}} \rangle \\
& + 2\langle (P\delta\phi_{\vec{k}}) | \tilde{H} + J_n | \phi_n \rangle \langle \phi_n | \phi_{\vec{k}} \rangle
\end{aligned} \tag{23}$$

where

$$\tilde{H} = f + \sum_{i=1}^{n-1} 2J_i - K_i \tag{24}$$

and

$$P = 1 - \sum_{i=1}^n |\phi_i\rangle \langle \phi_i| \tag{25}$$

The energy of the continuum electron is

$$\epsilon = E - E^{\text{core}} \tag{26}$$

where  $E^{\text{core}}$  is the Koopman's theorem energy of the ionic core

$$E^{\text{core}} = E^{\text{HF}} - \epsilon_n \tag{27}$$

That  $\phi_n$  is an eigenfunction of  $H^{\text{HF}}$  [Eq. (22)] reduces Eq. (23) to<sup>30</sup>

$$\begin{aligned}
0 = & \langle (P\delta\phi_{\vec{k}}) | \tilde{H} - \epsilon + J_n + K_n | P\phi_{\vec{k}} \rangle \\
& + 2(\epsilon_n - \epsilon) \langle \delta\phi_{\vec{k}} | \phi_n \rangle \langle \phi_n | \phi_{\vec{k}} \rangle ,
\end{aligned} \tag{28}$$

which must hold for all  $\delta\phi_{\vec{k}}$ . If we consider the case where  $\delta\phi_{\vec{k}} = \phi_n$  then it follows that if  $\epsilon \neq \epsilon_n$  then  $\langle \phi_{\vec{k}} | \phi_n \rangle = 0$ . Thus if  $\phi'_{\vec{k}}$  satisfies

$$0 = \langle (P\delta\phi'_{\vec{k}}) | \tilde{H} - \epsilon + J_n + K_n | P\phi'_{\vec{k}} \rangle \quad (29)$$

for all  $\delta\phi'_{\vec{k}}$  and with  $\epsilon \neq \epsilon_n$ , then  $\phi_{\vec{k}} = P\phi'_{\vec{k}}$  satisfies Eq. (28). So, solving Eq. (29) will give us the correct continuum wave function in the FCHF approximation.

There are several points to note about Eq. (29). First, Eq. (29) constrains the solution  $P\phi'_{\vec{k}}$  to be orthogonal to the occupied orbitals. Thus, this form of the scattering equation is entirely equivalent to the standard undetermined Lagrange multiplier form<sup>10,31</sup>

$$(\tilde{H} - \epsilon + J_n + K_n) \phi_{\vec{k}} = \sum_{i=1}^n \lambda_i \phi_i \quad (30)$$

where  $\lambda_i$  are undetermined multipliers and  $\phi_{\vec{k}}$  is subject to the condition

$$\langle \phi_{\vec{k}} | \phi_i \rangle = 0 \quad , \quad i = 1, 2, \dots, n \quad (31)$$

Secondly, the continuum solution must be constrained to be orthogonal to the doubly occupied orbitals since, unlike in the electron-neutral closed shell HF scattering case, the continuum orbital and the occupied orbitals are not eigenfunctions of the same one-electron Hamiltonian. Lastly, the general open-shell scattering problem would require the solution of Eq. (23), but as we have seen, since we are using the FCHF approximation, the scattering equations can be simplified to yield Eq. (29).

A scattering equation of the form of Eq. (2) can be obtained from Eq. (29) giving

$$(-\frac{1}{2}\nabla^2 + V^{\text{orth}} - \epsilon)\phi_{\vec{k}} = 0 \quad . \quad (32)$$

The potential  $V^{\text{orth}}$  is a generalized Phillips-Kleinman pseudopotential<sup>32</sup>

$$V^{\text{orth}} = V - LQ - QL + QLQ \quad (33)$$

where  $L$ ,  $Q$ , and  $V$  are defined by

$$L = -\frac{1}{2}\nabla^2 - \epsilon + V \quad , \quad (34)$$

$$Q = \sum_{i=1}^n |\phi_i\rangle\langle\phi_i| \quad , \quad (35)$$

and

$$V = \sum_{i=1}^{n-1} (2J_i - K_i) + J_n + K_n - \sum_{\alpha} \frac{Z_{\alpha}}{r_{i\alpha}} \quad . \quad (36)$$

Thus we use the pseudopotential  $V^{\text{orth}}$  to treat both the static-exchange interaction and the effects of constraining the continuum solution to be orthogonal to the occupied bound orbitals.

### C. Photoionization Cross Sections and Asymmetry Parameters

The photoionization cross section for going from an initial bound state  $\Psi_i$  to the continuum state  $\Psi_{f, \vec{k}}$  due to linearly polarized light in the dipole length and dipole velocity approximations is proportional to the square of the dipole matrix elements

$$\frac{L}{k, \hat{n}} = (k)^{\frac{1}{2}} \langle \Psi_i | \vec{r} \cdot \hat{n} | \Psi_{f, \vec{k}}^{(-)} \rangle \quad (37)$$

for the dipole length form and

$$I_{\vec{k}, \hat{n}}^{\vec{L}, \vec{V}} = \frac{(k)^{\frac{1}{2}}}{E} \langle \Psi_i | \vec{\nabla} \cdot \hat{n} | \Psi_{f, \vec{k}}^{(-)} \rangle \quad (38)$$

for the velocity form. In Eqs. (37) and (38),  $E$  is the photon energy,  $\hat{n}$  is the direction of polarization of the light, and  $\vec{k}$  is the momentum of the photoelectron. The factor of  $(k)^{\frac{1}{2}}$  in Eqs. (37) and (38) is required to change the normalization of the continuum functions,  $\Psi_{f, \vec{k}}^{(-)}$ , from momentum to energy normalized. The doubly differential photoionization cross section in the body-fixed frame is then

$$\frac{d^2\sigma}{d\Omega_{\vec{k}} d\Omega_{\hat{n}}} = \frac{4\pi^2 E}{c} |I_{\vec{k}, \hat{n}}^{\vec{L}, \vec{V}}|^2 \quad (39)$$

If the wave functions used to calculate the photoionization cross section were exact eigenfunctions of the electronic Hamiltonian, then the dipole length and dipole velocity forms of the cross section would be equivalent. Thus the equality of these two forms is a necessary but not sufficient condition that the computed cross sections are accurate. In this sense, the difference between the length and velocity forms can be viewed as an estimate of the minimum error in the calculation.<sup>22, 33</sup>

To treat the angular dependence of the cross section on the target orientation the dipole matrix elements are expanded in terms of spherical harmonics

$$I_{\vec{k}, \hat{n}}^{\vec{L}, \vec{V}} = \left(\frac{4\pi}{3}\right)^{\frac{1}{2}} \sum_{\ell m \mu} I_{\ell m \mu}^{\vec{L}, \vec{V}} Y_{\ell m}^*(\Omega_{\vec{k}}) Y_{1\mu}^*(\Omega_{\hat{n}}) \quad (40)$$

The partial-wave matrix elements are then given by

$$I_{\ell m \mu}^L = (k)^{1/2} \langle \Psi_i | r_\mu | \Psi_{f, k \ell m}^{(-)} \rangle \quad (41)$$

for the dipole length form, and

$$I_{\ell m \mu}^V = \frac{(k)^{1/2}}{E} \langle \Psi_i | \nabla_\mu | \Psi_{f, k \ell m}^{(-)} \rangle \quad (42)$$

for the dipole velocity form, where

$$r_\mu = \begin{cases} \mp (x \pm iy)/2^{1/2} & \text{for } \mu = \pm 1 \\ z & \text{for } \mu = 0 \end{cases} \quad (43)$$

and

$$\nabla_\mu = \begin{cases} \mp \left( \frac{\partial}{\partial x} \right) \pm i \left( \frac{\partial}{\partial y} \right) / 2^{1/2} & \text{for } \mu = \pm 1 \\ \frac{\partial}{\partial z} & \text{for } \mu = 0. \end{cases} \quad (44)$$

The total photoionization cross section averaged over all polarizations and photoelectron directions is then

$$\sigma^{L, V} = \frac{4\pi^2}{3c} E \left( \sum_{\mu} D_{\mu} \right) \quad (45)$$

where

$$D_{\mu} = \sum_{\ell} | I_{\ell, \Delta m - \mu, \mu}^{L, V} |^2 \quad (46)$$

Note that for linear molecules we have

$$\Delta m = m(\Psi_i) - m(\text{ion core}) = \mu + m(\text{photoelectron}). \quad (47)$$

There are two other averaged photoionization cross sections of interest as suggested by Wallace and Dill.<sup>15</sup> The first is the usual Integrated Target Angular Distribution (ITAD). The ITAD corresponds to the photoionization experiment where the target orientation is not resolved. This is the form of the photoionization cross section measured in the usual gas phase experiment. When the cross section in Eq. (39) is averaged over all target orientations the ITAD is found to be of the form

$$\frac{d\sigma^{L,V}}{d\Omega_{\hat{k}}} = \frac{\sigma^{L,V}}{4\pi} \left( 1 + \beta_{\hat{k}}^{L,V} P_2(\cos \theta) \right). \quad (48)$$

The angle  $\theta$  is the angle between the direction of polarization of the light and the momentum of the electron and  $P_2(\cos \theta)$  is the Legendre polynomial of degree 2. The asymmetry parameter  $\beta_{\hat{k}}$  is given by<sup>34</sup>

$$\begin{aligned} \beta_{\hat{k}}^{L,V} &= \frac{3}{5} (1/\sum_{\mu} D_{\mu}) \sum_{\substack{\ell m \mu \\ \ell' m' \mu' \\ \mu''}} (-1)^{m-\mu'} I_{\ell m \mu}^{L,V} \\ &\times (I_{\ell' m' \mu'}^{L,V})^* [(2\ell+1)(2\ell'+1)]^{1/2} (11\ 00 | 20) \\ &\times (\ell \ell' 00 | 20) (11 - \mu \mu' | 2 \mu'') (\ell \ell' - m - m' | 2 - \mu'') \end{aligned} \quad (49)$$

where  $(j_1 j_2 m_1 m_2 | j_3 m_3)$  is a Clebsch-Gordan coefficient. Note that the asymmetry parameter  $\beta_{\hat{k}}$  depends only on the photon energy and that the subscript  $\hat{k}$  implies only that  $\beta_{\hat{k}}$  describes the distribution of the photoelectrons and not that  $\beta_{\hat{k}}$  depends on their direction. The second averaged photoionization cross section we will consider is the Integrated Detector Angular Distribution (IDAD). The IDAD corresponds to the experiment where the target orientation is fixed in the laboratory frame of reference and the cross section is then integrated over all possible directions of emission of the photoelectron. Wallace and Dill<sup>15</sup> have suggested that the IDAD cross section would be useful in determining the orientation of a photoionized target in the laboratory frame. When the cross section given Eq. (39) is integrated over all photoelectron directions the IDAD is found to be of the form

$$\frac{d\sigma^{L,V}}{d\Omega_{\hat{n}}} = \frac{\sigma^{L,V}}{4\pi} \left( 1 + \beta_{\hat{n}}^{L,V} P_2(\cos \theta) \right). \quad (50)$$

The angle  $\theta$  in this case is the angle between the direction of the polarization of the light and the molecular z-axis. The asymmetry parameter  $\beta_{\hat{n}}$  is given by

$$\beta_{\hat{n}}^{L,V} = [2D_0 - (D_{-1} + D_{+1})] / (\sum_{\mu} D_{\mu}). \quad (51)$$

### III. RESULTS AND DISCUSSION

#### A. Final-State Wave Functions

The final-state wave functions used in this study of photoionization are constructed using the FCHF approximation. The bound orbitals in this approximation come from the HF wave function of the neutral molecule. We have constructed a HF wave function for the neutral  $N_2$  molecule using a double-zeta plus d functions contracted Gaussian basis of the form  $(9s5p2d/4s3p2d)$ .<sup>35, 36</sup> The d-function exponents were 1.5836 and 0.4691 which are the exponents appropriate to representing a Slater function with exponent  $\xi = 2.20$ .<sup>36</sup> The bond length was taken as 2.068 au. The HF energy for this basis set is  $E = -108.973235$  au. and the quadrupole moment for the neutral  $N_2$  molecule in the basis set is  $\theta_{ZZ} = -0.9923$  au.<sup>36</sup>

To compute the final-state continuum wave function we must evaluate the various matrix elements given in Eq. (14). We have used a single-center expansion approach to evaluate all such matrix elements.<sup>6, 30, 37</sup> The use of single-center techniques implies that all functions (e. g., scattering functions, occupied orbitals,  $1/r_{12}$ ,  $G^{c(-)}$ ) are expanded about a common origin (taken to be the bond center for  $N_2$ ) as a sum of spherical harmonics times radial functions. The radial integrals are computed by putting the radial functions on a grid and then using Simpson's rule. The angular integrals can then be done analytically. Actual calculations use standing-wave boundary conditions thus allowing radial wave functions to be represented by real-valued functions.

There are several parameters which describe the maximum  $\ell$  included in such spherical harmonic expansions. Using a notation similar to that of Robb and Collins,<sup>10,38</sup> we define our expansion parameters as follows:

- 1)  $\ell_m$  = maximum  $\ell$  included in the expansion of scattering functions ( $\chi_i$ 's of Eq. (14)), of the Coulomb Green's function, and of the projection orbitals ( $\phi_i$  of Eq. (35)),
- 2)  $\ell_s^{\text{ex}}$  = maximum  $\ell$  included in the expansion of the scattering functions in the exchange terms,
- 3)  $\ell_i^{\text{ex}}$  = maximum  $\ell$  included in the expansion of the occupied orbitals in the exchange terms,
- 4)  $\ell_i^{\text{dir}}$  = maximum  $\ell$  included in the expansion of the occupied orbitals in the direct potential,
- 5)  $\lambda_m^{\text{ex}}$  = maximum  $\ell$  included in the expansion of  $1/r_{12}$  in the exchange terms,
- 6)  $\lambda_m^{\text{dir}}$  = maximum  $\ell$  included in the expansion of  $1/r_{12}$  in the direct potential (not including the nuclear terms).

Also note that we always include terms up to  $\lambda = 2\ell_m$  in the expansion of the nuclear potential. We have expanded all radial integrands on a grid of 800 points extending to  $r = 64.0$  au. The smallest step size in this grid is 0.01 au which is used out to  $r = 2.0$  au. The largest step size is 0.16 au.

For the purposes of this study we have grouped the six parameters listed above as follows

$$\text{i) } \ell_{\text{max}}^{\text{dir}} = \ell_m, \ell_i^{\text{dir}}, \lambda_m^{\text{dir}}$$

$$\text{ii) } \ell_{\max}^{\text{exc}} = \ell_{\text{S}}^{\text{ex}}, \lambda_{\text{m}}^{\text{ex}}.$$

For all calculations on  $\text{N}_2$  considered here we have fixed  $\ell_{\text{i}}^{\text{ex}}$  to be  $\ell_{\text{i}}^{\text{ex}} = 16(1\sigma_{\text{g}}), 10(2\sigma_{\text{g}}), 10(3\sigma_{\text{g}}), 15(1\sigma_{\text{u}}), 9(2\sigma_{\text{u}}), 9(1\pi_{\text{u}})$ . These values correspond to having normalized the expansions of the various orbitals to better than 0.99.

To study the general convergence in this system we have initially considered four sets of parameters:

$$\text{A) } \ell_{\max}^{\text{dir}} = 20, \ell_{\max}^{\text{exc}} = 20$$

$$\text{B) } \ell_{\max}^{\text{dir}} = 30, \ell_{\max}^{\text{exc}} = 20$$

$$\text{C) } \ell_{\max}^{\text{dir}} = 40, \ell_{\max}^{\text{exc}} = 20$$

$$\text{D) } \ell_{\max}^{\text{dir}} = 30, \ell_{\max}^{\text{exc}} = 30.$$

We have used these four sets of parameters to calculate the photoionization cross section in the  $3\sigma_{\text{g}} \rightarrow k\sigma_{\text{u}}$  channel of  $\text{N}_2$ . This channel was chosen since it contains a shape resonance which makes the computed cross section more sensitive to the parameters of the potential than in a nonresonant channel. The results for parameter sets A, B, and C are shown in Fig. 1. On the scale shown in Fig. 1, the cross section with parameter set D cannot be distinguished from that of set B. The difference between sets B and C is less than 5% in the cross section. We consider the accuracy of set B to be adequate considering the FCHF approximation within which we are computing these cross sections. Thus, except where noted, we have used this set of parameters with  $\ell_{\max}^{\text{dir}} = 30$  and  $\ell_{\max}^{\text{exc}} = 20$  for all other calculations in

in this study. A more detailed discussion of the convergence of the energy of peak cross sections in the  $3\sigma_g \rightarrow k\sigma_u$  channel is given in Section III. C of this paper.

The scattering basis sets, corresponding to the set  $R$  of Eq. (10), which were used to obtain scattering solutions of the various possible symmetries, are given in Table I. The basis sets are constructed both from Cartesian Gaussian functions which are of the form

$$\phi_{\alpha, \ell, m, n, \bar{A}}(\bar{r}) = N(x - A_x)^\ell (y - A_y)^m (z - A_z)^n e^{-\alpha |\bar{r} - \bar{A}|^2} \quad (52)$$

centered at the nuclei, and spherical Gaussians of the form

$$\phi_{\alpha, \ell, m, \bar{A}}(\bar{r}) = N |\bar{r} - \bar{A}|^\ell e^{-\alpha |\bar{r} - \bar{A}|^2} Y_{\ell m}(\Omega_{\bar{r} - \bar{A}}) \quad (53)$$

centered at the expansion origin. We have examined the rate of convergence of the iterative Schwinger variational method with basis sets of this size. In Fig. 2 we present the results of photoionization calculations in the  $3\sigma_g \rightarrow k\sigma_u$  channel using the  $\sigma_u$  basis set given in Table I. The cross section without iteration (Eq. (10)) and from the first iteration (Eq. (14) with  $n = 1$ ) are both given in Fig. 2. The cross section obtained from the second iteration is indistinguishable from that given for the first iteration on the scale presented in Fig. 2. Thus, for all other channels we have only presented cross sections from the results of the first iteration. We have assured the adequacy of the basis sets for the other scattering symmetries, given in Table I, by comparing

the zero-iteration cross section to the one-iteration cross section. In all the other channels considered here, this difference is small and of the same order as that we have obtained in the  $3\sigma_g \rightarrow k\sigma_u$  channel.

### B. Initial state wave function

Swanson and Armstrong<sup>22</sup> found that inclusion of correlation effects in the initial-state wave function while using only the FCHF approximation for the final state significantly improved the computed cross section when compared to using only a HF initial-state wave function. In this study we have examined effects of initial-state correlation on the computed photoionization cross sections of molecular nitrogen. As initial-state wave functions we have used the HF wave function described in the previous section and a CI wave function containing "singles-plus-doubles" excitations.<sup>39</sup>

In order to limit the size of the CI wave function, the virtual orbital space was taken to be a restricted set of orbitals. The virtual orbitals were obtained by performing a separated-pair type MC-SCF calculation.<sup>29,40</sup> The orbital occupation in the HF wave function is

$$(1\sigma_g)^2 (2\sigma_g)^2 (3\sigma_g)^2 (1\sigma_u)^2 (2\sigma_u)^2 (1\pi_{ux})^2 (1\pi_{uy})^2. \quad (54)$$

Note that we have performed the initial-state calculations in  $D_{2h}$  symmetry. In the separated-pair calculation the valence electron pairs are expanded in orthogonal natural orbitals. The wave function we used for  $N_2$  may be represented as

$$\begin{aligned}
& (1\sigma_g)^2 (2\sigma_g, 5\sigma_g, 5\sigma_u)^2 (3\sigma_g, 4\sigma_g, 3\sigma_u, 4\sigma_u, 3\pi_{ux}, 3\pi_{uy}, \\
& 3\pi_{gx}, 3\pi_{gy})^2 (1\sigma_u)^2 (2\sigma_u, 6\sigma_g, 6\sigma_u)^2 (1\pi_{ux}, 1\pi_{gx}, 2\pi_{ux}, 2\pi_{gx})^2 \\
& (1\pi_{uy}, 1\pi_{gy}, 2\pi_{uy}, 2\pi_{gy})^2, \tag{55}
\end{aligned}$$

where the orbital listed within each pair of parentheses represents the natural orbitals of a particular pair function. The energy of this separated-pair wave function for  $N_2$  is -109.054 489 au. The orbitals in each pair function which are doubly occupied in the HF approximation were not allowed to vary from their HF form. This constraint made the evaluation of the photoionization cross sections simpler since in matrix elements of the form of Eqs. (41) and (42), this restriction allows only the continuum orbital in the final state to be nonorthogonal to the orbitals in the correlated initial-state wave function. Having only one nonorthogonal orbital in the final state causes the configurations in the initial-state wavefunction, differing from the reference HF configuration by three or more spin-orbitals, not to contribute to the photoionization cross section.

Hence we have chosen a linear combination of configurations differing from the HF configuration by no more than two orbitals to represent the correlated initial state wave function. The virtual orbital space was taken to be the set of orbitals determined in the separated-pair calculation. We have also restricted the calculation by requiring the  $1\sigma_g$  and  $1\sigma_u$  orbitals to remain doubly occupied in all

configurations. The resulting wave function has 386 spatial configurations in  $D_{2h}$  symmetry, from which 570 spin-eigenfunctions are constructed. The energy of this CI wave function is -109.173 549 au.

### C. Photoionization leading to the $X^2\Sigma_g^+$ state of $N_2^+$

Photoionization leading to the  $X^2\Sigma_g^+$  state of  $N_2^+$  is of primary interest due to the appearance of a shape resonance in the cross section. In the one-electron picture used here this channel corresponds to photoionization from the  $3\sigma_g$  orbital into a continuum orbital of either  $\sigma_u$  or  $\pi_u$  symmetry. The maximum  $\ell$  included in the expansion of the scattering solution (Eq. (7)) is  $\ell_p = 7$  for the continuum solutions of  $\sigma_u$  symmetry and  $\ell_p = 5$  for continuum solutions of  $\pi_u$  symmetry. The ionization potential we used for this channel was  $IP = 15.6 \text{ eV}$ .<sup>3,11</sup>

There have been several studies of the shape resonance in this channel using the FCHF approximation.<sup>3,9,10</sup> Among these studies there is a disagreement of about 3 eV in the position of the peak photoionization due to the resonance. For the  $3\sigma_g - k\sigma_u$  channel alone, Rescigno *et al.*<sup>3</sup> obtained a peak cross section at a photon energy of  $\sim 28 \text{ eV}$  whereas both Raseev *et al.*<sup>9</sup> and Robb and Collins<sup>10</sup> obtained the peak cross section at  $\sim 31 \text{ eV}$ . Figure 2 shows that the peak cross section in our calculation is at  $\sim 29 \text{ eV}$ .

The discrepancy between our peak cross section energy and those of Raseev *et al.* and Robb and Collins could be due either to the different targets used or the different expansion parameters used. To see if the difference in the targets is important, we have performed a

calculation in which we used similar expansion parameters to those used by Raseev et al.<sup>9</sup> For this calculation we have taken as our expansion parameters  $\ell_m = 13, \ell_s^{\text{ex}} = 9, \ell_i^{\text{ex}} = 7$  for all  $i, \ell_i^{\text{dir}} = 50, \lambda_m^{\text{ex}} = 5, \lambda_m^{\text{dir}} = 14$ . Using these parameters we obtain the peak cross section energy at 30.7 eV. Thus the difference between using a target wave function constructed from Gaussian functions as in the present study or from Slater type functions as in the studies by Raseev et al.<sup>9</sup> and Robb and Collins<sup>10</sup> is seen to be small. Thus most of the difference between the results of Raseev et al.<sup>9</sup> and Robb and Collins<sup>10</sup> and our present results must be due to the lack of convergence of the expansion parameters in the earlier studies.

In order to examine the behavior of the peak cross section with respect to the  $\ell$  expansion used, we have performed an additional set of calculations. The very small difference between the B and D calculations discussed in Sec. III.A indicates that the exchange potential is converged with  $\ell_{\text{max}}^{\text{exc}} = 30$ . Thus the only variations in  $\ell$  that we will consider here are those in  $\ell_{\text{max}}^{\text{dir}}$ . We have thus performed calculations with  $\ell_{\text{max}}^{\text{exc}} = 30$  and  $\ell_{\text{max}}^{\text{dir}} = 34, 38, 42, 46, 50$ . We have computed the photoionization cross section for the  $3\sigma_g \rightarrow k\sigma_u$  channel at three photoelectron energies, 0.47, 0.50, and 0.53 au, which correspond to photon energies of 28.4, 29.2, and 30.0 eV. Using these three energies we then used polynomial interpolation to obtain the photon energy of the peak cross section. We have plotted the resulting energies against  $1/(\ell_{\text{max}}^{\text{dir}})^3$  in Fig. 3. As can be seen from Fig. 3, the peak energies fall on a straight line when plotted against  $1/(\ell_{\text{max}}^{\text{dir}})^3$ . Thus we have empirically determined the relationship given in Eq. (1), i. e. ,

$$E_{\max}^{\ell} - E_{\max}^{\infty} \propto \frac{1}{\ell^3} .$$

The extrapolated energy for the peak cross section is then 28.7 eV.

We believe that this functional dependence of the resonance energy on  $\ell_{\max}^{\text{dir}}$  is due to the interaction of resonant function of  $\sigma$  symmetry, which satisfies the appropriate cusp condition at a nucleus, and the nuclear potential at that point. To test this conjecture we computed the potential integral of a s-type Slater function of exponent  $\xi = 2.0$ , which has the correct cusp condition at its origin, with a point charge at the center of the Slater function. This integral was performed using a single center expansion about an origin 1.034 au away from the center of the Slater function.<sup>41</sup> Note that this distance is the same as the distance from the expansion center to the nuclei in nitrogen. The convergence of this integral with  $\ell_{\max}$  was also found to obey the law given in Eq. (1), suggesting that this  $1/\ell^3$  convergence could be general for all  $\sigma$  shape resonances, although we do not have a rigorous proof of this. We have also observed this rate of convergence in the  $4\sigma_g \rightarrow k\sigma_u$  photoionization resonance in  $\text{CO}_2$ .<sup>19b</sup> Note that for resonances with  $m \neq 0$  ( $\pi, \delta$ , etc.) the convergence behavior will be different and one would expect these resonance energies to converge faster with increasing  $\ell$  than does the  $\sigma$  resonance discussed here.

In Fig. 4 we give the total cross section leading to the  $X^2\Sigma_g^+$  state of  $\text{N}_2^+$ . We have plotted the computed dipole length and dipole velocity cross sections, using both the HF and CI initial-state wave functions, along with the experimental results of Plummer *et al.*<sup>11</sup> and of Hamnett *et al.*<sup>13</sup> As in studies of atomic photoionization

by Swanson and Armstrong,<sup>22</sup> the correlated initial-state wave function brings the length and velocity forms of the cross section closer together in better agreement with the experimental results.

The feature at 23 eV in the experimental cross section has been attributed to autoionization from Rydberg states leading to the  $C^2\Sigma_u^+$  state of  $N_2^+$ .<sup>11,42</sup> To obtain such autoionization features theoretically one would have to include final state effects not present in the FCHF model used here.

In Fig. 5 we present our computed ITAD and IDAD asymmetry parameters. The effect of initial state correlation on the computed  $\beta$ 's is small. Thus for all the asymmetry parameters reported here, we will only present our most reliable results obtained using the CI initial-state wave function. The computed ITAD asymmetry parameters agree well with the experimental results of Marr et al.,<sup>12</sup> except for the values around the feature at 23 eV and at lower energies where autoionization features are important. We note that there are no dramatic changes in the  $\beta_k^{\wedge}$  values in the resonance region, in contrast to the significant  $\beta_k^{\wedge}$  effects which have been predicted in the  $4\sigma_g \rightarrow k\sigma_u$  photoionization resonance in  $CO_2$ .<sup>19b,43</sup> The results for the IDAD asymmetry parameter show that above the resonance energy the contribution from the  $k\sigma_u$  continuum channel drops off rapidly leaving only the contribution from the  $k\pi_u$  continuum.

#### D. Photoionization leading to the $A^2\Pi_u^+$ state of $N_2^+$

---

The photoionization channel leading to the  $A^2\Pi_u^+$  state of  $N_2^+$

corresponds in the one electron picture to ejecting an electron from the  $1\pi_u$  orbital into a continuum orbital having  $\sigma_g$ ,  $\pi_g$ , or  $\delta_g$  symmetry. For the ionization potential of this channel we have used  $IP = 16.7 \text{ eV}$ .<sup>3,11</sup> The maximum  $\ell$  included in the expansion of the scattering solution (Eq. (7)) was  $\ell_p = 6$  for continuum solutions of  $\sigma_g$ ,  $\pi_g$ , and  $\delta_g$  symmetries.

There is a well-known difficulty associated with using the FCHF approximation for the  $1\pi_u \rightarrow k\pi_g$  channel.<sup>4,5</sup> If the straightforward FCHF potential is used the photoionization cross section is unphysically large as shown in Fig. 6a. The potential used in this calculation was the usual singlet-coupled potential for the  $\pi_u^3 k\pi_g$  configuration,

$$V_{\pi}^1 = \sum_{\sigma} (2J_{\sigma} - K_{\sigma}) + 2J_{\pi^-} + J_{\pi^+} + K_{\pi^+} - K_{\pi^-} + 2S'_{\pi} - S''_{\pi} \quad (56)$$

where  $J$  and  $K$  are the usual Coulomb and exchange operators and  $S'$  and  $S''$  are defined by

$$S'_{\pi} \phi^+(\vec{r}_1) = \pi^+(\vec{r}_1) \int d^3\vec{r}_2 \frac{[\pi^-(\vec{r}_2)]^* \phi^-(\vec{r}_2)}{r_{12}} \quad (57)$$

and

$$S''_{\pi} \phi^+(\vec{r}_1) = \phi^-(\vec{r}_1) \int d^3\vec{r}_2 \frac{[\pi^-(\vec{r}_2)]^* \pi^+(\vec{r}_2)}{r_{12}} \quad (58)$$

The origin of the unphysical result presented in Fig. 6a is that the HF

potential given in Eq. (56) places the strong valence  $\pi \rightarrow \pi^*$  transition above the ionization threshold. This transition then appears as a large feature in the photoionization profile. If the appropriate  $\sigma \rightarrow \sigma^*$  correlations were included in the final-state wave function, then this transition would be brought below the ionization threshold in better agreement with experiment.<sup>5</sup> Instead of including final-state correlation in our calculation, we have chosen to modify the HF potential so that the  $\pi \rightarrow \pi^*$  oscillator strength is removed from the continuum.<sup>4</sup> We have tried three different ways of removing this deficiency of the HF potential. The first two methods are based on the observation that if an appropriate representation could be found for the  $\pi^*$  orbital, then the continuum solutions could be obtained using the singlet potential given in Eq. (56), with the additional condition that the continuum solution be orthogonal to the valence  $\pi^*$  orbital.<sup>4</sup> The orthogonality condition is imposed by using the appropriate Phillips-Kleinman potential. We have obtained the valence  $\pi^*$  orbital using two methods. The first method used was to obtain eigenfunctions of the singlet potential using only a valence basis set. For this calculation we used the same basis set as was used to obtain the HF wave function. The eigenvalue of the  $\pi_g^*$  orbital using the singlet potential was 2.08 eV. The second is to construct eigenfunctions of the triplet potential

$$V_{\pi}^3 = \sum_{\sigma} (2J_{\sigma} - K_{\sigma}) + 2J_{\pi-} + J_{\pi+} - K_{\pi+} - K_{\pi-} - S_{\pi}'' \quad (59)$$

The eigenvalue of the  $\pi_g^+$  orbital in our valence basis set for this potential was -10.15 eV. This eigenvalue corresponds to an excitation energy

of 6.49 eV for the transition to the  $A^3\Sigma_u^+$  state  $N_2$ .<sup>44</sup> Using the triplet  $\pi^*$  orbital and projected singlet potential was the original solution to this problem used by Rescigno et al.<sup>4</sup> An alternative to using the projected singlet potential is to use the triplet potential given in Eq. (59) directly to obtain the continuum solutions. The use of the triplet potential to solve the  $\pi \rightarrow \pi^*$  problem has been used by Padias et al. in photoionization studies of  $CO_2$ .<sup>45</sup> The photoionization cross sections obtained using these three modifications to the FCHF approximation are presented in Fig. 6b. We see that the triplet orbital with projected singlet scattering potential gives results very similar to those obtained from the triplet scattering potential. The singlet orbital with projected singlet scattering potential does not seem to be as satisfactory as the other two methods. This probably implies that the valence singlet  $\pi^*$  orbital has been contaminated by nonvalence contributions. The rest of the results for this channel were obtained using the triplet scattering potential, which seems to be the simplest approach to avoiding the  $\pi \rightarrow \pi^*$  problem.

In Fig. 7 we present the cross sections for photoionization leading to the  $A^2\Pi_u$  state. We give results obtained using the dipole length and dipole velocity forms of the cross section using both HF and CI type initial-state wave functions. We compare our results to the experimental data of Plummer et al.<sup>11</sup> and of Hamnett et al.<sup>13</sup> In this channel the effect of using a CI initial-state wave function is not very large. Inclusion of initial-state correlation does bring the length and velocity cross sections into slightly better agreement, however the effect is not as large as we found in the channel leading to the  $X^2\Sigma_g^+$  state of  $N_2^+$ .

In the experimental cross section the feature at 23 eV is again due to autoionization from Rydberg states leading to the  $C^2\Sigma_u^+$  state of  $N_2^+$ .<sup>11,42</sup>

The broad peaked shape of the cross section in this channel is due to the  $1\pi_u \rightarrow k\delta_g$  channel. The enhancement of the cross section in this channel is examined in more detail in Fig. 8 where the cross section and eigenphase sums of the  $1\pi_u \rightarrow k\delta_g$  channel are compared to those of the resonant  $3\sigma_g \rightarrow k\sigma_u$  channel. As can be seen from Fig. 8, the peak of the  $1\pi_u \rightarrow k\delta_g$  cross section is very broad when compared to the  $3\sigma_g \rightarrow k\sigma_u$  cross section. Also, the eigenphase sums indicate that the  $1\pi_u \rightarrow k\delta_g$  channel is not resonant. Thus the nonresonant energy dependence of the dipole matrix elements must determine the shape of the  $1\pi_u \rightarrow k\delta_g$  photoionization cross section of  $N_2$  in much the same manner as it does the shape of the  $2p \rightarrow kd$  photoionization cross section of Ne, as discussed by Cooper.<sup>46</sup>

We present in Fig. 9 the asymmetry parameters for this channel. Once again our computed  $\beta_{\hat{k}}$  agrees well with the experimental results of Marr *et al.*<sup>12</sup> The computed  $\beta_{\hat{n}}$ , which is very near in value to -1, reflects that the  $\mu = 0$  contribution ( $1\pi_u \rightarrow k\pi_g$ ) is very small.

#### E. Photoionization leading to the $B^2\Sigma_u^+$ state of $N_2^+$

In the one-electron picture, the photoionization channel leading to the  $B^2\Sigma_u^+$  state of  $N_2^+$  corresponds to ejecting an electron from the  $2\sigma_u$  orbital into a continuum orbital of  $\sigma_g$  or  $\pi_g$  symmetry. We used 18.8 eV for the ionization potential of this state.<sup>3,11</sup> The maximum  $\ell$  included in the expansion of the scattering solution (Eq. (7)) was  $\ell_p = 6$  for continuum solutions of both  $\sigma_g$  and  $\pi_g$  symmetry.

In Fig. 10 we present the calculated cross sections for this channel. In this case there seems to be little differential effect between length and velocity forms of the cross section on going from the HF initial-state wave function to the CI wave function. We also see in Fig. 10 that the present results are in fairly good agreement with the experimental results of Plummer et al.<sup>11</sup> and with those of Hamnett et al.<sup>13</sup>

In Fig. 11 we present the  $\beta$ 's for this channel. The agreement between the calculated  $\beta_{\hat{k}}$  and the experimental points of Marr et al.<sup>12</sup> is not as satisfactory in this channel as it was in the other two channels we have considered here. This difficulty is probably due to the inadequacy of the single particle hole state used in the FCHF approximation for this higher energy ionic state. A more accurate treatment would necessarily include a better representation of the final-state ionic wave function. The computed  $\beta_{\hat{n}}$  reflects that at low energy the main contribution to the cross section is from the  $2\sigma_u \rightarrow k\sigma_g$  channel, and that at higher energy the  $2\sigma_u \rightarrow k\pi_g$  channel becomes more important.

#### F. Total photoionization cross section of N<sub>2</sub>

We have summed the cross sections discussed above to obtain the total photoionization cross section of N<sub>2</sub> leading to the X <sup>2</sup>Σ<sub>g</sub><sup>+</sup>, A <sup>2</sup>Π<sub>u</sub><sup>+</sup>, and B <sup>2</sup>Σ<sub>u</sub><sup>+</sup> states of N<sub>2</sub><sup>+</sup>. These results are presented in Fig. 12 along with the total ionization cross sections obtained by Wight et al.<sup>14</sup> In order to make an appropriate comparison with our total cross section we have corrected Wight's total cross section by multiplying by the sum

of the branching ratios, obtained by Hamnett et al.,<sup>13</sup> for the three channels we have considered.

We can see from Fig. 12 that the effect of initial state correlation is to lower the length form and not to alter appreciably the velocity form of the cross section. The length form is now in excellent agreement with experimental results except for the 23eV feature which we mentioned earlier. In particular, the shape of the shoulder in the cross section due to the  $3\sigma_g \rightarrow k\sigma_u$  resonance, as well as the high energy fall off of the cross section are well reproduced using the FCHF model with initial-state correlation included.

It seems that the total calculated cross section is in better agreement with the experimental results than the individual partial channel cross sections are. This is probably due to effects of interchannel coupling which might redistribute the oscillator strength between different channels but does not seem to greatly affect the total cross section.

### G. Comparison with other theoretical methods

The partial cross sections for the three channels, which we have considered here, have been studied previously using the CMSM<sup>2</sup> and STMT<sup>3,4</sup> approaches to photoionization. In Fig. 13 we have compared our FCHF results obtained in the dipole length approximation using a HF initial-state wave function with results from the CMSM and STMT methods. The three methods are in qualitative agreement. The STMT results seem to be within 10-15% of our single-center results. The CMSM results are generally in worse agreement with the single-center results than are the STMT results.

## V. Conclusions

We have obtained photoionization cross sections of  $N_2$  using a single-center expansion technique and examined in detail the effect of the truncation of the single-center expansion on the energy of the peak cross section in the  $3\sigma_g \rightarrow k\sigma_u$  channel. We found that the peak energy for this resonance converged as  $1/\ell^3$ . This rate of convergence was also found in single-center expanded nuclear potential integrals where the orbitals involved were of  $\sigma$  symmetry. Thus the  $1/\ell^3$  convergence may be a general feature of  $\sigma$  symmetry shape resonances.

The coupled integral equations resulting from the single-center expansion of the Lippmann-Schwinger equation were solved using the iterative Schwinger variational method. We found that, with an adequate initial basis set, the iterative method converged to accurate static-exchange results in only one iteration.

We have used a frozen-core Hartree-Fock final state with a correlated initial state to compute molecular photoionization cross sections. This combination gives a good representation of the photoionization process except when two-electron resonances are important. We feel that it is important to obtain these accurate HF level final-state solutions before attempting to treat final-state correlation effects.

Acknowledgments

This material is based upon work supported by the National Science Foundation under Grant No. CHE79-15807. This research was also supported in part by an Institutional Grant from the United States Department of Energy, No. EY-76-G-03-1305. The research reported in this paper made use of the Dreyfus-NSF Theoretical Chemistry Computer which was funded through grants from the Camille and Henry Dreyfus Foundation, the National Science Foundation (Grant No. CHE78-20235), and the Sloan Fund of the California Institute of Technology.

We thank Professor W. A. Goddard III for making his molecular bound state computer codes available and J. Low for help with these programs. One of us (R. R. L. ) acknowledges support from a National Science Foundation Graduate Research Fellowship and from an Exxon Foundation Graduate Educational Fellowship. One of us (G. R. ) acknowledges a fellowship from IBM (Belgium).

References

- <sup>1</sup> See for example, Electron-Molecule and Photon-Molecule Collisions, ed. T. Rescigno, V. McKoy and B. Schneider (Plenum Press, New York, 1979).
- <sup>2</sup> J. W. Davenport, Phys. Rev. Lett. 36, 945 (1976), and Int. J. Quantum Chem. S11, 89 (1977).
- <sup>3</sup> T. N. Rescigno, C. F. Bender, B. V. McKoy, and P. W. Langhoff, J. Chem. Phys. 68, 970 (1978).
- <sup>4</sup> T. N. Rescigno, A. Gerwer, B. V. McKoy, and P. W. Langhoff, Chem. Phys. Lett. 66, 116 (1979).
- <sup>5</sup> G. R. J. Williams and P. W. Langhoff, Chem. Phys. Lett. 78, 21 (1981).
- <sup>6</sup> A. Temkin and K. V. Vasavada, Phys. Rev. 160, 109 (1967).
- <sup>7</sup> F. Hirota, Chem. Phys. Lett. 74, 67 (1980).
- <sup>8</sup> C. Duzy and R. S. Berry, J. Chem. Phys. 64, 2421 (1976).
- <sup>9</sup> G. Raseev, H. LeRouzo, and H. Lefebvre-Brion, J. Chem. Phys. 72, 5701 (1980).
- <sup>10</sup> W. D. Robb and L. A. Collins, Phys. Rev. A 22, 2474 (1980).
- <sup>11</sup> E. W. Plummer, T. Gustafsson, W. Gudat, and D. E. Eastman, Phys. Rev. A 15, 2339 (1977).

- <sup>12</sup>G. V. Marr, J. M. Morton, R. M. Holmes, and D. G. McCoy, J. Phys. B 12, 43 (1979).
- <sup>13</sup>A. Hamnett, W. Stoll and C. E. Brion, J. Electron Spectroscopy & Relat. Phenom. 8, 367 (1976).
- <sup>14</sup>G. R. Wight, M. J. Van der Wiel, and C. E. Brion, J. Phys. B 9, 675 (1976).
- <sup>15</sup>S. Wallace and D. Dill, Phys. Rev. B 17, 1692 (1978).
- <sup>16</sup>R. R. Lucchese, D. K. Watson, and V. McKoy, Phys. Rev. A 22, 421 (1980).
- <sup>17</sup>R. R. Lucchese, K. Takatsuka, D. K. Watson, and V. McKoy, "The Schwinger Variational Principle: An Approach to Electron-Molecule Collisions" in: Proceedings of the Symposium on Electron-Atom and Molecule Collisions, Universität Bielefeld (Plenum Press, London-New York, 1981).
- <sup>18</sup>R. R. Lucchese and V. McKoy, Phys. Rev. A 24, 770 (1981).
- <sup>19</sup>a) R. R. Lucchese and V. McKoy, J. Phys. Chem. 85, 2166 (1981);  
b) R. R. Lucchese and V. McKoy, "Studies of Differential and Total Photoionization Cross Sections of Carbon Dioxide," - in preparation.

- <sup>20</sup> D. K. Watson, T. N. Rescigno, and B. V. McKoy, *J. Phys. B*, 14, 1875 (1981).
- <sup>21</sup> R. R. Lucchese and V. McKoy, "Study of Electron Scattering by CO<sub>2</sub> at the Static-Exchange Level" *Phys. Rev. A*-submitted for publication.
- <sup>22</sup> J. R. Swanson and L. Armstrong, Jr., *Phys. Rev. A* 15, 661 (1977).
- <sup>23</sup> M. Abramowitz, "Coulomb Wave Functions" in Handbook of Mathematical Functions AMS 55, ed. M. Abramowitz and I. A. Stegun (National Bureau of Standards, 1972) p. 537, Washington, D.C.
- <sup>24</sup> G. Arfken, Mathematical Methods for Physicists, 2nd Edition (Academic Press, New York, 1970) p. 737.
- <sup>25</sup> W. H. Miller, *J. Chem. Phys.* 50, 407 (1969).
- <sup>26</sup> S. K. Adhikari and I. H. Sloan, *Phys. Rev. C* 11, 1133 (1975).
- <sup>27</sup> V. B. Belyaev, A. P. Podkopoyev, J. Wrzeczionko, and A. L. Zubarev, *J. Phys. B* 12, 1225 (1979).
- <sup>28</sup> M. E. Riley and D. G. Truhlar, *J. Chem. Phys.* 65, 792 (1976).
- <sup>29</sup> F. W. Bobrowicz and W. A. Goddard III, in Modern Theoretical Chemistry 3, ed. H. F. Schaefer III (Plenum, New York, 1977) p. 79.
- <sup>30</sup> R. R. Lucchese and V. McKoy, *Phys. Rev. A* 21, 112 (1980).

- <sup>31</sup> P. G. Burke and N. Chandra, *J. Phys. B* 5, 1696 (1972).
- <sup>32</sup> J. D. Weeks, A. Hazi, and S. A. Rice, in Advances in Chemical Physics Vol. XVI, (Interscience, New York, 1969) p. 283.
- <sup>33</sup> H. P. Kelly, *Chem. Phys. Lett.* 20, 547 (1973).
- <sup>34</sup> J. C. Tully, R. S. Berry, and B. J. Dalton, *Phys. Rev.* 176, 95 (1968).
- <sup>35</sup> T. H. Dunning, Jr., *J. Chem. Phys.* 53, 2823 (1970).
- <sup>36</sup> T. H. Dunning, Jr., *J. Chem. Phys.* 55, 3958 (1971).
- <sup>37</sup> A. W. Fliflet and V. McKoy, *Phys. Rev. A* 18, 1048 (1978).
- <sup>38</sup> L. A. Collins, W. D. Robb, and M. A. Morrison, *Phys. Rev. A* 21, 488 (1980).
- <sup>39</sup> I. Shavitt, in Modern Theoretical Chemistry 3, ed. H. F. Schaefer III (Plenum, New York, 1977) p. 189.
- <sup>40</sup> D. M. Silver, E. L. Mehler, and K. Ruedenberg, *J. Chem. Phys.* 52, 1174 (1970).
- <sup>41</sup> F. E. Harris and H. H. Michels, *J. Chem. Phys.* 43, S165 (1965).
- <sup>42</sup> K. Codling, *Astrophys. J.* 143, 552 (1966).
- <sup>43</sup> F. A. Grimm, T. A. Carlson, W. B. Dress, D. Agron, J. O. Thomson, and J. W. Davenport, *J. Chem. Phys.* 72, 3041 (1980).

- <sup>44</sup>J. B. Rose and V. McKoy, *J. Chem. Phys.* 55, 5435 (1971).
- <sup>45</sup>N. Padial, G. Csanak, B. V. McKoy, and P. W. Langhoff, *Phys. Rev. A* 23, 218 (1981).
- <sup>46</sup>J. W. Cooper, *Phys. Rev.* 128, 681 (1962).

TABLE I. Scattering basis sets used with the Schwinger variational expression.<sup>a</sup>

Symmetry of Continuum Solution	Type of Gaussian Function <sup>b</sup>	Exponents
$\sigma_g$	Cartesian - s	16.0, 8.0, 4.0, 2.0, 1.0, 0.5
	- z	1.0, 0.5
	Spherical - $\ell=0$	2.0, 1.0, 0.5
	- $\ell=2$	2.0, 1.0, 0.5
$\sigma_u$	Cartesian - s	16.0, 8.0, 4.0, 2.0, 1.0, 0.5
	- z	1.0, 0.5
	Spherical - $\ell=1$	4.0, 2.0, 1.0, 0.5
	- $\ell=3$	4.0, 2.0, 1.0, 0.5
	- $\ell=5$	1.0, 0.5
$\pi_u$	Cartesian - x	8.0, 4.0, 2.0, 1.0, 0.5
	- xz	0.5
	Spherical - $\ell=1$	1.0
	- $\ell=3$	1.0
$\pi_g$	Cartesian - x	8.0, 4.0, 2.0, 1.0, 0.5
	- xz	0.5
	Spherical - $\ell=2$	1.0
	- $\ell=4$	1.0
$\delta_g$	Cartesian - xy	4.0, 2.0, 1.0, 0.5, 0.25
	Spherical - $\ell=2$	1.0
	- $\ell=4$	1.0

<sup>a</sup>These basis sets correspond to the set R of Eq. (10).

<sup>b</sup>The basis functions are symmetry adapted functions constructed from either Cartesian or spherical Gaussian functions, as defined in the text, of the given type. Cartesian functions are centered at the nuclei and spherical functions are centered at the bond mid-point.

Figure Captions

- Fig. 1 Convergence of the  $3\sigma_g \rightarrow k\sigma_u$  photoionization cross section of  $N_2$  with varying potential parameters:  
 - - - - parameter set A ( $l_{\max}^{\text{dir}} = 20$ );  
 - - - - parameter set B ( $l_{\max}^{\text{dir}} = 30$ );  
 - - - - parameter set C ( $l_{\max}^{\text{dir}} = 40$ ).  
 For all three sets  $l_{\max}^{\text{exc}} = 20$ . These are results of noniterative calculations using the  $\sigma_u$  basis set of Table I in Eq. (10). One megabarn (Mb) is  $10^{-18} \text{ cm}^2$ .
- Fig. 2 Convergence of the  $3\sigma_g \rightarrow k\sigma_u$  photoionization cross section of  $N_2$  using the iterative Schwinger method:  
 - - - - iteration zero using Eq. (10); - - - - iteration one using Eq. (14).
- Fig. 3 Dependence of the energy of the peak photoionization cross section on  $l_{\max}^{\text{dir}}$  for the  $3\sigma_g \rightarrow k\sigma_u$  channel of  $N_2$ .
- Fig. 4 Photoionization cross section for the production of the  $X^2\Sigma_g^+$  state of  $N_2^+$ : HFL - in the dipole length approximation using a Hartree-Fock initial-state wave function; HFV - in the dipole velocity approximation using a Hartree-Fock initial-state wave function; CIL - in the dipole length approximation using a configuration interaction initial-state wave function; CIV - in the dipole velocity approximation using a configuration

initial-state wave function; ● - experimental results of Plummer et al. (Ref. 11); ■ - experimental results of Hamnett et al. (Ref. 13).

Fig. 5

Photoionization asymmetry parameters for the production of the  $X^2\Sigma_g^+$  state of  $N_2^+$ : (a) ITAD asymmetry parameter  $\hat{\beta}_k$ ; (b) IDAD asymmetry parameter  $\hat{\beta}_n$ ; ——— dipole length approximation using a correlated initial state; - - - - dipole velocity approximation using a correlated initial-state wave function; ● - experimental  $\hat{\beta}_k$  of Marr et al. (Ref. 12).

Fig. 6

Photoionization cross sections in the  $1\pi_u \rightarrow k\pi_g$  channel of  $N_2$  using various forms for the scattering potential: (a) unmodified potential compared with modified forms; (b) expanded scale showing modified potentials; ——— the cross section obtained using continuum solutions which are eigenfunctions of the triplet Hartree-Fock potential; - - - - using eigenfunctions of the singlet Hartree-Fock potential constrained to be orthogonal to a valence  $\pi_g$  eigenfunction of the triplet Hartree-Fock potential; - - - - using eigenfunctions of the singlet Hartree-Fock potential constrained to be orthogonal to a valence  $\pi_g$  eigenfunction of the singlet Hartree-Fock potential; - - - - - using eigenfunctions of the unmodified singlet Hartree-Fock potential.

- Fig. 7 Photoionization cross section for the production of the  $A^2\Pi_u$  state of  $N_2^+$  (same designations as in Fig. 4).
- Fig. 8 Comparison of photoionization in the  $3\sigma_g \rightarrow k\sigma_u$  channel with photoionization in the  $1\pi_u \rightarrow k\delta_g$  channel of  $N_2$ : (a) comparison of photoionization cross sections; (b) comparison of eigenphase sums; ———  $3\sigma_g \rightarrow k\sigma_u$  channel; - - - -  $1\pi_u \rightarrow k\delta_g$  channel.
- Fig. 9 Photoionization asymmetry parameters for the production of the  $A^2\Pi_u$  state of  $N_2^+$  (same designations as in Fig. 5).
- Fig. 10 Photoionization cross section for production of the  $B^2\Sigma_u^+$  state of  $N_2^+$  (same designations as in Fig. 4).
- Fig. 11 Photoionization asymmetry parameters for the production of the  $B^2\Sigma_u^+$  state of  $N_2^+$  (same designations as in Fig. 5).
- Fig. 12 Total photoionization cross section for the production of the  $X^2\Sigma_g^+$ ,  $A^2\Pi_u$ , and  $B^2\Sigma_u^+$  states of  $N_2^+$  (same designations as in Fig. 4):  $\blacktriangle$  total experimental cross sections of Wight et al. (Ref. 14) corrected to include only the contribution from these three channels using the experimental branching ratios of Hamnett et al. (Ref. 13).

Fig. 13

Comparison of different theoretical cross sections for the production of the  $X^2\Sigma_g^+$ ,  $A^2\Pi_u$ , and  $B^2\Sigma_u^+$  states of  $N_2^+$ : ——— present single center FCHF results; — — — — FCHF results obtained using the STMT approach (Refs. 3 and 4); - - - - CMSM model potential results (Ref. 2).

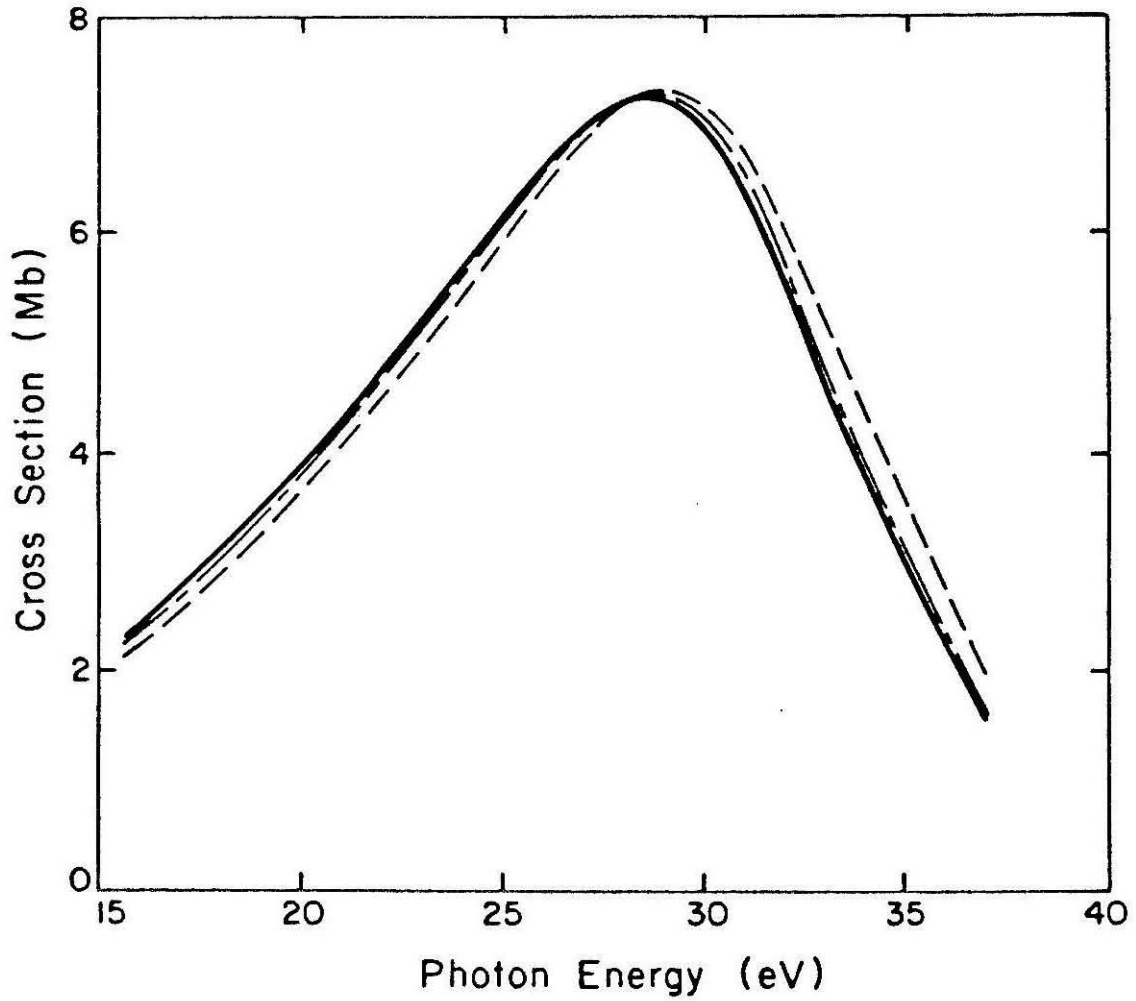


Figure 1

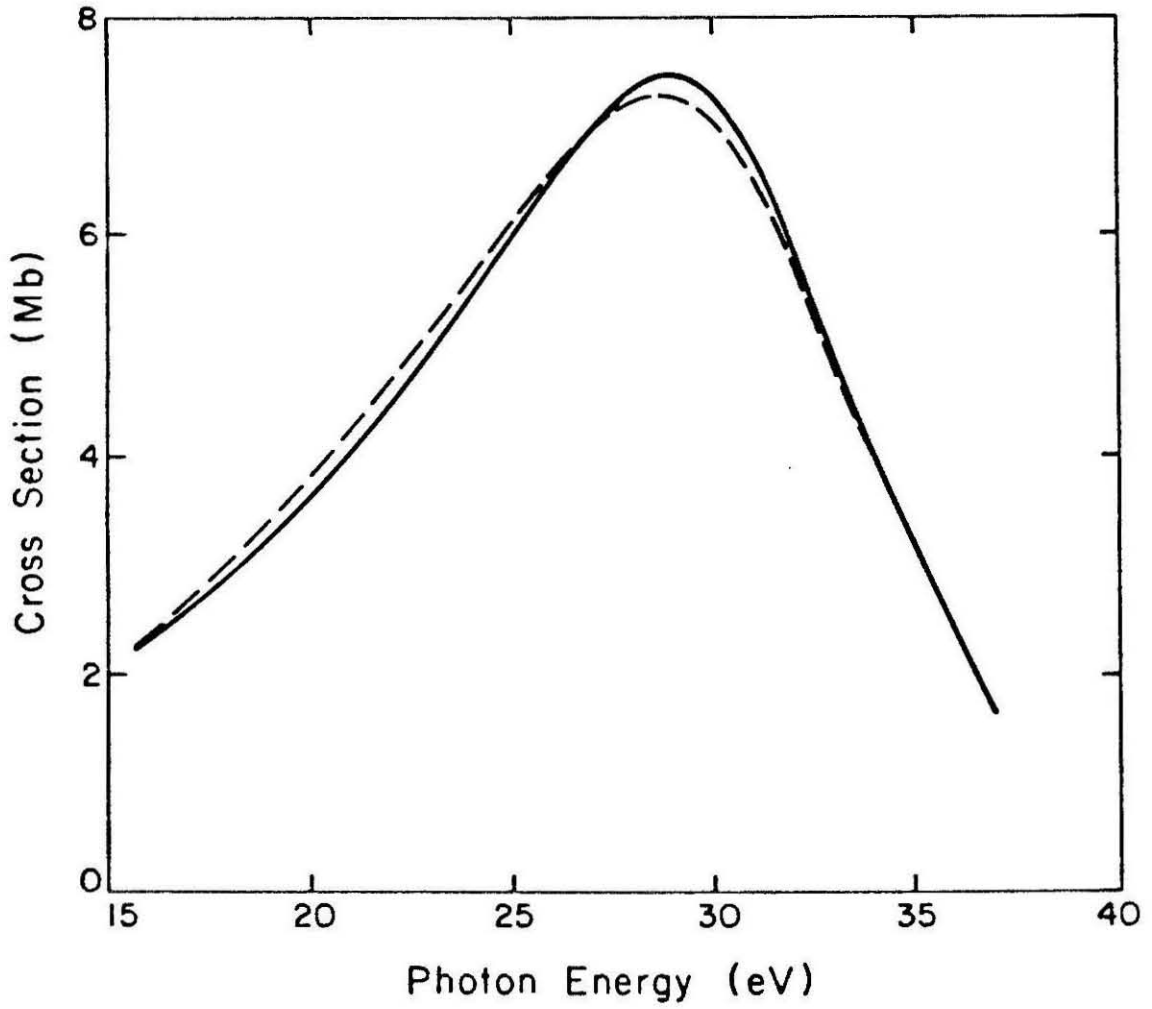


Figure 2

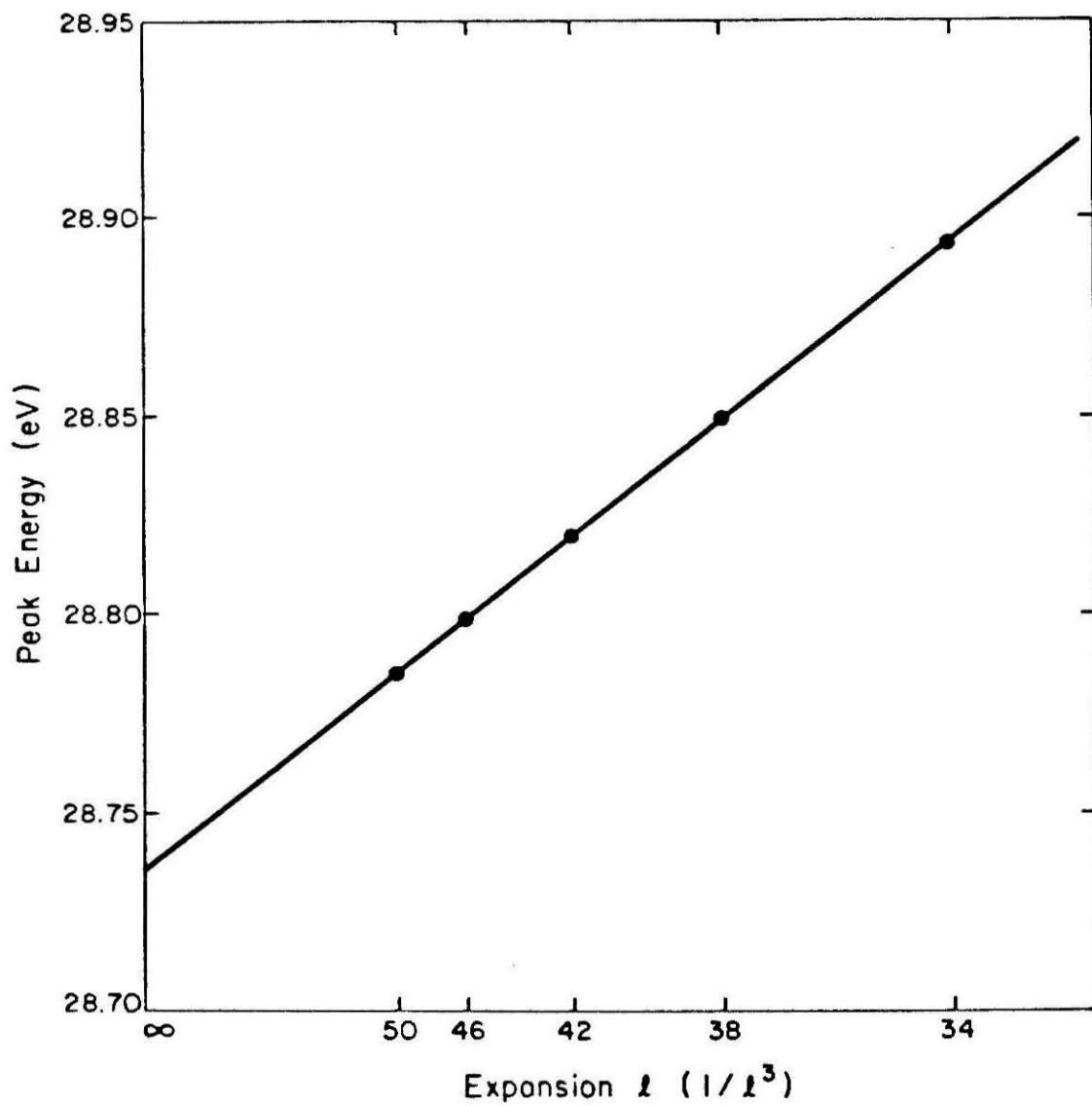


Figure 3

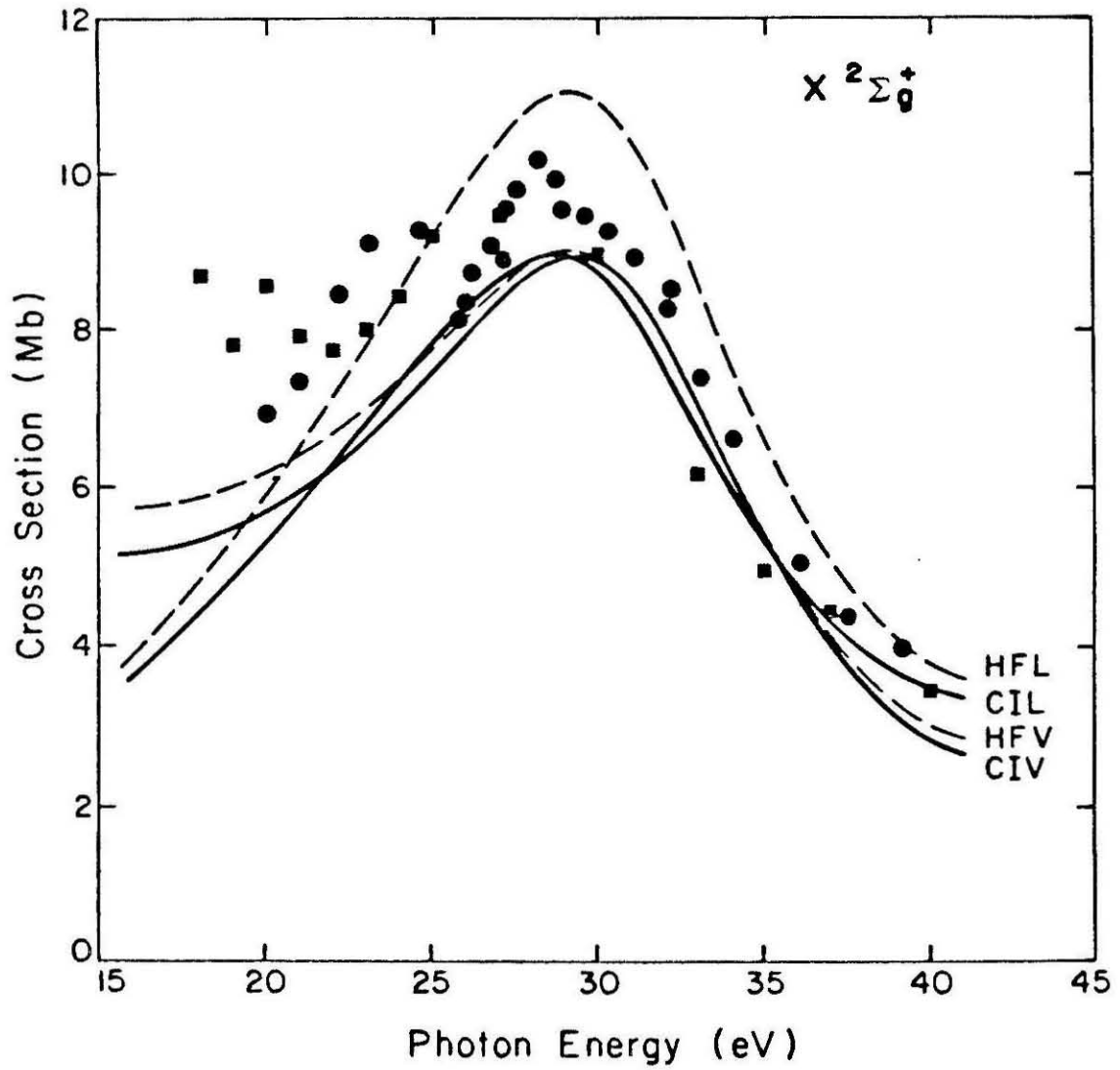


Figure 4

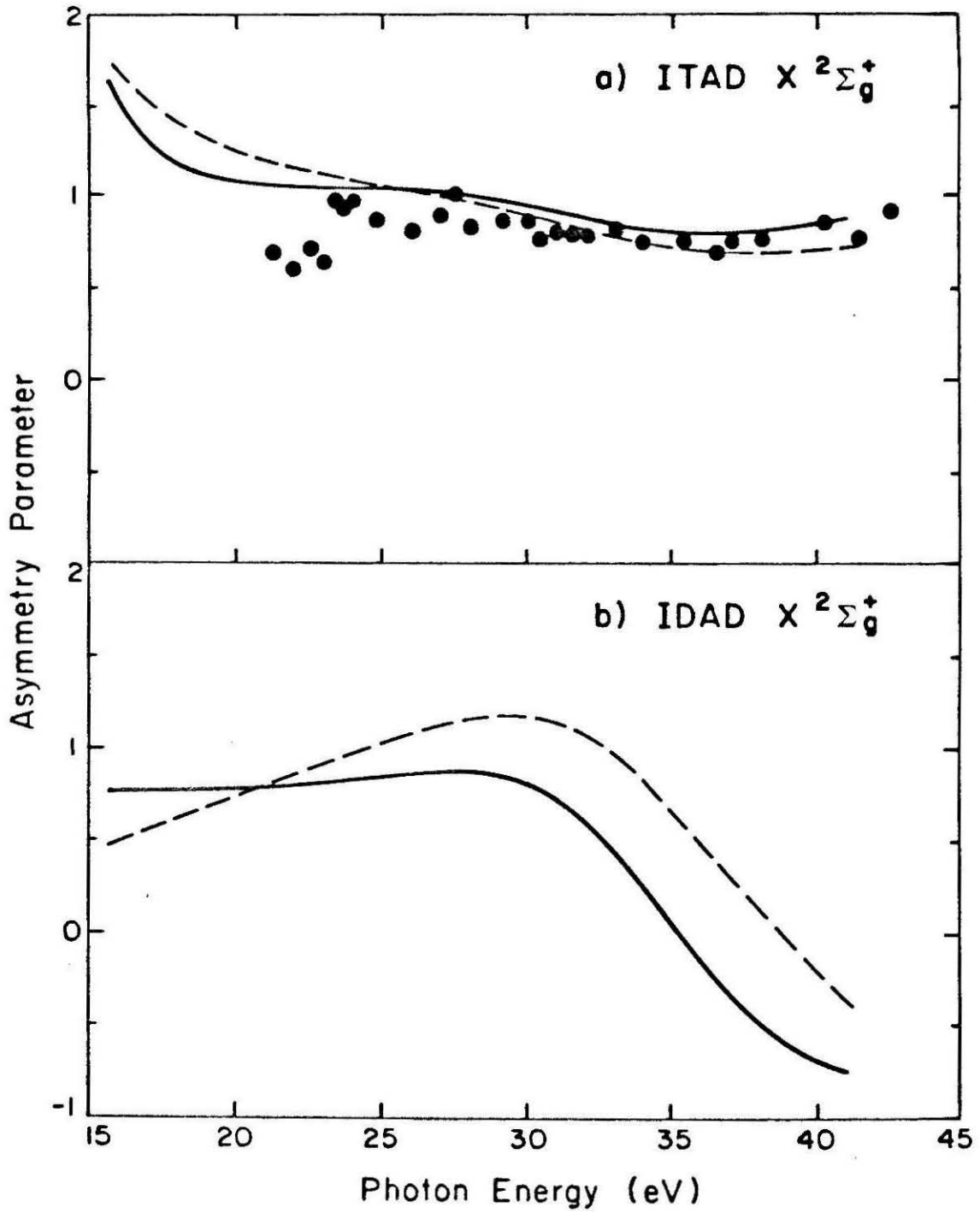


Figure 5

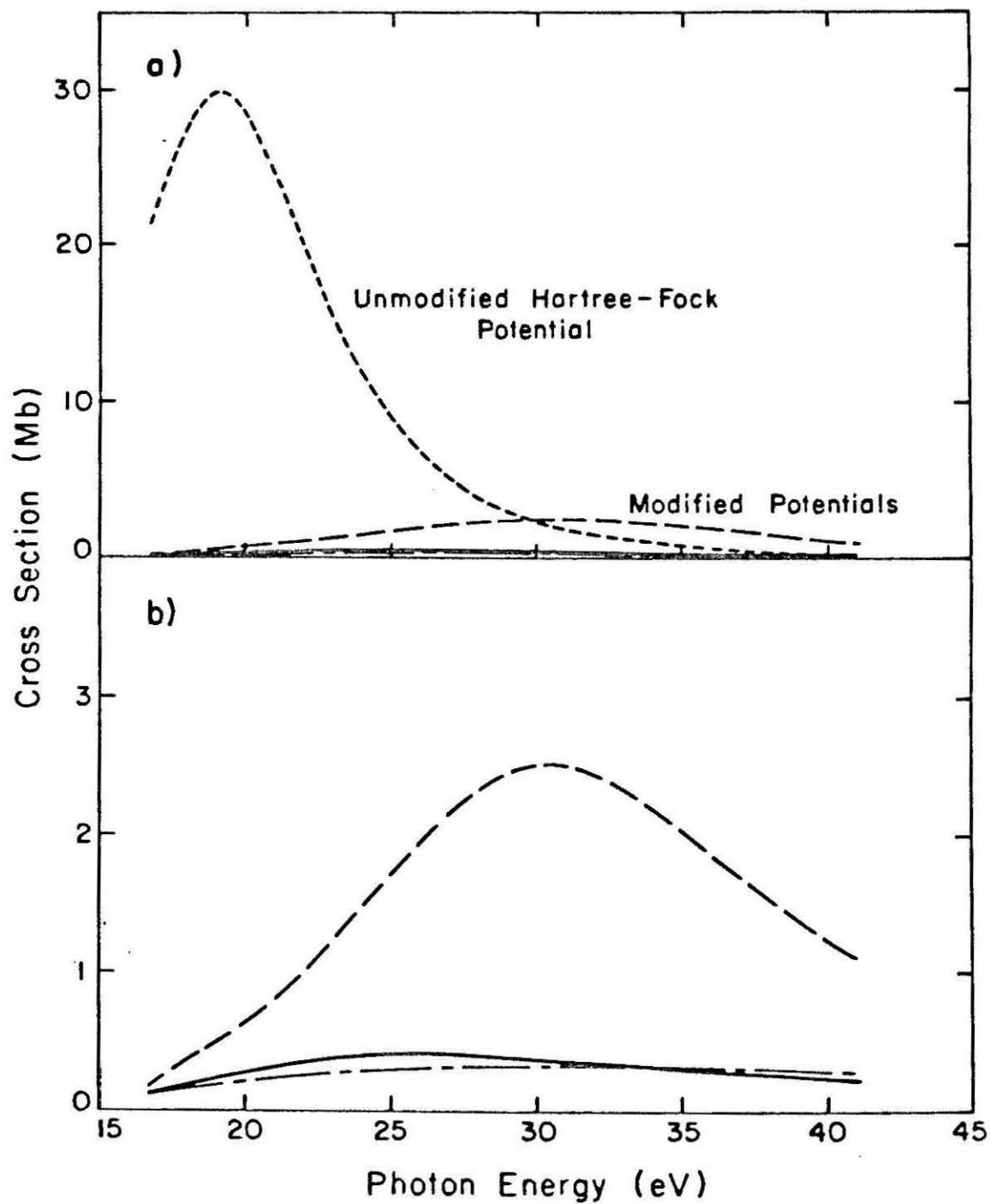


Figure 6

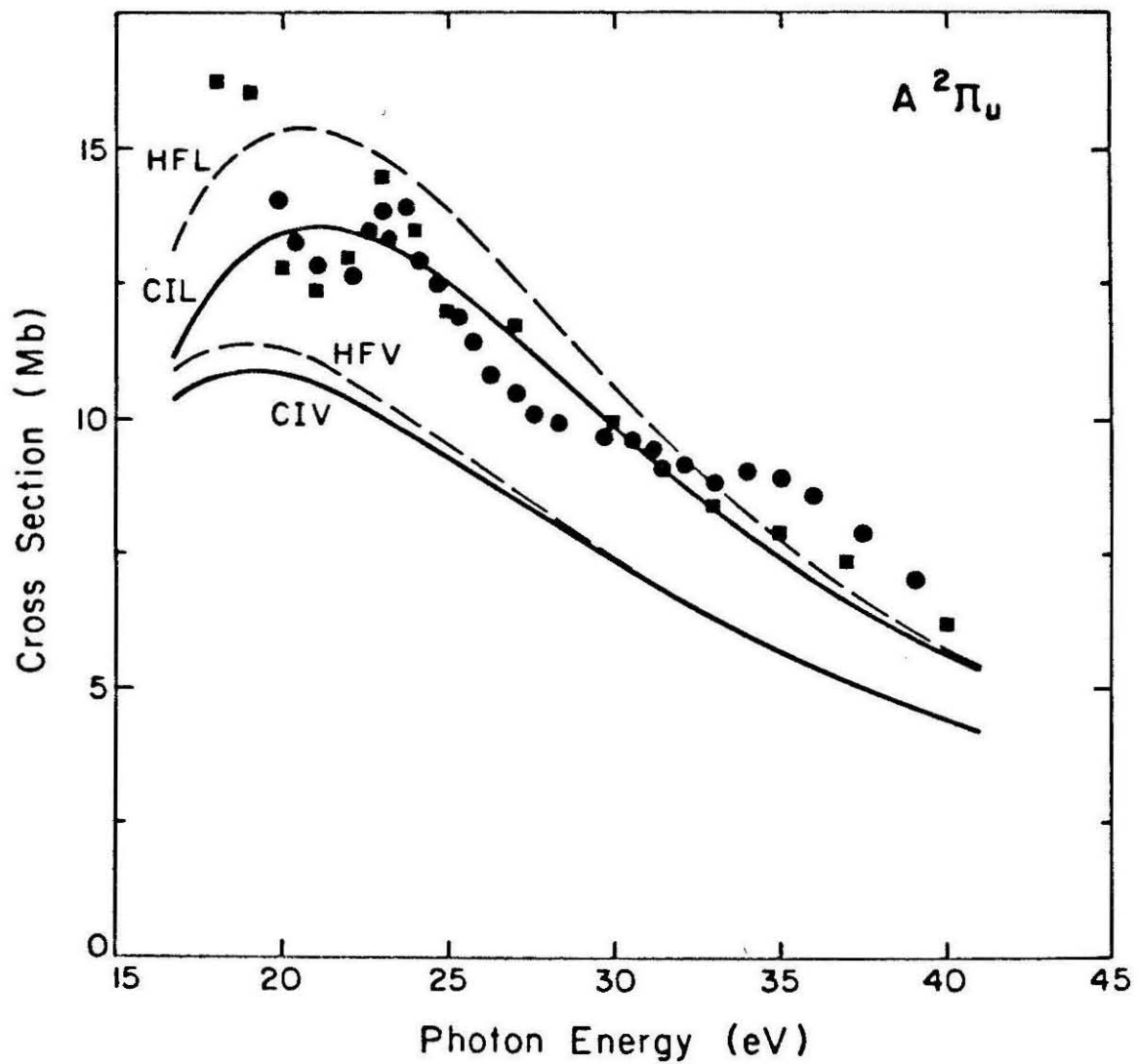


Figure 7

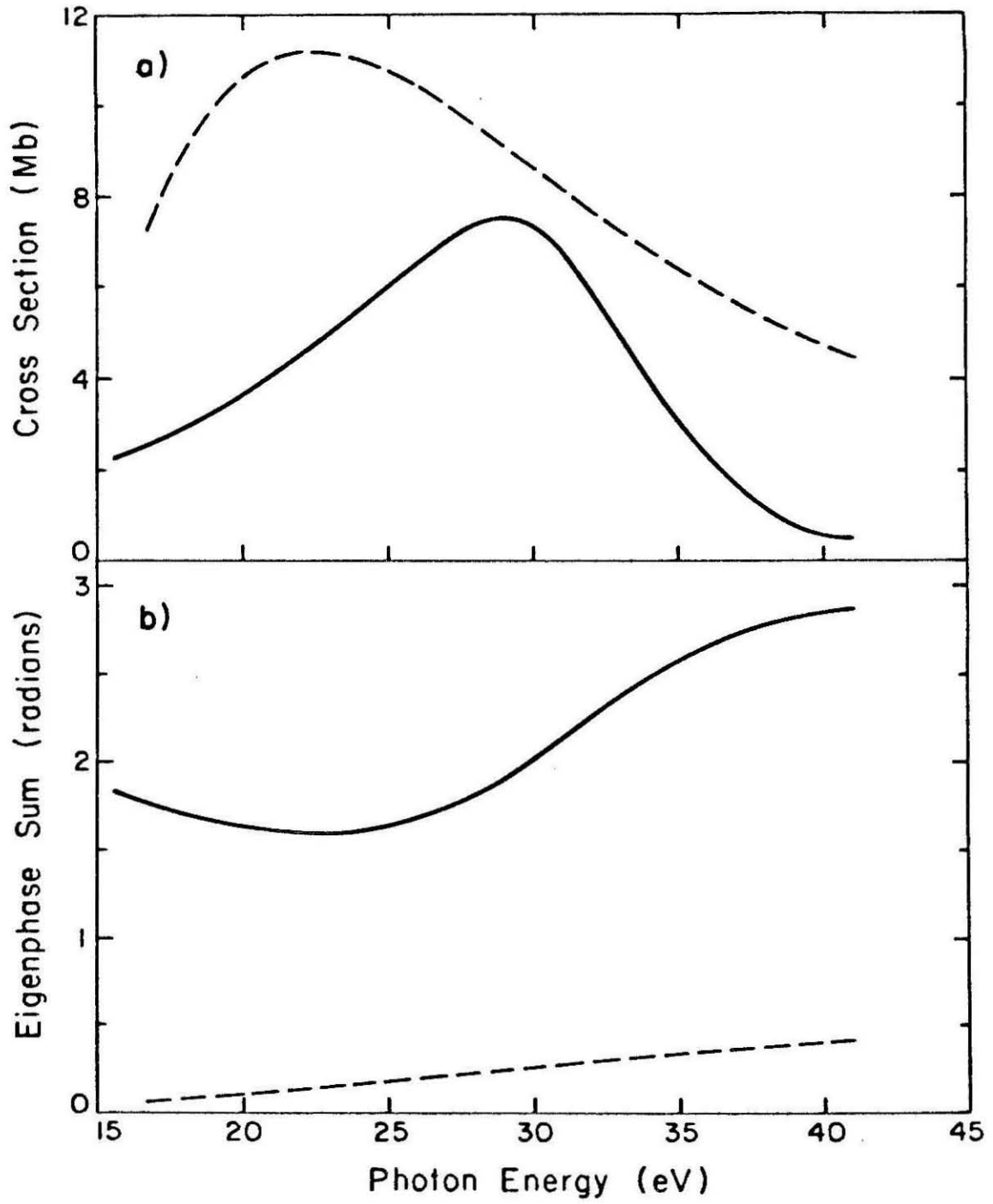


Figure 8

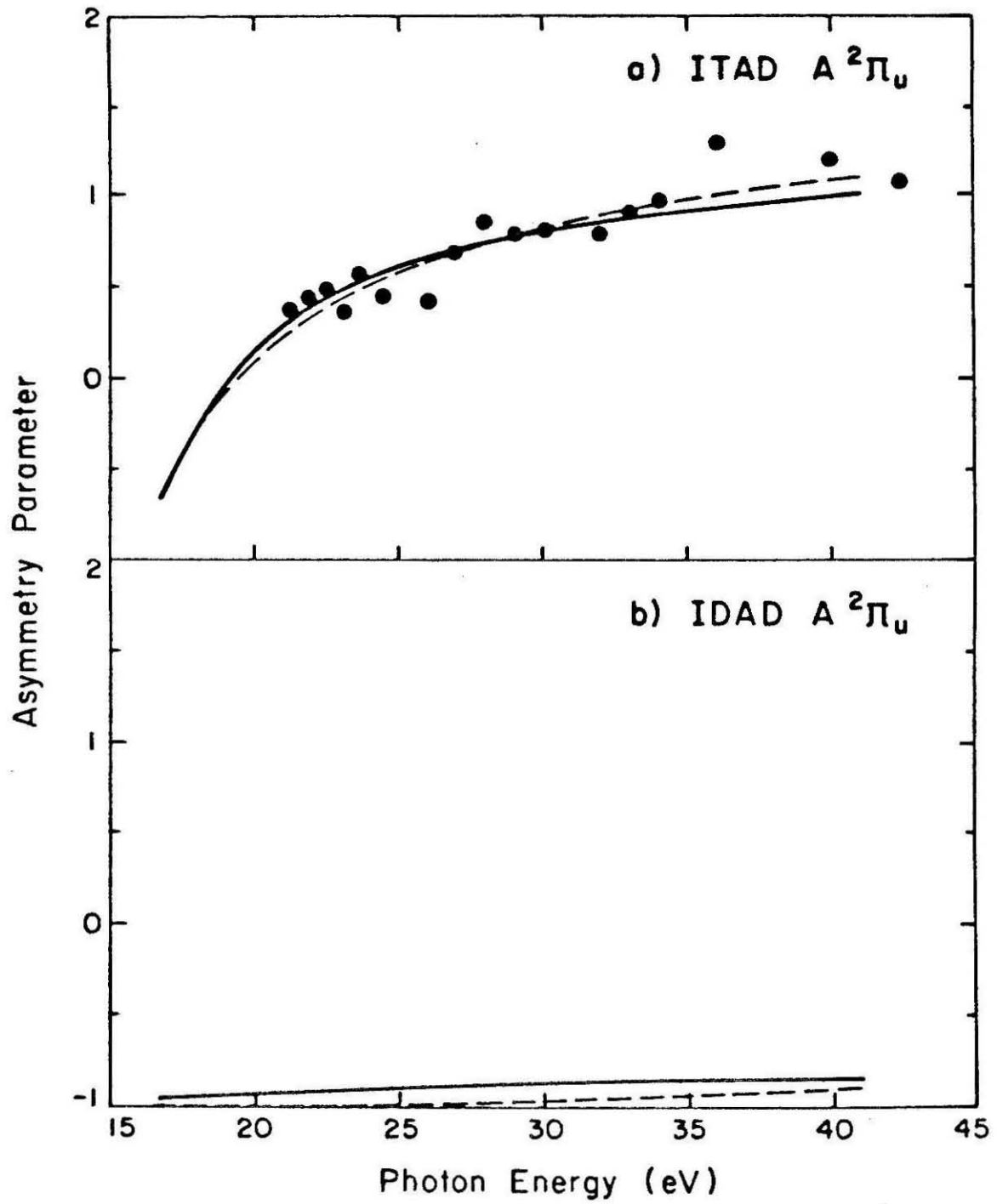


Figure 9

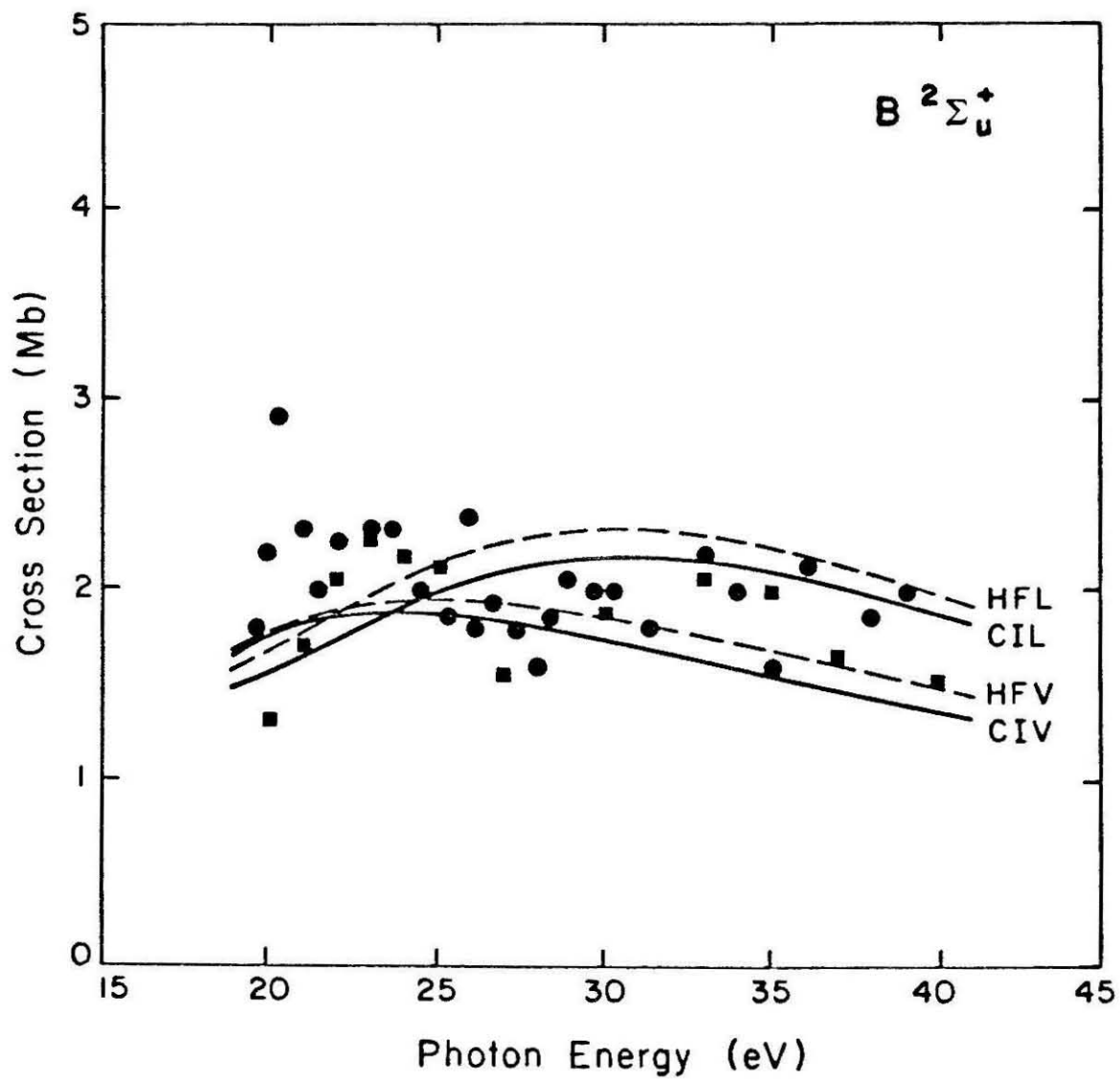


Figure 10

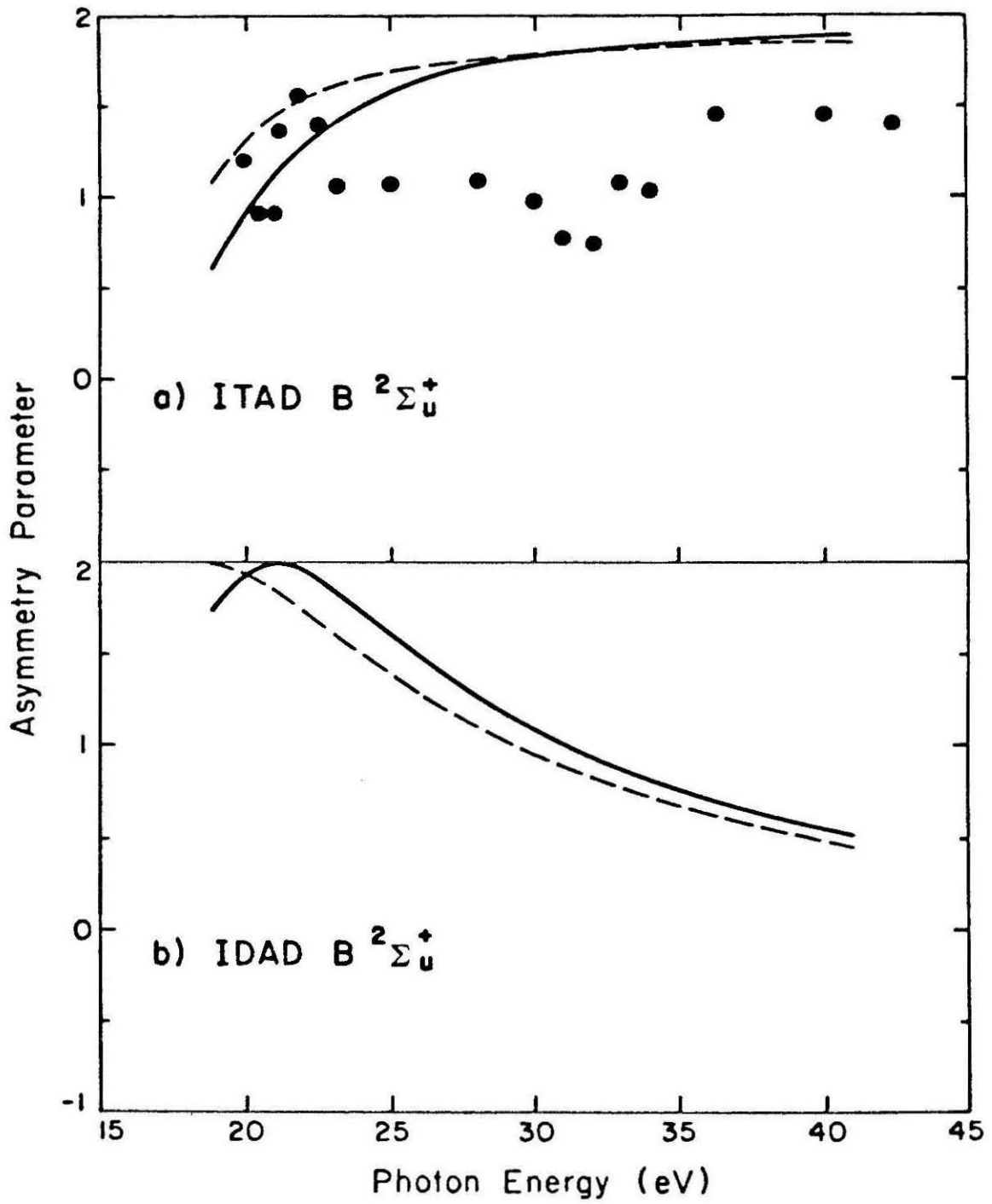


Figure 11

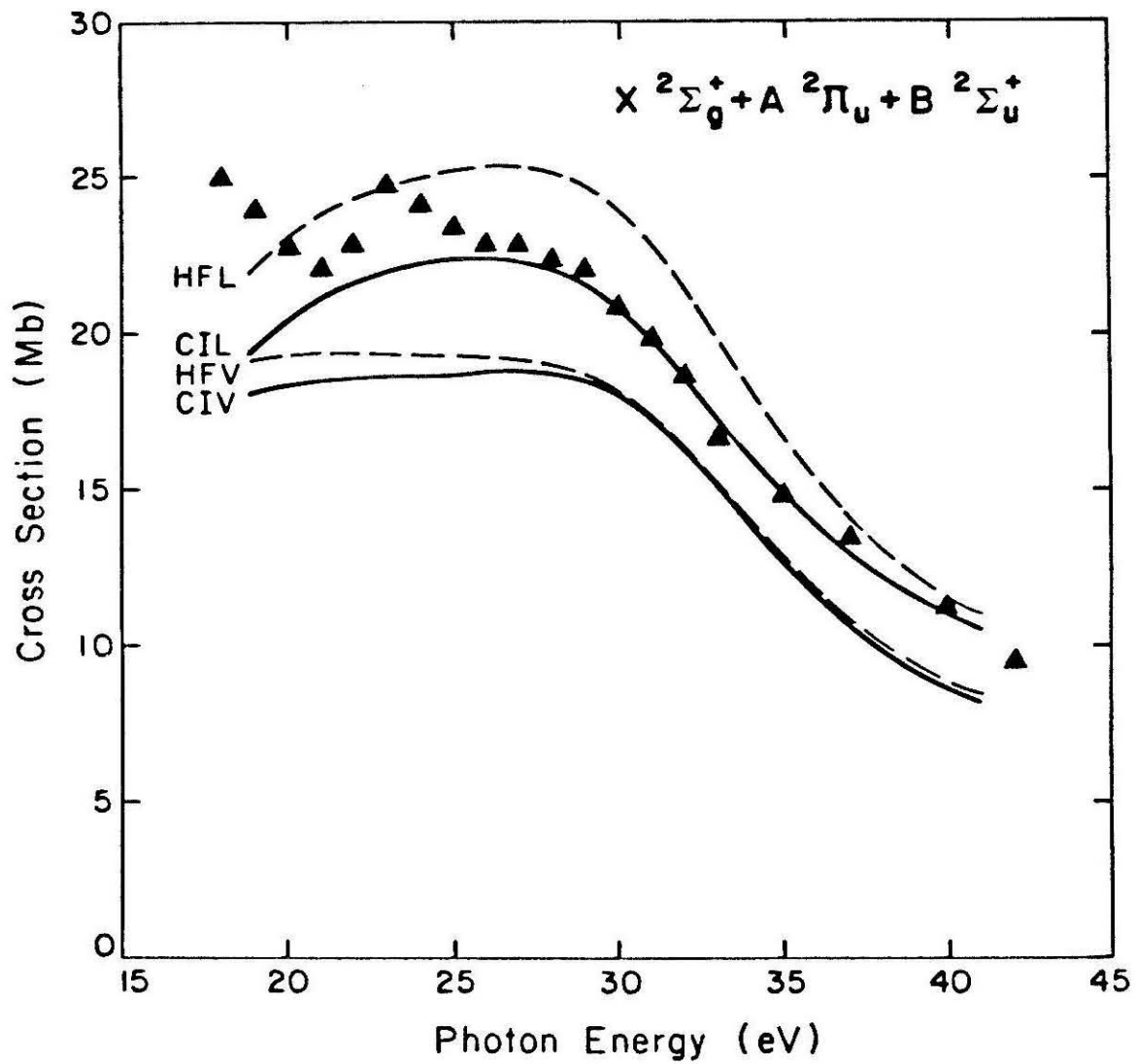


Figure 12

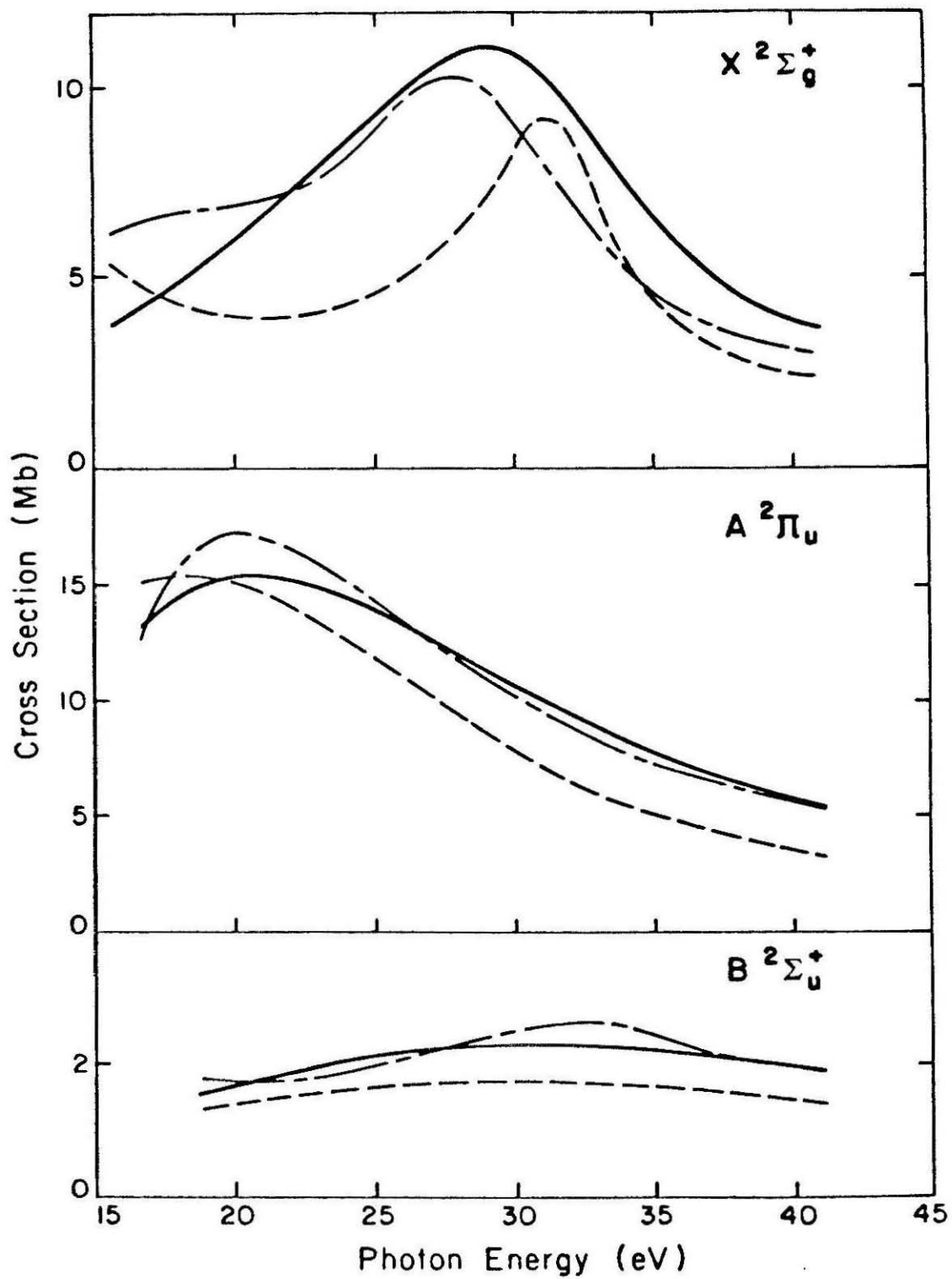


Figure 13

## SECTION B

Accurate Hartree-Fock Vibrational Branching Ratios  
in  $3\sigma_g$  Photoionization of  $N_2$

The shape resonance occurring in the photoionization of molecular nitrogen leading to the  $X^2\Sigma_g^+$  state of the ion is known to produce significant non-Franck-Condon effects in the final vibrational state distributions. These vibrational effects were first predicted by Dehmer et al (1979) and subsequently have been observed experimentally by West et al (1980). The original prediction by Dehmer et al (1979) using the continuum multiple scattering method (CMSM) was qualitatively correct but their computed vibrational branching ratio for the  $\nu' = 1$  vibrational state relative to the  $\nu = 0$  vibrational state was off by approximately a factor of two. Recently Raseev et al (1980) have studied vibrational effects in this system using an accurate Hartree-Fock single-center expansion method. The  $\nu' = 1/\nu' = 0$  branching ratio reported by Raseev et al (1980) is in much better agreement with the experimentally measured value of West et al (1980) than is the branching ratio obtained by Dehmer et al (1979). However, the results of Raseev et al (1980) are still low by about 25%.

In the present study we have re-examined the calculations of Raseev et al (1980) to determine whether the difference between the computed and experimental branching ratio is due to a breakdown of the adiabatic-nuclei frozen-core-Hartree-Fock model used in their study or whether the results given by Raseev et al (1980) were not fully converged solutions for this model. We have found two deficiencies in the calculation performed by Raseev et al (1980). The most important shortcoming of their calculation is that Raseev et al (1980) only computed the electronic transition matrix elements for three internuclear separations and obtained the value of these matrix elements at all other

points using a polynomial interpolation. We have found that it is important to compute the transition matrix elements at more internuclear separations since they are fairly rapidly varying functions of the internuclear separation. Another deficiency of the study of Raseev et al (1980) is that their potential expansion parameters are not well converged. We know from previous studies (Lucchese et al 1981) that with more accurate potential parameters the peak photoionization cross section in the fixed-nuclei approximation for the resonant  $3\sigma_g \rightarrow k\sigma_u$  channel of  $N_2$  is found to lie at a photon energy of 29 eV rather than at 31 eV as reported by Raseev et al (1980). When these two problems are corrected we have found that the adiabatic-nuclei frozen-core-Hartree-Fock  $\nu' = 1/\nu' = 0$  ratios are in very good agreement with the experimental values of West et al (1980).

We have repeated the calculations of Raseev et al (1980) correcting the two problems mentioned above. The frozen-core-Hartree-Fock approximation was used to describe the interaction between the photoelectron and the ionic core. To obtain the appropriate continuum solutions we have used the Schwinger variational method (Lucchese and McKoy 1980). For the purposes of this study we have not employed the iterative technique which has been applied to other systems (Lucchese et al 1980, Lucchese and McKoy 1981), since in our previous studies of the photoionization of  $N_2$  we found that the exact iterative cross section is in general very close to the initial noniterative result using only  $L^2$  basis functions (Lucchese et al 1981).

The scattering basis sets we have used for the  $3\sigma_g \rightarrow k\sigma_u$  and  $3\sigma_g \rightarrow k\pi_u$  photoionization channels of  $N_2$  are given in table 1. These

basis sets consist of both Cartesian Gaussian functions defined by

$$\phi^{\alpha, \ell, m, n, \underline{A}}(\underline{r}) = N (x - A_x)^\ell (y - A_y)^m (z - A_z)^n \times e^{-\alpha |\underline{r} - \underline{A}|^2} \quad (1)$$

and spherical Gaussian functions defined by

$$\phi^{\alpha, \ell, m, \underline{A}}(\underline{r}) = N |\underline{r} - \underline{A}|^\ell e^{-\alpha |\underline{r} - \underline{A}|^2} Y_{\ell m}(\Omega_{\underline{r} - \underline{A}}). \quad (2)$$

The continuum solutions which are used to obtain the photoionization cross section are given by

$$\psi_{klm}^{(-)}(\underline{r}) = \phi_{klm}^{c(-)}(\underline{r}) + \sum_{\alpha_i, \alpha_j \in R} \langle \underline{r} | G^{c(-)} U | \alpha_i \rangle \times [D^{-1}]_{ij} \langle \alpha_j | U | \phi_{klm}^{c(-)} \rangle \quad (3)$$

where  $[D^{-1}]_{ij}$  is the matrix inverse of

$$D_{ij} = \langle \alpha_i | U - U G^{c(-)} U | \alpha_j \rangle \quad (4)$$

and where  $U$  is the static-exchange interaction potential minus the long range Coulomb potential of the ionic core,  $G^{c(-)}$  is the Coulomb Green's function and  $R$  is the appropriate scattering basis set given in

table 1. All necessary integrals are computed by expanding all functions in truncated partial wave expansions with the resulting radial integrals put on a grid and computed using Simpson's rule. We have also constructed our continuum solutions subject to the constraint that they be orthogonal to the bound orbitals of the same symmetry. More details of this method can be found in previous papers (Lucchese et al 1981, Lucchese et al 1980, Lucchese and McKoy 1980).

The Hartree-Fock (HF) target wave function was constructed from a (9s5p2d/4s3p2d) contracted Cartesian Gaussian basis set (Dunning 1970, Dunning 1971). The computed HF energy of  $N_2$  for the equilibrium nuclear separation of  $R = 2.068$  au was  $E = -108.973235$  au, and the quadrupole moment for the neutral  $N_2$  molecule in this basis was  $-0.9923$  au.

The parameters used to expand the static-exchange potential were as follows:

- 1)  $l_m = 30$ , maximum  $l$  included in the expansion of the scattering functions and of the Coulomb Green's function,
- 2)  $l_s^{ex} = 30$ , maximum  $l$  included in the expansion of the scattering functions in the exchange terms,
- 3)  $l_i^{ex} = 24(1\sigma_g), 12(2\sigma_g), 12(3\sigma_g), 24(1\sigma_u), 12(2\sigma_u), 12(1\pi_u)$ , maximum  $l$  included in the expansion of the occupied orbitals in the exchange terms,
- 4)  $l_i^{dir} = 30$ , maximum  $l$  included in the expansion of the occupied orbitals in the static potential,
- 5)  $\lambda_m^{ex} = 30$ , maximum  $l$  included in the expansion of  $1/r_{12}$  in the exchange terms,

6)  $\lambda_m^{\text{dir}} = 60$ , maximum  $\ell$  included in the expansion of  $1/r_{12}$  in the static potential.

The grid used to compute all radial integrals consisted of 800 points extending out to  $r = 64.0$  au. These potential expansion parameters lead to substantially better convergence than those used by Raseev et al (1980).

We have computed the photoionization transition matrix elements both in the dipole length form

$$I_{\ell m \mu}^L(R) = (k)^{1/2} \langle \Psi_i(\underline{r}; R) | r_\mu | \Psi_{f, k \ell m}^{(-)}(\underline{r}; R) \rangle \quad (5)$$

and dipole velocity form

$$I_{\ell m \mu}^V(R) = \frac{(k)^{1/2}}{E} \langle \Psi_i(\underline{r}; R) | \nabla_\mu | \Psi_{f, k \ell m}^{(-)}(\underline{r}; R) \rangle \quad (6)$$

at five internuclear separations  $R = 2.268, 2.168, 2.068, 1.968$  and  $1.868$  au. The cross section for going from the ground vibrational state of  $N_2$  to the  $n$ 'th vibrational state of  $N_2^+$  is given by

$$\sigma_{\nu=0, \nu'=n}^{L, V} = \frac{4\pi^2}{3c} E \sum_{\ell m \mu} |\langle \chi_i^{\nu=0} | I_{\ell m \mu}^{L, V} | \chi_f^{\nu'=n} \rangle|^2 \quad (7)$$

where the  $\chi$ 's are the appropriate initial and final state vibrational wave functions,  $E$  is the photon energy and  $c$  is the speed of light. The asymmetry parameter  $\beta_{\hat{k}}$  is defined from the differential cross section for the photoelectron by

$$\frac{d\sigma_{\nu=0, \nu'=n}^{L, V}}{d\Omega_{\hat{k}}} = \frac{\sigma_{\nu=0, \nu'=n}^{L, V}}{4\pi} \left( 1 + \beta_{k, \nu=0, \nu'=n}^{L, V} P_2(\cos \theta) \right) \quad (8)$$

where  $\theta$  is the angle between the direction of the polarization of the light and the momentum of the electron.

The vibrational wave functions were obtained from numerical solution of the Schrödinger equation for the nuclear motion using RKR potentials to describe the potential surfaces. For the  $X^1\Sigma_g^+$  state of  $N_2$  we used the RKR curve of Benesch et al (1965). For the  $X^2\Sigma_g^+$  state of  $N_2^+$  we used the RKR curve of Singh and Rai (1966). The values of the potentials between the classical turning points were obtained using six point polynomial interpolation. The potential curves at  $R_e$ , 1.09768 Å for  $N_2$  and 1.116420 Å of  $N_2^+$  (Huber and Herzberg 1979), were also forced to have zero slope. The vibrational wave functions were then obtained using the method of Cooley (1961). With this approach we obtained the following Franck-Condon factors (FCF):  $(\nu=0, \nu'=0) = 0.917$ ,  $(\nu=0, \nu'=1) = 0.0786$ ,  $(\nu=0, \nu'=2) = 0.0043$ .

In figure 1 we present the cross section for photoionization leading to the first three vibrational levels of the  $X^2\Sigma_g^+$  state of  $N_2^+$ . We have divided the computed cross section given by equation (7) by the appropriate FCF given above to show the non-Franck-Condon nature of the photoionization in this spectral region. In figure 2 we present the computed asymmetry parameters and note that they also have a strong dependence on the final vibrational level. In figure 3 our computed  $\nu'=1/\nu'=0$  branching ratio is compared to the experimentally determined

branching ratio of West et al (1980) and those of the CMSM model (Dehmer et al (1979). From this figure we can clearly see that for photon energies greater than 26 eV the computed ratio is in very good agreement with the measured value of West et al (1980). At lower energies the differences are due to the autoionization features known to be present in the cross section at these energies and which are not included in the present study.

In conclusion we have shown that non-Franck-Condon vibrational effects due to the one-electron (shape) resonance in the photoionization of  $N_2$  can be well represented in the adiabatic-nuclei frozen-core-HF model used here. Thus inclusion of electron correlation effects should change the computed branching ratios very little except in regions where two-electron resonances (autoionization) are important. Thus the poor quantitative agreement between the CMSM branching ratios and the experimental values (West et al 1980) can be attributed solely to an inaccurate representation of the R dependence of the scattering potential in the CMSM model. Moreover, electron correlation effects are probably much smaller than had been anticipated by West et al (1980).

This research is based upon work supported by the National Science Foundation under Grant No. CHE79-15807. One of us (R. R. L.) acknowledges support from an Exxon Educational Foundation Fellowship. The research reported in this paper made use of the Dreyfus-NSF Theoretical Chemistry Computer which was funded through grants from the Camille and Henry Dreyfus Foundation, the National Science Foundation (Grant No. CHE78-20235), and the Sloan Fund of the

California Institute of Technology. This research was also supported in part by an Institutional Grant from the United States Department of Energy, No. EY-76-G-03-1305.

References

- Benesch W, Vanderslice J T, Tilford S G and Wilkinson P G 1965  
Astrophys. J. 142 1227-40
- Cooley J W 1961 Math. Comp. 15 363-74
- Dehmer J L, Dill D and Wallace S 1979 Phys. Rev. Lett. 43 1005-8
- Dunning T H Jr 1970 J. Chem. Phys. 53 2823-33
- Dunning T H Jr 1971 J. Chem. Phys. 55 3958-66
- Huber K P and Herzberg G 1979 Constants of Diatomic Molecules  
 (New York: Van Nostrand Reinhold)
- Lucchese R R and McKoy V 1980 Phys. Rev. A 21 112-23
- Lucchese R R, and McKoy V 1981 Phys. Rev. A 24 770.
- Lucchese R R, Watson D K and McKoy V 1980 Phys. Rev. A 22  
 421-6
- Lucchese R R, Raseev G and McKoy V 1981 "Studies of Differential  
 and Total Photoionization Cross Sections of Molecular Nitrogen"  
Phys. Rev. A - to be submitted
- Raseev G, Le Rouzo H and Lefebvre-Brion H 1980 J. Chem. Phys.  
72 5701-9
- Singh R B and Rai D K 1966 J. Mol. Spect. 19 424-34
- West J B, Parr A C, Cole B E, Ederer D L, Stockbauer R and  
 Dehmer J L 1980 J. Phys. B 13 L105-8

Table 1. Scattering basis sets used with the Schwinger variational expression.<sup>a</sup>

Photoionization Symmetry	Type of Gaussian Function <sup>b</sup>	Exponents
$3\sigma_g \rightarrow k\sigma_u$	Cartesian - s	16, 8, 4, 2, 1, 0.5
	- z	1, 0.5
	Spherical - $l = 1$	4, 2, 1, 0.5
	- $l = 3$	4, 2, 1, 0.5
	- $l = 5$	1, 0.5
	$3\sigma_g \rightarrow k\pi_u$	Cartesian - x
	- xz	0.5
	Spherical - $l = 1$	1.0
	- $l = 3$	1.0

<sup>a</sup> These basis sets correspond to the set R of equation (3) of the text.

<sup>b</sup> The basis functions are symmetry-adapted functions constructed from either Cartesian or spherical Gaussian functions, as defined in equations (1) and (2) of the text, of the type indicated. Cartesian functions are centered at the nuclei and spherical functions are centered at the bond mid-point.

Figure Captions

- Figure 1 Scaled photoionization cross sections of  $N_2$  leading to the  $\nu'$  vibrational level of the  $X^2\Sigma_g^+$  state of  $N_2^+$ : ——— dipole length approximation; — — — dipole velocity approximation. The cross sections given here must be multiplied by the Franck-Condon factors given in the text to yield their absolute magnitudes.
- Figure 2 Photoelectron asymmetry parameters for photoionization of  $N_2$  leading to the  $\nu'$  vibrational level of the  $X^2\Sigma_g^+$  state of  $N_2^+$ : ——— dipole length approximation; — — — dipole velocity approximation.
- Figure 3 Branching ratios for the production of the  $\nu' = 1/\nu' = 0$  vibrational levels of the  $X^2\Sigma_g^+$  state of  $N_2^+$  by photoionization of  $N_2$ : ——— present results using the frozen-core-HF dipole-length approximation; — — — present results using the frozen-core-HF dipole-velocity approximation; — — — — CMSM results from Dehmer et al. (1979); ● experimental results of West et al. (1980).

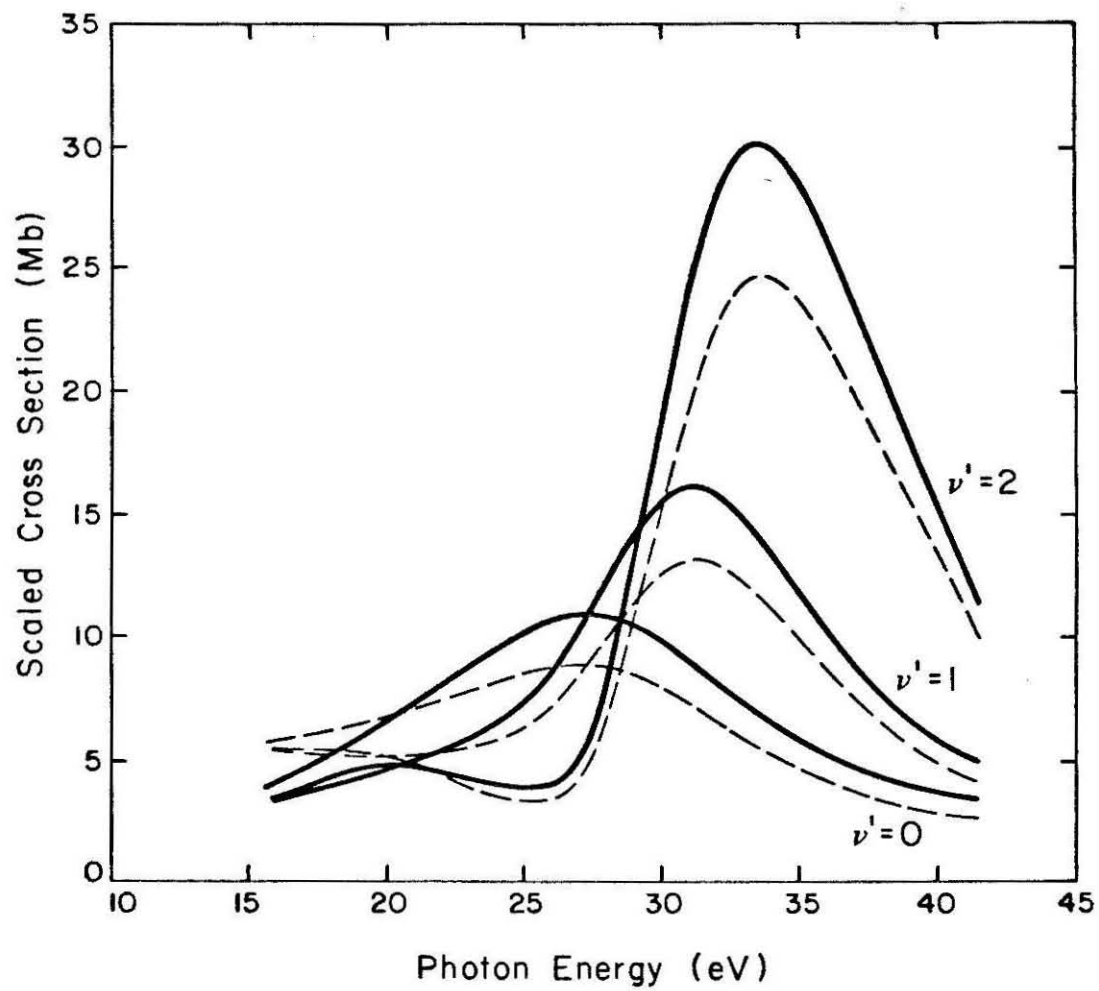


Figure 1

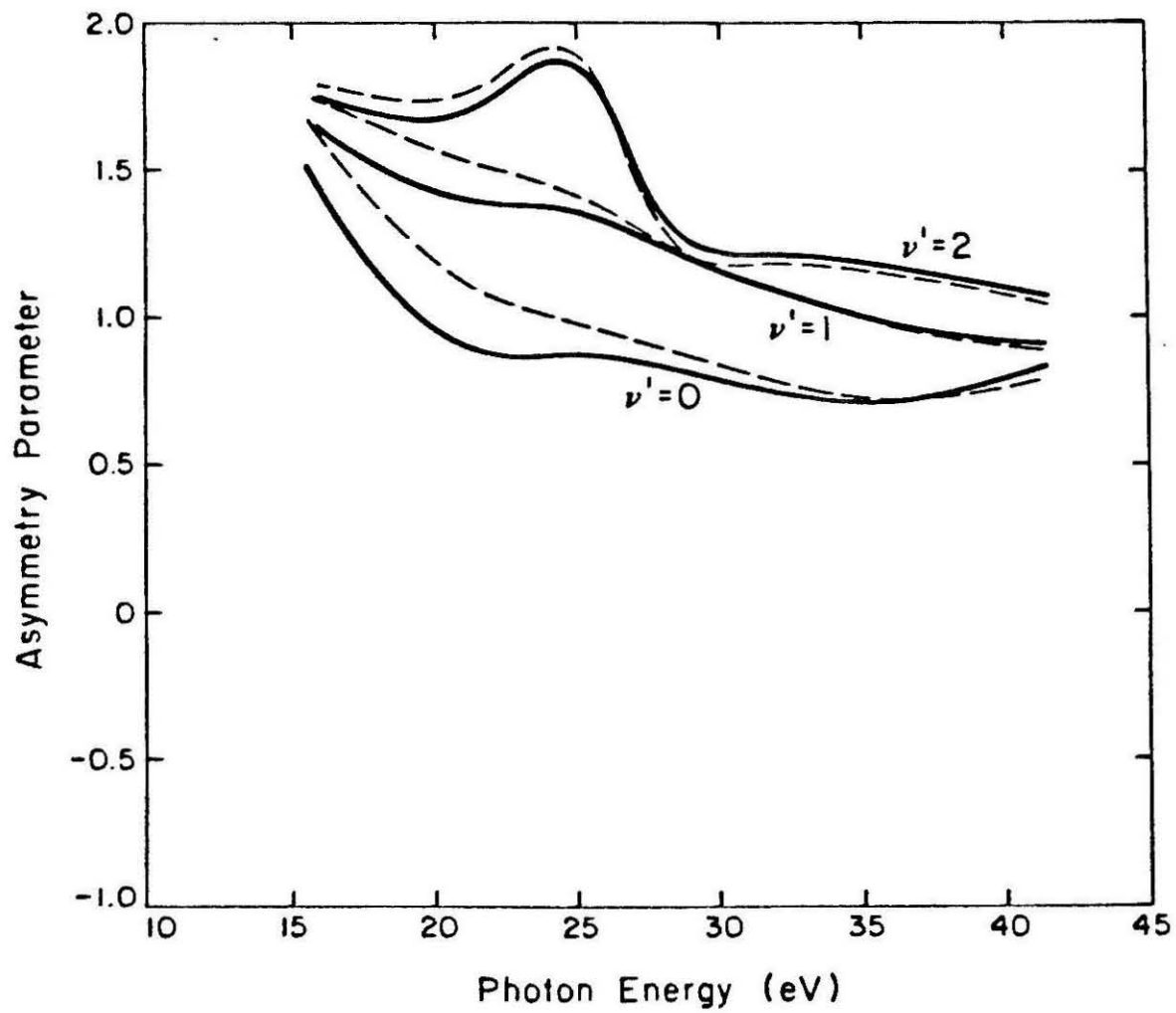


Figure 2

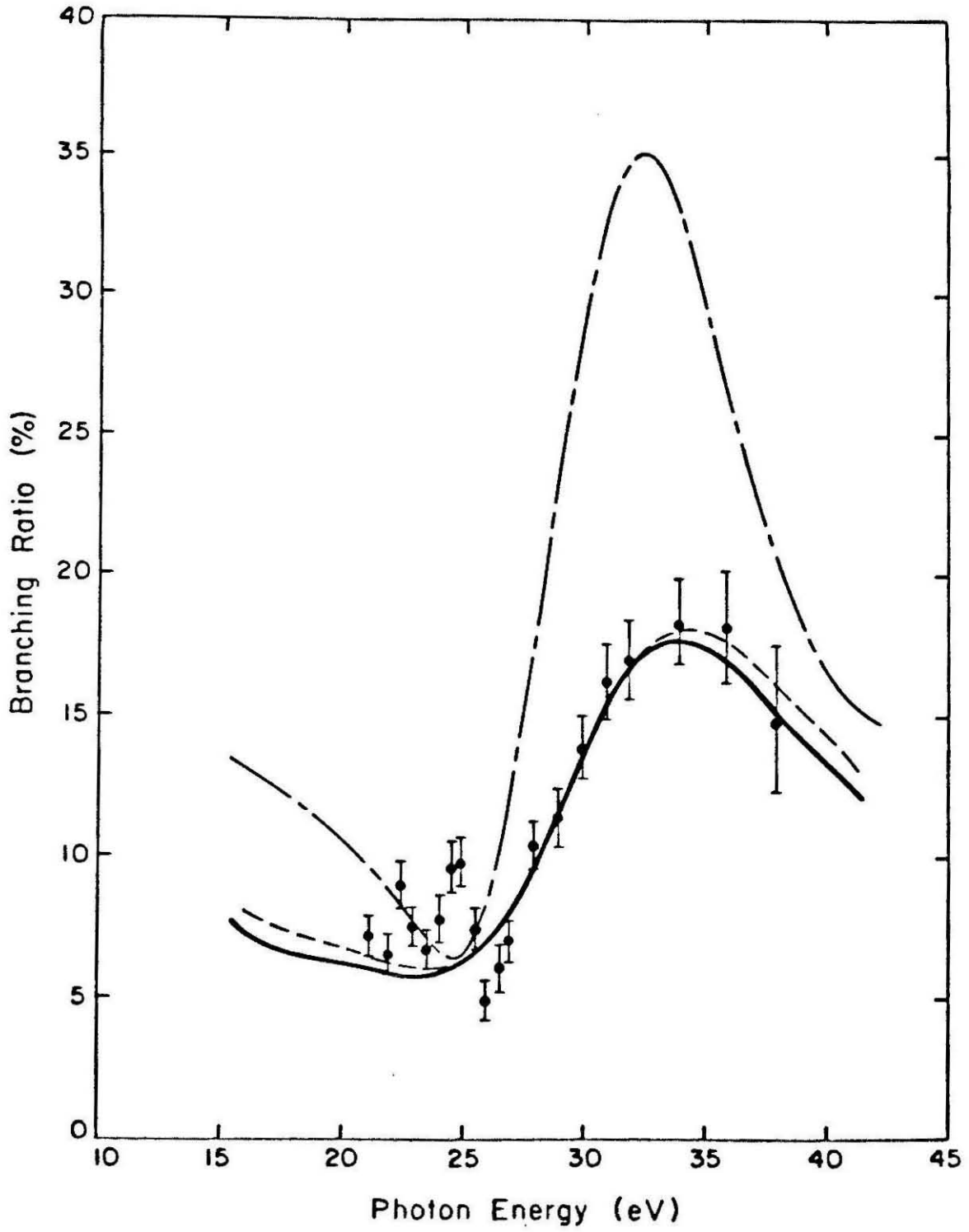


Figure 3

## SECTION C

Comparative Studies of a Shape-Resonant Feature  
in the Photoionization of CO<sub>2</sub>

Molecular photoionization has been the subject of many theoretical and experimental investigations in recent years. To date many of these studies of molecular photoionization cross sections have been carried out by the Stieltjes-Tchebycheff moment theory (STMT) approach developed by Langhoff and coworkers<sup>1</sup> and by the continuum multiple scattering method (CMSM) as developed by Dill and Dehmer.<sup>2</sup> In the STMT approach one obtains spectral moments of the oscillator strength distribution from the results of the diagonalization of the Hamiltonian over discrete basis functions. The underlying photoionization cross sections can then be extracted from the spectral moments. In most applications the approximate spectral moments were derived from pseudostates obtained from the diagonalization of the static-exchange Hamiltonian of the appropriate ion.<sup>3</sup> In the CMSM model the scattering potential is partitioned into spherical regions and approximated in these regions so that the resulting scattering equations can be readily solved. Photoionization cross sections can also be obtained from the solution of the scattering equation for the electron-molecular ion system provided the relevant equations can be solved for the choice of scattering potential. Methods for the accurate solution of these equations for diatomic and linear polyatomic systems at the static-exchange level are now available.<sup>4,5,6</sup> These methods are based on the single-center expansion technique and hence are not easily extended to more general polyatomic systems. They can, however, provide highly accurate differential and total photoionization cross sections at the static-exchange level.

In the course of our studies of the photoionization cross section of CO<sub>2</sub> by the Schwinger variational method<sup>6</sup> we have found that our

calculated partial photoionization cross section leading to the  $C^2 \Sigma_g^+$  state differs significantly from those previously obtained by both the STMT approach<sup>7</sup> and the CMSM model.<sup>8</sup> The  $C^2 \Sigma_g^+$  state of  $CO_2^+$  corresponds to ionization out of the  $4\sigma_g$  orbital. The feature of particular interest in this partial photoionization cross section is a fairly narrow shape resonance at a photon energy of about 40 eV. The partial photoionization cross section for this state obtained by the STMT approach<sup>7</sup> does not show this narrow shape resonance but has a broad peak at lower energy. In the CMSM model the fixed-nuclei cross section as given by Swanson et al.<sup>8</sup> does exhibit a very pronounced resonance in this region, but the peak height exceeds our calculated value by a factor of almost three.

In this letter we compare the photoionization cross section for the  $4\sigma_g$  level of  $CO_2$  obtained from the solution of the  $e-CO_2^+$  scattering equations with those obtained by the STMT approach<sup>7</sup> and the CMSM model.<sup>8</sup> There are substantial differences between our calculated values and those obtained by these two other methods. We will discuss why these differences suggest that it may be difficult for both the STMT approach and CMSM model to provide detailed quantitative information about such resonant features in molecular photoionization cross sections.

### Theory and Results

The rotationally unresolved, fixed-nuclei photoionization cross section is given by

$$\sigma_{if}(R) = \frac{4\pi^2\omega}{3} |\langle \Psi_i(\underline{r}, R) | \vec{\mu} | \Psi_f(\underline{r}, R) \rangle|^2 \quad (1)$$

where  $\vec{\mu}$  is the dipole moment operator and  $\omega$  the photon frequency. In eq 1  $\Psi_i(\underline{r}, R)$  is the initial state of the molecule and  $\Psi_f(\underline{r}, R)$  the final ionized state. For  $\Psi_i(\underline{r}, R)$  we use the ground state SCF wavefunction and for the  $(N-1)$  bound orbitals of  $\Psi_f(\underline{r}, R)$  we use the ground state SCF orbitals, i. e., the frozen core approximation. The continuum orbital in  $\Psi_f(\underline{r}, R)$  for the ejected electron is a solution of a one-particle Schrödinger equation with the static-exchange potential,  $V_{N-1}$ , of the ion. The continuum orbital satisfies the Schrödinger equation

$$\left(-\frac{1}{2}\nabla^2 + V_{N-1}(\underline{r}, R) - \frac{k^2}{2}\right)\psi_{\vec{k}}(\underline{r}, R) = 0 \quad (2)$$

where  $\frac{k^2}{2}$  is the kinetic energy of the ejected electron and  $\psi_{\vec{k}}$  satisfies the appropriate boundary conditions. It is the solution of this equation which is required to obtain the photoionization cross section through eq 1.

To obtain the continuum orbital  $\psi_{\vec{k}}$  it is convenient to work with the integral form of eq 2. The partial wave component of  $\psi_{\vec{k}}$ ,  $\psi_{k\ell m}$ , then satisfies the Lippmann-Schwinger equation

$$\psi_{k\ell m}^{(-)} = \phi_{k\ell m} + G_C^{(-)}(E) U \psi_{k\ell m}^{(-)} \quad (3)$$

where  $E = \frac{k^2}{2}$  and  $G_C^{(-)}(E)$  is the Coulomb Green's function with incoming-wave boundary conditions.<sup>9</sup> In eq 3  $U = 2V$  where  $V$  is the potential of the molecular ion with the Coulomb component removed and  $\phi_{k\ell m}$  is the regular Coulomb function. We have recently developed an iterative approach to the solution of the Lippmann-Schwinger equation

which is based on the Schwinger variational principle.<sup>6, 10</sup> Applications<sup>11, 12</sup> have shown that the method is a very effective approach to electron-molecule collisions at energies where partial wave coupling due to the nonspherical potentials and exchange effects are important. Details have been discussed elsewhere<sup>10</sup> and here we will discuss only some essential features of the method. In this approach we first solve the Lippmann-Schwinger eq 3, by assuming an approximate separable form for the potential U

$$U(\underline{r}, \underline{r}') \approx U^S(\underline{r}, \underline{r}') = \sum_{\alpha_i, \alpha_j} \langle \underline{r} | U | \alpha_i \rangle (U^{-1})_{ij} \langle \alpha_j | U | \underline{r}' \rangle \quad (4)$$

where the matrix  $(U^{-1})_{ij}$  is the inverse of the matrix  $U_{ij} = \langle \alpha_i | U | \alpha_j \rangle$ . At this stage the functions  $\alpha_i$  can be chosen to be entirely discrete basis functions and in this study we take them to be spherical Gaussian functions defined by

$$\phi_{\ell m}^A(\underline{r}) = N_{\ell m}^\alpha |\underline{r} - \underline{A}|^\ell e^{-\alpha |\underline{r} - \underline{A}|^2} Y_{\ell m}(\Omega_{\underline{r} - \underline{A}}) \quad (5)$$

The solutions of eq 3 for the approximate potential  $U^S$  of eq 4 is then simply

$$\psi_{k\ell m}^{S_0}(\underline{r}) = \phi_{k\ell m}(\underline{r}) + \sum_{\alpha_i, \alpha_j} \langle \underline{r} | G_C U | \alpha_i \rangle (D^{-1})_{ij} \langle \alpha_j | U | \phi_{k\ell m} \rangle \quad (6)$$

where the matrix  $(D^{-1})_{ij}$  is the inverse of the matrix

$$D_{ij} = \langle \alpha_i | U - U G_C U | \alpha_j \rangle . \quad (7)$$

The solutions of eq 6,  $\psi_{k\ell m}^{S_0}$ , can already provide useful estimates of the photoionization cross sections through eq 1. However, these scattering functions are only approximate solutions to the Lippmann-Schwinger equation for the actual potential  $U$ . The accuracy of these solutions depends on how well  $U^S$  approximates  $U$  in eq 4. To obtain more accurate and, if necessary, converged solutions to this static-exchange problem we have developed a method to iteratively improve the scattering functions of eq 6. This iterative method<sup>10</sup> is based on the use of the Schwinger variational principle and the solutions of eq 6 to obtain scattering functions which converge to the actual solutions of eq 3. This procedure contains criteria which allow one to determine when the exact solutions of the scattering problem have been obtained.<sup>10</sup>

We have used this procedure to study the photoionization cross section of the  $4\sigma_g$  level of  $CO_2$  in the static-exchange frozen-core approximation.<sup>7</sup> The SCF wavefunction for  $CO_2$  was constructed from a  $3s2p1d$  contracted Cartesian Gaussian basis set.<sup>13</sup> The SCF energy of  $CO_2$  in this basis set is  $-187.674286$  a. u. Table I shows the scattering basis set used in the calculation for the continuum orbital of  $\sigma_u$  symmetry. In Table II the eigenphases and eigenphase sums for  $^1\Sigma_u^+$  symmetry as well as the photoionization cross sections are given. The results are obtained after one step in the iterative procedure.<sup>10</sup> The resonant nature of the scattering process in this symmetry is clearly evident although the eigenphase sum does not rise through a full  $\pi$  radians. The eigenphase sums in Table II have been obtained from

a K matrix truncated at  $L = 9$ . Thus these eigenphase sums may not be totally converged with respect to this truncation; however, the photoionization cross sections obtained from these solutions are well converged.

We will first compare our results for the  $k\sigma_u$  component of the  $4\sigma_g$  photoionization cross section with those obtained from the STMT approach as presented by Padiyal et al.<sup>7</sup> The  $k\pi_u$  component of this cross section is nonresonant and will be given later. The STMT approach is based on the fact that the exact moments of the cumulative oscillator strength distribution can be obtained from a calculation employing discrete basis ( $L^2$ ) functions only.<sup>1</sup> Once these moments have been computed the problem can be inverted and the underlying spectrum can be obtained. In practice the moments are computed by diagonalizing the static-exchange Hamiltonian for the appropriate ion in an  $L^2$  basis. This procedure gives the variational pseudospectrum  $\{\tilde{\epsilon}_i, \tilde{f}_i, i = 1, N\}$  where the  $\tilde{\epsilon}_i$  and  $\tilde{f}_i$  are the discrete transition frequencies and oscillator strengths respectively. From this spectrum, approximate moments can be defined by

$$\tilde{S}(-k) = \sum_{i=1}^N \tilde{\epsilon}_i^{-k} \tilde{f}_i . \quad (8)$$

The principal representation of order  $n$ ,  $\{\epsilon_i^{(n)}, f_i^{(n)}, i = 1, n\}$  is then defined by

$$\tilde{S}(-k) = \sum_{i=1}^n (\epsilon_i^{(n)})^{-k} f_i^{(n)} , \quad 0 \leq k \leq 2n - 1. \quad (9)$$

One can show that the Stieltjes densities defined by<sup>1</sup>

$$\frac{df_s^{(n)}}{d\epsilon} = 0 \quad 0 < \epsilon < \epsilon_1^{(n)}$$

$$\frac{df_s^{(n)}}{d\epsilon} = \frac{1}{2} (f_{i+1}^{(n)} + f_i^{(n)}) / (\epsilon_{i+1} - \epsilon_i) \quad \epsilon_i < \epsilon < \epsilon_{i+1} \quad (10)$$

$$\frac{df_s^{(n)}}{d\epsilon} = 0 \quad \epsilon_n < \epsilon$$

will converge to the correct oscillator strength densities in the limit of large  $n$  if the exact moments  $S(-k)$  are used. However, when the moments are obtained from a variational calculation, the principal representation of order  $N$  is identical to the variational pseudospectrum. Thus the Stieltjes densities in this case will converge to the Stieltjes density of the variational pseudospectrum.

In Figure 1 we compare our calculated  $4\sigma_g \rightarrow k\sigma_u$  cross sections with those of the STMT method given by Padiál et al.<sup>7</sup> We show both the Stieltjes density of the variational pseudospectrum and the final smoothed cross section of ref 7. A comparison of these results show that the low order moment theory, i. e. ,  $n \ll N$  in eq 8 and 9, used by Padiál et al.<sup>7</sup> has smoothed away the resonant feature in this channel. The Stieltjes densities do not begin to show this resonance-like feature until one goes to order  $n = 15$  where  $N = 24$ . Cross sections obtained from such a high order moment analysis may not always be reliable. We believe that this comparison shows that in order to obtain an accurate representation of a fairly narrow shape resonance, in this case of width 3 eV, one must have considerably more than the two

pseudostates which are present in the resonance region in this calculation.<sup>7</sup>

Next we compare our  $4\sigma_g \rightarrow k\sigma_u$  cross sections with those of the CMSM model.<sup>8</sup> The CMSM method is a model potential approach which is described in detail elsewhere.<sup>2</sup> One of the approximations employed in the CMSM model is a local-exchange approximation. In Figure 2, we show our calculated  $4\sigma_g \rightarrow k\sigma_u$  cross sections and those of the CMSM model given by Swanson et al.<sup>8</sup> Clearly the CMSM model does show a very narrow resonance but the magnitude of the fixed-nuclei photoionization cross section given by the model exceeds our value by almost a factor of three. It is unclear if the disagreement between our results and those of the CMSM model is due to the local-exchange approximation alone<sup>14</sup> or whether it is due in part to the other approximations inherent in the CMSM model.

In Figure 2 we also show the  $4\sigma_g \rightarrow k\sigma_u$  photoionization cross section obtained in the CMSM model by averaging the cross section for each nuclear configuration over the ground state vibrational wavefunction. This R-averaging reduces the cross section considerably from the fixed-nuclei values calculated at equilibrium geometry giving a result much closer in magnitude to our fixed-nuclei cross sections. We believe that this dramatic effect due to vibrational averaging in the region of the resonance is unphysical and is an artifact of the CMSM model. One can hence expect that the CMSM model would overestimate non-Franck-Condon effects in the calculation of vibrational branching ratios in the region of resonances. This feature of the CMSM model had already been noted for vibrational branching ratios in the photoionization of the  $3\sigma_g$  level in  $N_2$ .<sup>5</sup>

Finally, in Figure 3 we compare our calculated photoionization

cross section for the  $C^2 \Sigma_g^+$  ( $4\sigma_g^{-1}$ ) ion of  $CO_2$  with the  $(e, 2e)$  measurements of Brion and Tan.<sup>15</sup> These experimental results do not indicate any significant enhancement in the  $C^2 \Sigma_g^+$  cross section around 40 eV. This discrepancy may be due to interchannel coupling or other effects which could reduce its apparent magnitude to a level which would be difficult to identify easily in current experiments. A more detailed description of our calculations for the photoionization cross sections of  $CO_2$  including the energy dependence of the asymmetry parameters is in preparation.

Acknowledgment. This research is based upon work supported by the National Science Foundation under Grant No. CHE79-15807. One of us (R. R. L.) acknowledges support from an Exxon Educational Foundation Fellowship. The research reported in this paper made use of the Dreyfus-NSF Theoretical Chemistry Computer which was funded through grants from the Camille and Henry Dreyfus Foundation, the National Science Foundation (Grant No. CHE78-20235), and the Sloan Fund of the California Institute of Technology.

References

- (1) Langhoff, P. W. "Stieltjes-Tchebycheff Moment-Theory Approach to Molecular Photoionization Studies," in Electron-Molecule and Photon-Molecule Collisions, Eds. Rescigno, T. N. ; McKoy, B. V. ; Schneider, B. (Plenum Press, N. Y. , 1979), pp. 183-224.
- (2) Dill, D. ; Dehmer, J. L. J. Chem. Phys. 1974, 61, 692.
- (3) See, for example, Rescigno, T. N. ; Bender, C. F. ; McKoy, B. V. ; Langhoff, P. W. J. Chem. Phys. 1978, 68, 970.
- (4) Robb, W. D. ; Collins, L. A. Phys. Rev. A 1980, 22, 2474.
- (5) Raseev, G. ; Le Rouzo, H. ; Lefebvre-Brion, H. J. Chem. Phys. 1980, 72, 5701.
- (6) Lucchese, R. R. ; McKoy, V. "An Iterative Approach to the Schwinger Variational Principle Applied to Electron-Molecular Ion Collisions," Phys. Rev. A 1981, in press.
- (7) Padial, N. ; Csanak, G. ; McKoy, B. V. ; Langhoff, P. W. Phys. Rev. A 1981, 23, 218.
- (8) Swanson, J. R. ; Dill, D. ; Dehmer, J. L. J. Phys. B 1980 13, L231.
- (9) See, for example, Taylor, J. R. "Scattering Theory" (Wiley: New York, 1972), p. 169.
- (10) Lucchese, R. R. ; Watson, D. K. ; McKoy, V. Phys. Rev. A 1980, 22, 421.
- (11) Lucchese, R. R. ; McKoy, V. "Studies of Elastic Scattering of Electrons by CO<sub>2</sub>" Phys. Rev. A - to be published.
- (12) Lucchese, R. R. ; McKoy, V. "Photoionization Cross Sections in Acetylene" Phys. Rev. A - to be published.

(13) Dunning, Jr., T. H.; Hay, P. J. "Gaussian Basis Sets for Molecular Calculations" in Methods of Electronic Structure Theory; Schaefer III, H. F., Ed. (Plenum: New York, 1977), pp. 1-27.

(14) For an example of such discrepancies in atomic systems, see Kennedy, D. J.; Manson, S. T. Phys. Rev. A 1972, 5, 227.

(15) Brion, C. E.; Tan, K. H. Chem. Phys. 1978, 34, 141.

TABLE I. Scattering Basis Set for  $\sigma_u$  Symmetry<sup>a</sup>

$\ell$	$m$	Center <sup>b</sup>	$\alpha$ 's
0	0	O	16.0, 8.0, 4.0, 2.0, 1.0, 0.5
1	0	O	1.0, 0.5
1	0	C	4.0, 2.0, 1.0, 0.5
3	0	C	4.0, 2.0, 1.0, 0.5
5	0	C	1.0, 0.5

<sup>a</sup> The 18 basis functions given are symmetry adapted functions constructed from spherical Gaussian functions of the given  $\ell$  and  $m$ . See text for definition.

<sup>b</sup> The O-C bond distance was taken to be 2.1944 a. u.

TABLE II. Eigenphase Sums and Cross Sections for  $4\sigma_g \rightarrow k\sigma_u$  Photoionization Channel in  $\text{CO}_2$

Photon Energy <sup>a</sup> (eV)	Eigen Phase Sum	1	3	Eigen Phases <sup>b</sup>			Cross Section <sup>c</sup> (Mb)
				5	7	9	
19.55	1.43	1.36	0.06	0.01	0.00	0.00	0.57
23.00	1.25	1.19	0.03	0.01	0.01	0.00	1.79
27.00	1.06	1.14	-0.13	0.04	0.01	0.00	2.75
31.00	0.87	-0.32	1.11	0.06	0.01	0.00	3.06
35.00	0.71	-0.49	1.08	0.10	0.02	0.01	3.28
38.00	0.69	-0.57	1.06	0.18	0.02	0.01	3.89
39.50	0.76	-0.58	1.05	0.27	0.02	0.01	4.61
41.00	0.97	-0.55	1.04	0.45	0.02	0.01	5.79
42.50	1.47	0.80	1.09	-0.45	0.02	0.01	5.79
44.00	2.07	1.41	0.95	-0.33	0.03	0.01	2.35
47.00	2.51	1.70	0.94	-0.18	0.03	0.01	0.20
50.00	2.54	1.70	0.91	-0.12	0.04	0.01	0.16

<sup>a</sup>The vertical ionization potential to produce the  $\text{C}^2\Sigma_g^+$  ionic state was taken to be 19.4 eV.

<sup>b</sup>The value of  $l$  given corresponds roughly to the principal component of the eigenphase.

<sup>c</sup>In megabarns ( $10^{-18} \text{ cm}^2$ ).

Figure Captions

- Fig. 1      Comparison of STMT and Schwinger photoionization cross sections in  $4\sigma_g \rightarrow k\sigma_u$  channel of  $\text{CO}_2$ :  
 ————— Schwinger; — — — STMT from ref. 7;  
 ----- Stieltjes density of variational pseudospectrum.
- Fig. 2      Comparison of CMSM and Schwinger photoionization cross sections in  $4\sigma_g \rightarrow k\sigma_u$  channel of  $\text{CO}_2$ : ————— Schwinger;  
 — — — fixed-nuclei; CMSM from ref. 8; — . — . — .  
 R-averaged CMSM from ref. .8.
- Fig. 3      Comparison of Schwinger photoionization cross sections with experimental results in  $4\sigma_g \rightarrow k\sigma_u + k\pi_u$  channel of  $\text{CO}_2$ : ————— Schwinger; + experimental results of Brion and Tan from ref. 15.

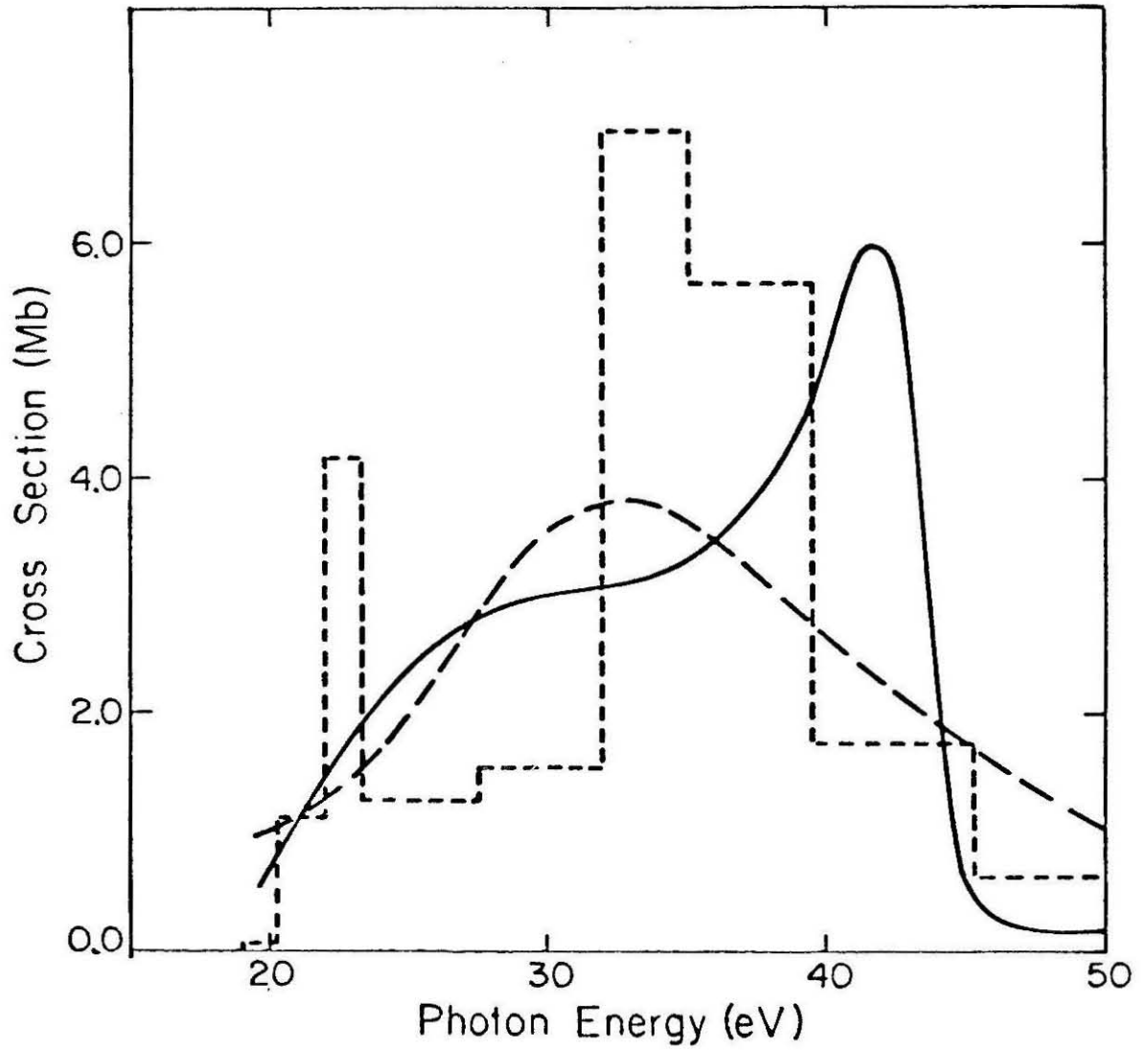


Figure 1

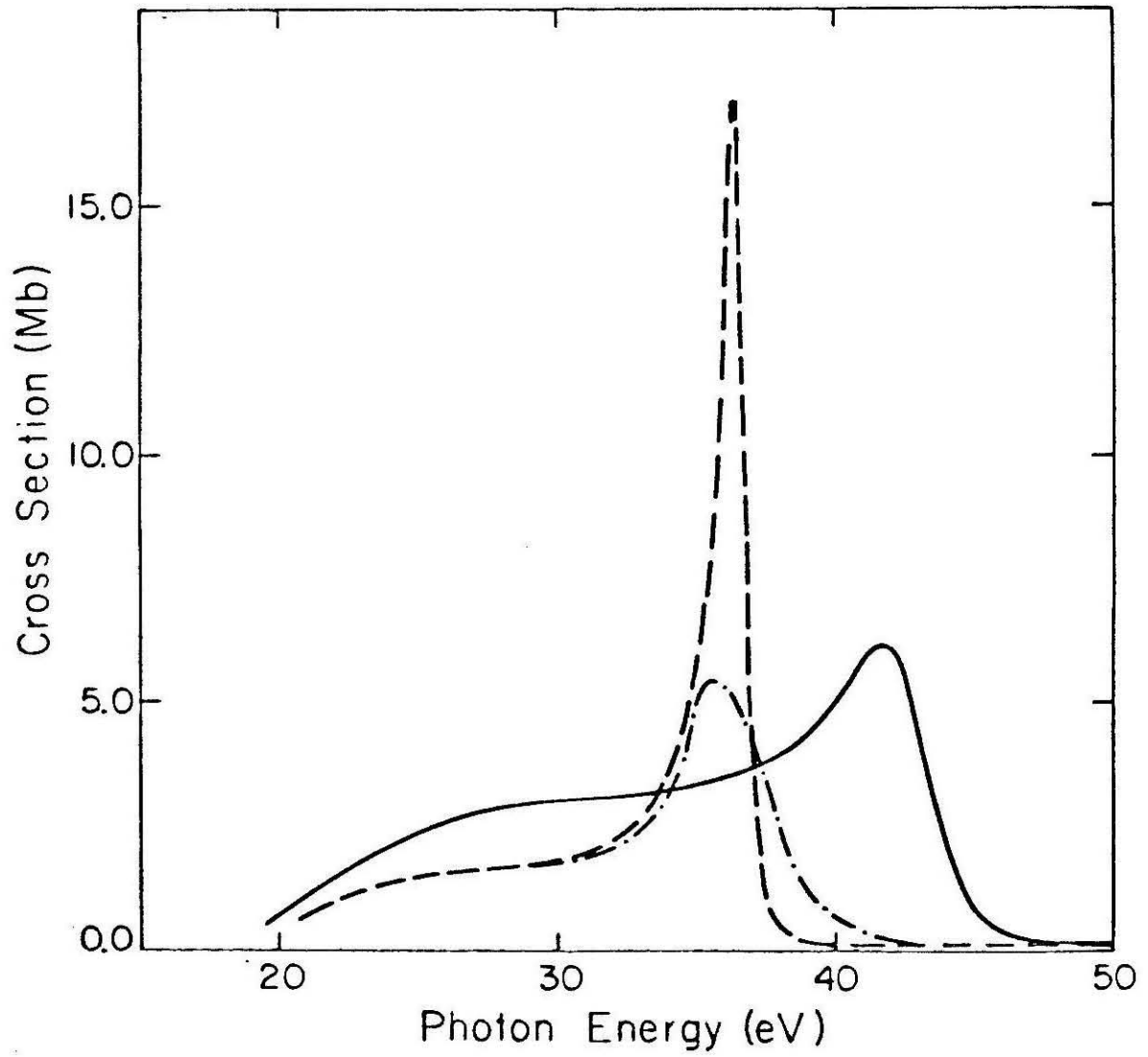


Figure 2

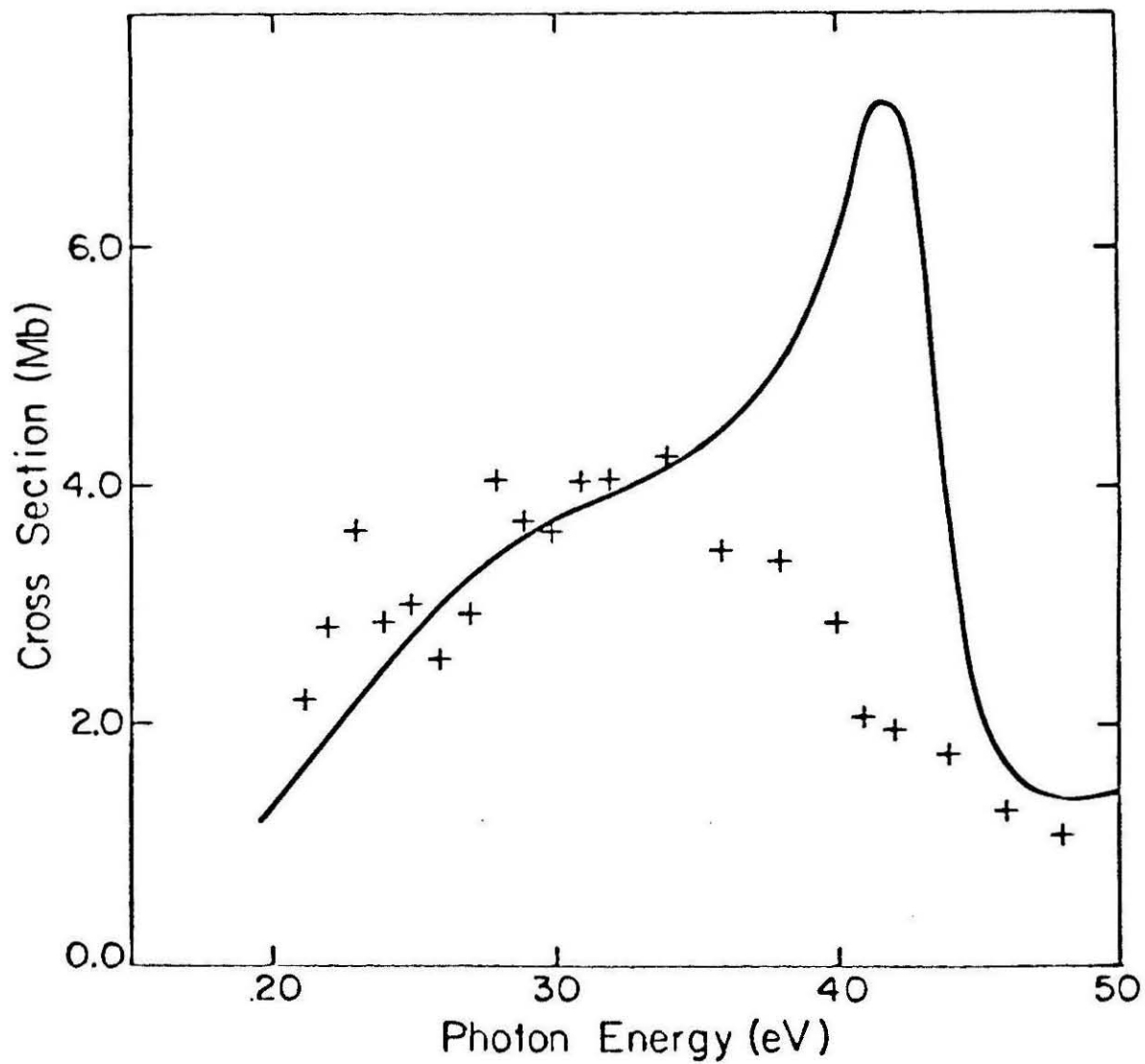


Figure 3

SECTION D

Studies of Differential and Total Photoionization  
Cross Sections of Carbon Dioxide

## I. INTRODUCTION

Several recent theoretical studies have investigated the partial-channel photoionization cross sections and photoelectron angular distributions of carbon dioxide. They include the comprehensive work by Padial et al.<sup>1</sup> which employed the Stieltjes-Tchebycheff Moment Theory (STMT) approach to obtain photoionization cross sections, and the studies of Swanson et al.<sup>2,3</sup> which used the Continuum Multiple Scattering Method (CMSM) to compute both cross sections and photoelectron angular distributions. Both the CMSM and STMT approaches obtained photoionization cross sections within a Hartree-Fock final-state framework. The present study is directed at obtaining accurate Hartree-Fock final-state continuum wave functions which are then used to compute both differential and integral photoionization cross sections. Comparison of the present results with available experimental data and with the results of the STMT and CMSM methods allow us to examine the accuracy of the Hartree-Fock final-state model and the utility of the STMT and CMSM methods.

The theoretical approach used here is identical to the approach used in an earlier study of the photoionization of  $N_2$ .<sup>4</sup> We have used the fixed-nuclei approximation with the final-state photoionization wave function computed using the Frozen-Core Hartree-Fock (FCHF) approximation. To study initial-state correlation effects, we have computed the photoionization cross section using both a Hartree-Fock (HF) initial-state wave function and a Configuration Interaction (CI) initial-state wave function. The FCHF final-state wave functions were

obtained using the iterative Schwinger variational method,<sup>5,6,7</sup> which we found to be an effective approach for obtaining HF continuum solutions in our study of the photoionization of  $N_2$ .<sup>4</sup>

We have studied the photoionization of  $CO_2$  from the valence molecular orbitals ( $1\pi_g$ ,  $1\pi_u$ ,  $3\sigma_u$ , and  $4\sigma_g$ ) and from the K-shell orbitals ( $1\sigma_g$ ,  $1\sigma_u$ , and  $2\sigma_g$ ). Of particular interest in this system are the narrow shape resonances which occur for continuum solutions of  $\sigma_u$  symmetry.<sup>2,3,8-10</sup> Such shape resonances can lead to an enhancement in the photoionization cross section, marked changes in the photoelectron angular distribution and non-Franck-Condon vibrational effects.

We compare our valence shell photoionization cross sections of  $CO_2$  to the (e, 2e) cross sections of Brion and Tan,<sup>11</sup> to the synchrotron source cross sections of Gustafsson et al.,<sup>12</sup> and to the fluorescence cross sections of Lee et al.<sup>13</sup> and Carlson et al.<sup>14</sup> The carbon K-shell cross sections are compared to the electron energy loss data of Wight and Brion<sup>15</sup> and the oxygen K-shell cross sections to the photoabsorption cross sections of Barrus et al.<sup>16</sup> We also compare our asymmetry parameters to the experimental data of Katsumata et al.,<sup>17</sup> of Carlson et al.<sup>18a</sup> and of Grimm et al.<sup>18b</sup> We find good agreement between experimental data and the present theoretical results. There are, however, two noticeable disagreements. The first major disagreement is the lack of experimental observation of the computed resonant enhancement of the photoionization cross section leading to the  $C^2\Sigma_g^+$  state of  $CO_2^+$ . However, the experimentally

determined asymmetry parameters of Carlson et al.<sup>18</sup> do lend support to the existence and to the predicted position of this shape resonance. The second area of disagreement is that the experimental cross section has a peak at a photon energy of 21 eV which is not obtained in the present results. We have tentatively attributed this discrepancy to the effects of autoionization which have not been included here.

We also compare our results to the published results of the STMT<sup>1</sup> and CMSM<sup>2,3</sup> methods. In a previous paper<sup>9</sup> we discussed the relationship between the results of the Schwinger method used here and the results of the STMT and CMSM methods for photoionization leading to the  $C^2\Sigma_g^+$  state of  $CO_2^+$ . In the present paper we compare the results of the Schwinger method with those of the STMT and CMSM method leading to other states of  $CO_2^+$ . As in the case of the  $C^2\Sigma_g^+$  channel discussed in the earlier paper,<sup>9</sup> we find that the STMT method as applied by Padiál et al.<sup>1</sup> does not reliably obtain the cross section in the region of narrow shape resonances found in the photoionization of  $CO_2$ . Also due to limitations of the computer program used by Padiál et al.<sup>1</sup> the incorrect HF potentials were used in the calculations of the  $\pi \rightarrow \delta$  partial channels contribution. This led to somewhat different results than those obtained here using the correct HF potential. We have also compared our results with the CMSM results of Swanson et al.<sup>2,3</sup> As indicated in Ref. 9 we find that the CMSM method does show the narrow shape resonances found here, but the resonant CMSM cross sections are too large by a factor of about 2 and the positions of the resonances are at different energies than found here.

## II. METHOD

### A. Final-state wave functions

The final-state photoionization wave functions used in this study were obtained using the FCHF approximation. In the FCHF model the final-state wave function is described by a single electronic configuration in which the ionic core orbitals are constrained to be identical to the HF orbitals of the neutral molecule. The Lippmann-Schwinger equation for the remaining continuum electron is (in atomic units)

$$\Psi_{\vec{k}}^{(\pm)} = \Psi_{\vec{k}}^{c(\pm)} + G^{c(\pm)} U \Psi_{\vec{k}}^{(\pm)}, \quad (1)$$

with  $U(\vec{r}) = 2V(\vec{r})$ , where  $V(\vec{r})$  is the appropriate short-range potential describing the scattering process and  $G^{c(\pm)}$  is the Coulomb Green's function defined by

$$G^{c(\pm)} = (\nabla^2 + \frac{2}{r} + k^2 \pm i\epsilon)^{-1}. \quad (2)$$

In Eq. (1),  $\Psi_{\vec{k}}^{c(\pm)}$  is a pure Coulomb scattering function. In the FCHF approximation,  $V$  is a generalized Phillips-Kleinman pseudopotential<sup>19</sup> which constrains the continuum orbital to be orthogonal to the occupied molecular orbitals. For photoionization from the  $n$ 'th (nondegenerate) orbital of a closed-shell molecule containing  $n$  doubly occupied molecular orbitals, the potential  $V$  is given by<sup>4</sup>

$$V = V^{SE} - LQ - QL + QLQ + \frac{1}{r} \quad (3)$$

where

$$L = -\frac{1}{2} \nabla^2 - \frac{k^2}{2} + V^{\text{SE}}, \quad (4)$$

$$Q = \sum_{i=1}^n |\phi_i\rangle \langle \phi_i|, \quad (5)$$

and  $V^{\text{SE}}$  is the static-exchange potential

$$V^{\text{SE}} = \sum_{i=1}^{n-1} (2J_i - K_i) + J_n + K_n - \sum_{\alpha} \frac{Z_{\alpha}}{r_{i\alpha}}. \quad (6)$$

In Eq. (6), the functions  $\phi_i$  are the  $n$  molecular orbitals,  $Z_{\alpha}$  is the nuclear charge of the  $\alpha$ 'th nucleus, and  $J_i$  and  $K_i$  are the usual Coulomb and exchange operators.<sup>20</sup>

We solve the Lippmann-Schwinger equation using the iterative Schwinger variational method which has been described in detail elsewhere.<sup>4-7</sup> Using this iterative method, the continuum solution at the  $n$ 'th iteration is expanded in a partial-wave series

$$\Psi_{\vec{k}}^{(-)S_n}(\vec{r}) = \left(\frac{2}{\pi}\right)^{1/2} \sum_{\ell=0}^{\ell p} \sum_{m=-\ell}^{+\ell} i^{\ell} \psi_{k\ell m}^{(-)S_n}(\vec{r}) Y_{\ell m}^*(\Omega_{\vec{k}}) \quad (7)$$

where an infinite sum over  $\ell$ 's has been truncated at  $\ell = \ell p$ . The set of partial-wave scattering solutions at the  $n$ 'th iteration

$$S_n = \{ \psi_{kl_1 m}^{S_n}, \dots, \psi_{kl_p m}^{S_n} \} \quad (8)$$

is obtained from the previous set of solutions,  $S_{n-1}$ , using

$$\begin{aligned} \psi_{klm}^{(-)S_n}(\vec{r}) &= \phi_{klm}^{c(-)}(\vec{r}) + \sum_{\chi_i, \chi_j \in R \cup S_{n-1}} \langle \vec{r} | G^{c(-)} U | \chi_i \rangle [D^{-1}]_{ij} \\ &\quad \times \langle \chi_j | U | \phi_{klm}^{c(-)} \rangle, \end{aligned} \quad (9)$$

where  $[D^{-1}]_{ij}$  is the matrix inverse of

$$D_{ij} = \langle \chi_i | U - UG^{c(-)} U | \chi_j \rangle. \quad (10)$$

The set of functions  $R$  in Eq. (9) is composed of  $L^2$  functions, which, in the present study, are taken to be spherical Gaussian functions defined by

$$\chi^{\alpha, \ell, m, \vec{A}}(\vec{r}) = N_{\alpha \ell m} |\vec{r} - \vec{A}|^\ell e^{-\alpha |\vec{r} - \vec{A}|^2} Y_{\ell m}(\Omega_{\vec{r} - \vec{A}}). \quad (11)$$

The  $L^2$  basis sets,  $R$ , for the various scattering symmetries are given in Tables I and II. Note that in Eq. (9), the set of functions  $S_{-1}$  is taken to be the null set. When the wave functions given by this iterative scheme do converge it can be shown that they are solutions of the Lippmann-Schwinger equation given in Eq. (1).<sup>5</sup>

These continuum solutions are then used to compute photoionization cross sections. The cross section for ionization of an initial bound state  $\Psi_i$  to the continuum state  $\Psi_{f, \vec{k}}$  by linearly polarized light is given in the dipole length approximation by

$$\frac{d^2\sigma^L}{d\Omega_{\vec{k}} d\Omega_{\hat{n}}} = \frac{4\pi^2 E}{c} k \left| \langle \Psi_i | \vec{r} \cdot \hat{n} | \Psi_{f, \vec{k}}^{(-)} \rangle \right|^2, \quad (12)$$

and in the dipole velocity approximation by

$$\frac{d^2\sigma^V}{d\Omega_{\vec{k}} d\Omega_{\hat{n}}} = \frac{4\pi^2}{cE} k \left| \langle \Psi_i | \vec{\nabla} \cdot \hat{n} | \Psi_{f, \vec{k}}^{(-)} \rangle \right|^2, \quad (13)$$

where  $E$  is the photon energy,  $\hat{n}$  is the direction of the polarization of the light,  $c$  is the speed of light, and  $\vec{k}$  is the asymptotic momentum of the photoelectron. When these cross sections are averaged over all possible orientations of the molecule in the laboratory frame the resulting differential cross section is of the form

$$\frac{d\sigma^{L, V}}{d\Omega_{\vec{k}}} = \frac{\sigma^{L, V}}{4\pi} \left[ 1 + \beta_{\vec{k}}^{L, V} P_2(\cos \theta) \right] \quad (14)$$

where  $\theta$  is the angle between the direction of polarization of the light and the momentum of the photoelectron. For all channels considered in this study we have computed both the total cross section  $\sigma^{L, V}$  and

the asymmetry parameters  $\beta_{\hat{k}}^{L, V}$ .

To compute the final-state continuum wave functions we must evaluate the various matrix elements given in Eq. (9). We have used a single-center expansion approach to evaluate all such matrix elements. In actual scattering calculations we use standing-wave boundary conditions thus allowing radial wave functions to be represented by real-valued functions. We define our partial-wave expansion parameters as follows:

- 1)  $\ell_m$  = maximum  $\ell$  included in the expansion of scattering functions ( $\chi_i$ 's of Eq. (9)), of the Coulomb Green's function and of the projection orbitals ( $\phi_i$  of Eq. (5)),
- 2)  $\ell_s^{\text{ex}}$  = maximum  $\ell$  included in the scattering functions in the exchange terms,
- 3)  $\ell_i^{\text{ex}}$  = maximum  $\ell$  included in the expansion of the occupied orbitals in the exchange terms,
- 4)  $\ell_i^{\text{dir}}$  = maximum  $\ell$  included in the expansion of the occupied orbitals in the direct potential,
- 5)  $\lambda_m^{\text{ex}}$  = maximum  $\ell$  included in the expansion of  $1/r_{12}$  in the exchange terms,
- 6)  $\lambda_m^{\text{dir}}$  = maximum  $\ell$  included in the expansion of  $1/r_{12}$  in the direct potential.

As usual we have included nuclear potential terms up to  $\lambda = 2\ell_m$ . We have expanded all radial integrals on a grid of 1000 points extending out to  $r = 90$  au. The smallest step size in the grid was 0.005 au which was used for points within 0.1 au of the nuclei. A step size of

0.01 au was used for all other points out to  $r = 3.0$  au. The largest step size in the remainder of the grid was 0.16 au.

In studying the convergence of the single-center method we fixed some of the expansion parameters. We have taken  $\ell_i^{\text{dir}} = 59$ ,  $\ell_s^{\text{ex}} = \ell_m$ , and  $\lambda_m^{\text{dir}} = 2\ell_m$ . We also fixed  $\ell_i^{\text{ex}}$  to be  $\ell_i^{\text{ex}} = 38(1\sigma_g)$ ,  $10(2\sigma_g)$ ,  $24(3\sigma_g)$ ,  $16(4\sigma_g)$ ,  $39(1\sigma_u)$ ,  $23(2\sigma_u)$ ,  $15(3\sigma_u)$ ,  $15(1\pi_u)$ ,  $16(1\pi_g)$ . These values for  $\ell_i^{\text{ex}}$  correspond to having normalized the expansions of the various orbitals to better than 0.99. The value for  $\ell_p$  of Eq.(7) was fixed at  $\ell_p = 10$ .

Thus we have only retained two independent parameters,  $\ell_m$  and  $\lambda_m^{\text{ex}}$  to define the single-center expansion. To study the convergence of the static-exchange potential of  $\text{CO}_2$ , we have considered five combinations of values of  $\ell_m$  and  $\lambda_m^{\text{ex}}$ :

- A)  $\ell_m = 59$ ,  $\lambda_m^{\text{ex}} = 40$
- B)  $\ell_m = 55$ ,  $\lambda_m^{\text{ex}} = 40$
- C)  $\ell_m = 51$ ,  $\lambda_m^{\text{ex}} = 40$
- D)  $\ell_m = 47$ ,  $\lambda_m^{\text{ex}} = 40$
- E)  $\ell_m = 59$ ,  $\lambda_m^{\text{ex}} = 30$ .

We have used these five sets of parameters to compute the energy of the peak cross section of the resonant  $4\sigma_g \rightarrow k\sigma_u$  photoionization channel of  $\text{CO}_2$ . The peak energy of such a shape resonance is a sensitive test of the convergence of these parameters. The peak energies were obtained from a zero iteration calculation ( $n = 0$ ) using Eq.(9). The resulting peak photon energies were,  $E_{\text{max}}^{\text{A}} = 41.79$  eV,  $E_{\text{max}}^{\text{B}} = 41.85$  eV,  $E_{\text{max}}^{\text{C}} = 41.92$  eV,

$E_{\max}^D = 42.01 \text{ eV}$  and  $E_{\max}^E = 41.82 \text{ eV}$ . To test the effect of the iterative procedure on these results, we performed one iteration using parameter set A and obtained a first iteration result of  $E_{\max}^{A'} = 41.79 \text{ eV}$ . Thus the peak energy was unchanged by one iteration, and the procedure seems well converged by the first iteration. All other results presented in this paper were obtained using the results of the first iteration of Eq. (9) (i. e., using the  $S_1$  scattering functions). In an earlier study we found empirically that the energy of the peak cross section in a  $\sigma$  symmetry shape resonance converges with partial wave expansion as

$$E_{\ell m}^{\ell} - E^{\infty} \propto 1/\ell_m^2. \quad (15)$$

The results of parameter sets A-D satisfy this relationship well with an extrapolated  $E^{\infty} = 41.57 \text{ eV}$ . Thus we see that parameter set A is within 0.3 eV of the fully converged result. Also, we note that the  $\lambda_m^{\text{ex}}$  parameter seems to be at least as well converged at  $\lambda_m^{\text{ex}} = 40$ . Thus for all further calculations in  $\text{CO}_2$  we have used the parameter set A.

### B. Initial-State Wave Functions

We have studied the effects of initial state correlation on the photoionization cross section by calculating cross sections using both a HF wave function and a CI wave function as the initial state.

The HF basis set was a [3s2p1d] contracted Cartesian Gaussian basis set.<sup>21</sup> With a R(C-O) bond length of 2.2944 au, the HF energy in this basis was  $E = -187.674286$  au.

The CI initial-state wave function contained "single-plus-double excitation" type configurations. These are the only configurations which have a non-zero contribution to the photoionization cross section when the final state is computed using the FCHF approximation.<sup>4</sup> The virtual orbital space for the CI calculation was a restricted set of molecular orbitals obtained from a separated-pair calculation. The separated-pair wave function was of the form

$$\begin{aligned}
 & (1\sigma_g)^2 (2\sigma_g)^2 (3\sigma_g)^2 (4\sigma_g, 6\sigma_g, 4\sigma_u, 6\sigma_u)^2 (1\sigma_u)^2 (2\sigma_u)^2 (3\sigma_u, 5\sigma_g, 5\sigma_u)^2 \\
 & (1\pi_{ux}, 3\pi_{ux}, 2\pi_{gx})^2 (1\pi_{uy}, 3\pi_{uy}, 2\pi_{gy})^2 (1\pi_{gx}, 3\pi_{gx}, 2\pi_{ux})^2 \\
 & (1\pi_{gy}, 3\pi_{gy}, 2\pi_{uy})^2,
 \end{aligned} \tag{16}$$

where the orbitals within each pair of parentheses represent natural orbitals of a particular pair function. Also, the orbitals in each pair function which are doubly occupied in the HF approximation were not allowed to vary. The energy of this separated-pair wave function for  $\text{CO}_2$  was  $E = -187.707766$  au.

The CI wave function was then taken to be a linear combination of configurations constructed from the orbitals determined in the separated-pair calculation and differing from the HF configuration by no more than two orbitals. We have also restricted the calculation by requiring the  $1\sigma_g$ ,  $2\sigma_g$ , and  $1\sigma_u$  orbitals to remain doubly occupied in all configurations. The

resulting wave function had 505 spatial configurations in  $D_{2h}$  symmetry from which 797 spin eigenfunctions were constructed. The energy of the CI wave function was  $E = -187.943937$  au.

### III. Results and Discussion

#### A. Valence-Shell Photoionization

Of primary interest here is the photoionization from the valence orbitals of  $\text{CO}_2$ . These photoionization channels lead to the four lowest states of  $\text{CO}_2^+$  which are the  $(1\pi_g)^{-1} X^2\Pi_g$  state obtained by ionizing an electron from the  $1\pi_g$  orbital with a vertical ionization potential (IP) of 13.8eV, the  $(1\pi_u)^{-1} A^2\Pi_u$  state with an IP of 17.7eV, the  $(3\sigma_u)^{-1} B^2\Sigma_u^+$  state with an IP of 18.2eV, and the  $(4\sigma_g)^{-1} C^2\Sigma_g^+$  state with an IP of 19.4eV.<sup>22</sup>

In Fig. 1 we present the cross sections leading to the  $X^2\Pi_g$  and  $C^2\Sigma_g^+$  states of  $\text{CO}_2^+$ . Both of these channels contain narrow shape resonances in the partial channels where the continuum orbital is of  $\sigma_u$  symmetry. In the computed photoionization cross sections, these resonances are apparent. In the  $X^2\Pi_g$  channel, the resonance produces a shoulder in the cross section at a photon energy of 35eV and in the  $C^2\Sigma_g^+$  channel the resonance produces a prominent peak in the cross section at 42eV. In Fig. 1 we present four different theoretical cross sections for each channel. These four cross sections were obtained using the HF initial-state wave function with the dipole length (HFL) and dipole velocity (HFV) approximations, as well as using the

correlated initial-state wave function, discussed in section II B, in the dipole length (CIL) and dipole velocity (CIV) approximations.

As noted previously by Padial et al.<sup>1</sup>, if the correct singlet HF potential were used in obtaining the  $1\pi_g - k\pi_u$  partial channel cross section, then the cross section would be spuriously enhanced at low photon energy. This difficulty is due to a strong  $1\pi_g - 2\pi_u$  ( $n - \pi^*$ ) transition which is incorrectly placed above the ionization threshold in the HF approximation. Thus we have been forced to use the triplet coupled potential to obtain the cross section in the  $1\pi_g - k\pi_u$  photoionization channel. This is the only channel where we did not use the correct singlet HF potential.

The difference between the length and velocity forms of the cross sections in Fig. 1 can be viewed as an estimate of the minimum error in these calculations.<sup>23, 24</sup> In our previous study of the photoionization of  $N_2$  we found that in nonresonant regions of the photoionization cross section, the inclusion of initial-state correlation tended to reduce the cross section in both the length and velocity approximations, whereas in the region of the photoionization cross section dominated by a shape resonance, the inclusion of initial-state correlation differentially lowered the length form of the cross section relative to the velocity form, bringing the two approximations into close agreement.<sup>4</sup> The same trends can be seen in the two channels

given in Fig. 1. In the  $C^2\Sigma_g^+$  channel, inclusion of initial-state correlation brings the length form very close to the velocity form in the region of the resonance. In the  $X^2\Pi_g$  channel, this effect is not as noticeable since the cross at 35eV is not dominated by the resonant  $1\pi_g \rightarrow k\sigma_u$  partial channel.

In Fig. 1 the cross sections leading to the  $X^2\Pi_g$  and  $C^2\Sigma_g^+$  states are compared to the experimental data of Gustafsson *et al.*<sup>12</sup> and Brion and Tan.<sup>11</sup> The experimental results for the  $X^2\Pi_g$  channel fall between the length and velocity estimates of the cross section, although there is no reason for this to be generally true. There also seems to be some evidence of a shoulder in the experimental cross section at a photon energy of 35eV as was obtained in the theoretical cross section. The  $C^2\Sigma_g^+$  experimental cross sections do not contain any such evidence of the resonance enhancement seen theoretically. As has been noted by Swanson *et al.*<sup>2</sup>, both vibrational effects and final-state correlation would lower and broaden the theoretical cross section. In an earlier study,<sup>10</sup> we have examined the effects on this cross section of averaging the cross section over the symmetric stretch vibrational mode, and found that the peak resonant cross section was lowered by about 15%. Inclusion of vibrational effects of other modes would also be expected to lower the peak cross section. Thus the theoretical cross section using the FCHF final-state model and including averaging over all vibrational modes would probably not differ

from the experimental cross section by more than a few megabarns in the region of the 42eV resonance. However, there would still seem to be a qualitative discrepancy in this channel which may be attributed to the effects of final-state correlation.

In Fig. 2 we compare our fixed-nuclei HFL results for the  $X^2 \Pi_g$  and  $C^2 \Sigma_g^+$  channels to the cross sections given by the STMT and CMSM methods also using the fixed-nuclei dipole length form of the cross section. The STMT cross section of Padial *et al.*<sup>1</sup> for the  $X^2 \Pi_g$  channel agrees fairly well with the Schwinger cross section at high energy although there is no evidence of a shoulder in the STMT cross section at 35eV. At lower photon energies there is a larger disagreement between the STMT and Schwinger results. Most of the discrepancy at low energy is due to differences in the  $1\pi_g \rightarrow k\sigma_u$  partial channel. The STMT cross sections were extracted from the results of a diagonalization of the FCHF operator in a large  $L^2$  basis set of Cartesian Gaussian basis functions. These calculations were performed using standard bound state computer codes which require that the inter-electronic interactions be expressible in terms of the usual J and K operators.<sup>20, 25</sup> The singlet potential appropriate to the  $\pi^3 \delta$  case is not expressible in terms of J and K operators when real valued molecular orbitals are used. Thus the STMT results were instead obtained using a triplet-coupled potential which can be expressed in terms of J and K operators. To show the effect of using these different HF potentials, we present in Fig. 3 the results of

noniterative Schwinger calculations where both the triplet and singlet potentials have been used, and compare them to the STMT  $1\pi_g \rightarrow k\delta_u$  results of Padiyal et al.<sup>1</sup> Thus it can be seen that a large portion of the discrepancy in the  $1\pi_g \rightarrow k\delta_u$  channel is due to using the triplet potential in obtaining the STMT cross sections.

In Fig. 2a we also compare the Schwinger results for the  $X^2\Pi_g$  channel to the fixed-nuclei CMSM cross section of Swanson et al.<sup>2</sup> We can see that the CMSM cross sections are generally too small and that the shape resonance in the  $1\pi_g \rightarrow k\sigma_u$  partial channel is at a lower energy than that obtained using the Schwinger method. The fixed-nuclei resonant feature in the CMSM cross section is seen to be much more pronounced than the broad shoulder obtained using the Schwinger method.

In Fig. 2b, we compare the various theoretical cross sections for the  $C^2\Sigma_g^+$  channel. This comparison has been discussed in detail in an earlier paper.<sup>9</sup> Briefly, we can see that the STMT results show no evidence of a resonant enhancement of the photoionization cross section. In contrast, the results of the CMSM method show an unrealistically large and narrow resonant cross section, which differs from the Schwinger results in position by about 5eV and in magnitude by over a factor of two.

In Fig. 4 we present the computed asymmetry parameters for the  $X^2\Pi_u$  and  $C^2\Sigma_g^+$  channels. We have only presented the

results which were obtained using the correlated initial-state wave function. We found that initial-state correlation effects on the asymmetry parameter were small, and thus we chose only to present our most accurate results. We have compared the present results with available experimental data and to the values predicted by the CMSM method.<sup>3</sup>

The resonance in the  $X^2 \Pi_g$  channel at 35eV is barely visible as a slight bump in the dipole length asymmetry parameters. The CMSM asymmetry parameters of Swanson et al.<sup>3</sup> are seen to have a larger resonance effect than do the Schwinger values. Both the CMSM and Schwinger results are in reasonable accord with the two line source measurements of Katsumata et al.,<sup>17</sup> and with the continuous source measurements of Grimm et al.<sup>18 b</sup> As can be seen in Fig. 4b, the resonance in the  $C^2 \Sigma_g^+$  channel leads to very dramatic effects in the asymmetry parameters. The experimental results of Carlson et al.<sup>18 a</sup> show a fairly large dip in the  $\beta$  values around a photon energy of 40eV. Both the Schwinger and CMSM fixed-nuclei results overestimate the magnitude of the resonance effect. Inclusion of vibrational effects is known to make this feature shallower.<sup>3, 10</sup> Including just the symmetric stretch vibrational mode, in an earlier paper<sup>10</sup> we found that vibrational averaging of the cross section reduced the dip in the asymmetry parameter by about 25%. Thus if other vibrational degrees of freedom were considered in the

averaging, it would seem that the theoretical  $\beta$  could be in fairly good quantitative agreement with the experimental results using just the FCHF final-state approximation.

The cross sections leading to the production of the  $A^2\Pi_u$  and  $B^2\Sigma_u^+$  states of  $CO_2^+$  are given in Fig. 5. We have compared our cross sections to the experimental fluorescence cross sections of Lee *et al.*<sup>13</sup> for the  $A^2\Pi_u$  state, and to the fluorescence data of Carlson *et al.*<sup>14</sup> for the  $B^2\Sigma_u^+$  state. We have also presented cross sections which were derived by taking the ratios of the cross sections for the A and B states obtained from the photoelectron spectra by Samson and Gardner<sup>26</sup> and multiplying them by the total cross section for the A and B states given by Brion and Tan.<sup>11</sup> The cross section for the  $B^2\Sigma_u^+$  state is in reasonably good agreement with results obtained from fluorescence measurements, whereas the cross section for the  $A^2\Pi_u$  state has a more serious disagreement with the experimental fluorescence data in the region of 21eV photon energy. The limited number of photoelectron measurements available seem to indicate the reverse situation, with agreement between theory and photoelectron experiments being good in the A channel and a major disagreement in the 21eV photon energy range in the B channel. The comparison of the present theoretical results with the photoelectron results thus seem to indicate that near the photon energy of 21eV, a large contribution to the correct cross section for the  $B^2\Sigma_u^+$  channel

must come from multi-electron effects in the final state. One possible effect which would enhance the cross section would be autoionization due to higher lying ionic states. The lowest multi-electron ionic state, which has been identified, has an IP of 23eV and has been characterized by Domcke et al.<sup>27</sup> as being dominated by the  $(1\pi_g)^{-2}(2\pi_u)$  configuration. This autoionization enhancement would be analogous to the enhancement due to the  $C^2\Sigma_u^+$  state in the photoionization cross section of  $N_2$  which is characterized by the  $(1\pi_u)^{-1}(3\sigma_g)^{-1}(1\pi_g)$  configuration.

It is clear from Fig. 5 that the fluorescence cross section disagrees strongly with the photoelectron cross section in the region of the feature which we suggest is due to autoionization. We can speculate that in this region there is a mechanism whereby a large fraction of the molecules which are initially in the B state cross over to the A state before the molecule fluoresces. Such a cross over mechanism has been suggested by Samson and Gardner;<sup>26</sup> however, they assumed that the crossover rate would be independent of the photon energy. As discussed by Gustafsson et al.<sup>12</sup>, such a photon-energy-independent mechanism does not agree with experimental evidence since, as can be seen in Fig. 5, at 40.8eV the cross section derived from fluorescence and photoelectron measurements are in much better agreement than at 21.2eV. This suggests that such a mechanism must depend on the photon energy and in particular the presence of autoionization in the cross section must strongly effect the

crossover rate.

It is of interest also to note that both the  $A^2 \Pi_u$  and  $B^2 \Sigma_u^+$  channels exhibit rising eigenphase sums in the partial channels where the continuum electron has  $\sigma_g$  and  $\pi_g$  symmetry. In the case of the  $\pi_g$  continuum channels, these rising eigenphase sums can be attributed to very broad shape resonances at about 22eV above threshold.

The resonant rise in the eigenphase sums in the  $\sigma_g$  channels occurs at low energy and is due to a rising eigenphase which is primarily s-wave. In Fig. 6 we give both the eigenphase sums and cross sections for the  $1\pi_u \rightarrow k\sigma_g$  and  $3\sigma_u \rightarrow k\sigma_g$  channels. The effects of the resonance-like features on the cross sections in these two channels are markedly different, with the  $1\pi_u \rightarrow k\sigma_g$  channel showing a minimum and the  $3\sigma_u \rightarrow k\sigma_g$  showing a maximum in the region of interest. As can be seen in Fig. 5b, the effect of initial state correlation on the maximum in the  $3\sigma_u \rightarrow k\sigma_g$  cross section is to increase the difference between length and velocity forms of the cross section. This effect is different from that found for cross sections dominated by shape resonances discussed earlier, where length and velocity forms are brought closer together by initial state correlations. Thus it seems that these two  $\sigma_g$  photoionization continuum channels are being affected by a one-electron resonant process which is qualitatively different from the usual shape resonance, which is characterized by a rising eigenphase corresponding to a higher value of  $\ell$ , i. e.,  $\ell > 0$ .

In Fig. 7 we compare the present Schwinger results for the  $A^2\Pi_u$  and  $B^2\Sigma_u^+$  channels with the cross sections obtained by Padiál et al.<sup>1</sup> using the STMT method. The peak in the STMT cross section in the  $A^2\Pi_u$  channel is shifted to a lower energy than that obtained using the Schwinger method. As was the case in the  $X^2\Pi_g$  channel, most of the cross section comes from the  $\pi - \delta$  partial channel. The STMT results were again obtained using the triplet potential in this channel, and this may account for the shift of the peak cross section to lower energy. In the  $B^2\Sigma_u^+$  channel both the  $3\sigma_u \rightarrow k\sigma_g$  and  $3\sigma_u \rightarrow k\pi_g$  features are at lower energy in the STMT cross sections. The source of these discrepancies is uncertain.

In Fig. 8 we present the computed asymmetry parameters for the  $A^2\Pi_u$  and  $B^2\Sigma_u^+$  channels. The present results are compared with those of the CMSM method and to experimental results. The agreement between the two theoretical calculations is fairly good, and both theoretical results agree fairly well with experimental results except for the 40.8eV measurement of Katsumata et al.<sup>17</sup> in the  $B^2\Sigma_u^+$  channel.

In Fig. 9a we compare the sum of our  $A^2\Pi_u$  and  $B^2\Sigma_u^+$  cross sections with the experimental results of Gustafsson et al.<sup>12</sup> and of Brion and Tan.<sup>11</sup> Due to the small difference between the IPs of these two states, neither of these two continuous source photoelectron experiments resolved the individual branching

ratios for these two channels. The Schwinger results are seen to agree fairly well with the experimental data for photon energies above 24eV. Below 24eV the computed cross section is too small. This error must be due to final state correlation effects as we discussed earlier.

The total valence shell cross sections are given in Fig. 9b. Here we have summed the four theoretical cross sections leading to the  $X^2\Pi_g$ ,  $A^2\Pi_u$ ,  $B^2\Sigma_u^+$ , and  $C^2\Sigma_g^+$  states of  $CO_2^+$  given above and compare them to the sum of the experimental cross sections leading to these four states given by Brion and Tan.<sup>11</sup> The feature at a photon energy of 21eV is again apparent in the experimental cross section and not in the theoretical cross section. The other major discrepancy between theory and experiment is the shoulder at 42eV in the theoretical cross section due to the resonance in the  $C^2\Sigma_g^+$  channel. As noted earlier, the magnitude of this feature would be reduced somewhat by vibrational averaging.

### B. K-shell Photoionization

As we have seen in the previous section, photoionization from the outer valence shell of  $CO_2$  is fairly well represented by the use of the FCHF final-state approximation. Photoionization from the inner valence orbitals ( $3\sigma_g$ ,  $2\sigma_u$ ) should be strongly affected by final state correlation. This breakdown of the single particle picture for the inner valence ionic states has been discussed by Domcke et al.<sup>27</sup> However, the K-shell photoionization

should be fairly well described by the simple hole states used in the FCHF model.

We have computed the oxygen and carbon K-shell photoionization cross sections of  $\text{CO}_2$ . The K-shell IPs were taken to be 297.5eV for carbon and 541.1eV for oxygen.<sup>28</sup> Since the initial-state correlated wave function discussed in section II B does not include any correlation effects involving the K-shell electrons, we have only computed the HFL and HFV forms of the photoionization cross section.

In Fig. 10a we present the computed carbon K-shell photoionization cross section of  $\text{CO}_2$ . We have compared the present theoretical results to those of Padial *et al.*<sup>1</sup> obtained using the STMT method and to the experimental energy loss cross sections of Wight and Brion.<sup>15</sup> We have arbitrarily normalized the relative cross sections given in Ref. 15 to the Schwinger results at a photon energy of 325eV. The Schwinger and STMT results are in good mutual agreement with both cross sections showing a pronounced peak due to a  $2\sigma_g \rightarrow k\sigma_u$  shape resonance. Both of the FCHF level theoretical results are seen to be in only rough agreement with the experimental data which shows evidence of strong final state correlation effects (e. g., shake-up states). In Fig. 10b we give the computed photoelectron asymmetry parameters which show a strong feature around a photon energy of 304eV due

to the  $2\sigma_g \rightarrow k\sigma_u$  shape resonance.

The photoionization cross section for the oxygen K-shell is given in Fig. 11. The theoretical cross section we have presented is the sum of the cross sections for photoionizing electrons out at the nearly degenerate  $1\sigma_g$  and  $1\sigma_u$  molecular orbitals of  $\text{CO}_2$ . The effect of the narrow shape resonance in the  $1\sigma_g \rightarrow k\sigma_u$  channel is evident at a photon energy of 560eV. We have compared our cross sections to the experimental absorption measurements of Barrus et al.<sup>16</sup> and to the STMT results of Padial et al.<sup>1</sup> The broad feature in the experimental cross section at a photon energy of 560eV seems to be due in part to the shape resonance in the  $1\sigma_g \rightarrow k\sigma_u$  channel. However, the fixed-nuclei FCHF model gives a much narrower width to this feature. Vibrational averaging would tend to broaden this peak within the FCHF approximation. The shoulder in the experimental cross section at 554eV is not found using the FCHF approximation and is thus probably due to final state correlation. The STMT results of Padial et al.<sup>1</sup> do not show the narrow resonance which is present in this system in the FCHF approximation. In the STMT cross section, the oscillator strength from the resonance has been smeared out over a large energy range in much the same manner as the  $\text{C}^2\Sigma_g^+$  cross section was unphysically smoothed out by the STMT method.<sup>9</sup> The computed asymmetry parameters for this channel are given in Fig. 11b. The effects of the shape resonance

are once again clearly evident.

#### IV. Conclusion

Accurate fixed-nuclei FCHF photoionization cross sections of  $\text{CO}_2$  have been presented. Comparison of the present results with those of the STMT<sup>1</sup> and CMSM<sup>2,3</sup> methods have shown that both the STMT and CMSM methods provide useful qualitative information about the cross sections but these methods can fail to reproduce some important features in photoionization cross sections. The present results have been found to be in reasonably good agreement with experimental data. Comparison of experimental and computed cross sections for the  $A^2\Pi_u$  and  $B^2\Sigma_u^+$  channels has yielded indirect evidence of a possible autoionization feature at a photon energy of 21eV. These results also provide direct evidence of narrow shape resonances in those partial channels where the continuum electron has  $\sigma_u$  symmetry. The effects of these resonances on differential photoionization cross sections has been computed to be substantial. Such shape resonances can also be expected to exhibit strong non-Franck-Condon vibrational effects. Both vibrational effects and autoionization can be studied using FCHF continuum wave functions such as those obtained here and will be the subject of future research.

ACKNOWLEDGMENTS

We want to thank T. A. Carlson for making available to us experimental asymmetry parameters prior to publication. One of us (RRL) acknowledges support from an Exxon Foundation Graduate Educational Fellowship. This material is based upon work supported by the National Science Foundation under Grant No. CHE80-40870. The research reported in this paper made use of the Dreyfus-NSF Theoretical Chemistry Computer which was funded through grants from the Camille and Henry Dreyfus Foundation, the National Science Foundation (Grant No. CHE78-20235), and the Sloan Fund of the California Institute of Technology.

References

- <sup>1</sup>N. Padial, G. Csanak, B. V. McKoy, and P. W. Langhoff, Phys. Rev. A 23, 218 (1981).
- <sup>2</sup>J. R. Swanson, D. Dill, and J. L. Dehmer, J. Phys. B 13, L213 (1980).
- <sup>3</sup>J. R. Swanson, D. Dill, and J. L. Dehmer, J. Phys. B 14, L207 (1981).
- <sup>4</sup>R. R. Lucchese, G. Raseev, and V. McKoy, "Studies of Differential and Total Photoionization Cross Sections of Molecular Nitrogen," Phys. Rev. A - accepted for publication.
- <sup>5</sup>R. R. Lucchese, D. K. Watson, and V. McKoy, Phys. Rev. A 22, 421 (1980).
- <sup>6</sup>R. R. Lucchese and V. McKoy, Phys. Rev. A 24, 770 (1981).
- <sup>7</sup>R. R. Lucchese, K. Takatsuka, D. K. Watson, and V. McKoy, "The Schwinger Variational Principle: An Approach to Electron-Molecule Collisions" in: Proceedings of the Symposium on Electron-Atom and Molecule Collisions, Universität Bielefeld, Germany, May 5-14, 1980 (Plenum Press, London-New York, 1981).
- <sup>8</sup>F. Grimm, T. A. Carlson, W. B. Dress, P. Agron, J. O. Thomson, and J. W. Davenport, J. Chem. Phys. 72, 3041 (1980).
- <sup>9</sup>R. R. Lucchese and V. McKoy, J. Phys. Chem. 85, 2166 (1981).
- <sup>10</sup>R. R. Lucchese and V. McKoy, "Vibrational Effects in the Photoionization Shape Resonance Leading to the  $C^2\Sigma_g^+$  State of  $CO_2^+$ "- in prep.
- <sup>11</sup>C. E. Brion and K. H. Tan, Chem. Phys. 34, 141 (1978).
- <sup>12</sup>T. Gustafsson, E. W. Plummer, D. E. Eastman, and W. Gudat, Phys. Rev. A 17, 175 (1978).

- <sup>13</sup> L. C. Lee, R. W. Carlson, and D. L. Judge, *J. Phys. B* 9, 855 (1976).
- <sup>14</sup> R. W. Carlson, D. L. Judge, and M. Ogawa, *J. Geophys. Res.* 78, 3194 (1973).
- <sup>15</sup> G. R. Wight and C. E. Brion, *J. Electron Spectrosc. Related Phenomena* 3, 191 (1974).
- <sup>16</sup> D. M. Barrus, R. L. Blake, A. J. Burek, K. C. Chambers, and A. L. Pregenzer, *Phys. Rev. A* 20, 1045 (1979).
- <sup>17</sup> S. Katsumata, Y. Achiba, and K. Kimura, *J. Electron Spectrosc. Related Phenomena* 17, 229 (1979).
- <sup>18</sup> a) T. A. Carlson, M. O. Krause, F. A. Grimm, J. D. Allen, Jr., D. Mehaffy, P. R. Keller, and J. W. Taylor, *Phys. Rev. A* 23, 3316 (1981); b) F. A. Grimm, J. D. Allen, Jr., T. A. Carlson, M. O. Krause, D. Mehaffy, P. R. Keller, and J. W. Taylor, "Angle-Resolved Photoelectron Spectroscopy of CO<sub>2</sub> with Synchrotron Radiation," preprint.
- <sup>19</sup> J. D. Weeks, A. Hazi, and S. A. Rice, in Advances in Chemical Physics, Vol. XVI (Interscience, New York, 1969) p. 283.
- <sup>20</sup> F. W. Bobrowicz and W. A. Goddard III, in Methods of Electronic Structure Theory, ed. H. F. Schaefer III (Plenum, New York, 1977). p. 79.
- <sup>21</sup> T. H. Dunning, Jr., and P. J. Hay, "Gaussian Basis Sets for Molecular Calculations," in Methods of Electronic Structure Theory, ed. H. F. Schaefer III (Plenum, New York, 1977) p. 1.
- <sup>22</sup> D. W. Turner, C. Baker, A. D. Baker, and C. R. Brundle, Molecular Photoelectron Spectroscopy (Wiley, London, 1970).

- <sup>23</sup> J. R. Swanson and L. Armstrong, Jr., *Phys. Rev. A* 15, 661 (1977).
- <sup>24</sup> H. P. Kelly, *Chem. Phys. Lett.* 20, 547 (1973).
- <sup>25</sup> J. B. Rose and V. McKoy, *J. Chem. Phys.* 55, 5435 (1971).
- <sup>26</sup> J. A. R. Samson and J. L. Gardner, *J. Geophys. Res.* 78, 3663 (1973).
- <sup>27</sup> W. Domcke, L. S. Cederbaum, J. Schirmer, W. von Niessen, C. E. Brion, and K. H. Tan, *Chem. Phys.* 40, 171 (1979).
- <sup>28</sup> K. Siegbahn, C. Nordling, G. Johansson, J. Hedman, P. F. Heden, K. Hamrin, U. Gelius, T. Bergmark, L. O. Werme, R. Manne, and Y. Baer, ESCA Applied to Free Molecules (North-Holland, Amsterdam, 1969).

TABLE I. Scattering basis sets of  $\sigma$  symmetry used in the Schwinger variational expression.<sup>a</sup>

Number of Functions	$1\sigma_u, 3\sigma_u - k\sigma_g$			Exponents <sup>b</sup>
	Center	$\ell$	$m$	
7	O	0	0	32.0-0.5
5	O	1	0	8.0-0.5
3	O	2	0	2.0-0.5
7	C	0	0	32.0-0.5
5	C	2	0	8.0-0.5
3	C	4	0	2.0-0.5
$1\pi_u - k\sigma_g$				
6	O	0	0	32.0-2.0, 0.5
4	O	1	0	8.0-1.0
2	O	2	0	2.0, 1.0
1	O	3	0	1.0
2	O	4	0	1.0, 0.5
1	O	5	0	1.0
6	C	0	0	32.0-1.0
4	C	2	0	8.0-1.0
2	C	4	0	2.0, 1.0
2	C	6	0	1.0, 0.5
1	C	8	0	0.5
$1\sigma_g, 2\sigma_g, 4\sigma_g, 1\pi_g \rightarrow k\sigma_u$				
7	O	0	0	32.0-0.5
5	O	1	0	8.0-0.5
3	O	2	0	2.0-0.5
7	C	1	0	32.0-0.5
5	C	3	0	8.0-0.5
3	C	5	0	2.0-0.5

<sup>a</sup>These basis sets are composed of spherical Gaussian functions as defined in Eq. (11) and correspond to the set R of Eq. (9).

<sup>b</sup>The notation 32.0-0.5 denotes a geometric series of exponents starting with 32.0 and ending with 0.5 with a ratio between succeeding exponents of 2.0.

TABLE II. Scattering basis sets of  $\pi$  and  $\delta$  symmetry used in the Schwinger variational expression.<sup>a</sup>

Number of Functions	$1\sigma_u, 3\sigma_u, 1\pi_u - k\pi_g$			Exponents
	Center	$l$	$m$	
6	O	1	1	16.0-0.5
5	O	2	1	8.0-0.5
5	C	2	1	8.0-0.5
3	C	4	1	2.0-0.5
$1\sigma_g, 2\sigma_g, 4\sigma_g, 1\pi_g - k\pi_u$				
6	O	1	1	16.0-0.5
5	O	2	1	8.0-0.5
5	C	1	1	8.0-0.5
3	C	3	1	2.0-0.5
$1\pi_u \rightarrow k\delta_g$				
5	O	2	2	8.0-0.5
3	O	3	2	2.0-0.5
2	O	4	2	1.0, 0.5
5	C	2	2	4.0-0.25
3	C	4	2	1.0-0.25
3	C	6	2	1.0-0.25
$1\pi_g \rightarrow k\delta_u$				
5	O	2	2	8.0-0.5
3	O	3	2	2.0-0.5
4	C	3	2	4.0-0.5
2	C	5	2	1.0, 0.5

<sup>a</sup>See notes of TABLE I.

### Figure Captions

**Figure 1** Photoionization cross section for the production of the  $X^2\Pi_g$  and  $C^2\Sigma_g^+$  states of  $CO_2^+$ : ——— present results using the dipole length approximation and the CI initial-state wave function; — — — — present results using the dipole velocity approximation and the CI initial-state wave function; — — — — present results using the dipole length approximation and the HF initial-state wave function; - - - - - present results using the dipole velocity approximation and the HF initial-state wave function; ○ - experimental results of Brion and Tan (Ref. 11); □ - experimental results of Gustafsson et al. (Ref. 12). One megabarn (Mb) is  $10^{-18}$  cm<sup>2</sup>.

**Figure 2** Comparison of different theoretical cross sections for the production of the  $X^2\Pi_g$  and  $C^2\Sigma_g^+$  states of  $CO_2^+$ : ——— present single-center FCHF results; — — — — FCHF results obtained using the STMT approach (Ref. 1); — — — — fixed-nuclei CMSM results (Ref. 2).

Figure 3 Cross sections obtained using different scattering potentials in the  $1\pi_g \rightarrow k\delta_u$  photoionization channel of  $\text{CO}_2$ : ——— present results using correct singlet potential; — — — — present results using triplet potential; — — — — results of STMT method (Ref. 1) using triplet potential.

Figure 4 Photoelectron asymmetry parameters for photoionization leading to the  $X^2\Pi_g$  and  $C^2\Sigma_g^+$  states of  $\text{CO}_2^+$ : ——— present results using the dipole length approximation and a CI initial-state wave function; — — — — present results using the dipole velocity approximation and a CI initial-state wave function; — — — — fixed-nuclei CMSM results (Ref. 3);  $\circ$  - experimental data of Grimm et al. (Ref. 18);  $\square$  - experimental data of Katsumata et al. (Ref. 17).

Figure 5 Photoionization cross section for the production of the  $A^2\Pi_u$  and  $B^2\Sigma_u^+$  states of  $\text{CO}_2^+$ , for definitions of the lines see Fig. 1:  $\Delta$  - experimental fluorescence data of Lee et al. (Ref. 13) for the A state and of Carlson et al. (Ref. 14) for the B state;  $\square$  - experimental photoelectron cross sections obtained by taking the total A + B cross sections of Brion and Tan ( Ref. 11) and using the A/B ratios of Samson and Gardner (Ref. 26) to compute individual A and B cross sections.

- Figure 6 Eigenphase sums and cross sections for the  $1\pi_u \rightarrow k\sigma_g$  and  $3\sigma_u \rightarrow k\sigma_g$  photoionization channels of  $\text{CO}_2$ :  
 —————  $1\pi_u \rightarrow k\sigma_g$  channel; - - - -  $3\sigma_u \rightarrow k\sigma_g$  channel
- Figure 7 Comparison of different theoretical cross sections for the production of the  $A^2\Pi_u$  and  $B^2\Sigma_u^+$  states of  $\text{CO}_2^+$ :  
 ————— present single-center FCHF results;  
 - - - - FCHF results obtained using the STMT approach (Ref. 1).
- Figure 8 Photoelectron asymmetry parameters for photoionization leading to the  $A^2\Pi_u$  and  $B^2\Sigma_u^+$  states of  $\text{CO}_2^+$ , see Fig. 4 for definitions of lines and symbols.
- Figure 9 Total photoionization cross sections for the production of the  $A^2\Pi_u + B^2\Sigma_u^+$  and  $X^2\Pi_g + A^2\Pi_u + B^2\Sigma_u^+ + C^2\Sigma_g^+$  states of  $\text{CO}_2^+$ , see Fig. 1 for definitions of lines and symbols.
- Figure 10 Photoionization cross sections and photoelectron asymmetry parameters for carbon K-shell photoionization in  $\text{CO}_2$ : ————— present results using the dipole length approximation and the HF initial-state wave function; - - - - present results using the dipole velocity approximation and the HF initial-state wave function; - - - - results obtained using the STMT

approach (Ref. 1); - - - - - experimental results of Wight and Brion (Ref. 15) normalized to the present results at a photon energy of 325 eV.

Figure 11

Photoionization cross sections and photoelectron asymmetry parameters for oxygen K-shell photoionization in  $\text{CO}_2$ , see Fig. 10 for definitions of the lines:  $\circ$  - absolute photoabsorption cross sections of Barrus et al. (Ref. 16).

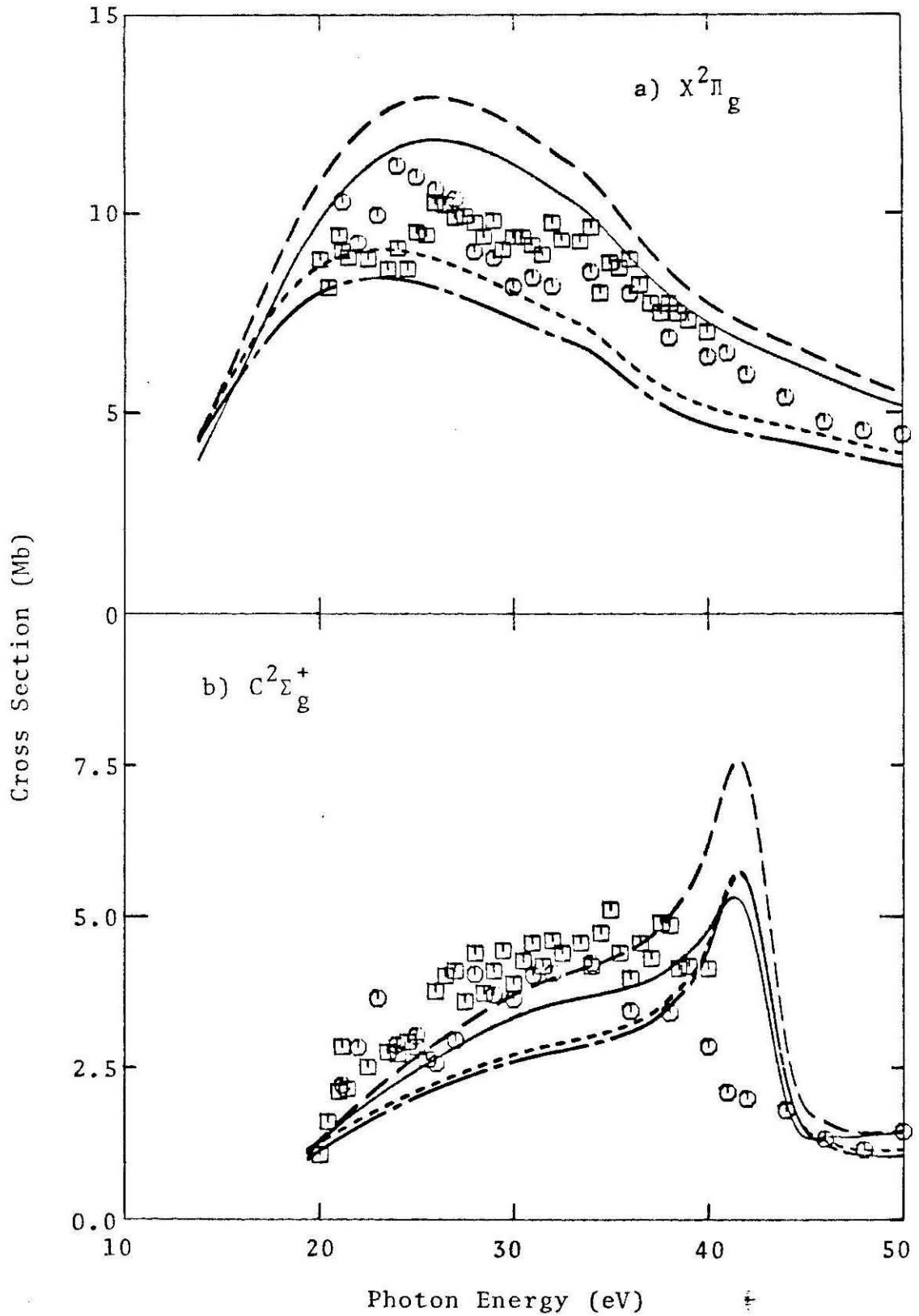


Figure 1

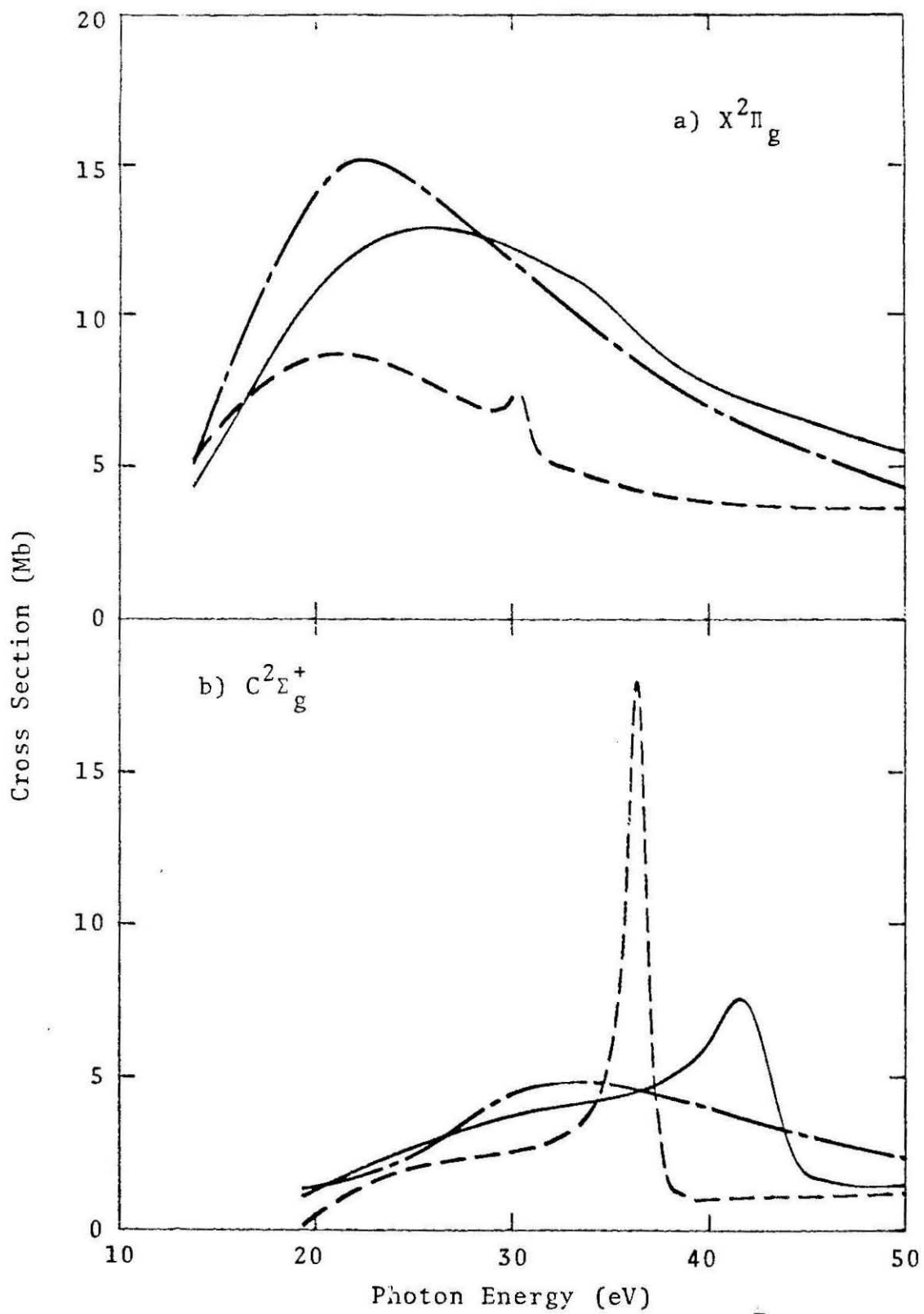


Figure 2

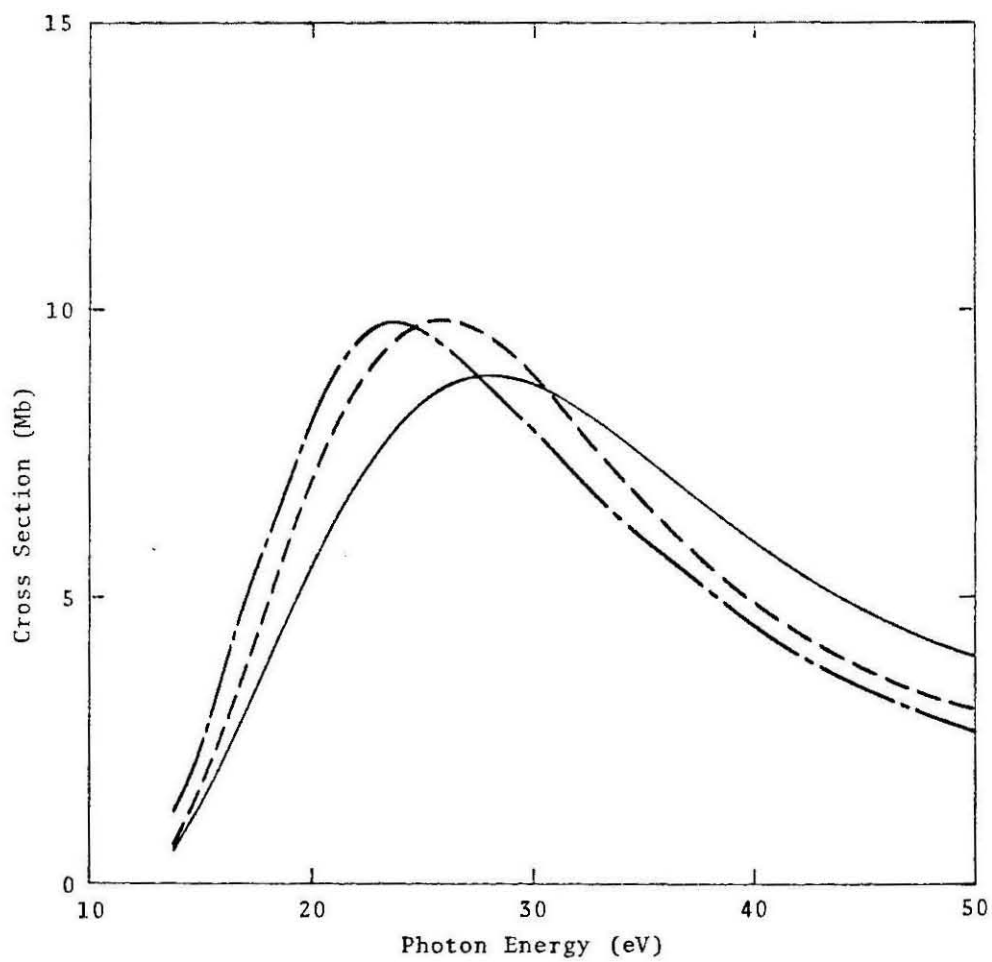


Figure 3

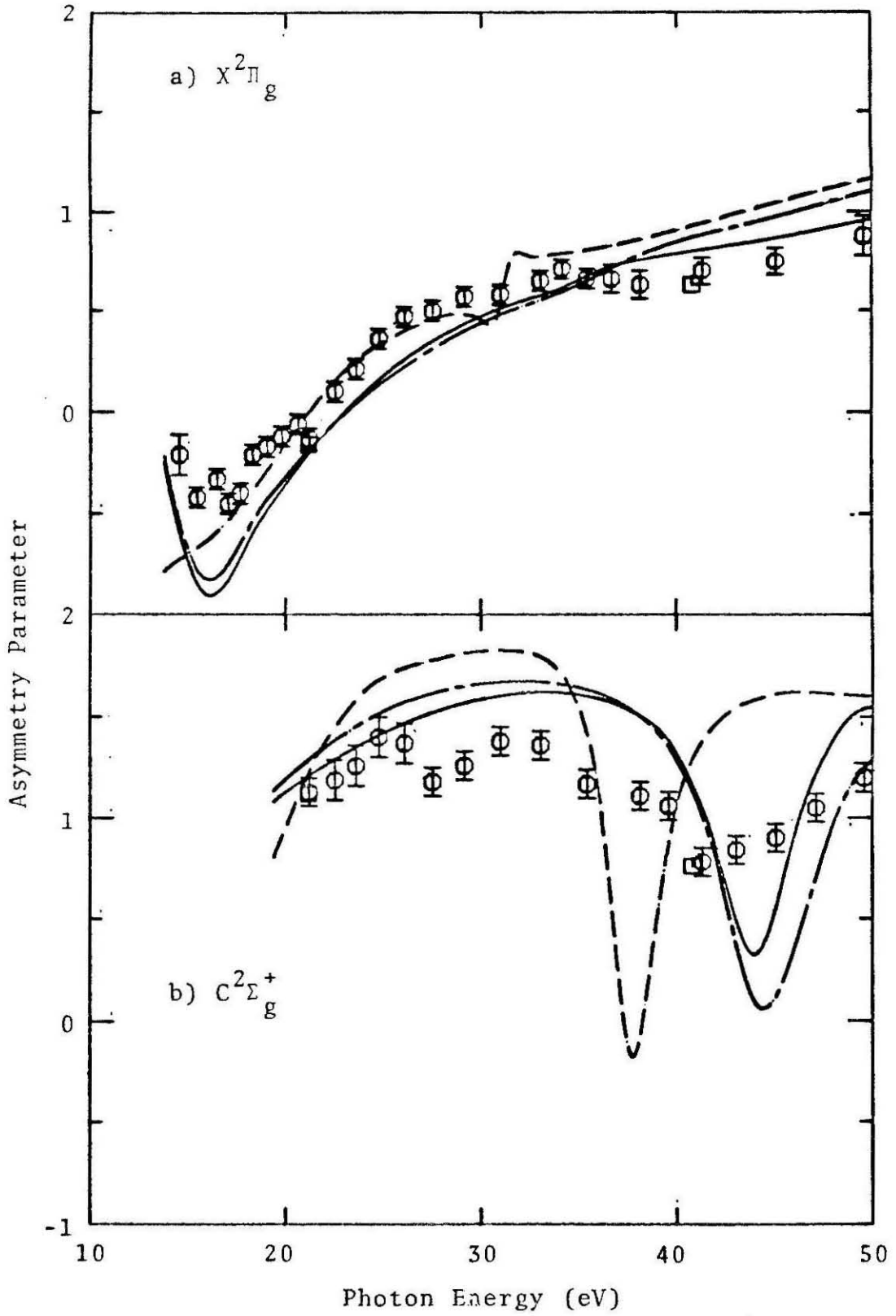


Figure 4

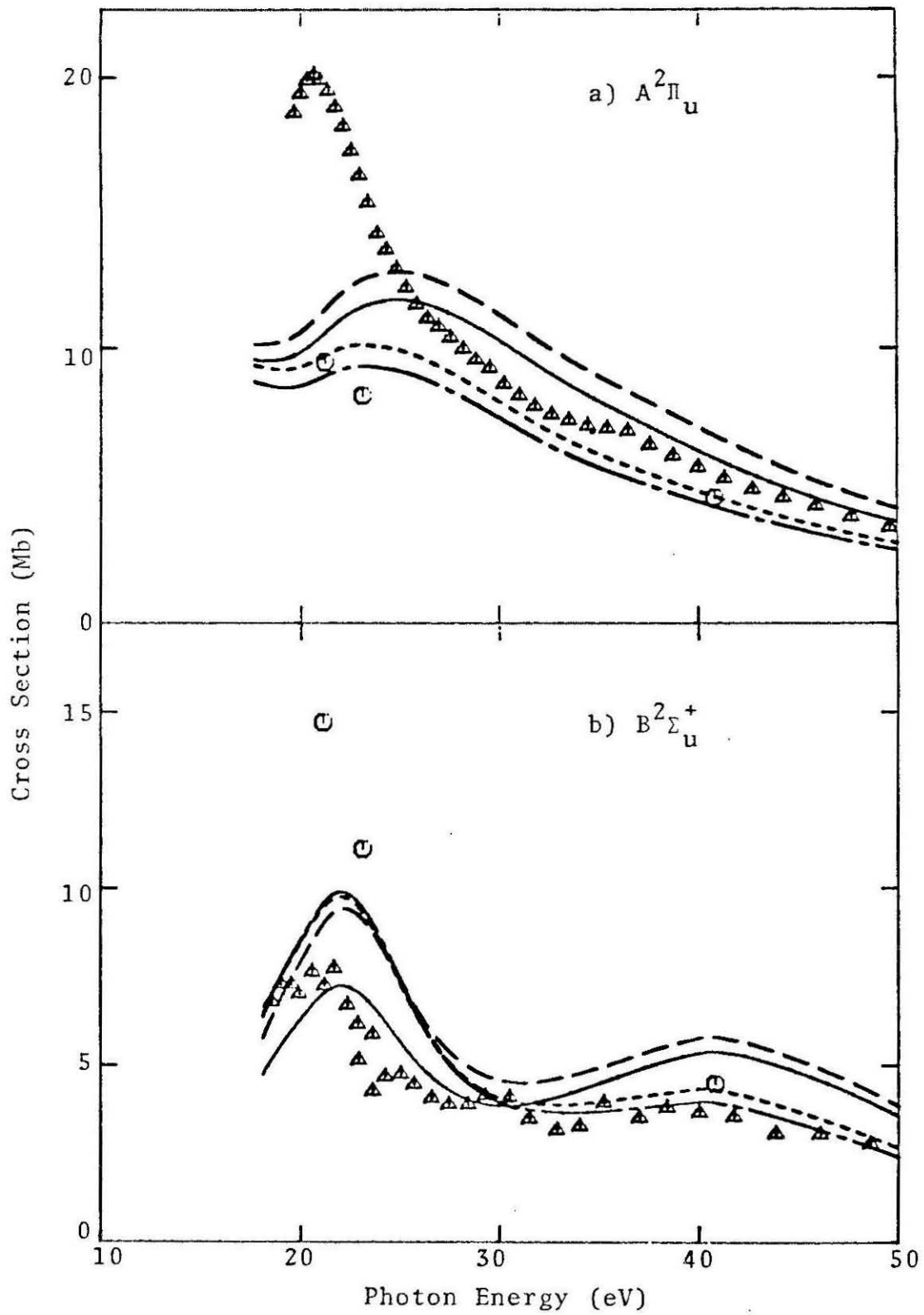


Figure 5

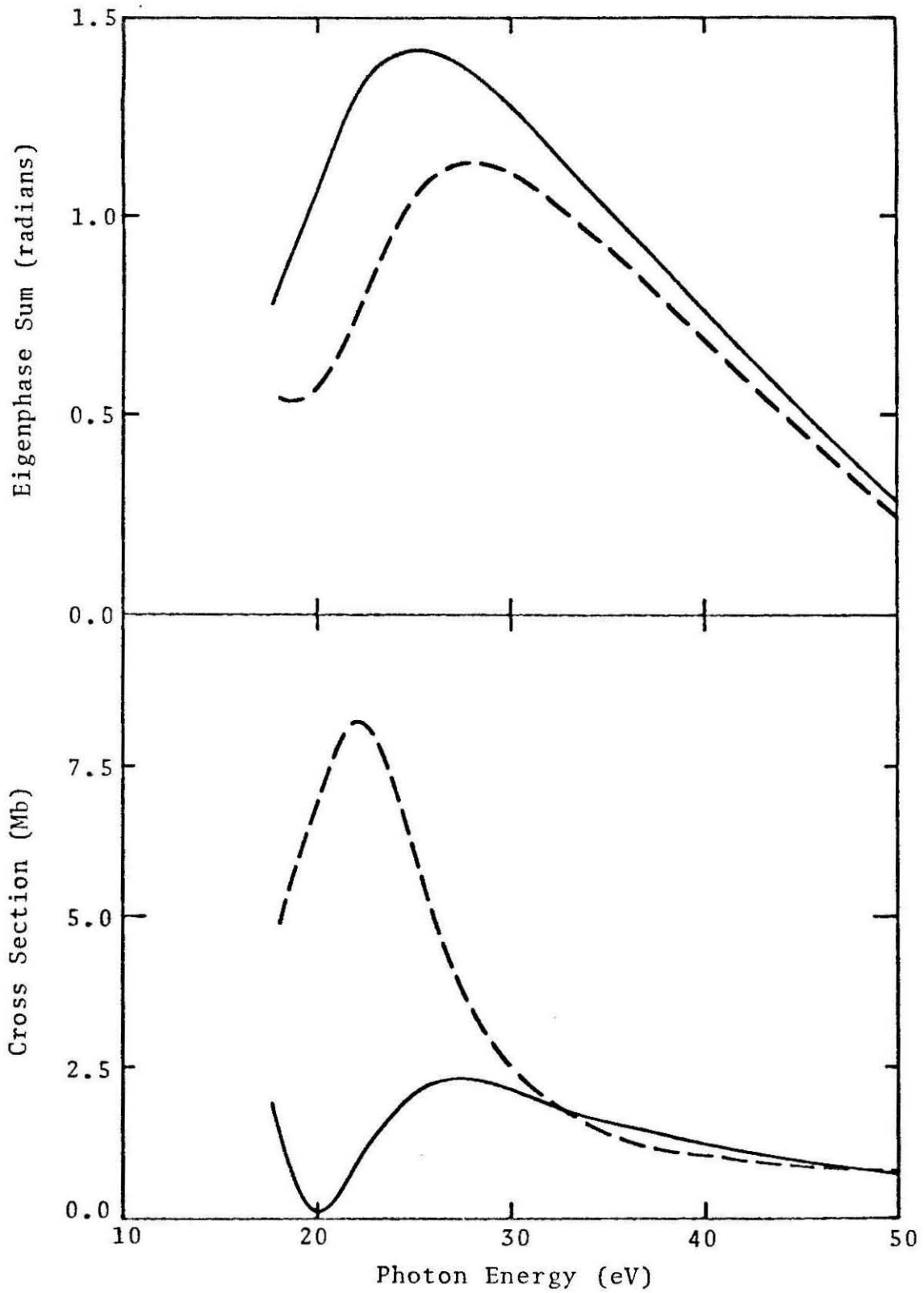


Figure 6

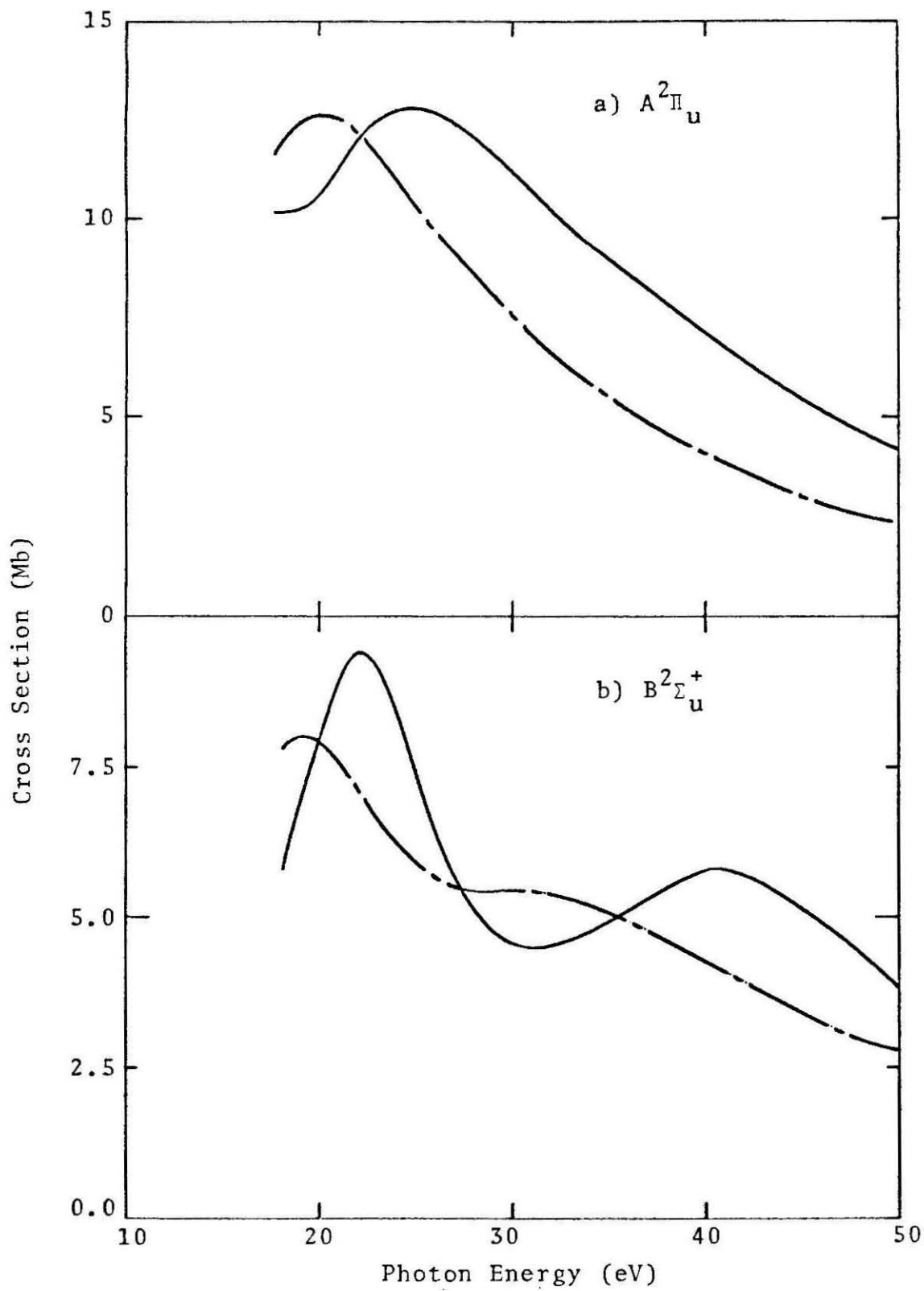


Figure 7

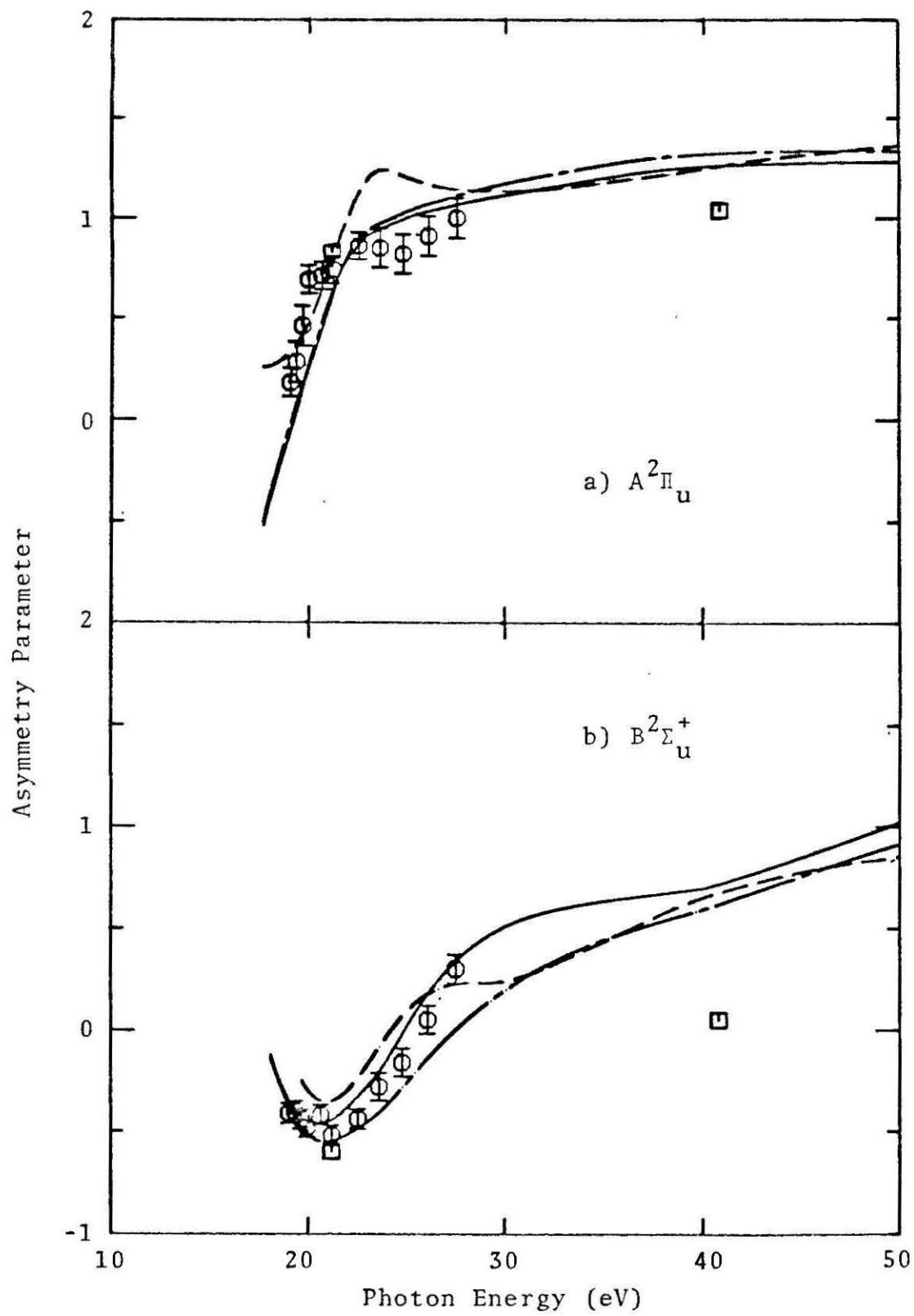


Figure 8

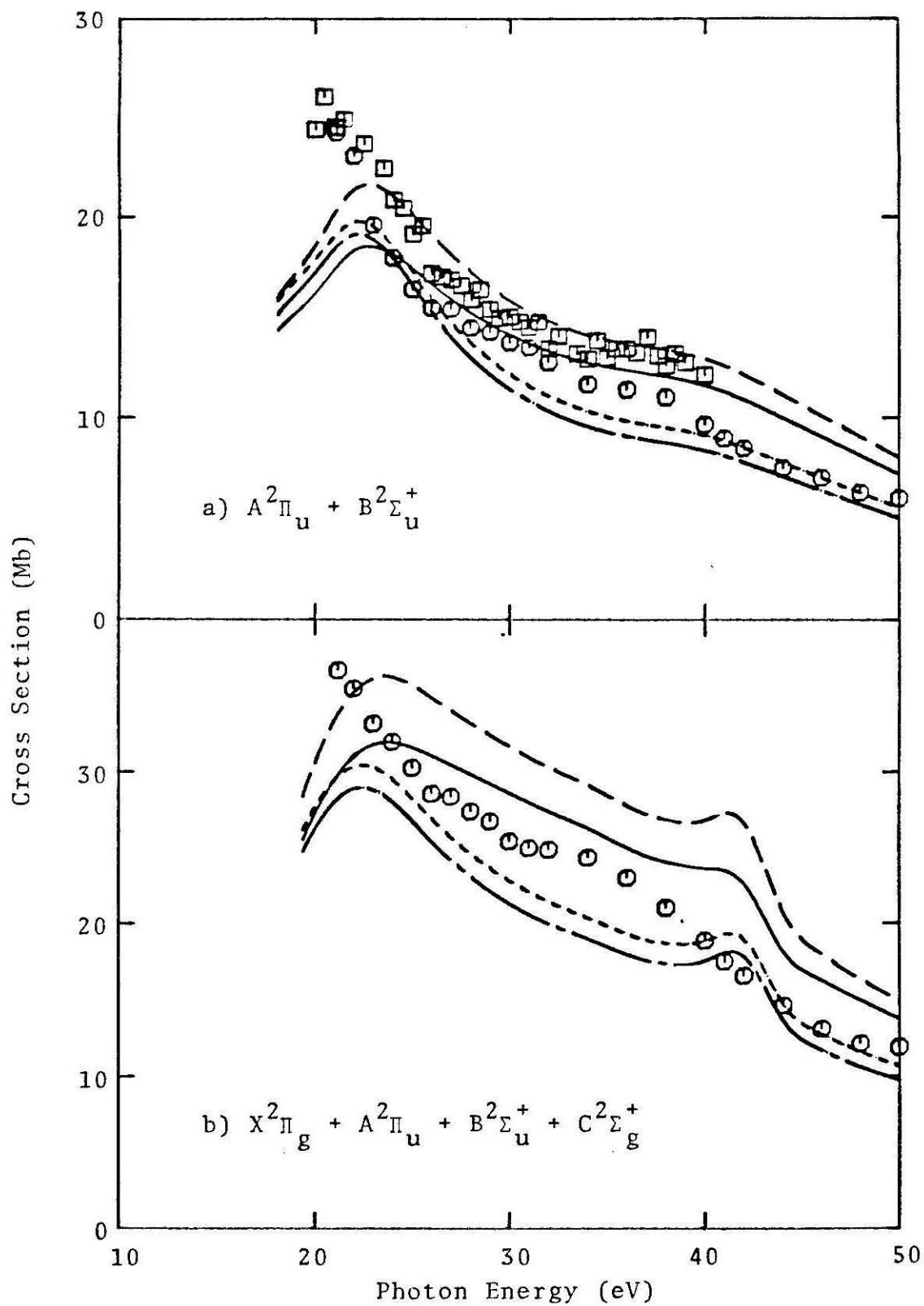


Figure 9

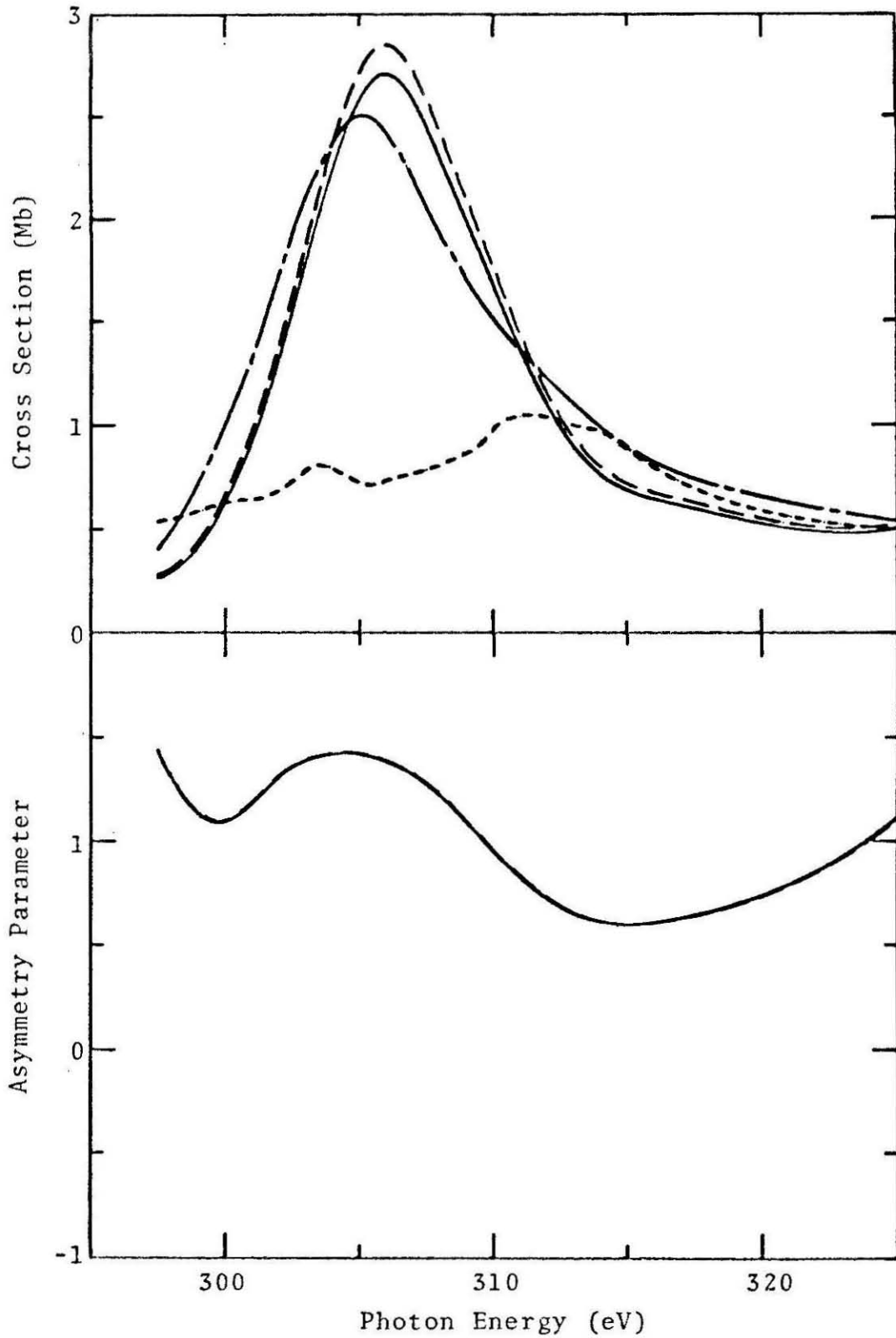


Figure 10

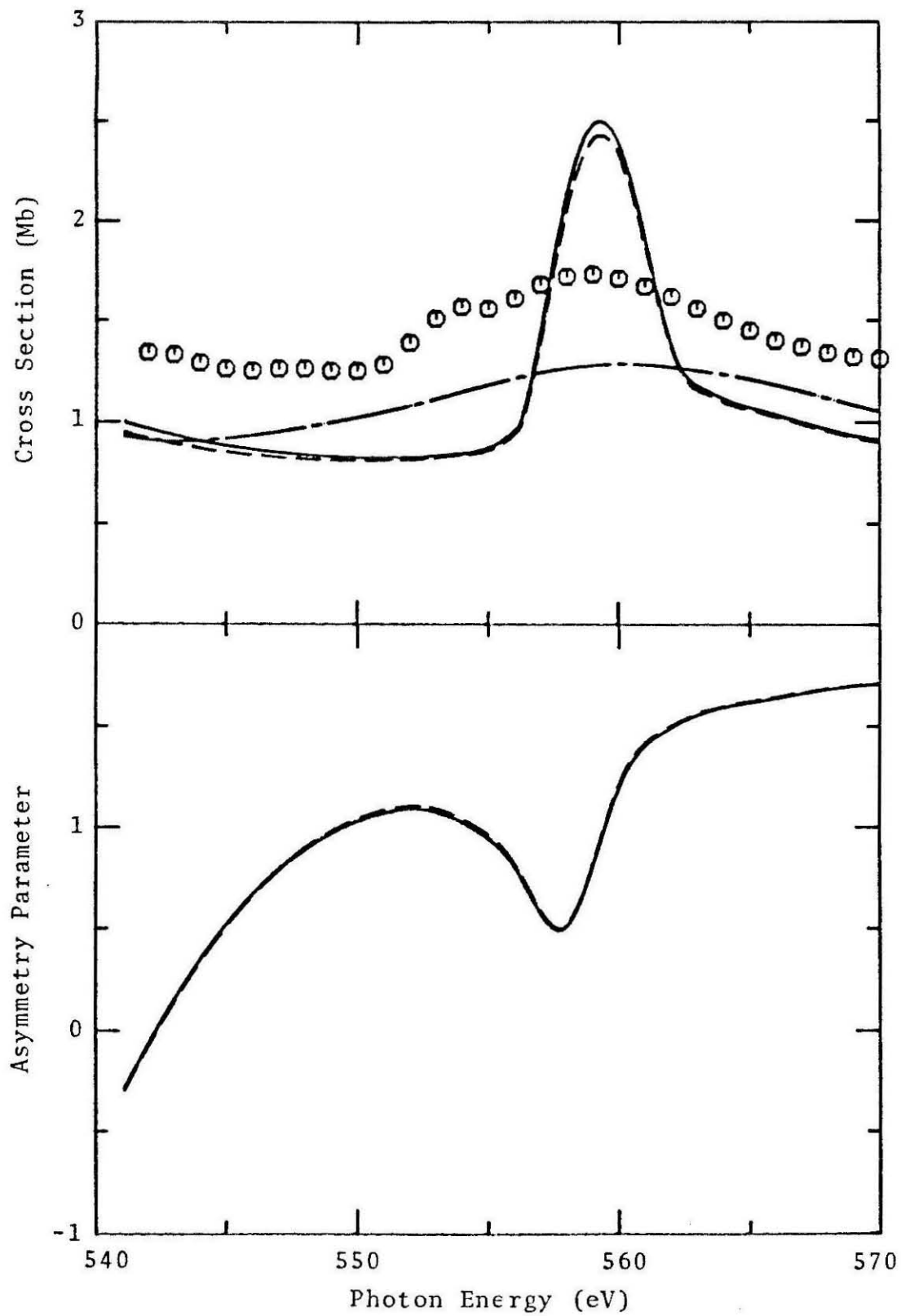


Figure 11

## SECTION E

Vibrational Effects in the Photoionization Shape  
Resonance Leading to the  $C^2\Sigma_g^+$  State of  $CO_2^+$

## I. INTRODUCTION

Recently,<sup>1</sup> we have compared the partial photoionization cross section leading to the  $C^2 \Sigma_g^+ [(4\sigma)^{-1}]$  state of  $CO_2^+$  as obtained by the continuum multiple scattering model<sup>2</sup> with that given by the direct solution of the scattering equations for the  $e-CO_2^+$  system. In these studies<sup>1</sup> we explicitly solved the scattering equations for the continuum orbital of the ejected electron in the field of the static-exchange potential of the molecular ion. The feature of particular interest in this channel was the narrow shape resonance which was predicted by the continuum multiple scattering model (CMSM) to have a peak value of 18 Mb at a photon energy of about 37 eV for the nuclei fixed at the ground state equilibrium geometry. In contrast, the photoionization cross sections obtained from the solution of the  $e-CO_2^+$  static-exchange collision equations show a somewhat broader resonance feature with a peak value of about 7 Mb at a photon energy of 42 eV.<sup>1</sup> Moreover, Swanson *et al.*<sup>2</sup> found that vibrational averaging of the fixed-nuclei CMSM cross sections resulted in a considerable reduction and broadening of the resonant peak relative to the results obtained at the equilibrium nuclear configuration. Specifically, vibrational averaging reduced the fixed-nuclei cross section from its peak value of 18 Mb at the ground state equilibrium geometry to a value of 6 Mb. Although photoionization cross sections near a shape resonance can be expected to be sensitive to changes in internuclear separation, we<sup>1</sup> suggested that this dramatic reduction of the cross section at the equilibrium geometry due to vibrational averaging in the region of the resonance

was unphysical and an artifact of the CMSM. Since vibrational motion can indeed lead to important effects in molecular photoionization, it is necessary to quantitatively assess the actual magnitude of the effect of vibrational averaging on molecular photoionization in the region of shape resonances.

In this paper we present vibrationally averaged cross sections and asymmetry parameters for photoionization of the  $4\sigma_g$  level of  $\text{CO}_2$  leading to the  $\text{C } ^2\Sigma_g^+$  state of  $\text{CO}_2^+$ . These results are obtained by averaging the fixed-nuclei photoionization cross sections and asymmetry parameters at five values of the internuclear coordinates over the ground vibrational wave function of the symmetric stretch mode of the molecule. At each internuclear geometry the cross sections are obtained from the solution of the  $e\text{-CO}_2^+$  collisional equations with the full static-exchange potential of the ion. These results show that vibrational averaging, in fact, reduces the peak intensity of the fixed-nuclei resonant cross section at the ground state equilibrium geometry by about 15%. These results are in strong contrast to those of the CMSM where vibrational averaging reduced the intensity of the resonance by 70% in this channel.<sup>2</sup> These results clearly suggest that the CMSM does not provide a quantitatively realistic description of this resonant photoionization cross section and the effects of vibrational averaging on these cross sections.

In the next section we briefly outline our method of solution of the  $e\text{-CO}_2^+$  scattering equations. We then present both the fixed-nuclei and vibrationally averaged cross sections and asymmetry

parameters. We compare our results with those of the CMSM and experimental results where available.

## II. THEORY AND RESULTS

The fixed-nuclei photoionization cross section for going from an initial bound state  $\Psi_i$  to the continuum state  $\Psi_{f, \vec{k}}^{(-)}$  due to linearly polarized light is given in the dipole length approximation by

$$\frac{d^2 \sigma^L(R)}{d\hat{\Omega}_{\vec{k}} d\hat{\Omega}_{\hat{n}}} = \frac{4\pi^2 E k}{c} \left| \langle \Psi_i(R) | \vec{r} \cdot \hat{n} | \Psi_{f, \vec{k}}^{(-)}(R) \rangle \right|^2, \quad (1)$$

and in the dipole velocity approximation by

$$\frac{d^2 \sigma^V(R)}{d\hat{\Omega}_{\vec{k}} d\hat{\Omega}_{\hat{n}}} = \frac{4\pi^2 k}{cE} \left| \langle \Psi_i(R) | \vec{\nabla} \cdot \hat{n} | \Psi_{f, \vec{k}}^{(-)}(R) \rangle \right|^2, \quad (2)$$

where  $E$  is the photon energy,  $\hat{n}$  is the direction of the polarization of the light,  $c$  is the speed of light, and  $\vec{k}$  is the asymptotic momentum of the photoelectron. When these cross sections are averaged over all possible molecular orientations in the laboratory frame, the resulting differential cross section is of the form

$$\frac{d\sigma^{L,V}(R)}{d\Omega_{\hat{k}}} = \frac{\sigma^{L,V}(R)}{4\pi} [1 + \beta_{\hat{k}}^{L,V}(R) P_2(\cos \theta)] \quad (3)$$

where  $\theta$  is the angle between the direction of the polarization of the light and the momentum of the photoelectron.

The adiabatic-nuclei cross section can then be obtained from the fixed-nuclei results by averaging over the vibrational degrees of freedom. If only the ground vibrational state is initially populated and we sum over all final vibrational states then, by ignoring the dependence of  $k$  on the vibrational energy levels, we obtain the following vibrationally averaged cross sections<sup>3</sup>

$$\sigma_{\text{ave}}^{L,V} = \langle \chi_i | \sigma^{L,V}(R) | \chi_i \rangle \quad (4)$$

and

$$\beta_{\hat{k},\text{ave}}^{L,V} = \frac{\langle \chi_i | \sigma^{L,V}(R) \beta_{\hat{k}}^{L,V}(R) | \chi_i \rangle}{\langle \chi_i | \sigma^{L,V}(R) | \chi_i \rangle}, \quad (5)$$

where  $\chi_i$  is the ground vibrational wave function. In this study we assume that the vibrational motion of  $\text{CO}_2$  is harmonic and we have only considered the effects of averaging over the symmetric stretching mode.

We have computed the vibrational averages by performing a

five point Gaussian quadrature where the square of the vibrational wave function is the weight function. Thus with a symmetric stretch vibrational frequency of  $1388.17 \text{ cm}^{-1}$  for  $\text{CO}_2$ ,<sup>4</sup> we have computed the fixed-nuclei cross sections at  $R(\text{C-O}) = 2.0892, 2.1445, 2.1944, 2.2443,$  and  $2.2996 \text{ au}$ . The quadrature weights were then  $0.011257, 0.222076, 0.533333, 0.222076, 0.011257$ , respectively.

The initial state function ( $\Psi_i$  of Eqs. (1) and (2)) was represented by a SCF wave function which was constructed from a 3s2p1d contracted Cartesian Gaussian basis set.<sup>5</sup> The SCF energy of  $\text{CO}_2$  in this basis set is  $-187.674286 \text{ au}$  at the equilibrium  $R(\text{C-O}) = 2.1944 \text{ au}$ . The final state wave functions ( $\Psi_{f, \vec{k}}^{(-)}$  of Eqs. (1) and (2)) were obtained using the Frozen-Core-Hartree-Fock (FCHF) approximation. This implies that all the bound orbitals were fixed as their initial state forms. The continuum orbital representing the photoelectron was then determined by solving the appropriate static-exchange Lippmann-Schwinger equation

$$\psi_{\vec{k}}^{(-)} = \phi_{\vec{k}} + G_c^{(-)}(E) U \psi_{\vec{k}}^{(-)}, \quad (6)$$

where  $E = k^2/2$ ,  $G_0^{(-)}(E)$  is the Coulomb Green's function,  $U$  is the static-exchange potential with the  $1/r$  component removed, and  $\phi_{\vec{k}}$  is a Coulomb scattering function. We have solved Eq. (6) using the Schwinger variational method.<sup>6</sup> We have not employed the iterative technique which has been applied to other systems,<sup>7,8</sup> since in our previous studies of the photoionization of  $\text{CO}_2$  we found that the exact iterative cross section for photoionization leading to the  $\text{C } ^2\Sigma_g^+$  state of  $\text{CO}_2^+$

was very close to the initial noniterative result obtained using the  $L^2$  basis functions given in Table I.<sup>9</sup> Using the Schwinger variational expression the solutions of Eq. (6) are given by<sup>6,7</sup>

$$\psi_{\vec{k}}^{(-)}(\vec{r}) = \phi_{\vec{k}}(\vec{r}) + \sum_{\alpha_i, \alpha_j \in R} \langle \vec{r} | G_c^{(-)} U | \alpha_i \rangle [D^{-1}]_{ij} \langle \alpha_i | U | \phi_{\vec{k}} \rangle \quad (7)$$

where  $[D^{-1}]_{ij}$  is the matrix inverse of

$$D_{ij} = \langle \alpha_i | U - U G_c^{(-)} U | \alpha_j \rangle. \quad (8)$$

The sets of functions  $R$  used in Eq. (7) are composed of spherical Gaussian functions defined by

$$\alpha^{\gamma, \ell, m, n, \vec{A}}(\vec{r}) = N |\vec{r} - \vec{A}|^\ell e^{-\gamma |\vec{r} - \vec{A}|^2} Y_{\ell m}(\Omega_{\vec{r} - \vec{A}}). \quad (9)$$

In Table I we give the elements of these sets for the two scattering symmetries considered here. The necessary integrals are computed by expanding all functions in truncated partial wave expansions with the resulting radial integrals put on a grid and computed using Simpson's rule. We have used the same grid and expansion parameters as were used in our earlier study of  $\text{CO}_2$  photoionization.<sup>9</sup> The grid contained

1000 points extending out to  $r = 90$  au. The smallest step size was 0.005 au and the largest step size was 0.16 au. We have expanded the static potential including terms up to  $\lambda_m^{\text{dir}} = 118$ . In the exchange integrals, the occupied orbitals were expanded to a high enough  $\ell$  such that the orbitals were normalized to better than 0.99, and the expansion of  $1/r_{12}$  was truncated at  $\lambda_m^{\text{ex}} = 40$ . All other partial-wave expansions were truncated at  $\ell_m = 59$ .

In Fig. 1 we present the fixed-nuclei photionization cross sections of  $\text{CO}_2$  leading to the  $\text{C } ^2\Sigma_g^+$  state of  $\text{CO}_2^+$  for the five internuclear separations given above. We have taken the vertical ionization potential for the  $\text{C } ^2\Sigma_g^+$  state of  $\text{CO}_2^+$  to be 19.4 eV.<sup>10</sup> We can see that the photoionization cross sections depend fairly strongly on  $R$  in the region of the shape resonance in this channel. The longer internuclear separations produce a lower energy resonance, and the shorter internuclear separations produce a higher energy resonance. In Fig. 2 we compare the present dipole length static-exchange level cross sections, both vibrationally-averaged and fixed-nuclei, with those obtained using the CMSM approach,<sup>2</sup> and with the experimental results of Brion and Tan.<sup>11</sup> We can see that the effect of averaging on the static-exchange cross section is to broaden the resonant feature and to reduce the cross section. As can be seen in Fig. 2, the CMSM fixed-nuclei and vibrationally averaged cross sections exhibit the same qualitative trend. However, the CMSM cross sections show a much larger drop in the peak cross section due to vibrational averaging. The experimental total cross section does not show any resonance

feature in this channel.

In this study we have not included the effects of initial or final state correlation. One way of estimating such correlation effects is by computing the photoionization cross section in both dipole length and velocity forms. In Fig. 3 we present the length and velocity forms of the vibrationally averaged cross section leading to the  $C^2\Sigma_g^+$  state of  $CO_2^+$  and compare them to the experimental results of Brion and Tan.<sup>11</sup> The difference between the length and velocity cross sections can be viewed as an estimate of the minimum error due to correlation.<sup>12</sup> In actual applications<sup>8, 9, 13</sup> we have found that the exact cross sections tend to lie between the length and velocity forms, except where auto-ionization is important. The lack of agreement between theory and experiment shown in Fig. 3 indicates that correlation effects will have to be explicitly included before quantitative agreement will be achieved.

In Fig. 4 we examine the effects of vibrational averaging on the photoelectron asymmetry parameters in the  $C^2\Sigma_g^+$  channel. We have compared the static-exchange results obtained here with the CMSM results of Swanson *et al.*<sup>14</sup> and with experimental data of Katsumata *et al.*<sup>15</sup> and Carlson *et al.*<sup>16</sup> Unlike the experimental total photoionization cross sections,<sup>11</sup> the experimental asymmetry parameters<sup>16</sup> do show a resonant feature at a photon energy of 40 eV, in reasonable agreement with the present theoretical results. Once again the vibrational averaging of the CMSM results produces a larger quantitative change than does vibrational averaging of the static-exchange results.

### III. CONCLUSION

We have shown that the effect of vibrational averaging on the static-exchange photoionization cross section of  $\text{CO}_2$  leading to the  $\text{C } ^2\Sigma_g^+$  state of  $\text{CO}_2^+$  is a 15% reduction in the peak resonant cross section. A similar reduction in the feature in the computed photoelectron asymmetry parameters was also obtained. This is in contrast to the larger effects predicted by the CMSM calculations.<sup>2, 14</sup> It is also of interest to note that the resonant vibrational effects obtained here for the photoionization of  $\text{CO}_2$  are much larger than those obtained by Raseev *et al.*<sup>17</sup> for the resonant photoionization of  $\text{N}_2$  leading to the  $\text{X } ^2\Sigma_g^+$  state of  $\text{N}_2^+$ . This seems to follow directly from the fact that the shape resonance in  $\text{CO}_2$  is much narrower than that in  $\text{N}_2$ .

The present theoretical results do not yet agree quantitatively with experimental results. However, the experimental asymmetry parameters of Carlson *et al.*<sup>16</sup> lend strong support to the theoretical prediction of a shape resonance occurring in the  $\text{C } ^2\Sigma_g^+$  channel near a photon energy of 40 eV.

### ACKNOWLEDGMENTS

This material is based upon work supported by the National Science Foundation under Grant No. CHE80-40870. The authors acknowledge computing support from the National Center for Atmospheric Research (NCAR) which is sponsored by the National Science

Foundation. One of us (RRL) acknowledges support from an Exxon Foundation Graduate Educational Fellowship. The research reported in this paper made use of the Dreyfus-NSF Theoretical Chemistry Computer which was funded through grants from the Camille and Henry Dreyfus Foundation, the National Science Foundation (Grant No. CHE78-20235), and the Sloan Fund of the California Institute of Technology.

References

- <sup>1</sup> R. R. Lucchese and V. McKoy, *J. Phys. Chem.* 85, 2166 (1981).
- <sup>2</sup> J. R. Swanson, D. Dill, and J. L. Dehmer, *J. Phys. B* 13, L105 (1980).
- <sup>3</sup> D. M. Chase, *Phys. Rev.* 104, 838 (1956).
- <sup>4</sup> G. Herzberg, Electronic Spectra of Polyatomic Molecules (Van Nostrand Reinhold, New York, 1966) p. 598.
- <sup>5</sup> T. H. Dunning, Jr., and P. J. Hay, "Gaussian Basis Sets for Molecular Calculations" in Methods of Electronic Structure Theory, ed. H. F. Schaefer III (Plenum, New York, 1977).
- <sup>6</sup> R. R. Lucchese and V. McKoy, *Phys. Rev. A* 21, 112 (1980).
- <sup>7</sup> R. R. Lucchese, D. K. Watson, and V. McKoy, *Phys. Rev. A* 22, 421 (1980).
- <sup>8</sup> R. R. Lucchese and V. McKoy, *Phys. Rev. A* 24, 770 (1981).
- <sup>9</sup> R. R. Lucchese and V. McKoy, "Studies of Differential and Total Photoionization Cross Sections of Carbon Dioxide," *Phys. Rev. A* - submitted for publication.
- <sup>10</sup> D. W. Turner, C. Baker, A. D. Baker, and C. R. Brundle, Molecular Photoelectron Spectroscopy (Wiley, London, 1970).
- <sup>11</sup> C. E. Brion and K. H. Tan, *Chem. Phys.* 34, 141 (1978).
- <sup>12</sup> H. P. Kelly, *Chem. Phys. Lett.* 20, 547 (1973).
- <sup>13</sup> R. R. Lucchese, G. Raseev, and V. McKoy, "Studies of Differential and Total Photoionization Cross Sections of Molecular Nitrogen," *Phys. Rev. A* - accepted for publication.

- <sup>14</sup> J. R. Swanson, D. Dill, and J. L. Dehmer, *J. Phys. B* 14, L207 (1981).
- <sup>15</sup> S. Katsumata, Y. Achiba, and K. Kimura, *J. Electron Spectrosc. Related Phenomena* 17, 229 (1979).
- <sup>16</sup> T. A. Carlson, M. O. Krause, F. A. Grimm, J. D. Allen, Jr., D. Mehaffy, P. R. Keller, and J. W. Taylor, *Phys. Rev. A* 23, 3316 (1981).
- <sup>17</sup> G. Raseev, H. Le Rouzo, and H. Lefebvre-Brion, *J. Chem. Phys.* 72, 5701 (1980).

TABLE I. Scattering basis sets used with the Schwinger variational expression.<sup>a</sup>

$4\sigma_g \rightarrow k\sigma_u$				
Number of Functions <sup>b</sup>	Center	$\ell$	$m$	Range of Exponents
7	O	0	0	32.0-0.5
5	O	1	0	8.0-0.5
3	O	2	0	2.0-0.5
7	C	1	0	32.0-0.5
5	C	3	0	8.0-0.5
3	C	5	0	2.0-0.5
$4\sigma_g \rightarrow k\pi_u$				
6	O	1	1	16.0-0.5
5	O	2	1	8.0-0.5
5	C	1	1	8.0-0.5
5	C	3	1	8.0-0.5

<sup>a</sup>These basis sets are composed of spherical Gaussian functions as defined in Eq. (9) and correspond to the set R of Eq. (7).

<sup>b</sup>Total number of basis functions on a given center with the same value of  $\ell$  and  $m$ . The exponents of the basis set form a geometric series with a ratio of 2.0.

### Figure Captions

- Figure 1: Fixed-nuclei photoionization cross sections of  $\text{CO}_2$  leading to the  $\text{C } ^2\Sigma_g^+$  state of  $\text{CO}_2^+$ . The five curves correspond from left to right to  $R(\text{C-O}) = 2.2996, 2.2443, 2.1944, 2.1445,$  and  $2.0892$  au. One megabarn (Mb) is  $10^{-18} \text{ cm}^2$ .
- Figure 2: Comparison of the CMSM results from Ref. 2 and the present static-exchange results for the photoionization cross section of  $\text{CO}_2$  leading to the  $\text{C } ^2\Sigma_g^+$  state of  $\text{CO}_2^+$ : ——— cross section averaged over the symmetric stretch vibrational mode; — — — — equilibrium fixed-nuclei cross section; ● - experimental results of Brion and Tan from Ref. 11.
- Figure 3: Vibrationally averaged photoionization cross section leading to the  $\text{C } ^2\Sigma_g^+$  state of  $\text{CO}_2^+$ : ——— dipole length static-exchange cross section; — — — — dipole velocity static-exchange cross section; ● - experimental results of Brion and Tan from Ref. 11.
- Figure 4: Comparison of the CMSM results from Ref. 14 and the present static-exchange results for the photoelectron asymmetry parameter for photoionization leading to the  $\text{C } ^2\Sigma_g^+$  state of  $\text{CO}_2^+$ : ——— asymmetry parameter averaged over the symmetric stretch vibrational mode;

Figure Captions (continuation)

— — — — equilibrium fixed-nuclei asymmetry parameter; ● - experimental data of Carlson et al. from Ref. 16; ■ - experimental data of Katsumata et al. from Ref. 15.

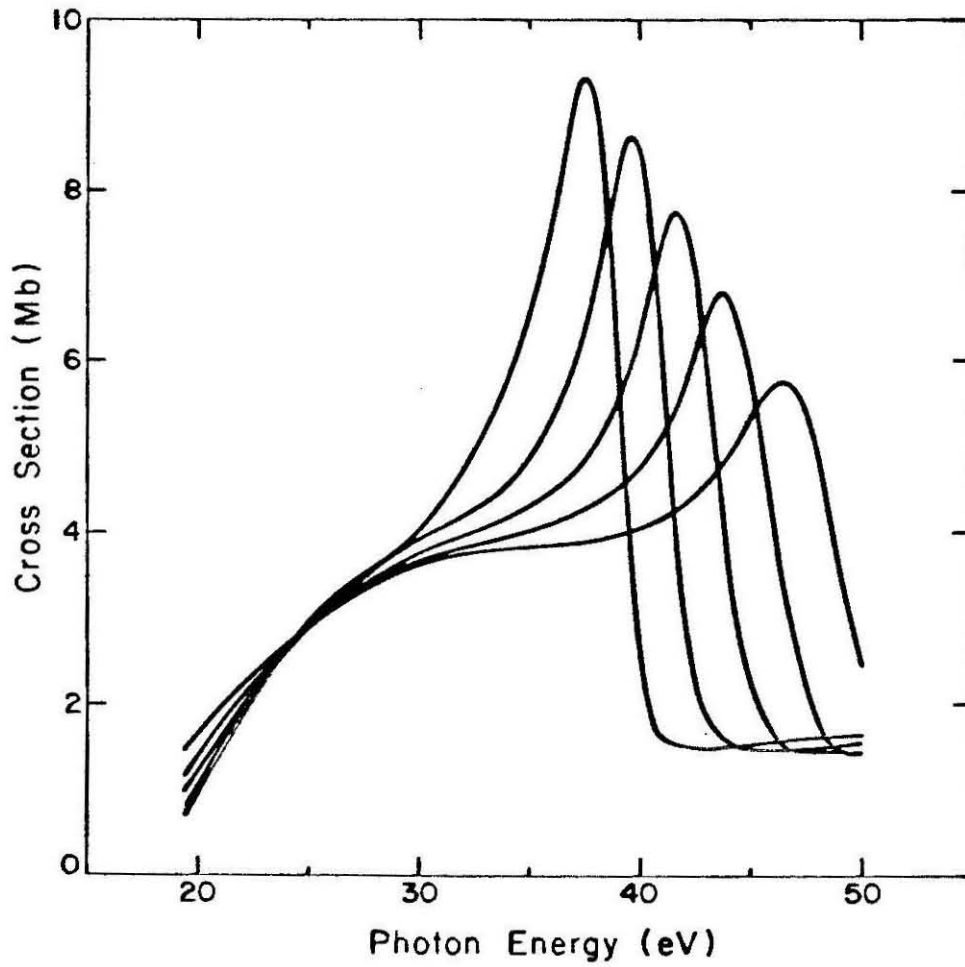


Fig. 1

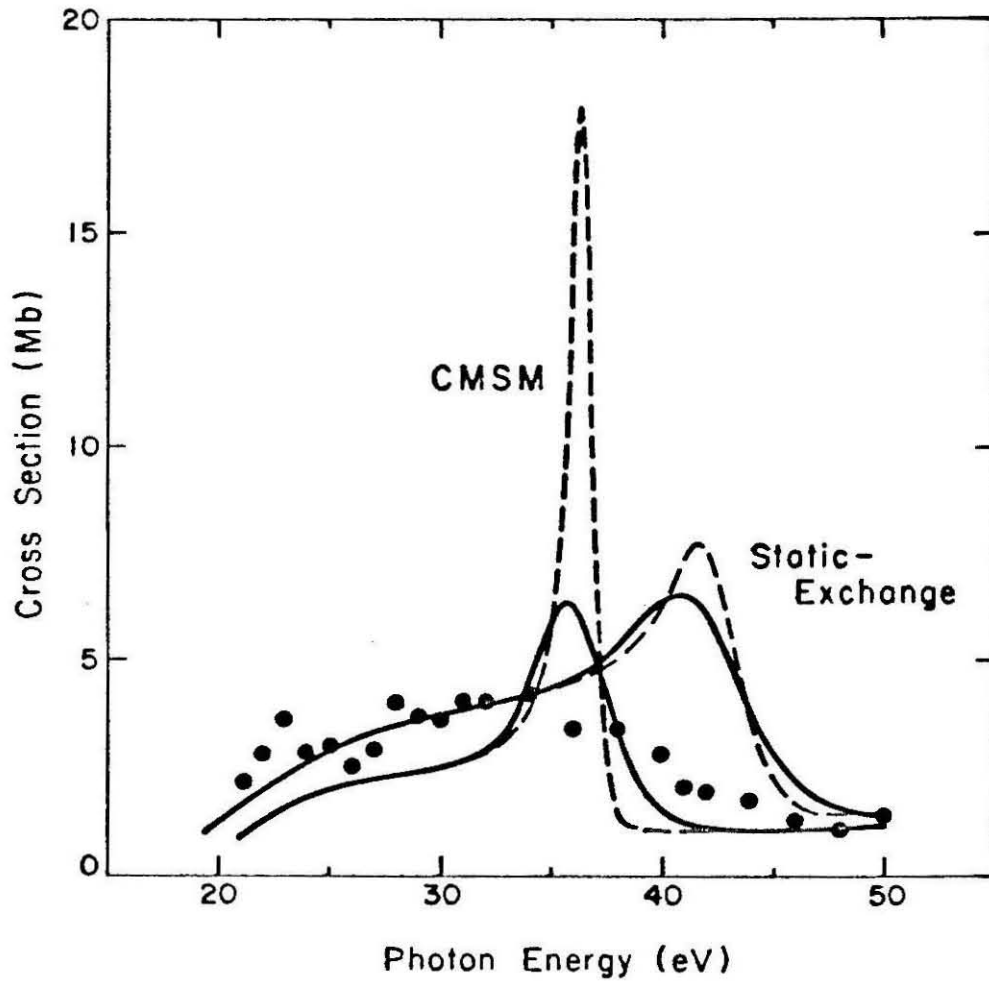


Fig. 2

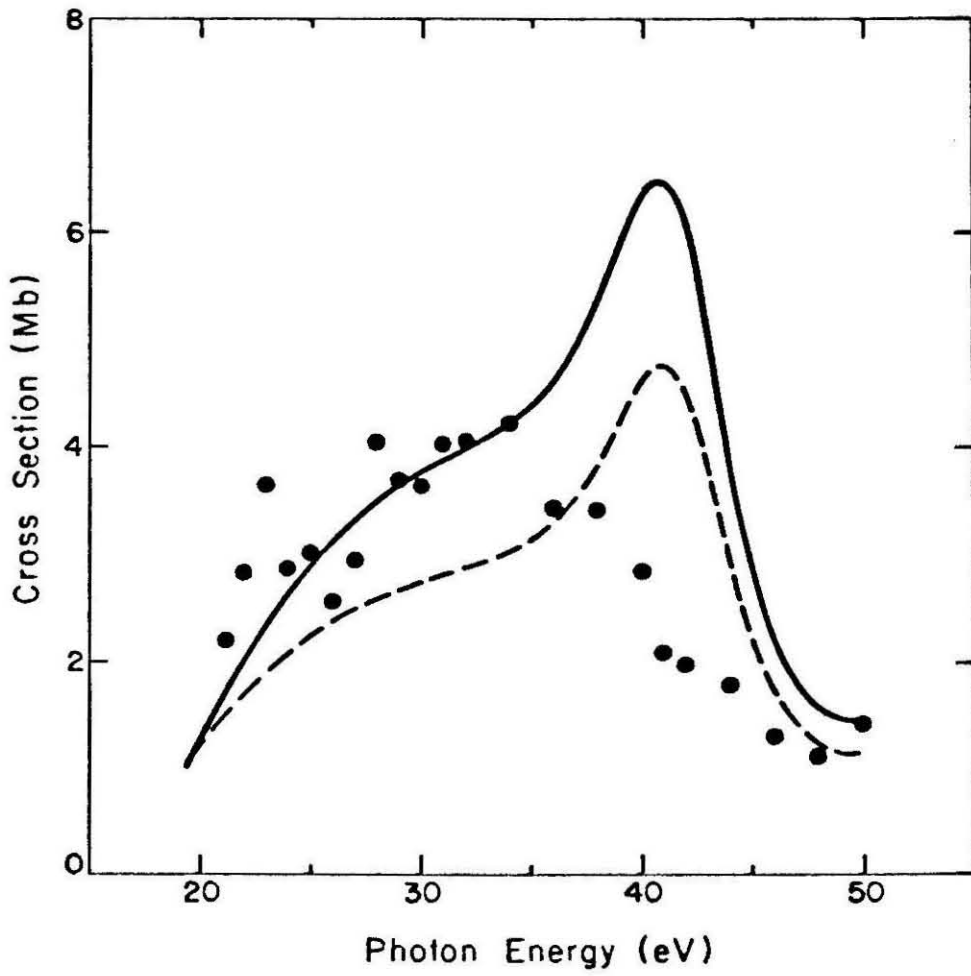


Fig. 3

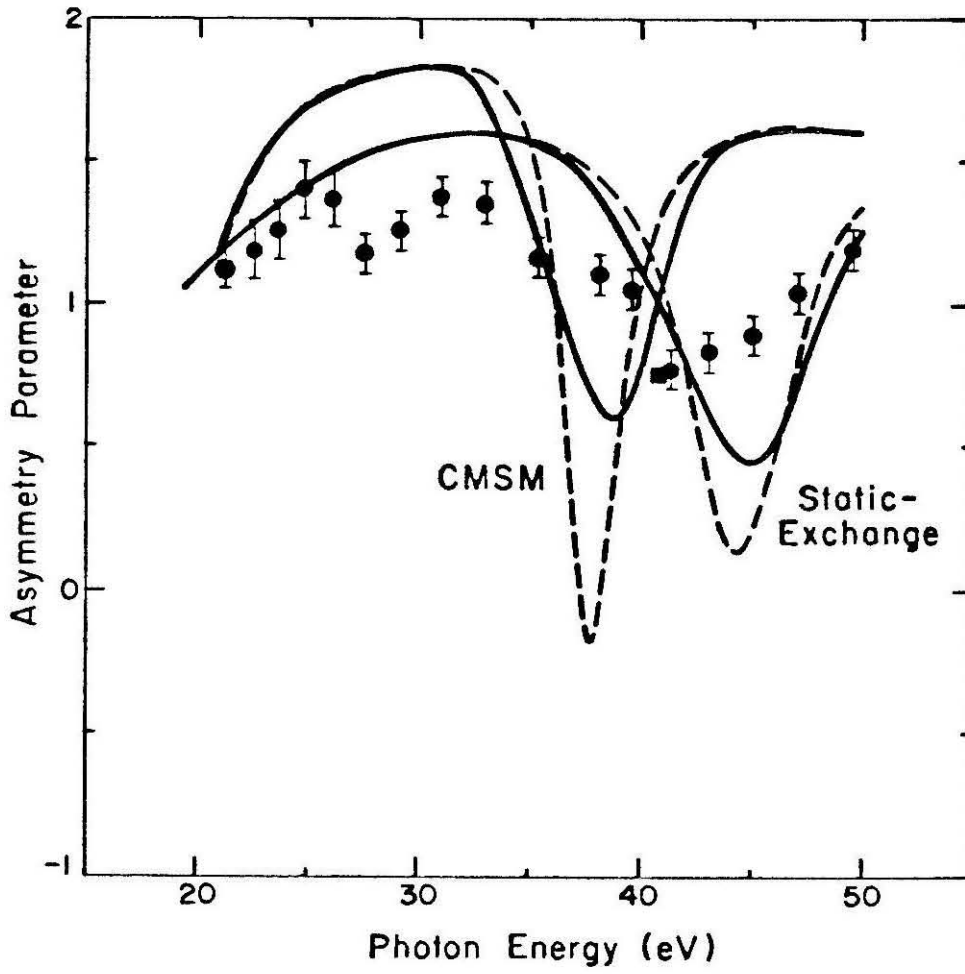


Fig. 4

Propositions

Robert Ross Lucchese

- I. NEW METHOD FOR EFFICIENT COMPUTATION OF MCSCF WAVE FUNCTIONS. It is proposed that the integral transformation method of Beebe and Linderberg will allow the efficient determination of MCSCF wave functions. In the Beebe and Linderberg method, repeated integral transformations are performed with great ease. Thus, this method should be ideally suited for use in MCSCF procedures. Details are given on how this transformation procedure would be applied to the SRMCASE method of Yarkony.
- II. TREATMENT OF POLARIZATION EFFECTS USING A SCHWINGER VARIATIONAL METHOD. It is proposed that the effects of polarization in low-energy electron-molecule scattering can be treated using a multichannel Schwinger formalism. Polarization pseudo-states would be constructed which reflect the effects of the incoming electron on the target electrons. These pseudo-states could be included in the wave function using the target state expansion method. The final scattering wave function would then be obtained from a Schwinger variational expression. Application of this procedure to  $e^-H_2$  scattering is discussed.
- III. MEASUREMENT OF THE POLARIZATION OF FLUORESCENCE OF THE  $B^2\Sigma_u^+$  STATE OF  $CO_2^+$  FOLLOWING PHOTOIONIZATION OF  $CO_2$ . We propose that the measurement of the polarization of fluorescence of the  $B^2\Sigma_u^+$  state of  $CO_2$  would provide a good comparison between experiment and theory. This experiment should also give strong evidence for shape resonances in the photoionization of  $CO_2$  leading to the  $B^2\Sigma_u^+$  state of  $CO_2^+$ . We have computed the expected polarization using previous theoretical results.
- IV. COMPUTATION OF  $S_{-1}$  OSCILLATOR STRENGTH SUM RULE FOR  $N_2$  AND  $CO$ . We propose to calculate the  $S_{-1}$  sum rule for  $N_2$  and  $CO$  using standard bound state techniques. The needed matrix elements are given and possible basis set effects are discussed.
- V. A HYBRID ITERATIVE SCHWINGER VARIATIONAL METHOD FOR SCATTERING SYSTEMS CONTAINING DIPOLAR POTENTIALS. In the spirit of the R-matrix method, we propose to solve the scattering problem with long-range potentials by dividing space into two regions. In the inner region where the interaction potential contains both local and non-local terms, we will use the iterative Schwinger variational technique to solve the scattering problem. In the outer region where the potential has only a local component, we will use the integral equations method to obtain scattering solutions. The form of the integral equations method is discussed along with possible applications.

PROPOSITION I  
NEW METHOD FOR EFFICIENT COMPUTATION  
OF MCSCF WAVE FUNCTIONS

ABSTRACT

It is proposed that the integral transformation method of Beebe and Linderberg will allow the efficient determination of MCSCF wave functions. In the Beebe and Linderberg method, repeated integral transformations are performed with great ease. Thus, this method should be ideally suited for use in MCSCF procedures. Details are given on how this transformation procedure would be applied to the SRMCASE method of Yarkony.

Computing electronic wave functions for molecules whose symmetry corresponds to non-abelian point groups is in general more complicated than it is for molecules of lower symmetry. In fact, for some open-shell systems the standard SCF procedures (e.g., Goddard's GVB<sup>(1)</sup>) are not applicable, since they assume a restricted energy expression of the form

$$E = 2 \sum_i f_i h_{ii} + \sum_{i>j} (a_{ij} J_{ij} + b_{ij} K_{ij}). \quad (1)$$

Yarkony has presented the Symmetry-Restricted Annihilation of Singles (SRAS) method,<sup>(2)</sup> which allows for the variational determination of such wave functions. Recently, he has generalized the method to compute optimized multiconfiguration wave functions.<sup>(3,4)</sup> The generalized method is called the Symmetry Restricted Multiconfiguration Annihilation of Single Excitations (SRMCASE) method. The most serious computational difficulty in this method is the need for a full two-electron integral transformation during each iteration. I propose to overcome this computational difficulty by using the novel integral transformation method of Beebe and Linderberg.<sup>(5)</sup>

An MCSCF wave function is the wave function of a given form which gives the lowest variational energy. Given the expansion of the wave function in the form

$$\Psi(S, \Gamma^\alpha) = \sum_{\substack{i=1,m \\ j=1,d(i)}} t_{ij} \psi(S, \Gamma^\alpha, i, j) \quad (2)$$

where  $\psi(S, \Gamma^\alpha, i, j)$  is the  $j$ th symmetry-adapted configuration arising from the  $i$ th electron occupancy, and  $t_{ij}$  are expansion coefficients. The symmetry-adapted configurations are constructed from orbitals  $j \Gamma_\ell^\alpha$  which are linear combinations of symmetry-adapted orbitals, given by

$$j \Gamma_\ell^\alpha = \sum_m C_{j,m}^\alpha A_m(\alpha, \ell) \quad (3)$$

where the subscript  $\ell$  denotes transformation according to the  $\ell$ th column of the irreducible representation, and  $A_m(\alpha, \ell)$  is a symmetry-adapted atomic orbital. The conditions that the function  $\Psi(S, \Gamma^\alpha)$  is an energy minimum within the required form are

$$\delta_{t_{ij}} E = 0 \quad (4a)$$

and

$$\delta_{C_{jm}^\alpha} E = 0 \quad (4b)$$

for  $j$  occupied orbitals. The SRMCASE method generates the optimal wave function using an iterative two-step procedure. The first step is the optimization of the configuration expansion coefficients  $t_{ij}$  with the orbital expansion coefficients  $C_{jm}^\alpha$  fixed. This is performed by standard Configuration Interaction (CI) techniques.<sup>(6)</sup> The second step is the optimization of the orbital expansion coefficients with the  $t_{ij}$  fixed. This orbital optimization is performed using a generalized form of Brillouin's theorem and the Iterative Natural Orbital (INO) technique.<sup>(7)</sup> In the form of a generalized

Brillouin's theorem, the second condition, in Eq. (4b), becomes

$$\langle \Psi_{SE_j^i}(S, \Gamma^\alpha, \gamma) | H | \Psi(S, \Gamma^\alpha) \rangle = 0 \quad (5)$$

where  $\Psi_{SE_j^i}(S, \Gamma^\alpha, \gamma)$  is the result of an excitation operator acting on  $\Psi(S, \Gamma^\alpha)$ , which is defined by

$$\begin{aligned} \Psi_{SE_j^i}(S, \Gamma^\alpha, \gamma) = & \sum_{\ell=1, m(\Gamma^\alpha)} \{ (j\Gamma_\ell^\gamma)^\dagger (i\Gamma_\ell^\gamma) \\ & \lambda \in \{ \alpha \beta \} \\ & - (i\Gamma_\ell^\gamma)^\dagger (j\Gamma_\ell^\gamma) \} \Psi(S, \Gamma^\alpha). \end{aligned} \quad (6)$$

If the  $t_{ij}$  coefficients were known, then the optimum orbitals could be obtained by performing INO iterations. This involves setting up a Hamiltonian matrix of all such matrix elements as in Eq. (5), and diagonalizing it. Next, the one-electron density matrix is constructed and diagonalized, yielding a new set of orbitals. This procedure could be repeated until convergence is achieved. In the present application, both the  $t_{ij}$  and the orbital expansions must be optimized simultaneously. It has been found<sup>(4)</sup> that successive alternations of optimizations of the  $t_{ij}$  and the orbitals produced the quickest convergence.

The optimization of the wave functions, as described above, requires the construction of many different matrix elements of the Hamiltonian. These matrix elements are composed of sums of various one- and two-electron molecular integrals. Thus every time the orbital basis set is changed by an INO

iteration, all of the two-electron integrals must be transformed.

In actual implementation of any general MCSCF procedure, the bulk of the computational efforts will be devoted to the repeated two-electron integral transformations. The transformation method of Beebe and Linderberg<sup>(5)</sup> would seem to be ideally suited to such applications. I will describe how they propose integral transformations should be performed. Then I will describe how Beebe and Linderberg's procedure could be utilized with the SRMCASE method described above.

In discussing the transformation scheme proposed by Beebe and Linderberg, consider the one-electron orbitals to be composed of functions  $\phi_\alpha(\mathbf{r}) = \langle \mathbf{r} | \alpha \rangle$ , then let the distribution  $\psi_k(\mathbf{r})$  be given by

$$\psi_k(\mathbf{r}) = \phi_\alpha(\mathbf{r})\phi_\beta(\mathbf{r}). \quad (7)$$

If there are  $N$  basis functions  $\phi_\alpha$ , then there will be  $M = N(N+1)/2$  distributions  $\psi_k$ . The potential due to the two-electron operator  $V = 1/r_{12}$  can be represented by

$$V^I = \sum_{k,\ell=1}^M V|k\rangle [d^{-1}]_{k\ell} \langle \ell|V \quad (8)$$

for  $d_{k\ell} = \langle k|V|\ell\rangle$ . This reproduces all matrix elements of the various distributions exactly, i.e.,

$$\langle k|V^I|\ell\rangle = \langle k|V|\ell\rangle. \quad (9)$$

Beebe and Linderberg suggest that the distribution basis in which  $d$  is diagonal provides a good representation of  $V^I$ . Here the projected potential is given by

$$V^I = \sum_{k=1}^M V|k\rangle \frac{1}{d_{kk}} \langle k|V \quad (10)$$

The key point is that, when the eigenvalues of  $d$  become small enough, the contribution from those small eigenvalues can be neglected with no loss in the accuracy of the reproduced integrals. Thus the expansion of the potential can be terminated

$$V^I = \sum_{k=1}^v V|k\rangle \frac{1}{d_{kk}} \langle k|V \quad (11)$$

where  $v < M$ . With this truncation of the potential, any two-electron integral is given by

$$\langle \ell | V^I | m \rangle = \sum_{k=1}^v L_{\ell k} L_{mk} \quad (12a)$$

where

$$L_{\ell k} = \langle \ell | V | k \rangle / \sqrt{d_{kk}} \quad (12b)$$

When integrals over a new basis set are required, the distribution tables are easily transformed using

$$L_{(\alpha', \beta')k} = \sum_{\alpha=1}^N \sum_{\beta=1}^N C_{\alpha'\alpha} C_{\beta'\beta} L_{(\alpha, \beta)k} \quad (13)$$

This integral transformation method seems ideally suited for the needs of an MCSCF procedure. The efficiency of the Beebe and Linderberg method is dependent upon the actual value of  $v$ , compared to its maximum possible value  $N(N+1)/2$ . If  $v \propto N^2$  then this procedure will probably not be faster than traditional transformation methods. However, if  $v \propto N$ , as Beebe and Linderberg suggest as the most probable dependence, then in the application to MCSCF methods, this procedure will have greater efficiency. In this case, the transformation of the distribution tables would require a computational effort proportional to  $N^4$ , and each integral would then only take  $N$  additional multiplications. Thus if all  $N^4$  integrals are needed, the transformation time would be proportional to  $N^5$ . In general, an MCSCF procedure would require less than the full  $N^4$  integrals. It is for this reason that the Beebe and Linderberg procedure is attractive, since only those integrals explicitly required would be constructed.

As was suggested in Ref. 4, the most flexible approach to implementing the SRMCASE method is probably using some form of symbolic formula tape method. The formula tape method consists of symbolic formulas for each Hamiltonian matrix element. In the INO procedure described above, each matrix element is a sum of contributions from various integrals with coefficients which are functions of the  $t_{ij}$  coefficients. These symbolic formulas can be computed once, then reused during each iteration, and can also be used again at different geometries which have the same symmetry. In standard CI

procedures, the formula tape is combined with the transformed integrals to produce the final Hamiltonian. In the present use, the integrals are not formed ahead of time--instead, the distribution tables are used. The most efficient Hamiltonian construction procedure is that of Yoshimine.<sup>(8)</sup> This procedure would be modified in that, instead of having a certain set of integrals held in the computer memory at one time, the appropriate distribution tables would be in the core. Then as the formulas for each integral are processed, that particular integral would be constructed from the distribution tables. The formula tape would be organized so that each integral would only be constructed once. By using the distribution tables in this manner, integrals not required in the construction of the Hamiltonian would never be computed.

The use of the Beebe and Linderberg transformation method would seem to be the best way to implement the SRMCASE method of Yarkony. The chief uncertainty concerning the utility of this method is the dependence of  $v$  on  $N$ . It would seem that for basis sets which are of an extended nature  $v$  would likely be of a lower order of dependence on  $N$ , since these high quality basis sets are more nearly linearly dependent. That is, in such basis sets each new function would be in some part redundant as to the information it contains about the potential. However, for large molecular systems where minimal basis sets must be employed, I would suspect that  $v$  might be more nearly proportional to  $N^2$ . If the proposed scheme for implementing Yarkony's SRMCASE method does prove to be efficient as is hoped, then it

might also be competitive with other general MCSCF procedures for molecules of low symmetry.

## References

1. F.W. Bobrowicz and W.A. Goddard, Modern Theoretical Chemistry, ed. H.F. Schaefer, Plenum, New York (1977), Vol. 3, Ch. 4.
2. D.R. Yarkony, H.F. Schaefer and C.F. Bender, J. Chem. Phys. 64, 981 (1976).
3. D.R. Yarkony, J. Chem. Phys. 66, 2045 (1977).
4. R.R. Lucchese and D.R. Yarkony, J. Chem. Phys. 68, 2696 (1978).
5. N.H.F. Beebe and J. Linderberg, "Simplifications in the Generation and Transformation of Two-Electron Integrals in Molecular Calculations", unpublished.
6. For detailed discussion, see I. Shavitt, Modern Theoretical Chemistry, ed. H.F. Schaefer, Plenum, New York (1977), Vol. 3, pp. 189-275.
7. C.F. Bender and E.R. Davidson, J. Chem. Phys. 40, 2675 (1966).
8. M. Yoshimine, J. Comp. Phys. 11, 449 (1973).

---

PROPOSITION II  
TREATMENT OF POLARIZATION EFFECTS  
USING A SCHWINGER VARIATIONAL METHOD

ABSTRACT

It is proposed that the effects of polarization in low-energy electron-molecule scattering can be treated using a multichannel Schwinger formalism. Polarization pseudo-states would be constructed which reflect the effects of the incoming electron on the target electrons. These pseudo-states could be included in the wave function using the target state expansion method. The final scattering wave function would then be obtained from a Schwinger variational expression. Application of this procedure to  $e^-H_2$  scattering is discussed.

One of the unusual features of electron-atom or electron-molecule scattering is the very low energy behavior of the total elastic cross sections of some systems. In heavy rare gas atoms, such as Ar, Kr, and Xe,<sup>(1)</sup> and in some organic molecules such as methane, ethane, and propane,<sup>(2)</sup> sharp minima in the elastic electron-molecule scattering cross sections are observed with the incident electron having kinetic energy in range of 0.1-0.2 eV. These minima are known as Ramsauer-Townsend (RT) minima. In the theoretical study of  $e^-$ -Ar,<sup>(3)</sup> the feature is strongly dependent upon polarization effects. Physically, polarization is the redistribution of the target electrons due to the presence of the incident scattering electron. At higher incident kinetic energy these polarization effects become less important and approximations ignoring them, such as the static-exchange approximation, are better able to describe the scattering process. However, polarization must be included to obtain the proper low energy dependence of the elastic cross section.

I propose that a multichannel version of the Schwinger variational method using polarization pseudo-states in a manner similar to that used by Schneider,<sup>(4)</sup> should allow the accurate determination of low energy polarization effects in electron-molecule scattering. To demonstrate the proposed method, I will consider  $e^-$ -H<sub>2</sub> scattering. In this system, the effects of polarization can clearly be seen in the low energy elastic cross section. At 3 eV the elastic cross section of  $e^-$ -H<sub>2</sub> has a maximum and falls off towards zero as the kinetic energy of

the scattered electron approaches zero.<sup>(5)</sup> This feature in the elastic cross section is due to polarization, since in the static-exchange approximation, the cross section rises monotonically as the incident electron energy goes to zero.<sup>(6)</sup>

A standard procedure for dealing with multichannel scattering is the target state expansion method.<sup>(7)</sup> In this method, the total wave function is written as

$$\Psi(X, X_{\text{tar}}) = \sum_{\alpha} \chi_{\alpha}(X) \phi_{\alpha}(X_{\text{tar}}) \quad (1)$$

where  $\{\phi_{\alpha}\}$  are eigenfunctions of the target Hamiltonian and  $\{\chi_{\alpha}\}$  are one-electron orbitals describing the incident electron. If all target states are included in the expansion, then the scattering solution will be exact. In actual applications the expansion must be truncated. In most cases only a few important terms are retained.

In principle, polarization effects could be treated by including enough target states in the expansion of the wave function given in Eq. (1). Unfortunately, the effects of polarization are not rapidly convergent with increasing numbers of target states included in the expansion. As discussed by Burke and Mitchell,<sup>(8)</sup> for rare gas atoms, typically 50% of the polarization effects come from continuum states of the target.

A solution to the slow convergence of target states was given by Damburg and Karule.<sup>(9)</sup> They suggested that inclusion of states which reflected the effect of a static electric field would be more effective in treating the polarization due to the

incident electron. Burke et al.<sup>(10)</sup> showed that this procedure substantially improved the results in  $e^-$ -H scattering.

The method I propose to use to calculate polarization pseudo-states is the same as that used by Schneider.<sup>(4)</sup> This method is an adaptation of the scheme proposed by McLean and Yoshimine to calculate static polarizabilities of molecular systems.<sup>(11)</sup> The first step is to calculate one-electron polarized orbitals. This is done by calculating one-electron orbitals which are eigenfunctions of an effective Hamiltonian. This Hamiltonian has a potential that is the sum of the potentials due to the other electrons in the target, which are described by the orbitals of the unperturbed system plus a potential due to an applied electric field. The electric field is simulated by placing a point charge at a large distance from the molecule. The point charge must be far enough away from the target so that the target wave function does not have an appreciable amplitude in the vicinity of the charge. The one-electron orbital is obtained by diagonalizing the Hamiltonian in a finite basis set. For the application considered here, the basis set used will be a set of Cartesian Gaussian functions

$$\phi_{k\ell m}^{\mathbf{A},\alpha}(\mathbf{r}) = N_{k\ell m} (x-A_x)^k (y-A_y)^\ell (z-A_z)^m e^{-\alpha|\mathbf{r}-\mathbf{A}|^2} \quad (2)$$

where  $N_{k\ell m}$  is a normalization constant and  $\mathbf{A}$  is the center of the Gaussian, which is usually either one of the nuclear centers or the center of mass of the molecule. For each different occupied target molecular orbital, a different

polarization orbital can be constructed. The polarized orbitals are then orthogonalized with respect to each other and with respect to the occupied orbitals.

As Schneider suggested,<sup>(4)</sup> the target ground state and polarization pseudo-states can then be obtained by diagonalizing the  $N+1$  electronic Hamiltonian in a space spanned by Slater determinants constructed from the Hartree-Fock orbitals of the ground state combined with the polarized orbitals. The one-electron basis set could be even expanded further to include more orbitals. This would produce a target wave function of increasing complexity, which makes the ensuing scattering calculation increasingly more difficult.

The simplest possible form of the Schwinger pseudo-state method proposed here for  $e^-$ - $H_2$  scattering, would be obtained by calculating one polarized orbital of  $\sigma_u$  symmetry and to compute a scattering wave function which is an expansion of three pseudo-states. Thus the total wave function would be given by

$$\Psi = \Phi_1 + \Phi_2 + \Phi_3 \quad (3)$$

where

$$\Phi_1 = [1\sigma_g^\alpha 1\sigma_g^\beta \chi^1 \alpha] \quad (4a)$$

$$\begin{aligned} \phi_2 = & \frac{\sqrt{2}}{3} [1\sigma_g \alpha 1\sigma_u \alpha \chi^2 \beta] - \frac{\sqrt{1}}{6} [1\sigma_g \beta 1\sigma_u \alpha \chi^2 \alpha] \\ & - \frac{\sqrt{1}}{6} [1\sigma_g \beta 1\sigma_u \alpha \chi^2 \alpha] \end{aligned} \quad (4b)$$

$$\phi_3 = \frac{\sqrt{1}}{2} [1\sigma_g \alpha 1\sigma_u \beta \chi^3 \alpha] - \frac{\sqrt{1}}{2} [1\sigma_g \beta 1\sigma_u \alpha \chi^3 \alpha] \quad (4c)$$

and where  $1\sigma_g$  is the ground state Hartree-Fock orbital and  $\chi^1$ ,  $\chi^2$  and  $\chi^3$  are scattering functions to be determined.

The Lippmann-Schwinger equation for such an expansion of the total wave function is of the form<sup>(12)</sup>

$$\chi^{n(+)} = \chi_o^n + G_o^{(+)}(E-E_n) \sum_m U_{nm} \chi^{m(+)} \quad (5)$$

where  $E_n$  is the energy of the  $n$ th target state and  $E$  is the electronic energy of the whole system. In a more general vector notation, Eq. (5) becomes

$$\chi^{(+)} = \chi_o + \underline{G}_o^{(+)}(E) \underline{U} \chi^{(+)} \quad (6)$$

where

$$G_o^{(+)}(E) = \begin{pmatrix} G_o^{(+)}(E-E_1) & & 0 \\ & \ddots & \\ 0 & & G_o^{(+)}(E-E_n) \\ & & & \ddots \end{pmatrix} \quad (7)$$

The  $U_{nm}$  are matrix elements of the potential. For example, in  ${}^2\Sigma_g$  scattering the orbital  $\chi^1$  has gerade symmetry. In that case  $U_{21}\chi^1$  would be given by

$$U_{21}\chi^1 = \sqrt{6}\{ \langle 1\sigma_u | \square | 1\sigma_g 1\sigma_g \rangle \langle 1\sigma_g | \chi_g^1 \rangle - \langle 1\sigma_u | \square | \chi_g^1 1\sigma_g \rangle \} \quad (8)$$

where

$$\langle a | b \rangle = \int d^3r a(\mathbf{r}) b(\mathbf{r}) \quad (9a)$$

and

$$\langle a | \square | bc \rangle(\mathbf{r}) = c(\mathbf{r}) \int d^3r' \frac{a(\mathbf{r}') b(\mathbf{r}')}{|\mathbf{r} - \mathbf{r}'|} \quad (9b)$$

Expand the wave function  $\chi^{(+)}$  in a basis set

$$\chi^{(+)} = \sum_i C_i f_i \quad (10)$$

where the expansion functions are Cartesian Gaussian functions

$$f_i = \begin{pmatrix} 0 \\ \vdots \\ \phi_\alpha(\mathbf{r}) \\ \vdots \\ 0 \end{pmatrix} \quad (11)$$

Then inserting this expansion into a Schwinger expression identical in form to that used in the single channel case gives for the Schwinger variational T matrix

$$T = \sum_{ij} U | f_i \rangle (D^{-1})_{ij} \langle f_j | U \quad (12)$$

where  $D_{ij} = \langle f_i | U - U G_0^{(+)} U | f_j \rangle$ .

For elastic scattering

$$\chi_0^1(\underline{r}) = e^{i\mathbf{k}_1 \cdot \underline{r}} \quad (13a)$$

and

$$\chi_0^i(\underline{r}) = 0 \quad \text{for } i > 1, \quad (13b)$$

with  $k_i = \sqrt{2(E - E_i)}$ .

Then the scattering amplitude defined by

$$\chi_{k_1}^{1(+)}(\underline{r})_{r \rightarrow \infty} = e^{i\mathbf{k}_1 \cdot \underline{r}} + f_{k_1}(\hat{r}) \frac{\exp(i\mathbf{k}_1 \cdot \underline{r})}{r} \quad (14)$$

is given by

$$f_{k_1}(\hat{r}) = \frac{-1}{4\pi} \langle \chi_{0,\hat{r}} | T | \chi_{0,k_1} \rangle \quad (15)$$

or, in the case considered here

$$f_{k_1}(\hat{r}) = \frac{1}{4\pi} \sum_{ij} \langle e^{i\mathbf{k}_1 \cdot \hat{r}} | \sum_m U_{1m} | f_i \rangle \quad (16)$$

$$\times (D^{-1})_{ij} \langle f_j | \sum_m U_{m1} | e^{i\mathbf{k}_2 \cdot \underline{r}} \rangle .$$

The numerical methods for calculating these matrix elements would be identical to those presented for the Schwinger variational method at the static-exchange level.<sup>(13)</sup> However, it is interesting to look at the partial wave form of the free particle Green's function. When  $E > E_n$  the Green's function is the standard result<sup>(14)</sup>

$$G_o^{(+)}(E-E_n; r, r') = -k_n \sum_{\ell, m} i^\ell j_\ell(kr_<) h_\ell^{(+)}(kr_>) Y_{\ell m}(\hat{r}) Y_{\ell m}^*(\hat{r}') \quad (17)$$

When  $E < E_n$ , as will be the case with closed channels, the Green's function is

$$G_o^{(+)}(E-E_n; r, r') = -ik_n' \sum_{\ell, m} i^\ell j_\ell(ik_n' r_<) h_\ell^{(+)}(ik_n' r_>) Y_{\ell m}(\hat{r}) Y_{\ell m}^*(\hat{r}') \quad (18)$$

where  $k_n = \sqrt{2(E_n - E)}$ . (18)

Then note that in terms of modified Bessel functions, <sup>(15)</sup>

$$j_\ell(ikr) = i^\ell \frac{\sqrt{\pi}}{2kr} I_{\ell+1/2}(kr) \quad (19a)$$

and

$$h_\ell^{(+)}(ikr) = \frac{2}{\pi} \frac{\sqrt{\pi}}{2kr} i^{-(\ell+1)} K_{\ell+1/2}(kr) \quad (19b)$$

so

$$G_o^{(+)}(E-E_n; r, r') = -\sum_{\ell, m} i^\ell \frac{1}{\sqrt{rr'}} I_{\ell+1/2}(k_n' r_<) \quad (20)$$

$$K_{\ell+1/2}(k_n' r_>) Y_{\ell m}(\hat{r}) Y_{\ell m}^*(\hat{r}')$$

The implementation of this method should be very straightforward. All the numerical integrations can be performed by known procedures. Since the radial functions for the continuum

electron are known explicitly in both open and closed channels, the iterative Schwinger variational method could also be applied here to obtain improved solutions.<sup>(16)</sup> The formalism developed here is naturally directly applicable to multichannel scattering with suitable choice of target states. It would seem that just as polarization effects are important near zero momentum in elastic scattering, polarization effects would be important just after threshold in an inelastic channel. It is conceivable that the polarization pseudo-state method presented here could also be used to treat inelastic polarization threshold effects.

## References

1. C. Ramsauer and R. Kollath, *Ann. Phys. Lpz.* 4, 91 (1930).
2. D.L. McCorkle, L.G. Christophorou, D.V. Maxey and J.G. Carter, *J. Phys. B* 11, 3067 (1978).
3. A.W. Yau, R.P. McEachran and A.D. Stauffer, *J. Phys. B* 11, 2907 (1978).
4. B.I. Schneider, *Chem. Phys. Lett.* 51, 578 (1971).
5. F. Linder and H. Schmidt, *Z. Naturf.* 26a, 1603 (1971).
6. A. Klonover and U. Kaldor, *J. Phys. B* 11, 1623 (1978).
7. J.R. Taylor, *Scattering Theory*, Wiley, New York (1972), p. 380.
8. P.G. Burke and J.F.B. Mitchell, *J. Phys. B* 7, 665 (1974).
9. R.J. Damburg and E. Karule, *Proc. Phys. Soc.* 90, 637 (1967).
10. P.G. Burke, D.F. Gallaher and S. Geltman, *J. Phys. B* 2, 1142 (1969).
11. A.D. McLean and M. Yoshimine, *J. Chem. Phys.* 46, 3682 (1967).
12. B.H. Brandsen and J.S.C. McKee, *Proc. Phys. Soc. A* 70, 398 (1957).
13. R.R. Lucchese and V. McKoy, *Phys. Rev. A* 21, 112 (1980).
14. A. Messiah, *Quantum Mechanics*, Vol 1, Wiley, New York, p. 497 (1966).
15. M. Abramowitz and I.A. Stegun, *Handbook of Mathematical Functions*, National Bureau of Standards, Washington, D.C. (1972), p. 443.
16. R.R. Lucchese, D.K. Watson and V. McKoy, *Phys. Rev. A* 22, 421 (1980).

## PROPOSITION III

MEASUREMENT OF THE POLARIZATION  
OF FLUORESCENCE OF THE  $B^2\Sigma_u^+$  STATE OF  $CO_2^+$   
FOLLOWING PHOTOIONIZATION OF  $CO_2$ ABSTRACT

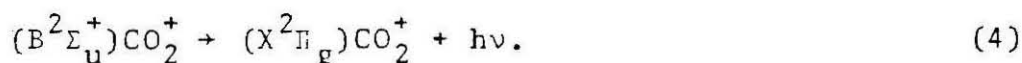
We propose that the measurement of the polarization of fluorescence of the  $B^2\Sigma_u^+$  state of  $CO_2$  would provide a good comparison between experiment and theory. This experiment should also give strong evidence for shape resonances in the photoionization of  $CO_2$  leading to the  $B^2\Sigma_u^+$  state of  $CO_2^+$ . We have computed the expected polarization using previous theoretical results.

When comparing theoretical quantum mechanical calculations of reaction cross sections to experimental data, one usually must sum over individual computed cross sections to obtain the result equivalent to what is measured. Such summed theoretical cross sections can often be more accurate than the individual cross sections due to cancelation of errors. Thus, it is of great interest to theoreticians when a new experimental technique which allows more detailed measurements to be made is developed since this allows for more accurate assessments of theoretical models. Recently Poliakoff et al.<sup>(1)</sup> have reported on such a method which measures the relative contributions to molecular photoionization coming from degenerate continuum states. This method is based on the measurement of the polarization of the fluorescence coming from an excited ionic state produced by polarized ionizing light.

We propose that the experimental technique of Poliakoff et al.<sup>(1)</sup> be applied to the measurement of the photoionization cross sections for producing the  $B^2\Sigma_u^+$  state of  $CO_2^+$ . The first application of this technique was to the photoionization of  $N_2$  leading to the  $B^2\Sigma_u^+$  state of  $N_2^+$  which then fluoresces down to the  $X^2\Sigma_g^+$  state of  $N_2^+$ .<sup>(1)</sup> The comparison between theory and experiment was not very satisfactory in this case. One possible indication that the theory is suspect here is that the theoretical photoelectron asymmetry parameters are also in poor agreement with the experiment.<sup>(1)</sup> In contrast, the theoretical asymmetry



and the fluorescence by



The  $B^2\Sigma_u^+ \rightarrow X^2\Pi_g$  transition of  $CO_2^+$  produces emission at a wavelength of 2890 Å. This feature is prominent in the ultraviolet spectrum of the atmosphere of Mars.<sup>(4)</sup> The average angles between absorption and fluorescence are then given in Table I along with the resulting polarizations. When these processes are averaged over, we obtain for the "pure  $\sigma_g$ " photoionization  $P_{\sigma_g} = -1/13$  and "pure  $\pi_g$ " photoionization  $P_{\pi_g} = 1/27$ . Then defining R as the ratio of the intensities  $R = D_{\pi_g}^2/D_{\sigma_g}^2$ , we obtain for the true polarization

$$P = \frac{R - 1}{13 + 27R}. \quad (5)$$

One particularly interesting aspect of the  $B^2\Sigma_u^+$  channel in  $CO_2$  photoionization is the appearance of shape resonances in both the  $\sigma_g$  and  $\pi_g$  channels.<sup>(2)</sup> In Fig. 1a we present the theoretical R ratios from Ref. 2 and in Fig. 1b we have predicted the polarization, obtained by using Eq. (5), which should be observed experimentally. As can be seen in Fig. 1, the R ratio changes dramatically as a function of energy reflecting the  $\sigma_g$  resonance at a photon energy of 22 eV and the  $\pi_g$  resonance at 42 eV. These large changes in R are directly related to the predicted energy dependence of the fluorescence polarization.

We feel that the proposed experimental measurement of the fluorescence polarization of the  $B^2\Sigma_u^+$  state of  $CO_2^+$  would show dramatic effects due to shape resonant photoionization and should provide a good comparison between theory and experiment.

## References

1. E.D. Poliakoff, J.L. Dehmer, D. Dill, A.C. Parr, K.H. Jackson and R.N. Zare, Phys. Rev. Lett. 46, 907 (1981).
2. See Chapter III, Section D of this thesis.
3. M. McClintock, W. Demtröder and R.N. Zare, J. Chem. Phys. 51, 5509 (1969).
4. R.W. Carlson, D.L. Judge and M. Ogawa, J. Geophys. Res. 78, 3194 (1973).

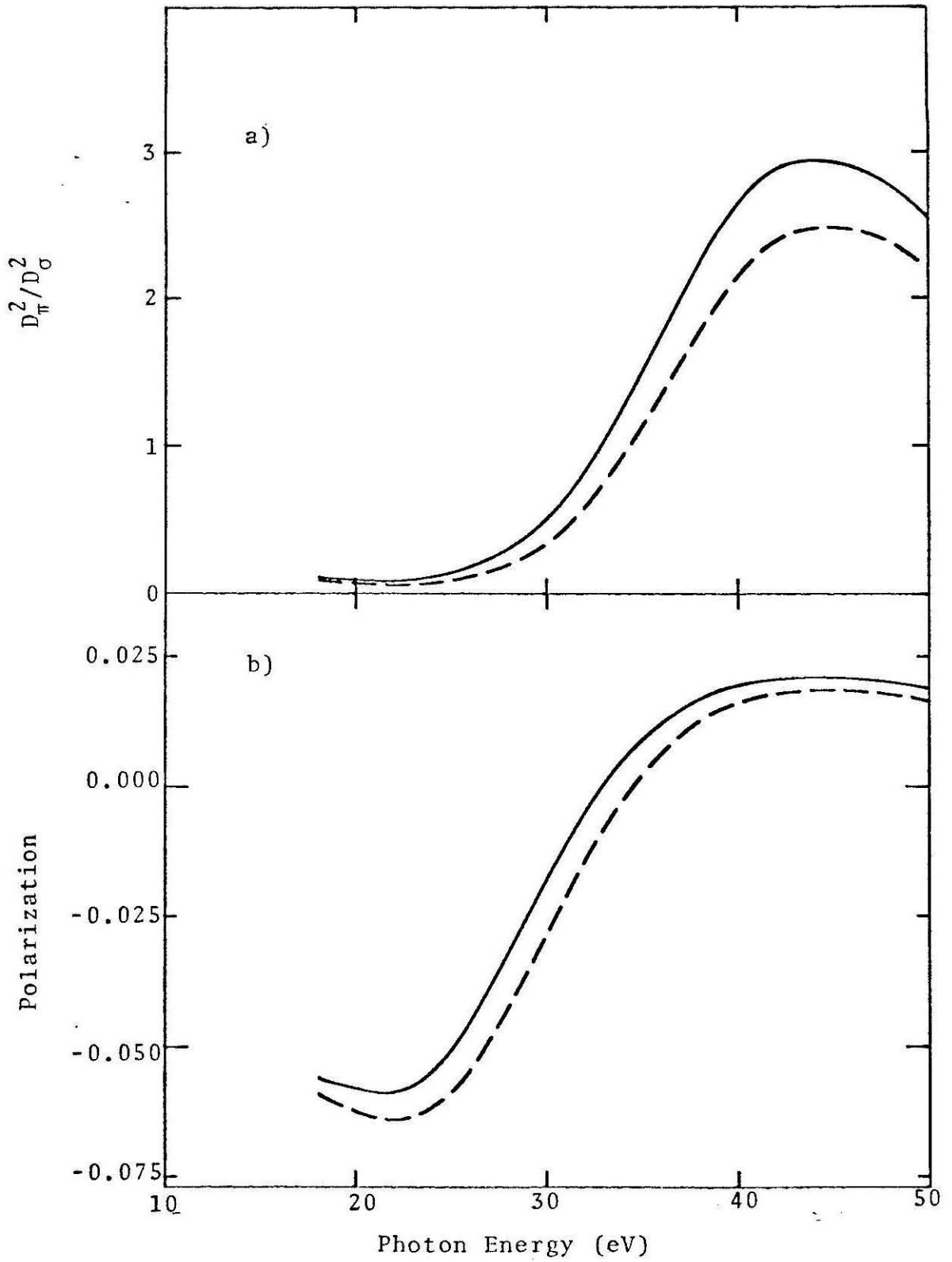
Table I. Average angles between absorption and fluorescence for various processes in photoionization leading to the  $B^2\Sigma_u^+$  state of  $CO_2^+$ .

Continuum Channel	Rotational <sup>a</sup> Branch	$\alpha$	P
$\sigma_g$	$P\uparrow R\uparrow$ , $P\downarrow R\downarrow$	$45^\circ$	1/7
$\sigma_g$	$P\uparrow R\uparrow$ , $Q\downarrow$	$90^\circ$	-1/3
$\pi_g$	$P\uparrow R\uparrow$ , $P\downarrow R\downarrow$	$45^\circ$	1/7
$\pi_g$	$P\uparrow R\uparrow$ , $Q\downarrow$	$90^\circ$	-1/3
$\pi_g$	$Q\uparrow$ , $P\downarrow R\downarrow$	$90^\circ$	-1/3
$\pi_g$	$Q\uparrow$ , $Q\downarrow$	$0^\circ$	1/2

<sup>a</sup>The notation  $P\uparrow R\uparrow$  ,  $Q\downarrow$  implies that the process proceeds through the  $P(\Delta j = -1)$  or  $R(\Delta j = +1)$  rotational branches in absorption and through the  $Q(\Delta j = 0)$  branch in emission.

FIGURE 1

- a) The predicted  $D_{\pi}^2/D_{\sigma}^2$  ratios for photoionization leading to the  $B^2\Sigma_u^+$  state of  $CO_2^+$  from Ref. 2.
- b) The computed polarization parameter for fluorescence of the  $B^2\Sigma_u^+$  state of  $CO_2^+$ : ————— dipole length FCHF with correlated initial state; - - - - - dipole velocity FCHF with correlated initial state.



PROPOSITION IV  
COMPUTATION OF  $S_{-1}$  OSCILLATOR STRENGTH  
SUM RULE FOR  $N_2$  AND CO

ABSTRACT

We propose to calculate the  $S_{-1}$  sum rule for  $N_2$  and CO using standard bound state techniques. The needed matrix elements are given and possible basis set effects are discussed.

The moments of the dipole oscillator strength for atomic or molecular systems are defined as <sup>(1)</sup> (in atomic units)

$$S_k(x) = \sum_{j \neq q} (E_j - E_q)^k f(x)_{qj} \quad (1)$$

where  $f(x)_{qj}$  is the oscillator strength for a transition going from the  $q$  state (e.g., the ground state) to the  $j$  state (e.g., an excited state) and is defined as

$$f(x)_{qj} = 2(E_j - E_q) \langle \psi_q | \mu_x | \psi_j \rangle \langle \psi_j | \mu_x | \psi_q \rangle. \quad (2)$$

The moments corresponding to integer values of  $k$  are of interest for several reasons. One interesting application involving oscillator moments is the Stieltjes-Tchebycheff Moment Theory (STMT) approach to the calculation of photoionization cross sections developed by Langhoff<sup>(2)</sup> and others. The STMT methods obtain approximate moments and then invert the moment theory problem to obtain the underlying oscillator strengths. Various of the moments (also known as sum rules) also have physical interpretations.<sup>(1)</sup>  $S_{-3}$  is the norm of the first order perturbation wave function, where the perturbation is an electric field.  $S_{-2}$  is the static polarizability.  $S_{-1}$  is known as the size or approximate polarizability of a system, and  $S_0$  is the Reiche-Thomas-Kuhn sum rule and is just equal to the number of electrons in the system (in the fixed-nuclei approximation).

Here we will discuss the  $S_{-1}$  sum rule. As pointed out by Berkowitz,<sup>(3)</sup> this sum rule has apparently been computed only for atomic systems and  $H_2$ . We propose to calculate  $S_{-1}$

for molecular systems such as  $N_2$  and CO. The molecular systems  $N_2$  and CO are of particular interest since experimental estimates of  $S_{-1}$  are given by Berkowitz,<sup>(3)</sup> and these systems are small enough so that computation of accurate theoretical  $S_{-1}$  sums should be possible.

The  $S_{-1}$  sum rule is obtained from Eq. (1) with  $k = -1$ , and is

$$S_{-1}(x) = 2 \sum_{j \neq q} \langle \psi_q | \mu_x | \psi_j \rangle \langle \psi_j | \mu_x | \psi_q \rangle, \quad (3)$$

where the dipole operator is

$$\mu_x = -\sum_i x_i. \quad (4)$$

Using completeness of states, we can rewrite Eq. (3) to give

$$\begin{aligned} S_{-1}(x) &= 2 \langle \psi_q | (-\sum_i x_i) (-\sum_j x_j) | \psi_q \rangle \\ &\quad - 2 |\langle \psi_q | -\sum_i x_i | \psi_q \rangle|^2. \end{aligned} \quad (5)$$

Eq. (5) can then be slightly rewritten to give

$$\begin{aligned} S_{-1}(x) &= 4 \langle \psi_q | \sum_i x_i \sum_j x_j | \psi_q \rangle \\ &\quad + 2 \langle \psi_q | \sum_i x_i^2 | \psi_q \rangle \\ &\quad - 2 |\langle \psi_q | \sum_i x_i | \psi_q \rangle|^2. \end{aligned} \quad (6)$$

We thus propose to compute the ground state  $S_{-1}$  sum rule by directly computing the ground state wave function,  $\psi_q$ , using standard CI methods<sup>(4)</sup> and then evaluating the expression given in Eq. (6).

To evaluate Eq. (6), we need to note that the matrix elements needed are of an operator of the form

$$M = \sum_i f_i + \sum_{i>j} g_{ij}. \quad (7)$$

which is also the form of the electronic Hamiltonian. Matrix elements of such operators between many-electron wave functions which are sums of Slater determinants can be computed using the Condon-Slater rules.<sup>(5)</sup> Thus to compute the matrix elements in Eq. (6), one could easily modify a standard Hamiltonian construction program to use products of dipole matrix elements instead of the usual two-electron Coulombic integrals. Such dipole matrix elements are readily available from one-electron property programs.

The main question here is how accurate must the ground state wave function be in order to obtain accurate  $S_{-1}$  sums. There are two parts to this question. First, what kind of one-electron basis set must be used in the CI wave function; and second, what level of excitations, relative to the Hartree-Fock reference configuration, must be included in the CI expansion? I believe that an extended basis with polarization functions would be required since such basis sets are needed to obtain accurate one-electron properties of molecular systems.<sup>(6)</sup> One expects that a CI expansion of the "singles-plus-doubles" type would be adequate for wave functions which are dominated by a single reference configuration.

I think it is interesting to apply such bound state techniques as indicated above to the problem of computing the

$S_{-1}$  sum which formally involves summations over continuum states since such bound state methods can easily include extensive correlation effects which are very difficult to include in the direct continuum state calculation. Another note of interest is that this same technique could be applied to computing  $S_{+1}$  by computing dipole velocity matrix elements.

## References

1. J.O. Hirschfelder, W. Byers Brown and S.T. Epstein, in Advances in Quantum Chemistry Vol. 1, Academic Press, New York (1964), p. 255.
2. P.W. Langhoff, "Stieltjes-Tchebycheff Moment-Theory Approach to Molecular Photoionization Studies", in Electron-Molecule and Photon-Molecule Collisions, eds. T. Rescigno, V. McKoy and B. Schneider, Plenum Press, New York (1979), p. 183.
3. J. Berkowitz, Photoabsorption, Photoionization, and Photoelectron Spectroscopy, Academic Press, New York (1979).
4. I. Shavitt, in Modern Theoretical Chemistry 3, ed. H.F. Schaefer III, Plenum, New York (1977), p. 189.
5. C.S. Johnson, Jr. and L.G. Pedersen, Problems and Solutions in Quantum Chemistry and Physics, Addison-Wesley, Reading, MA (1974), p. 234.
6. H.F. Schaefer III, The Electronic Structure of Atoms and Molecules, Addison-Wesley, Reading, MA (1972), p. 81.

## PROPOSITION V

A HYBRID ITERATIVE SCHWINGER  
VARIATIONAL METHOD FOR SCATTERING  
SYSTEMS CONTAINING DIPOLAR POTENTIALSABSTRACT

In the spirit of the R-matrix method, we propose to solve the scattering problem with long-range potentials by dividing space into two regions. In the inner region where the interaction potential contains both local and non-local terms, we will use the iterative Schwinger variational technique to solve the scattering problem. In the outer region where the potential has only a local component, we will use the integral equations method to obtain scattering solutions. The form of the integral equations method is discussed along with possible applications.

The iterative Schwinger variational method has been found to work very well for those problems where the potential is of not too long of a range. Thus for systems such as  $e\text{-H}_2$ ,  $e\text{-N}_2$  and  $e\text{-CO}_2$  scattering,<sup>(1)</sup> where the asymptotic interaction potential goes as  $1/r^3$ , we have found rapid convergence of the iterative method. However, for systems which contain dipolar potentials ( $1/r^2$ ) such as  $e\text{-LiH}$ <sup>(2)</sup> and  $e\text{-CO}^+$ <sup>(3)</sup>, the iterative method is found to be more slowly convergent. In particular in  $e\text{-CO}^+$  scattering where there are both resonant and non-resonant scattering effects, we found that it was difficult to find a satisfactory initial basis set with which to start the iterative procedure.<sup>(4)</sup> We observed that one basis set would work well at some scattering energies while it lead to a non-convergent iterative procedure at other energies.

There are several approaches to solving this problem. One suggestion has been the use of a different variational functional.<sup>(3)</sup> Another approach now being considered<sup>(5)</sup> is the use of the integral equations method of Morrison<sup>(6)</sup> which would treat the static potential exactly and represent the exchange terms by a separable potential of the Schwinger type.<sup>(1)</sup> I propose here a third possible approach to the long-range static potential problem. In the spirit of the R-matrix method,<sup>(7)</sup> I suggest that for some boundry  $r = r_c$ , we can compute the scattering wave function for  $r < r_c$  using the iterative Schwinger variational method, then we could obtain the solutions from the integral equations method for  $r > r_c$ .

For most systems of interest all of the non-local potential effects (exchange and orthogonality) are of the same range as the molecular orbitals. In  $\text{CO}^+$ , for example,<sup>(4)</sup> the most diffuse orbital is very small at  $r = 20$  au whereas the dipole potential is only down to  $10^{-5}$  by  $r = 100$  au. Thus for the region from  $r = 20$  au to  $r = 100$  au, the only interaction potential is a static potential which can be most easily be handled by the integral equations method of Morrison.<sup>(6)</sup> By not using the iterative Schwinger variational method in this intermediate region ( $r > r_c$ ), we hope to improve the convergence of the method in the inner region ( $r < r_c$ ).

To see how the integral equations method can be used in the intermediate region, consider the potential to be a sum of two pieces,  $U(r)$  a local potential and  $U'(r, r')$  a short range non-local potential such that  $U'(r, r')$  is zero if  $r > r_c$  or  $r' > r_c$ . Then assume that we have obtained solutions valid for  $r < r_c$  using the iterative Schwinger variational method which satisfy

$$\begin{aligned} \psi^c(r) = & F(r) - 1/k \int_0^{r_c} dr' F(r_<) G(r_>) U(r') \psi^c(r') \\ & - 1/k \int_0^{r_c} dr' F(r_<) G(r_>) \int_0^{r_c} dr'' U'(r', r'') \psi^c(r'') \end{aligned} \quad (1)$$

where  $F$  are regular (at the origin) zero-potential solutions, and  $G$  are irregular zero-potential solutions. The equations presented here can be viewed as either single channel equations or multi-channel equations where the functions then represent matrix functions. The total solutions then satisfy

$$\begin{aligned} \psi^\infty(r) = & F(r) - 1/k \int_0^\infty dr' F(r_<) G(r_>) U(r') \psi^\infty(r') \\ & - 1/k \int_0^{r_c} dr' F(r_<) G(r_>) \int_0^{r_c} dr'' U'(r', r'') \psi^\infty(r'') \end{aligned} \quad (2)$$

Assuming that

$$\psi^\infty(r) = \psi^c(r)A$$

for  $r < r_c$  and matching the functions at  $r = r_c$  we obtain

$$\begin{aligned} \psi^\infty(r) = & F(r) + G(r)K^c(1-B) \\ & - 1/k G(r) \int_{r_c}^r dr' F(r') U(r') \psi^\infty(r') \\ & + 1/k F(r) \int_{r_c}^r dr' G(r') U(r') \psi^\infty(r') \\ & - F(r)B \end{aligned} \quad (3)$$

where

$$B = 1/k \int_{r_c}^\infty dr' G(r') U(r') \psi^\infty(r') \quad (4)$$

and

$$\begin{aligned} K^c = & - 1/k \int_0^{r_c} dr' F(r') \{ U(r') \psi^c(r') \\ & + \int_0^{r_c} dr'' U'(r', r'') \psi^c(r'') \}. \end{aligned} \quad (5)$$

Now we can transform Eq. (3) by rewriting it in terms of  $\psi^V$  defined as

$$\psi^V(r) = \psi^\infty(r) (1-B)^{-1}. \quad (6)$$

Then Eq. (3) becomes

$$\begin{aligned} \psi^V(r) = & F(r) + G(r)K^C - 1/k G(r) \int_{r_c}^r dr' F(r')U(r')\psi^V(r') \\ & + 1/k F(r) \int_{r_c}^r dr' G(r')U(r')\psi^V(r'). \end{aligned} \quad (7)$$

This is then an inhomogeneous Volterra type integral equation which can be integrated in a very straightforward manner.<sup>(8)</sup>

Once the wave function  $\psi^V$  has been computed, the physical solution  $\psi^\infty$  can be obtained by matching  $\psi^V$  and  $\psi^\infty$  at  $r = \infty$ .

Doing this we obtain

$$(1 - B) = (1 + C)^{-1} \quad (8)$$

where

$$C = 1/k \int_{r_c}^{\infty} dr' G(r')U(r')\psi^V(r') \quad (9)$$

so that

$$\psi^\infty(r) = \psi^V(r)(1 + C)^{-1} \quad (10)$$

and the final K matrix is given by

$$K^\infty = \{K^C - 1/k \int_{r_c}^{\infty} dr' F(r')U(r')\psi^V(r')\}(1 + C)^{-1}. \quad (11)$$

I feel that this hybrid method should allow us to treat problems with long-range ( $1/r^2$ ) interaction potentials without any loss of efficiency compared to the use of the iterative Schwinger variational expression with shorter range ( $1/r^3$ ) potentials. Such an improved method would be very useful when considering non-symmetric linear systems such as CO, HCN, N<sub>2</sub>O

and non-linear systems such as  $\text{H}_2\text{O}$  and  $\text{H}_2\text{CO}$ , as well as in applications to inelastic scattering.

## References

1. See thesis.
2. D.K. Watson, T.N. Rescigno and B.V. McKoy, *J. Phys. B* 14, 1875 (1981).
3. M.T. Lee, K. Takatsuka and V. McKoy, "Application of a new variational functional for electron-molecule collisions: An extension of the Schwinger variational principle", *J. Phys. B*, accepted for publication.
4. R.R. Lucchese and V. McKoy, unpublished.
5. M.E. Smith, R.R. Lucchese and V. McKoy, in preparation.
6. M.A. Morrison, "The Coupled-Channels Integral-Equations Method in the Theory of Low-Energy Electron-Molecule Scattering", in Electron-Molecule and Photon-Molecule Collisions, eds. T. Rescigno, V. McKoy and B. Schneider, Plenum Press, New York (1979), p. 15.
7. B.I. Schneider, "The R-Matrix Method for Electron-Molecule Scattering: Theory and Computation", in Electron-Molecule and Photon-Molecule Collisions, eds. T. Rescigno, V. McKoy and B. Schneider, Plenum Press, New York (1979), p. 77.
8. C.E. Fröberg, Introduction to Numerical Analysis, 2nd ed., Addison-Wesley, London (1969), p. 329.